DEVELOPMENT AND VALIDATION OF TDR-BASED SENSORS FOR THERMAL CONDUCTIVITY AND SOIL SUCTION MEASUREMENTS

by

NAN ZHANG

Presented to the Faculty of the Graduate School of

The University of Texas at Arlington

In Partial Fulfillment of the Requirements

For the Degree of

DOCTOR OF PHILOSOPHY

THE UNIVERSITY OF TEXAS AT ARLINGTON

August 2015

Acknowledgements

First, I would like to express my deepest appreciation and gratitude to my advisor, Dr. Xinbao Yu, and co-advisor, Dr. Anand J. Puppala, for their unfailing excellent guidance and enthusiastic encouragement for the past three years. I appreciate the very constructive recommendations that they made for this research and their help in getting several papers published in high quality journals. Their support and patience have been an inspiration, and their friendship is truly precious to me. Their advice on both my research and my career has been invaluable.

I also would like to thank Dr. Sahadat Hossain and Dr. Nick Z. Fang for serving as my committee members, and Dr. Xinbao Yu, Dr. Ali Abolmaali, Dr. Laureano Hoyos, Dr. Sahadat Hossain, Dr. Bhaskar Chittoori and Dr. Chein-Pai Han for sharing their vast knowledge and experience with me during the geotechnical engineering classes and labs.

I also want to thank my colleagues in our research group, Dr. Asheesh Pradhan, Elmira Riahi, Yujie Hu, Karthik Bolla and Saurav Sinha for supporting and helping me throughout this research. I would like to extend my gratitude to Visiting Professors, Dr. Xinyu Hou, Dr. Zhaoyu Wang, and Dr. Xiang Chen for their excellent help and sincere encouragement.

In addition, I like to express my appreciation to my colleagues in Dr. Puppala's research group, Dr. Aravind Pedarla, Dr. Tejo Vikash Bheemasetti, Dr. Ujwalkumar Dashrath Patil, Dr. Pinit Ruttanaporamakul, Dr. Nagasreenivasu Talluri, Chatuphat Savigamin, Sadikshya Poudel, Rathna Mothkuri, Spoorthi Reballi, Praveen Vanga, Raju Acharya, Alejandro Pinobravo, Aritra Banerjee Santiago Caballero and Minh Hai Nguyen

for their contribution to this research. They are my best friends forever, and our friendship will never be forgotten.

I also would like to thank all the members of Department of Civil Engineering, Ms. Ginny Bowers, Ms. Sara Ridenour, Ms. Ava Chapman, and Mr. Paul Shover for their help during my PhD study at UTA.

At the end I would like to thank all of my friends who kept me motivated to reach my goal. Finally, a special thanks to my family and my beloved girlfriend, Zhuo Li. I could not have finished this work without their selfless support, encouragement, patience, and love.

July 30, 2015

Abstract

DEVELOPMENT AND VALIDATION OF TDR-BASED SENSORS FOR THERMAL CONDUCTIVITY AND SOIL SUCTION MEASUREMENTS

Nan Zhang, PhD

The University of Texas at Arlington, 2015

Supervising Professosrs: Xinbao Yu and Anand J. Puppala

Simultaneous measurement of soil thermal conductivity, moisture content, dry density, and soil suction is a challenging issue and very important to the design of geothermal-related structures such as geothermal energy piles (GEP), ground source heat pump (GSHP) systems, borehole thermal energy storage (BTES) systems, etc. The measurement of these properties is mainly done in laboratory conditions, which can be time consuming. Hence, an attempt is made in this research to develop a new field sensor that can provide these properties in about the same timeframe.

The TDR technique has been used successfully to measure soil moisture content and dry density by analyzing the soil dielectric constant (K_a) and the electrical conductivity (EC_b) obtained from TDR waveforms. The objective of this research is to develop a new thermo-time domain reflectometry (TDR) probe and a moisture/suction TDR probe to better achieve these measurements.

The thermo-TDR probe has three probes of the same diameter and length, with resistance wire embedded in the center probe, and three thermocouples installed in each probe. The probe calibrations for K_a and EC_b were completed by testing five different chemicals with known K_a values, and NaCl and KCl solutions with different concentrations. The probe was then evaluated by testing four different materials, i.e.,

three sands and kaolin clay, and validating them against the KD2 standard probe for measurement of soil thermal properties. Laboratory experiments employing the thermo-TDR probe were then performed on quartz sands, sand-sand mixtures, and sand-clay mixtures to study the effects of the quartz content, particle size, moisture content, dry density, and clay content on soil thermal conductivity.

Based on the experimental results on sand-clay mixtures, a continuum soil thermal conductivity prediction model was developed. The model overcame the shortcomings of the existing models, which accounts for the quartz content effect and prediction of soil thermal conductivity continuously over the entire range of soil types.

The moisture/suction TDR probe has two steel stainless probes and a gypsum block attached to half of the probes. The calibration of the probe is conducted by modified pressure plate tests to establish the relationship between K_a and the matric suction of the gypsum block. Laboratory experiments on silty sand, including the staged-drying test and absorption and desorption tests, were performed to evaluate the probe and to study the equilibrium or response time of the gypsum block being equilibrated with surrounding soils.

Table of Contents

List of Illustrations

List of Tables

Chapter 1

Introduction

1.1 Research Background

Soil is a complex substance consisting of three phases: solid (i.e., soil particles), liquid (i.e., water) and gas (i.e., air). It is the collection of natural bodies on the earth's surface, in places modified or even made by man of earthy materials, containing living matter and supporting or capable of supporting plants out of doors. Jenny (1941) addressed the question of which environmental factors are responsible for the soils we have today. Recognizing these factors is extremely useful for field scientists when looking over a landscape and predicting the soil types that are found upon it. These factors include parent materials, organisms, climate, and relief and time. The parent materials refer to the mud deposited by a river, sand deposited by an ocean, rock that weathers and breaks down, etc. The organism usually refers to vegetation and microorganisms, but includes the complete biological community. Climate affects soils by governing the rate at which chemical reactions can take place and the amount of percolating water that translocates materials from one part of the soil to another. Local relief is the environmental factor that has the greatest effect on the soils under certain conditions. All pedogenic (i.e., soil-forming) processes occur over time, and additional subsurface is formed as the soil matures with time.

Traditionally, the research in geotechnical engineering primarily focuses on the physical and mechanical properties of soils. However, the study of soil thermal properties (i.e., thermal conductivity, thermal diffusivity and heat capacity) is also important because the exploitation and utilization of geothermal energy is becoming an emerging area as the demand for new resources increases all over the world. Subsurface geothermal energy has a great potential of renewable, sustainable, clean (i.e., non-carbon dioxide emission)

and direct-use energy, particularly when it is connected with shallow or deep foundations (i.e., geothermal energy piles, heat pumps (i.e., ground source heat pump systems, and borehole thermal energy storage systems). In the design of the above geothermal structures, the soil thermal property is the most significant design parameter which not only governs the heat transfer process in soils but also determines the thermal efficiency of the entire system. In addition, soil thermal property needs to be studied as an application for engineering barriers in deep geological high-level radioactive waste disposal (HLWD).

The heat pump was invented in Austria in 1875 for the extraction of geothermal energy from the ground. At that time, geothermal energy could also be obtained by means of flat collectors, trench collectors, or borehole heat exchangers (up to 300 m depth, standard diameter of 32 to 120 mm). These systems were widely used for many years in Austria, and there are still around 100,000 heat pumps operating at present. Later, geothermal energy was increasingly obtained from foundation elements, such as rafts, piles, or diaphragm walls. The new innovation, known as “energy foundations,” combined heat pumps with foundation elements and was more cost effective than the conventional systems (Brandl, 2003).

Because soil thermal properties are affected by many factors, such as moisture content, dry density, soil mineral components, soil gradation, etc., a reliable, rapid measurement and an accurate prediction of soil thermal properties are essential and valuable to the design of structures for geothermal-related applications. Moreover, soil is always under unsaturated conditions when geothermal energy is extracted in the shallow depths, and the thermal properties of subsurface soils are changed by the drying and wetting cycles during the climate change in different seasons. Therefore, it is also

necessary to correlate soil thermal properties with soil suction to further investigate the thermo-hydro-mechanical (THM) coupling process in soils.

1.2 Problem Statement and Research Objectives

This research mainly focuses on the development and validation of time domain reflectometry-based sensors (i.e., TDR) for thermal conductivity and soil suction measurements. In previous studies, the measurement of these properties was done under laboratory conditions, which can be time consuming. Hence, an attempt was made in this research to develop a new field sensor that can provide these properties in about the same timeframe. The objective of this research was to develop a new thermo-TDR probe and a moisture/suction TDR probe to better achieve these measurement goals. Based on the previous studies, the problem statements in this study are summarized as follows,

1. Demand of simultaneous in situ measurements of soil thermal conductivity, moisture content, and dry density.
2. Lack of systematic and comprehensive evaluation of the thermo-TDR probe.
3. Application of TDR technique in simultaneous measurements of soil moisture content and matric suction in the field.
4. Discontinuity in the prediction of soil thermal conductivity in the existing soil thermal conductivity models.

Accordingly, the research objectives in this study are listed below,

1. Evaluate the performance of a newly-developed thermo-TDR probe for measuring soil thermal conductivity, moisture content, and dry density simultaneously.
2. Study the effects of particle size, fines content, and clay content on soil thermal conductivity.

3. Develop a new continuum soil thermal conductivity model, accounting for the effects of soil type, mineralogy, moisture content, and dry density.
4. Design and evaluate a new moisture/suction TDR probe for measuring soil moisture content and matric suction.

1.3 Dissertation Organization

This thesis consists of seven chapters: Introduction (Chapter 1), Literature review (Chapter 2), Design and evaluation of a thermo-TDR probe (Chapter 3), Laboratory experimental program on thermal conductivity (Chapter 4), Development of a continuum soil thermal conductivity model (Chapter 5), Design and evaluation of a moisture/suction TDR probe (Chapter 6), and Summary, conclusions and recommendations (Chapter 7).

Chapter 1 presents the introduction of this research, including the research background on the application of TDR-based sensors in thermal conductivity and soil suction measurements, the problem statement based on the previous studies, and the research objectives for this study.

Chapter 2 presents a summary of previous studies: (1) Time domain reflectoemetry (TDR) technique, (2) Soil thermal properties and applications, (3) Measurement of soil thermal properties, (4) Measurement of soil matric suction, and (5) Soil Thermal conductivity prediction models.

Chapter 3 presents the design and fabrication of the thermo-TDR probe, followed by probe calibration through testing KCl and NaCl solutions with different concentrations, using both the thermo-TDR probe and electrical conductivity (EC) meter; and the probe evaluation by testing three sands and one kaolin clay and comparing the results with the standard KD2 probe from Decagon Device (Decagon Devices, 2011).

Chapter 4 presents the laboratory experiments on quartz sands, sand-sand mixtures and sand-clay mixtures by using the thermo-TDR probe to study the effects of

particle size, fines content, and clay content on soil thermal conductivity. The KD2 probe was also used in the experiments for the comparison with the thermo-TDR probe.

Chapter 5 presents the development of a new continuum soil thermal conductivity model based on the previous experimental data on sand-clay mixtures. This model was proposed on the basis of the normalized thermal conductivity concept proposed by (Johansen, 1977), and it accounts for the effects of soil type, quartz content, moisture content, and dry density on soil thermal conductivity simultaneously.

Chapter 6 presents the design and evaluation of the moisture/suction TDR probe. The calibration relationship between dielectric constant (K_a) and matric suction of the gypsum block was obtained by pressure plate tests. The probe evaluation was conducted by testing silty sand in a stage-drying test, absorption test, and desorption test.

Chapter 7 provides the summary and conclusions of this research, and the recommendations for future study.

Chapter 2

Literature Review

2.1 Introduction

This research is aimed at the development and validation of two types of TDR-based sensors, which are the thermo-TDR probe and the moisture/suction TDR probe, for thermal conductivity and soil suction measurements. It also includes the laboratory program of the thermo-TDR probe and the development of a new continuum soil thermal conductivity prediction model.

This chapter summarizes the previous relevant studies regarding this research topic. It is subdivided into several subsections: (1) Time domain reflectometry (TDR) technique, including its measuring principles, algorithms for TDR waveform analysis, TDR software development, and the determination of moisture content and dry density; (2) Soil thermal properties, their influence factors and applications; (3) The measurement techniques of soil thermal properties, including steady state method, transient state method, and thermo-TDR probe; (4) The existing soil suction measurement methods; (5) The existing soil thermal conductivity models.

2.2 Time Domain Reflectometry (TDR) Technique

TDR technique is a relatively new method, but a promising tool for the tests in civil engineering. Based on the TDR technique, Drnevich et al. (2003) developed a “one step method” to estimate the soil moisture content and dry density simultaneously from the soil dielectric constant (K_a) and electrical conductivity (EC_b), which are analyzed and obtained from the reflected TDR waveforms (Yu and Drnevich, 2004). In geotechnical engineering, it is necessary to properly monitor in-situ soil compaction properties during most earthwork construction projects. The conventional in-situ soil compaction monitoring methods are always limited in their applications, whereas the TDR technique better

achieves its goals in the field (White, 2004). It can be used to measure both in-situ moisture content, as well as dry density, by the propagation of an electromagnetic wave going through the soils, and it has been implemented in many fields with success for applications in geotechnical engineering.

This section will describe the principles of the TDR technique and the related system design. The algorithms for TDR waveform analysis is then presented, followed by the statement on development of TDR software. The determination of moisture content and dry density by various traditional methods and the TDR technique are also provided in this section.

2.2.1 Introduction to TDR Technique and System Design

The TDR technique was derived from the same technology that was used in radar, which has been in use since the 1930s. It is similar to radar in that a short electromagnetic pulse is first generated and emitted, and then a reflection is measured. TDR can be also defined as a measurement device which relies on the use of remote electrical sampling to determine the location and nature of objects. A typical TDR system is primarily composed of a pulser, a sampler, an oscilloscope, and a coaxial cable, as shown in Figure 2-1.

The TDR pulser generates an electronic step pulse that travels into the coaxial cables. As the pulse travels down the coaxial cables, a difference is created between the inner and outer conductors of the coaxial cables, creating an electromagnetic field between the conductors (White, 2004). Figure 2-2 shows the diagram of the electromagnetic field in coaxial cables.

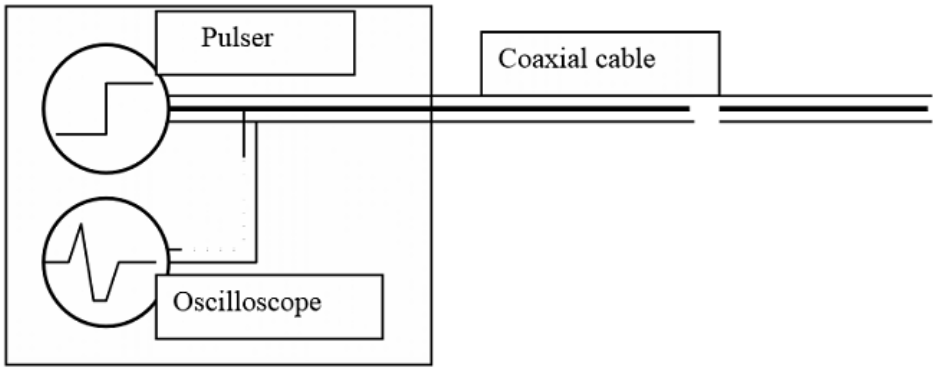

Figure 2-1 Schematic of a typical TDR system (O'Connor and Dowding, 1999)

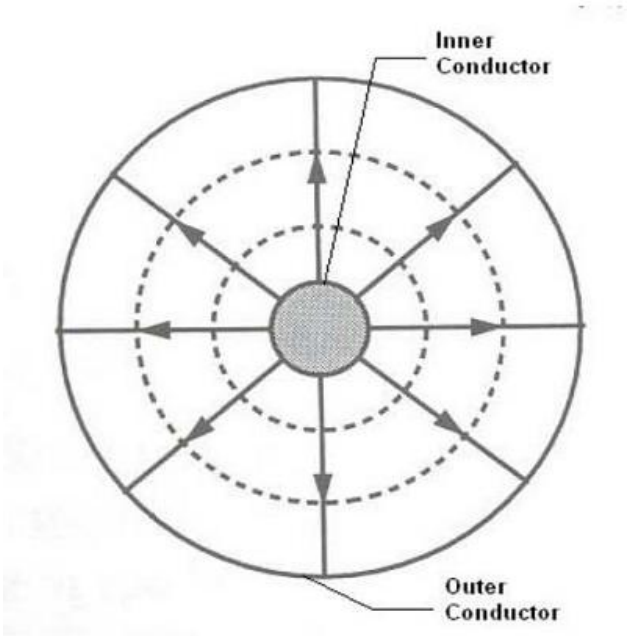

Figure 2-2 Diagram of electromagnetic field in coaxial cables (O'Connor and Dowding, 2004)

As the above electromagnetic field goes through the coaxial cables, it creates electromagnetic waves. The measured reflected waveforms (i.e., reflected TDR waveforms) are supposed to be uniform if the medium between the inner and outer conductors is uniform both geometrically and physically. But a reflection point can be

found from the reflected TDR waveforms when a discontinuity is encountered in the coaxial cables, such as the change of cable geometry or the medium between conductors. The time it takes for a reflection to occur, along with sign, length, and amplitude, is useful in determining both the location of the discontinuity or the nature of the medium. Similarly, soil moisture content property can be determined when inserting the coaxial cables into the soil using metallic spikes (e.g., steel rods). Figure 2-3 shows the TDR soil moisture system configuration. The inner conductor is connected to the inner probe, and outer conductors are connected to two outer probes. The soil tested in the electromagnetic field is between the inner probe and the outer probe.

Figure 2-4 depicts a typical reflected TDR waveform from a TDR system. There are two reflection points which can be observed at different locations. The first one is located at the air-soil interface from the probe head, where the medium between two conductors is suddenly changed, while the second one is located at the probe end, which is actually the end of the coaxial cables.

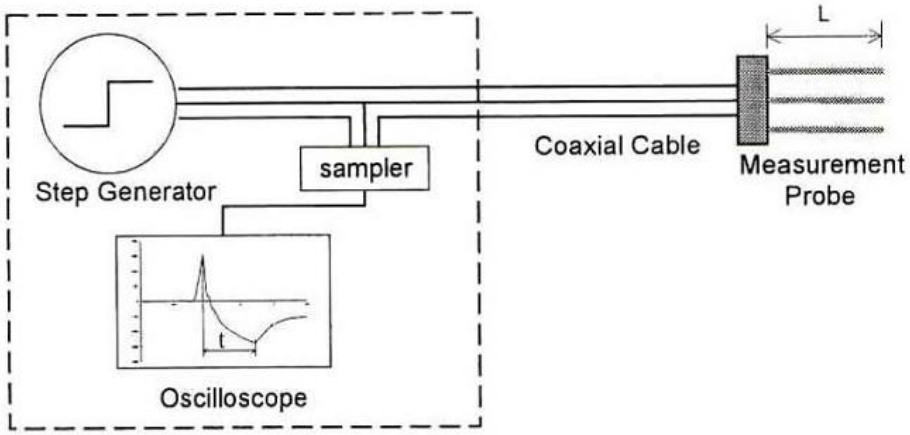

Figure 2-3 TDR soil moisture system configuration ((Drnevich et al., 2000)

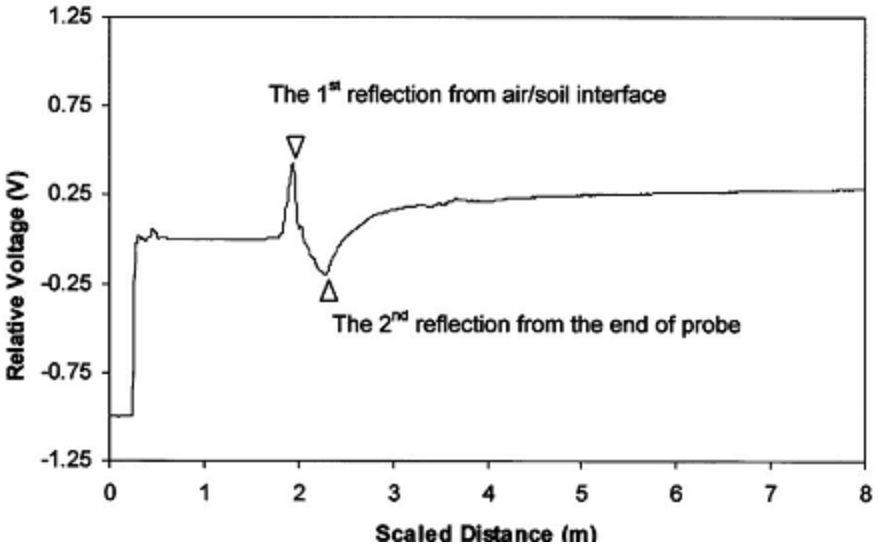

Figure 2-4 A typical reflected TDR waveform (Yu and Drnevich, 2004)

2.2.2 Algorithms for TDR Waveform Analysis

As discussed in the previous sections, soil dielectric constant (K_a) and electrical conductivity (EC_b) properties can be obtained from the reflected TDR waveforms. In theory, K_a is a function of travel time of the electromagnetic pulse along the waveguides. There are three commonly used approaches for getting travel time from the TDR waveforms (Timlin and Pachepsky, 1996): (1) Measure the signal trace manually, (2) Use a computer algorithm to find the initial point and end point of the trace by searching characteristic slope changes, and (3) Do an Inverse analysis of the TDR waveforms to obtain the parameters of transmission line simulated by the TDR system (Yanuka et al., 1988).

Figure 2-5 shows the two methods to manually identify the second reflection point. This manual method usually uses the tangent line method to determine the location of the reflection point. Topp et al. (1982) and Baker and Allmaras (1990) proposed two different tangent line methods. The basic idea is to draw tangent lines from characteristic

points along the TDR signal, and the intersections of the two tangent lines are regarded as the reflection points. But there is also a slight difference between these two methods' criteria of selecting characteristic points. The method proposed by Topp et al. (1982) uses two lines from the linear section of the TDR signal, while the method proposed by Baker and Allmaras (1990) uses one line from the linear section of the TDR waveforms and another line from a horizontal line going through the point where the voltage is a local minimum. The manual approach is more prone to be affected by the user's personal preference; therefore, the automation of the TDR waveform analysis is highly desirable.

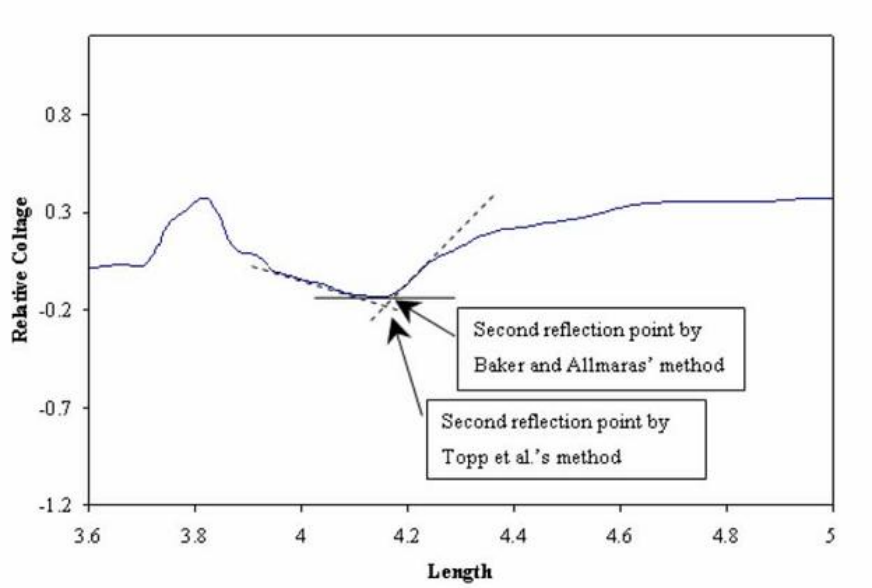

Figure 2-5 The example of two methods to manually identify the second reflection point (Drnevich et al., 2003)

The second method for the analysis of the TDR signal is based on the computer algorithm. This means that all the TDR waveforms analysis can be completed by using a computer algorithm to record the TDR signal, store the data, analyze the TDR waveforms, and calculate the K_a and EC_b of the test soil samples. Actually, the algorithm also follows the tangent line methods, as described above, to perform the TDR analysis

for selecting reflection points. It generally makes use of numerical differentiation, which can calculate the first derivative and find the location of the point with the highest first derivative. The numerical slope of the tangent line can be computed by,

$$k_i = \frac{d_{i+1} - d_{i-1}}{2\Delta} \tag{2.1}$$

where k_i is the calculated slope the tangent line at point i; d_{i+1} and d_{i-1} are the measured voltage levels on the TDR signal at point i+1 and i-1; Δ is the horizontal interval of the signal.

TDR signals include some unavoidable noise, affecting the analyzed results. Thus, it is highly recommended to use the average point method to remove the noise effect as much as possible. Figure 2-6 shows the use of the 5-point average method to smooth the derivative curve to improve the first derivative values. It has been found that the original data will become smoother by averaging multiple signals. Although the noise effect cannot be completely eliminated by this method, its level will be reduced considerably. In addition, the 7-point average method can also be utilized in some cases if the signal still contains a lot of noise after being processed by the 5-point method.

The characteristic points, which include the local maximum or minimum, and the points with the maximum first derivative in the TDR waveforms can then be identified. The locations and the slopes of the characteristic points are used to calculate the intersection and determine the location of reflection points.

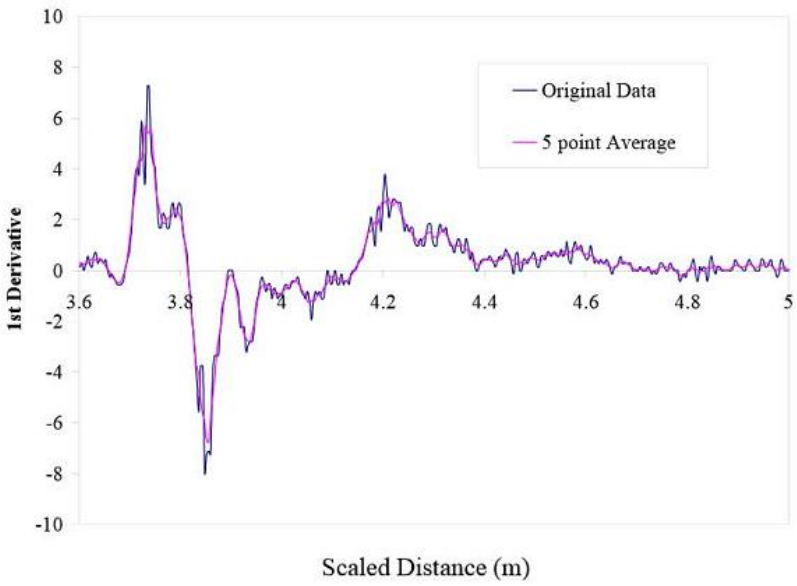

Figure 2-6 Use of 5 point average method to smooth the derivative curve to improve the first derivative values (Drnevich et al., 2003)

The third method for the analysis of TDR signals is by means of applying an inversion theory. It is the most complicated method for analyzing the TDR waveforms and calculating soil properties because it just physically describes the phenomena that occurs in the TDR systems. But the complexity of the TDR system makes it difficult to simulate the actual behaviors of the system, and some assumptions and simplifications need to be made before a solution can be obtained.

2.2.3 Development of TDR Software

The use of TDR software can certainly simplify the TDR waveforms analysis process significantly. The basic software is known as “PMTDR,” and it was developed by Campbell Scientific, Inc., especially for the Purdue TDR method. It is the acronym of Purdue Method Time Domain Reflectometry. There are also two other improved methods, which are called PMTDR-RDR and PMTDR-SM, respectively. The “hand-shaking” functions were incorporated into PMTDR-RDR to control the TDR100 signal

generator/sampler and to acquire the TDR waveform data. The “one step method” for in-situ measurements of soil moisture content and dry density was included and implemented in PMTDR-SM program.

PMTDR-SM is the acronym of Purdue Method TDR – Simplified Method. It is the software used automation of soil moisture content and dry density calculation by using “one step method” proposed by Yu and Drnevich (2004). This program has two parts: the MRP screen for field TDR tests, and the CMP screen for mold TDR tests, as shown in Figure 2-7 and Figure 2-8. The proper screen needs to be activated for the specific type of test being conducted.

After the TDR probe is inserted into the soil sample, the TDR waveforms can be obtained by clicking the button “Get Waveform.” It usually takes about 10 s to collect the data and display two waveforms on the screen. The upper waveform is used to calculate the soil dielectric constant (K_a), and the other at bottom is used to calculate the soil’s electrical conductivity (EC_b).

The analysis for the determination of soil moisture content and dry density can also be performed by clicking the “Start” button under the Wave Analysis, as shown in Figure 2-7 and Figure 2-8. Once the calibration relationships for K_a and EC_b have been established from the separate laboratory tests, the calibration coefficients a, b, c, and d can be inputted to the system. The soil moisture content and dry density can then be calculated by clicking the “Compute” button. In addition, the test results, including the test information, TDR waveforms data, and the results of the analyses, can be stored on the computer for further examination and analysis.

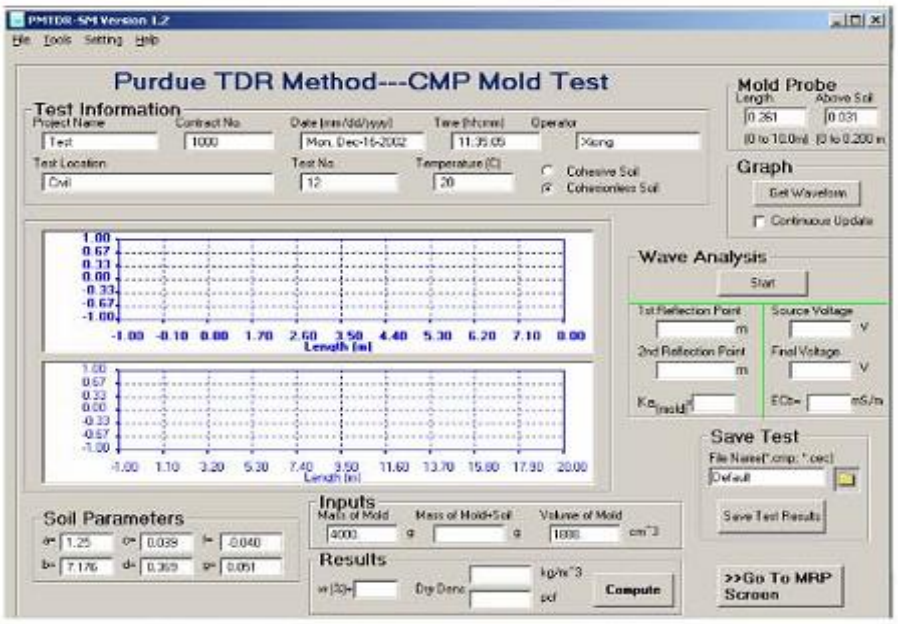

Figure 2-7 MRP screen for field TDR test

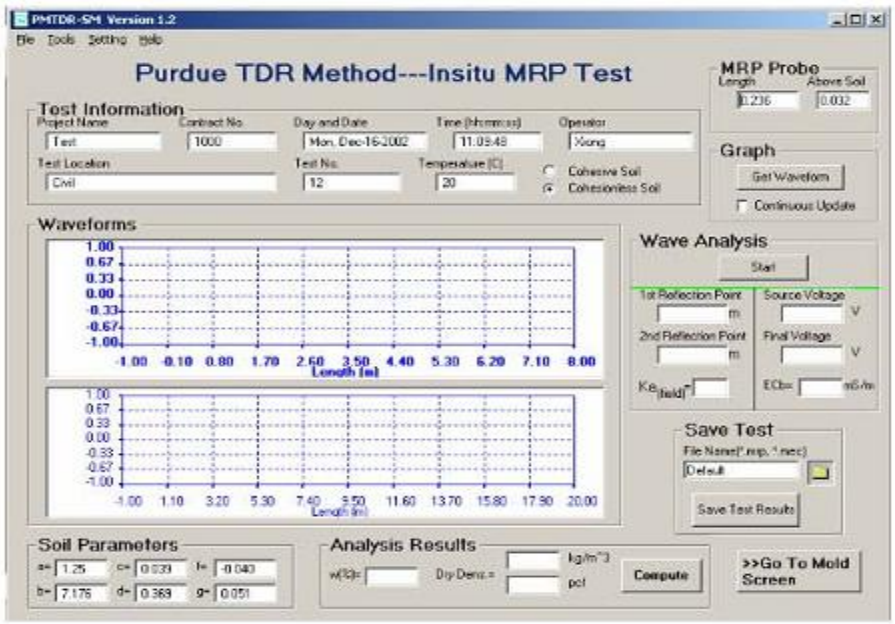

Figure 2-8 CMP screen for mold TDR test

2.2.4 Determination of Moisture Content and Dry Density

There are several methods in the ASTM Standards that can be used to measure soil moisture content and dry density, both in the laboratory and in-situ, as listed below.

For soil moisture content measurement:

1) Laboratory Determination of Water Content of Soil and Rock (ASTM D2216)
2) Microwave Oven Method (ASTM D4643)
3) Direct Heating Method (ASTM D4959)
4) Calcium Carbide Gas Pressure Tester Method (ASTM D4944)
5) Nuclear Method (Shallow Depth) (ASTM D3017)

For soil dry density measurement:

1) Nuclear Method (ASTM D5195)
2) Nuclear Method (shallow depth) (ASTM D3017)
3) Sleeve Method (ASTM D4564)
4) Drive-Cylinder Method (ASTM D2937)
5) Sand-Cone Method (ASTM D1556)
6) Rubber Balloon Method (ASTM D2167)

Among all the methods mentioned previously, the nuclear method is most commonly used for soil moisture and density measurements, but It requires training and special licensing to operate the equipment, and the field measurements are only as good as the calibration device. The drive sleeve is another widely used method, but it is not a nondestructive method. Both sand cone and rubber balloon methods are less likely to be adopted, and require a proficient and skilled test operator. The TDR-based “one step method” developed by Yu and Drnevich (2004) to determine soil moisture content and dry density will be presented in the following paragraph. Table 2-1 shows the comparison of current methods for soil moisture content and dry density measurements.

Table 2-1 Comparison of current methods of soil moisture content and dry density measurements (White, 2004)

Test	Application	Required Time	Major Source of Error
Oven Dry	Water Content	24 h	Considered as baseline measurement
Speedy Moisture	Water Content	15-20 min + calibration	Operator's ability to perform test correctly
Nuclear Method	Water Content, Dry density	30 min+ calibration	Highly dependent on proficient calibration
Sand Cone	Density	30 min+ calibration	Operator dependent

The TDR-based "One-Step Method" was proposed by Yu and Drnevich (2004), who stated that some previous calibration equations for K_a and EC_b are difficult to apply to geotechnical engineering for two reasons: (1) The calibration equations are expressed in terms of volumetric water content, whereas the gravimetric water content is mostly used in the field of geotechnical engineering; (2) The calibrations which incorporate the density effect, such as that in the Malicki et al. (1996) study, are complex and difficult to apply (Yu and Drnevich, 2004). The first equation in the "One-Step Method" was proposed by Siddiqui and Drnevich (1995) and expressed as follows,

$$\sqrt{K_a}\,\frac{\rho_w}{\rho_d} = a + bw \tag{2.2}$$

where a and b are the soil specific calibration constants; ρ_d is the dry density of soils; ρ_w is the density of water and w is the gravimetric water content.

Yu and Drnevich (2004) further argued that the electrical conductivity of the pore fluid is typically the dominating factor in the determination of the bulk electrical

conductivity of soils, and proposed a similar equation describing the relationship between the soil electrical conductivity and moisture content, expressed as follows,

$$\sqrt{EC_b}\,\frac{\rho_w}{\rho_d} = c + dw \tag{2.3}$$

where c and d are another two soil specific calibration constants. By combining and solving Equations 2.2 and 2.3, the other two equations to determine soil moisture content and dry density can be expressed as,

$$w = \frac{c\sqrt{K_a} - a\sqrt{EC_b}}{b\sqrt{EC_b} - d\sqrt{K_a}} \tag{2.4}$$

$$\rho_d = \frac{d\sqrt{K_a} - b\sqrt{EC_b}}{ad - cb}\rho_w \tag{2.5}$$

However, Yu and Drnevich (2004) did not obtain very satisfactory results when the above two equations were applied because of the dominance of pore fluid conductivity on Equation 2.3. Zhang et al. (2015a) designed a new thermo-TDR probe and estimated the soil moisture content and dry density using this method. The excellent agreement between predicted values and the actual measured results of three quartz sands reflected only 10% deviation.

2.3 Soil Thermal Properties and Applications

This section will introduce soil thermal properties, including thermal conductivity, thermal resistivity, thermal diffusivity, and heat capacity. The influence factors of soil thermal conductivity are also discussed from previous literatures. The applications of soil thermal conductivity in geotechnical engineering, especially in the exploitation and utilization of geothermal energy, are also presented.

2.3.1 Soil Thermal Properties

Soil thermal properties are a component of soil physics that have found important uses in engineering, climatology, and agriculture. These properties influence how the energy is partitioned in the soil profile. While related to soil temperature, it is more accurately associated with the heat transfer throughout the soils, by radiation, conduction, and convection. Soil thermal properties include thermal conductivity, thermal resistivity, thermal diffusivity, and heat capacity.

2.3.1.1 Thermal Conductivity

Thermal conductivity is an intrinsic soil property that describes its ability to conduct heat and is expressed in W $m^{-1}K^{-1}$. It can be called “heat flux” or “heat transfer” in that it is related to the movement of heat energy through the soils. The heat moves from an area of high temperature to a cooler area of low temperature as the heat redistributes itself to reach an equilibrium where it is evenly distributed through the soils. It appears primarily in Fourier's Law for heat conduction. Heat transfer occurs at a lower rate across materials of low thermal conductivity than across materials of high thermal conductivity. Correspondingly, the materials of high thermal conductivity are widely used in heat sink applications, and the others of low thermal conductivity are used as thermal insulation. Moreover, the reciprocal of thermal conductivity is thermal resistivity, usually expressed in Km W^{-1}.

The dimension of thermal conductivity is $M^1L^1T^{-3}\Theta^{-1}$. These variables are (M) mass, (L) length, (T) time, and (Θ) temperature. In Imperial units, thermal conductivity is measured in BTU/(hr·ft·°F)(Perry et al., 1997). Other units which are closely related to the thermal conductivity are in common use in the construction and textile industries. The construction industry makes use of units such as the R-value (i.e., resistance) and the U-value (i.e., conductivity). Although related to the thermal conductivity of a material used in

an insulation product, R and U values are dependent on the thickness of the products. Likewise the textile industry has several units, including the tog and the clo, which express thermal resistance of a material in a way analogous to the R values used in the construction industry.

Thermal conductivity is important in material science, research, electronics, building insulation, and related fields, especially where high operating temperatures are achieved. The thermal conductivities of solid particles in soils are shown in Table 2-2.

Table 2-2 Average values of thermal conductivities of solid particles computed from various sources (Côté and Konrad, 2005)

Material	ρ_s (g/cm^3)	λ (W m^{-1}K^{-1})
Rocks		
Anorthosite	2.73	1.8
Basalt	2.90	1.7
Diabase	2.98	2.3
Dolostone	2.90	3.8
Gabbro	2.92	2.2
Gneiss	2.75	2.6
Granite	2.75	2.5
Limestone	2.70	2.5
Marble	2.80	3.2
Quartzite	2.65	5.0
Sandstone	2.80	3.0
Schist	2.65	1.5
Shale	2.65	2.0
Syenite	2.80	2.0
Trap rock	2.90	2.0
Soil and organic matter		
Coal	1.35	0.26
Peat	1.50	0.25
Silt and clay	2.75	2.90

2.3.1.2 Thermal Diffusivity

In the heat transfer analysis, thermal diffusivity is the thermal conductivity divided by density and specific heat capacity at constant pressure (Lide and Haynes, 2009). It measures the ability of a material to conduct thermal energy relative to its ability to store thermal energy. It has the SI unit of m²/s. Thermal diffusivity is usually denoted by α and can be calculated by,

$$a = \frac{k}{\rho c_p} \tag{2.6}$$

where k is the thermal conductivity, W $m^{-1}K^{-1}$; ρ is the density, kg/m^3; c_p is the specific heat capacity, J $kg^{-1}K^{-1}$. In addition, ρc_p is the volumetric heat capacity, J m^{-3} K^{-1}.

Thermal diffusivity is the ratio of the time derivative of temperature to its curvature, quantifying the rate at which temperature concavity is "smoothed out." In a sense, thermal diffusivity is the measure of thermal inertia (Venkanna, 2010). In a substance with high thermal diffusivity, heat moves rapidly through it because the substance conducts heat quickly, relative to its volumetric heat capacity or 'thermal bulk'.

Thermal diffusivity is often measured with the flash method (Parker et al., 1961). It involves heating a strip or cylindrical sample with a short energy pulse at one end and analyzing the temperature change (reduction in amplitude and phase shift of the pulse) a short distance away (Blumm and Opfermann, 2002; Thermitus, 2010).

2.3.1.3 Heat Capacity

Heat capacity, also called thermal capacity, consists of specific heat capacity and volumetric heat capacity. It is a measurable physical quantity equal to the ratio of the heat added to (or removed from) an object to the resulting temperature change (Halliday et al., 2010). The SI unit of heat capacity is J K^{-1} and the dimensional form is $M^1L^2T^{-2}\Theta^{-1}$.

Specific heat capacity is the amount of heat needed to raise the temperature of a certain mass 1 degree Celsius.

Heat capacity is an extensive property of matter, meaning it is proportional to the size of the system. When expressing the same phenomenon as an intensive property, the heat capacity is divided by the amount of substance, mass, or volume, so that the quantity is independent of the size or extent of the sample. The molar heat capacity is the heat capacity per unit amount (SI unit: mole) of a pure substance, and the specific heat capacity, often simply called specific heat, is the heat capacity per unit mass of a material. Occasionally, in engineering contexts, the volumetric heat capacity is used.

2.3.2 Influence Factors of Soil Thermal Conductivity

Among the three soil thermal properties, thermal conductivity is the most important one and the one usually used in practices. As heat transfer in soils takes place primarily by conduction, with convection playing a significant role only in highly permeable soils (e.g., gravel), the major thermal properties of the soils that are of interest are the thermal conductivity and heat capacity. The heat capacity determines the amount of energy needed to change the temperature of the soils, and hence influences the time taken to reach steady state conditions, only the thermal conductivity of the soil influences the temperature field and heat flow in the soils at equilibrium (Haigh, 2012). This section presents the influence factors of soil thermal conductivity, including compositional factors (i.e., soil particle size, shape, gradation, and soil mineral component) and environmental factors (i.e., moisture content, dry density, and temperature).

2.3.2.1 Compositional Factors

As reported in previous literatures (Abu-Hamdeh, 2003; Abu-Hamdeh and Reeder, 2000; Cortes, 2015; De Vries, 1963; Farouki, 1981; Johansen, 1977; Kersten,

1949), there are some compositional factors that affect soil thermal conductivity, such as soil particle size, shape, gradation, and soil mineral components.

Soil is mainly composed of three phases: solid, liquid, and gas. The solid particles are surrounded by pore fluid that contains water and air, and it may consist of several different soil minerals, such as quartz, kaolinite, illinite, and montmorillonite. Quartz has the highest thermal conductivity among all the soil minerals, whereas the thermal conductivity of other minerals does not change considerably. Water may occur as liquid or vapor in the pore space, as ordinary water in the liquid state above 0^{o}C, or ice below 0^{o}C (Farouki, 1981).

The soil particle size and shape will affect the arrangement of solid primary or secondary particles; thereby determine the “soil structure” or packing. This also influences the soil thermal conductivity to some extent. For example, the finer grains in natural soils are usually aggregated into large secondary units of different shapes and sizes. If the orientation of the above large secondary units existing between the primary soil particles and macropores is parallel to the direction of heat flow or the imposed temperature gradient, the effect of the thermal conductivity of soils is increased since the heat transfer mainly relies on the solid phase in soils.

In addition, there is another factor that affects soil thermal conductivity, which is the number and nature of the interparticle physical contact points among soil particles. It should be note that most of the heat transfer takes place across these contact points, particularly when soil is under dry condition. This is because the air has a very low thermal conductivity compared with solid particles. The number of contact points is the dominating factor in this case. If the solid grains are cemented together by clay or other binders, the thermal conductivity is significantly improved as well (Chen, 2008; Farouki, 1981; Johansen, 1977; Zhang et al., 2015a; Zhang et al., 2015b).

Various changes in soil structure may occur naturally, leading to the change in density or porosity. For instance, drying and wetting cycles will cause shrinkage and swelling behaviors and will change the soil structure, with consequential change in soil thermal conductivity. The process of freezing and thawing also leads to the excessive compositional and structure changes, and affects soil thermal conductivity as a result.

Heat conduction in soils usually occurs either in soil particles (i.e., inside solid phase) or between solid phase and pore fluid (i.e., water or air). All the compositional factors of soil thermal conductivity mentioned above are correlated and need to be considered comprehensively to assess their effects.

2.3.2.2 Environmental Factors

The environmental factors of soil thermal conductivity include soil moisture content, dry density, and temperature, which had been studied by many researchers (Chen, 2008; Côté and Konrad, 2005; De Vries, 1963; Farouki, 1981; Johansen, 1977; Kersten, 1949; Lu et al., 2007; Zhang et al., 2015a).

As reported by De Vries (1963), the thermal conductivity of water at room temperature (20-25^{o}C) is 0.59 W $m^{-1}K^{-1}$, which is almost 22 times greater than that of air (0.025 W $m^{-1}K^{-1}$). Thus, as soil pore fluid, the effect of moisture content on soil thermal conductivity is evident. Based on the experimental studies in literatures (Yu et al., 2014a; Yu et al., 2014b), soil thermal conductivity at dry or nearly dry condition is much less than that at moist or fully saturated condition.

Moreover, there is always some water movement taking place in soils naturally due to the temperature changes or water drainage. In addition to conducting heat, the water movement leads to the changes in soil thermal conductivity owing to the changes in amount and state of water. The temperature gradients imposed in soils can cause water movement directly by setting up suction potentials and osmotic pressures. For

example, at relatively low temperatures (e.g., below 0^{o}C), the water may be frozen, leading to changes in the soil structure and soil thermal conductivity. At relatively high temperatures, the water may turn into vapor in soils, resulting in an increase in soil thermal conductivity because of the increasing activity of water or water vapor molecules.

The moisture migration and temperature have been recognized as a coupled process, with complicated interactions between the effects of moisture flow, temperature, and heat flow. Figure 2-9 shows the heat flow in soils under dry, unsaturated, and saturated conditions. The heat and mass transport are the two major physical processes occurring in arctic tundra soils (Nakano and Brown, 1971). The moisture and thermal regimes of such soils act in parallel in a complex manner and must be considered simultaneously (Guymon and Luthin, 1974). Some other relevant studies on this topic can be found in literature (Gylys et al., 2013; Qian-lin and Xiao-chun, 2011; Wu, 2013).

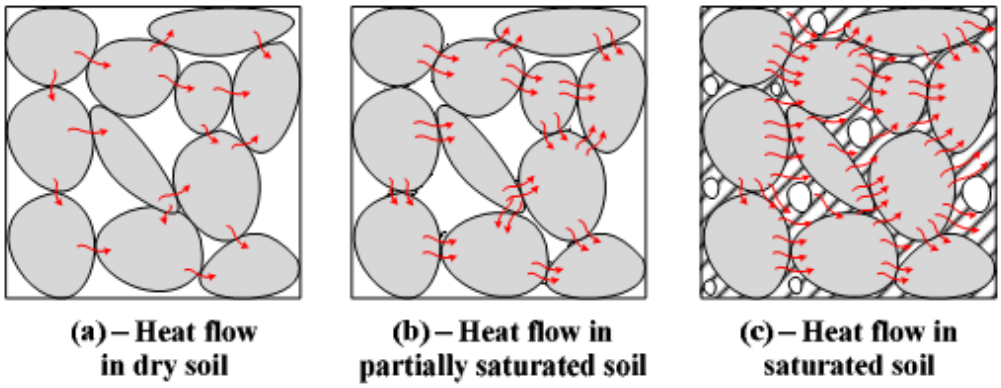

Figure 2-9 Heat flow in soils under dry, unsaturated and saturated conditions (Akrouch et al., 2015)

2.3.2.3 Other factors

This section will discuss some other factors that can influence soil thermal conductivity. It includes properties of soil components, ions, salts, additives, and hysteresis effects.

The surface of solid particles is the locus where physic-chemical reactions such as adsorption of water and of other molecules, binding of cementing substances, exchange of ions, and catalytic action may take place (Winterkorn, 1960). The specific surface area of soil particles primarily depends on its fines fraction. For example, the clay soils always have a larger surface area than sandy soils. Moreover, the more surface area the soil has, the more water it will absorb, resulting in a reduction of fluid water and then a decrease in soil thermal conductivity.

Irons and salts have greater influence on fine grained soils since they have high specific surface areas. Farouki (1981) stated that the bonds provided by the exchanged cations may make a contribution to the strength of clay. These bonds may also be expected to affect heat transfer process among soil particles. Significant changes in this heat transfer may result from any physico-chemical changes taking place in the particle surfaces where two single particles are in contact with each other, or in the region between these surfaces where the particles approach each other.

The additive effect on soil thermal conductivity is always encountered in some special cases where soils are treated with cement, lime, or other binders for strength improvement or other purpose. For example, Portland cement or asphalt is added to coarse granular materials, rendering ordinary concrete or bituminous concrete in road pavements.

The hysteresis effect not only takes place for soil thermal conductivity, but also for other soil properties. Some hysteresis effects have previously been mentioned, including the freeze-thaw cycle followed by the unfrozen moisture content's relationship with temperature, and the drying-wetting cycle followed by the suction-water content relationship. Experiments have shown that the thermal conductivity of soils depends on whether the particular moisture content is achieved by wetting or drying. It has also been

found that the thermal conductivity is much higher when it is produced by drying, especially in nearly dry state, because the drying process sets up the oriented water films to their fullest extent, thereby making heat transfer more effective.

2.3.3 Applications of Soil Thermal Conductivity

Studying soil thermal conductivity and its influence factors has many engineering applications, such as geothermal energy piles (GEP), borehole thermal energy storage (BTES), ground source heat pumps (GSHP) systems, and high level radioactive waste disposal (HLWD). In the above cases, the heat transfer process in soils or the heat exchange between soils and circulating fluid in pipes are the main concerns in the design of entire systems. Brandl (2006) finished a comprehensive review of energy foundations and other thermo-active ground structures. This section will introduce some typical engineering examples regarding the applications of soil thermal conductivity.

2.3.3.1 Geothermal Energy Piles (GEP)

Brandl (2003) presented that subsurface geothermal resources represent a great potential of direct use energy, especially in connection with deep foundations and heat pumps. The heat pump was invented about 140 years ago by the Austrian, Peter Ritter von Rittinger, for the extraction and utilization of geothermal energy from the ground. Combining traditional heat pumps with pile foundations, geothermal energy piles were developed as an innovative method which is also more cost effective and environmentally friendly because it uses sustainable, clean, and renewable energy.

Energy foundations may be raft foundation, piles, barrettes, or slurry trench systems (single elements or continuous diaphragm walls. In addition, energy foundations can be used to heat the buildings in the winter or cool the buildings in the summer. Figure 2-10 shows the scheme of heating/cooling an industrial building with energy piles. It is noted that the energy piles can be driven, bored, or augered piles of reinforced concrete.

The piles should have plastic pipes (HDPE) carrying a heat transfer medium, also called circulating fluid (i.e., water or air). In the pre-fabricated or in-situ cast concrete piles, the pipes are placed along the reinforcement cages. As shown in the Figure 2-10, there are two types of pipes, which are main pipes and absorber pipes, in energy piles. The absorber pipes are used to extract geothermal energy to heat or cool the buildings.

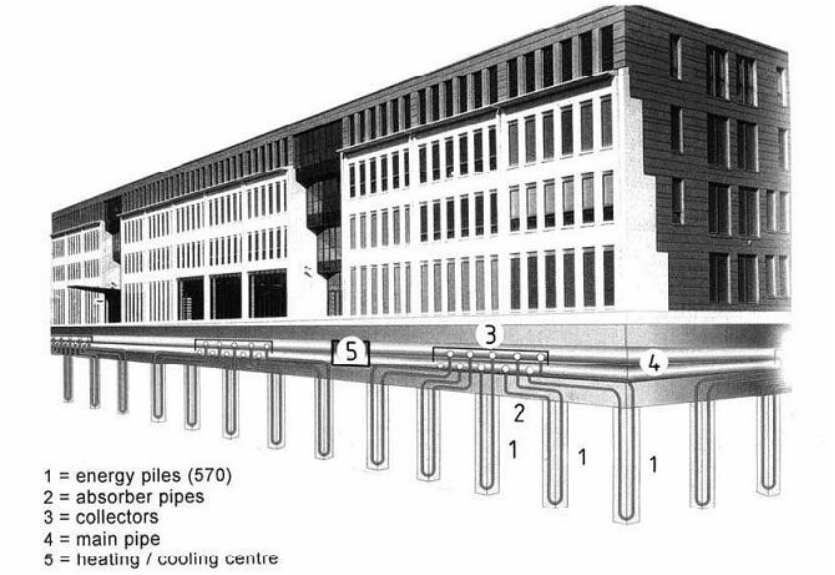

Figure 2-10 The scheme of heating/cooling an industrial building with energy piles (Brandl, 2003)

Figure 2-11 shows the scheme for heating/cooling a small one-familiy house with energy foundations. This kind system has been widely used for many years in Austria and can save 293000 m^3 of firewood each year. Figure 2-12 depicts the heat transport from soils to heat carrier fluid within the absorber pipe of an energy pile. It is obvious that there are seven different types of heat transfer processes taking place in the case of energy piles. The thermal efficiency of energy piles can be analyzed and calculated accordingly.

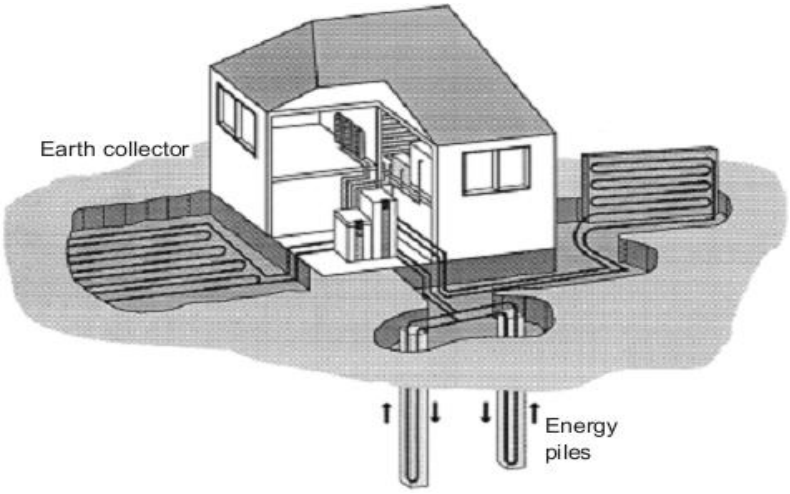

Figure 2-11 The scheme for heating/cooling a small one-familiy house with energy foundations (Brandl, 2006)

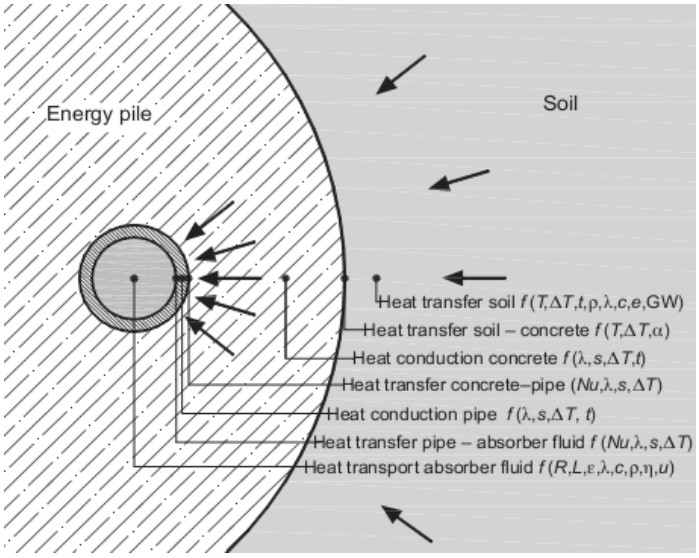

Figure 2-12 The heat transport from soils to heat carrier fluid within the absorber pipe of an energy pile (GW, ground water) (Brandl, 2006)

2.3.3.2 Borehole Thermal Energy Storage (BTES)

The borehole thermal energy storage (BTES) system is a type of underground structure for storing large quantities of solar heat collected in summer for use later in

winter. It is basically a large, underground heat exchanger. The system usually consists of an array of boreholes resembling standard drilled wells. After drilling, a plastic pipe with a “U” bend at the bottom is inserted down the borehole. To provide good thermal contact with the surrounding soil, the borehole is then filled with a high thermal conductivity grouting material.

Borehole thermal energy storage (BTES) is also an application of soil thermal conductivity, which can be used to store energy underground in soils. Ohga and Mikoda (2001) studied the energy performance of borehole thermal energy storage systems. The schematic of BTES is shown in Figure 2-13. This cooling and heating system is the closed-loop BHE, coupled with the heat pump. It consists of a high efficiency screw WSHP with new counter flow gas-liquid heat exchanger and BHE (as shown in Figure 2-14).

A cooling tower is usually added to balance the heat, which is injected into the ground and extracted from the ground. For example, if the heat injection is greater than the heat extraction, a cooling tower is used, as shown in Figure 2-15. Moreover, the energy consumption of the BTES system is decreased by 20%, compared with that of a conventional system using air source heat pump (ASHP).

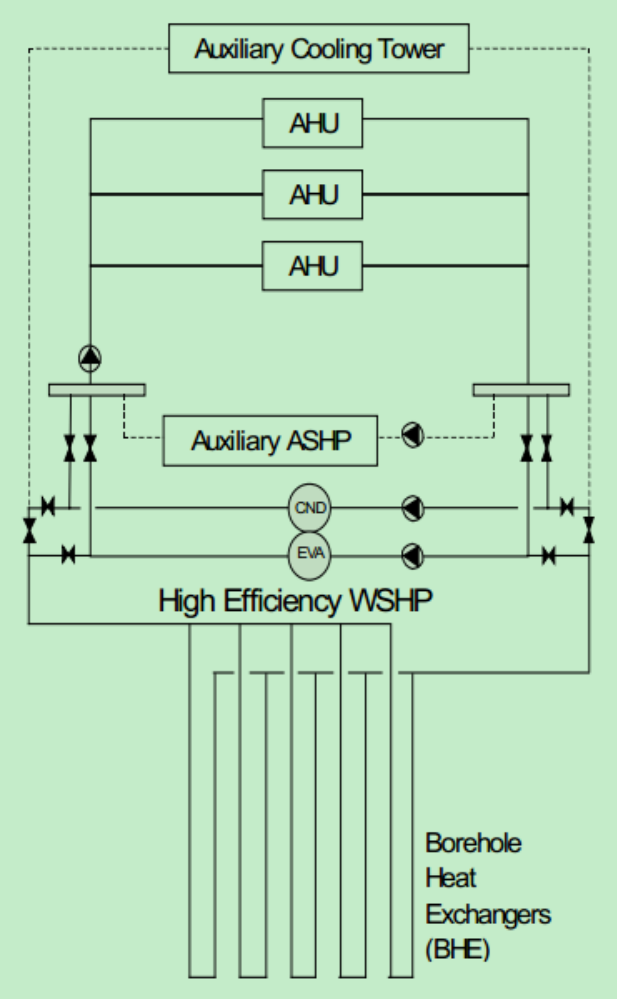

Figure 2-13 The schematic of BTES (Ohga and Mikoda, 2001)

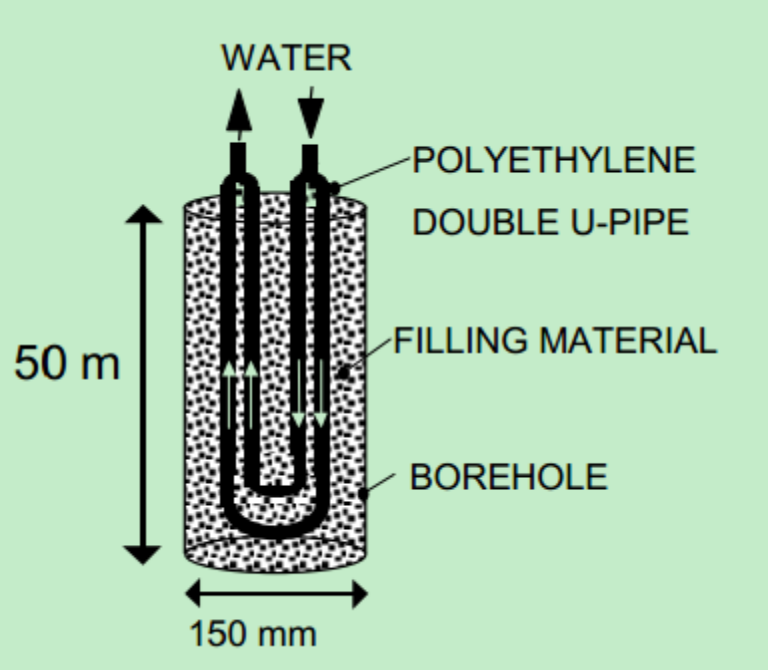

Figure 2-14 The schematic of borehole heat exchanger (Ohga and Mikoda, 2001)

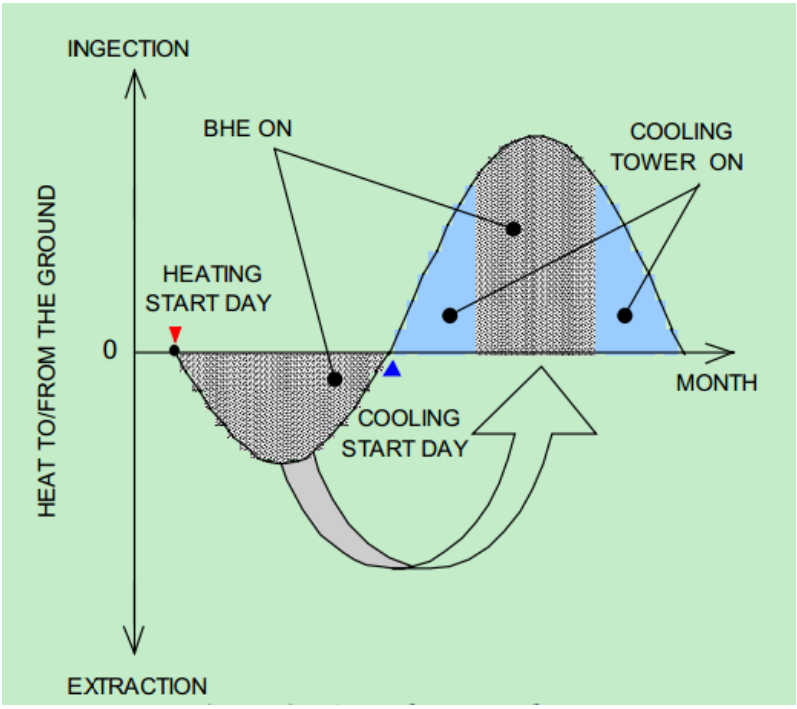

Figure 2-15 Annual heat balance (Ohga and Mikoda, 2001)

2.3.3.3 Ground Source Heat Pump (GSHP)

A ground source heat pump (GSHP) system is a central heating and cooling system that injects heat into the ground or extracts geothermal energy from the ground. It uses the soils as a heat source (in the winter) or a heat sink (in the summer). This design takes advantage of the moderate temperatures in the ground to boost efficiency and reduce the operational costs of heating and cooling systems, and can be combined with solar heating to create a geosolar system with even higher efficiency. GSHPs are also known as "geothermal heat pumps;" the heat (i.e., geothermal energy) does not come primarily from the soils, but from the sun. They are also called by other names, such as geoexchange, earth-coupled, and earth energy systems. GSHPs harvest heat absorbed at the soil's surface from solar energy. The temperature in the ground below 6 m is roughly equal to the mean annual air temperature at that latitude at the surface. The advantages of employing GSHP systems include: (1) It can lower your fuel bills, especially if you replace conventional electric heating; (2) It helps reduce home carbon emissions; (3) No fuel deliveries are needed, and the maintenance is minimal.

In GSHP systems, the heat from the ground can be absorbed at low temperatures into a circulating fluid inside a loop of pipe buried underground. The fluid then passes through a compressor that raises it to a higher temperature, which can then heat water for the heating and hot water circuits of the buildings. The cooled ground-loop fluid passes back into the ground where it absorbs further energy from the soils continuously, as long as heating is required.

Basically, the loop is laid flat or coiled in trenches about 2 m in depth. However, a vertical loop can be installed down into the soils to a depth of up to 100 m for a typical domestic home if there is not enough space in the field. The heat pumps have some impact on the environment since the electricity is needed to run the pumps, but the

geothermal energy extracted from the soils, the air or the water, is constantly renewed naturally. Figure 2-16 shows the schematic of a GHSP system for cooling (left) and heating (right).

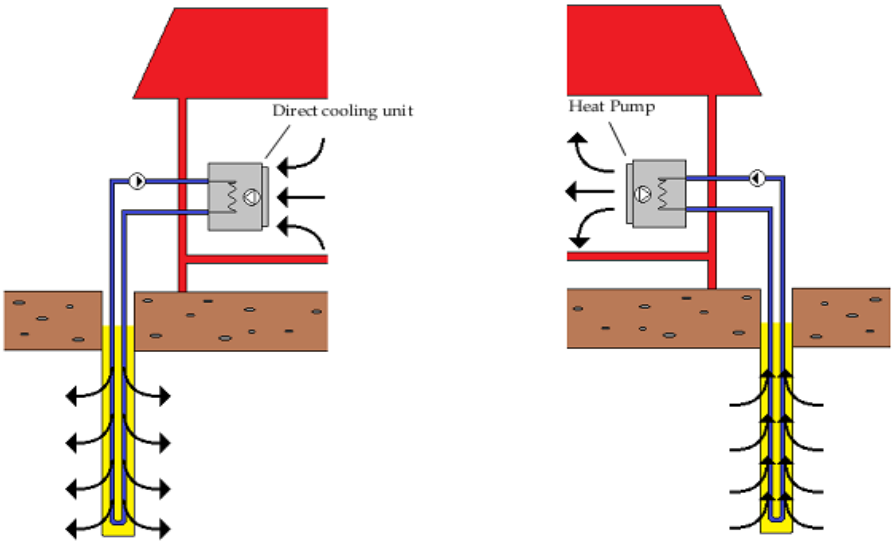

Figure 2-16 The schematic of GHSP system for cooling (left) and heating (right) (Monzo et al., 2011)

2.3.3.4 High Level Radioactive Waste Disposal (HLWD)

The term high-level radioactive waste (HLW) generally refers to the highly radioactive wastes requiring permanent isolation from man's environment that arise as a byproduct of nuclear power generation. In some countries, where the spent nuclear fuel arising from reactor operations is chemically reprocessed, the radioactive wastes include highly concentrated liquid solutions of nuclear fission products. These are later solidified, generally in a glass matrix in a process known as vitrification. Both the liquid solutions and the vitrified solids are considered as HLW. If the spent nuclear fuel is not reprocessed, it is considered as HLW to be disposed of by appropriate methods. Because HLW contains relatively high concentrations of both highly radioactive and

extremely long-lived radionuclides, special disposal practices are needed. The relative amount of HLW is small with respect to the total volume of radioactive waste produced in nuclear power programs, but it contains 99% of the radioactivity in this volume. Furthermore, it takes about 10,000 years for the radioactivity of such wastes to decay to the level which would have been generated by the original ore from which the nuclear fuel was produced, should this ore never have been mined.

Among the options discussed for disposing of HLW, an international consensus has emerged that deep geological disposal on land is the most appropriate means for isolating such wastes permanently from man's environment (Pigford, 1982; Polvani, 1977). However, the full range of options also includes disposal in geological formations under the deep ocean floor, disposal on the ocean floor, disposal in glaciated areas, extraterrestrial disposal, and destruction by nuclear transmutation. Extended storage, whether at production sites or in a centralized store, may be considered an acceptable waste management strategy, provided it is safe, not to be perpetuated for longer than feasible, and is to be replaced by a more permanent solution at a later date.

Figure 2-17 shows the storage hall for vitrified waste at La Hague. Canisters are stored in vaults, each with a number of channels, the round tops of which are visible in the picture. Each channel can hold up to twelve canisters stacked on top of each other. The storage facilities are modular, so that they can be extended as the need arises, and very compact. The technology used permits storage of all vitrified waste from 50 years' operation of France's 59 nuclear power plants on an area the size of a rugby field.

Figure 2-17 Storage hall for vitrified waste at La Hague

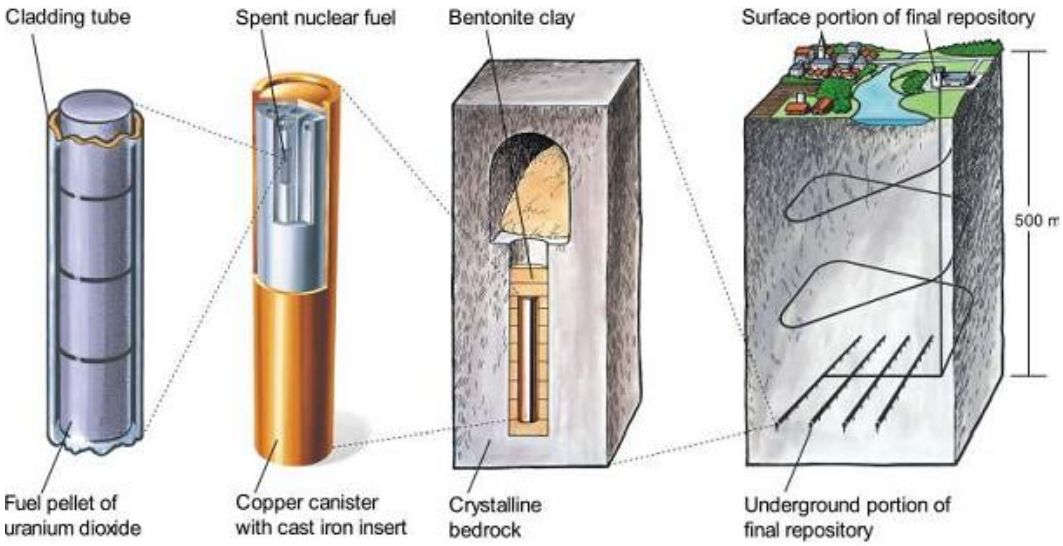

Figure 2-18 The Swedish concept for the disposal of spent nuclear fuel as an illustration of the multi-barrier concept (Bennett and Gens, 2008)

Figure 2-18 shows the multi-barrier concept for spent fuel disposal in Sweden. It has barriers at three levels. First is the waste matrix and initial waste package. In the

Swedish case, the solid fuel pellets and fuel-rod cladding provide barriers at this level. Second are engineered barriers, i.e., the copper canister with a cast iron insert, surrounded by compacted bentonite. Third is the host formation, e.g., the extensive crystalline bedrock.

It is noted that bentonite is usually used as engineering barriers in HLWD, and many researchers have studied the thermo-hydro-mechanical (THM) behavior of bentonite for HLWD application. For example, Tong et al. (2010) developed a fully coupled thermo-hydro-mechanical model for simulating multiphase flow, deformation, and heat transfer in buffer material and rock masses. Åkesson et al. (2009) conducted an experimental and numerical study on THM behavior of bentonite at high temperatures. Cui et al. (2000) proposed a thermo-mechanical model for saturated clays in unclear waste management program.

2.4 Measurement of Soil Thermal Properties

Various experimental methods had been developed to measure soil thermal properties (i.e., thermal conductivity, thermal diffusivity, and heat capacity) in the laboratory and in the field. In order to measure thermal conductivity, it is essential to set up a temperature gradient going through the soil specimen, but it may cause considerable moisture migration in unsaturated soils and affect measured results. Thus, the specific measurement method may actually change the property of soils it is attempting to measure. Although the moisture migration always occurs in the field, it will be smaller than that in the laboratory experiments.

This section will describe the measurement techniques of soil thermal properties, including the steady state methods, transient state methods, and thermo-TDR probe method. The advantages and disadvantages of each method are also presented in the following sections. The development and application of the thermo-TDR probe in the

measurement of soil thermal properties will be introduced as the main references in this research.

2.4.1 Steady State Methods

Steady state means that the temperature in soils does not change with time. Accordingly, the soil specimen is supposed to be in a steady state during the measurement of soil thermal properties in the experiments. But the attainment of such a steady state may take a long time after the initial temperature difference has been applied. There are four different types of steady state methods included and discussed in this section.

2.4.1.1 Heat Plate Method

Heat plate method is the most important steady state method for soil thermal properties measurement, and it has been standardized by ASTM C117. In Kaplar's (1971) study, two identical soil samples were placed above and below a flat-plate main heater unit which was surrounded by an outer guard heater. The guard eliminated the horizontal heat losses and caused heat from the main heater to flow vertically, up or down through the test samples. Thus, a temperature drop ΔT could be obtained across each sample with thickness of Δx. The thermal conductivity of the soil samples could then be calculated by,

$$k = \frac{Q}{A} \cdot \frac{\Delta x}{\Delta T} \tag{2.7}$$

where Q is the time rate of the heat flow; A is the test area of the samples.

The shortcomings of this method are the considerable time needed to achieve the steady state, and measurement error mainly from the unavoidable moisture migration due to the relatively high temperature difference (Hutcheon and Paxton, 1952). Moreover, the measured results may vary as much as 20% (De Vries, 1963; Jackson et al., 1978),

and it can be used only in laboratory. Another disadvantage of this method are the gravity effects which are consequential to vertical heat flow. Woodside and Cliffe (1959) found that the measured thermal conductivity was much greater with the heat flow upward than with heat flow downward. Vanpelt (1976) also obtained the similar results in his experiments.

2.4.1.2 Cylindrical Configuration Method

The cylindrical configuration method requires a line source heater with finite length, with soils placed in the surrounding annular space. The line source heater is considered as the main heater and is guarded by the upper and lower heaters. In 1949, Kersten tested soil thermal properties, using this method in a cylindrical arrangement. The heat was generated and flowed radially outward, going through the soil samples towards the cooling chamber. The temperature in the chamber was kept constant by circulating alcohol. Wolfe and Thieme (1964) used a similar setup to measure soil thermal conductivity at extreme low temperatures of around -180^{o}C. Flynn and Watson (1969) also adopted this method to test soils at very high temperatures (i.e., up to 1700^{o}C).

2.4.1.3 In Situ Sphere Method

Mochlinski (1964) developed this method in England via the National Physical Laboratory and the Electrical Research Association in application to underground power cables. The sphere may be hollow or solid, made of copper or aluminum, and can be used for in situ measurement of soil thermal conductivity. The diameter of the sphere can be 3-4 inch. It is assumed that the depth where the measurement is taken is large compared with the sphere radius. The thermal conductivity of soils can be calculated by,

$$k = \frac{Q}{4\pi r(T_1 - T_2)} \tag{2.8}$$

where r is the sphere radius; Q is the rate of heat supply to the sphere; T_2 is the temperature of the heat sink; T_1 is the temperature of the external surface of the sphere after a steady state has been attained.

2.4.1.4 Heat Meter Method

Scott (1964) presented that the thermal conductivity of soils in the field may be determined directly by using a heat meter to measure the temperatures at two points in soils and the heat flowing between these points. Van Wijk and Bruijn (1964) measured the soil thermal conductivity by applying a surface heat impulse with known intensity. A detailed description of the application and the theory of heat meters can be found in Schwerdtfeger's (1970) study. The important criterion is the ratio of the thermal conductivity of the meter to that of its surroundings. The design of it should give a value for this ratio, which is just high enough to remain above unity for the expected measuring thermal conductivity range. This may be difficult where the heat meter is required to register transient heat flows, so the sensor heat capacity should be set as low as possible, aiming for a high thermal diffusivity so that the transmission of temperature waves is not impeded.

2.4.2 Transient State Methods

Differing from the steady state method, the transient state method has been widely used recently, as it is more versatile and can be more easily performed in both the laboratory and in situ. Furthermore, this method requires much less time than the steady state methods and minimizes the moisture migration in the experiments, thereby providing more accurately measured soil thermal properties. The most representative transient state method is the probe method, including single-probe method and dual-probe method

The probe method was first suggested by Schleiermacher in 1888, and was used by Stalhane and Pyk (1931) to measure soils' thermal conductivity. In the experiments, the probe should be inserted into the soils very carefully, causing as little disturbance as possible. The probe has a line heater inside, generating thermal energy to heat the surrounding soils at a constant heating power, and a thermocouple, which is used to monitor temperature variations of the probe. Theoretically, the rate of temperature rise at the probe depends on the thermal conductivity of surrounding soils. More details will be presented in the following sections.

2.4.2.1 Probe Method

There are three types of probe methods, including single-probe method and dual-probe method. For single-probe method, there is only one probe, containing a line heater and a thermocouple embedded inside for soil thermal properties measurement. The theory of the probe method is based on the line heat source placed in a semi-infinite, homogeneous, and isotropic medium. The heat flowing from a heat source and going through a medium of thermal diffusivity α must comply with the general Fourier equation,

$$\frac{\partial T}{\partial t} = \alpha \frac{\partial^2 T}{\partial x^2} \tag{2.9}$$

For one-dimensional flow in the x direction, T is the temperature at time t. For cylindrical coordinates corresponding to the expanding radial field around the probe, the equation becomes,

$$\frac{\partial T}{\partial t} = \alpha \left(\frac{\partial^2 T}{\partial r^2} + \frac{1}{r} \frac{\partial T}{\partial r} \right) \tag{2.10}$$

where r is the radial distance from the line heat source. It can be assumed that the probe produces heat from t=0 at a constant rate q per unit length, the temperature rise ΔT in the medium can be calculated by,

$$\Delta T = \frac{q}{4\pi k}\left[-Ei\left(-\frac{r^2}{4\alpha t}\right)\right] \tag{2.11}$$

where Ei(-x) is an exponential integral; k is the thermal conductivity of the medium (Carslaw and Jaeger, 1959).

Farouki (1981) stated that the exponential integral may be approximated by a logarithm function for large values of time, so the temperature rise becomes proportional to the logarithm of time. A plot of temperature against the logarithm of time conforms to a straight line, and the thermal conductivity of soils can be calculated according to the following equation,

$$k = \frac{q}{4\pi(T_2 - T_1)}\ln\left(\frac{t_2}{t_1}\right) \tag{2.12}$$

where T_2 and T_1 correspond to the times t_2 and t_1, respectively. It should be emphasized that a real probe in a cylindrical shape of finite length is different from the idealized line heat source. The contact resistance exists between it and the medium. However, the measurement error is acceptable if the length of the probe is at least 22 times its diameter to ensure radial heat flow conditions all around the probe (Blackwell, 1956).

The dual-probe method is also based on the line heat theory. In an infinite medium, the temperature change is a function of time and radial distance away from the heat source. The mathematic expression is as follows (De Vries, 1952; Kluitenberg et al., 1993),

$$T(r,t) = \frac{Q}{4\pi\alpha}\left[Ei\left(\frac{-r^2}{4\alpha(t-t_o)}\right) - Ei\left(\frac{-r^2}{4\alpha t}\right)\right] \tag{2.13}$$

where T is the temperature change; t is time; t_o is the duration of the heat pulse; r is the radial distance; α is the soil thermal diffusivity; Ei(-x) is the exponential integral.

Abramowitz and Stegun (1972) proposed a formula to estimate the above exponential integral for $0 \le x \le 1$ and $1 \le x \le \infty$. The source strength is defined as $Q=q/\rho_c$ in which is the quantity of liberated heat and is the volumetric heat capacity. Through differentiating from Equation 2.13 with respect to time and setting the result to zero, Bristow et al. (1994a) provided the following solutions for volumetric heat capacity and thermal diffusivity,

$$\rho_c = \frac{q}{4\pi\alpha T_m}[Ei(\frac{-r^2}{4\alpha(t_m - t_0)}) - Ei(\frac{-r^2}{4\alpha t_m})] \quad (2.14)$$

$$\alpha = \frac{r^2}{4}[\frac{1}{(t_m - t_0)} - \frac{1}{t_m}] / \ln[\frac{t_m}{(t_m - t_0)}] \quad (2.15)$$

where t_m is the time when the maximum temperature occurs and T_m is the maximum temperature change.

According to the relationship among thermal conductivity, thermal diffusivity, and heat capacity, the soil thermal conductivity can be calculated by,

$$k = \frac{q}{4\pi T_m}[Ei(\frac{-\ln[t_m/(t_m - t_0)]}{t_0/t_m}) - Ei(\frac{-\ln[t_m/(t_m - t_0)]}{t_0/(t_m - t_0)})] \quad (2.16)$$

This method is also called “single point method” or “peak value method,” which does not require linear regression analysis as described for the single-probe method, because it estimates soil thermal properties using only a single point (t_m, T_m) of the recorded temperature variation.

2.4.2.2 Periodic Temperature Method

Forbes (1846) estimated the thermal diffusivity of soils in the fields by analyzing the attenuation and lag of the annual temperature wave in soils. The assumptions made in this mathematical derivation are that the annual temperature variation at the ground

surface can be represented by a sine wave, and soils do not change into other states. Hoekstra et al. (1973) measured the thermal diffusivity of a cylindrical soil sample in the laboratory by applying a sinusoidal temperature wave to its periphery. Then, the thermal diffusivity was estimated from the resulting amplitude ratio and the frequency of the wave. Farouki (1981) presented that this method is only suitable for the cases where there may be a moisture migration problem or changes in the thermal properties of soils, as it may occur in the frozen soils in the temperature range between -5 ^{o}C and 0 ^{o}C.

2.4.2.3 Thermal Shock Method

Shannon and Wells (1947) used the thermal shock method to measure the thermal diffusivity of soils by applying a sudden temperature change to the boundaries of a cylindrical soil sample and monitoring the temperature change at the center. The soil sample was inserted into a cooler water bath, and the change in temperature was monitored by a thermocouple, which had been placed in the center. The calculated thermal conductivity was shown to be in good agreement with the results obtained by the Kersten (1949) study, where the steady state method was employed for soil thermal properties measurements.

2.4.3 Thermo-TDR Probe Method

Ren et al. (1999) designed a new thermo-TDR probe for measuring soil water content, electrical conductivity, and thermal properties simultaneously. He is the first scholar who integrated the dual-probe heat pulse device with the TDR technique, aiming for soil thermal properties and moisture content measurements. Figure 2-19 indicates the schematic view of the thermo-TDR probe in his study.

Although the probe exhibits sufficiently high sensitivity and accuracy in soil thermal properties and moisture content measurements, there are still some issues that need to be solved. For example, the probe has a flat end, which causes some soil

disturbance during the insertion process, and the gaps between soils and the probe leads to inaccurate measurements. Moreover, a comprehensive evaluation of the probe requires more tests on other soil types. Additional study is needed on the effects of the heating power and heating duration on soil thermal properties because they must be selected very carefully to avoid moisture migration as much as possible during the test, since the measured results will be affected.

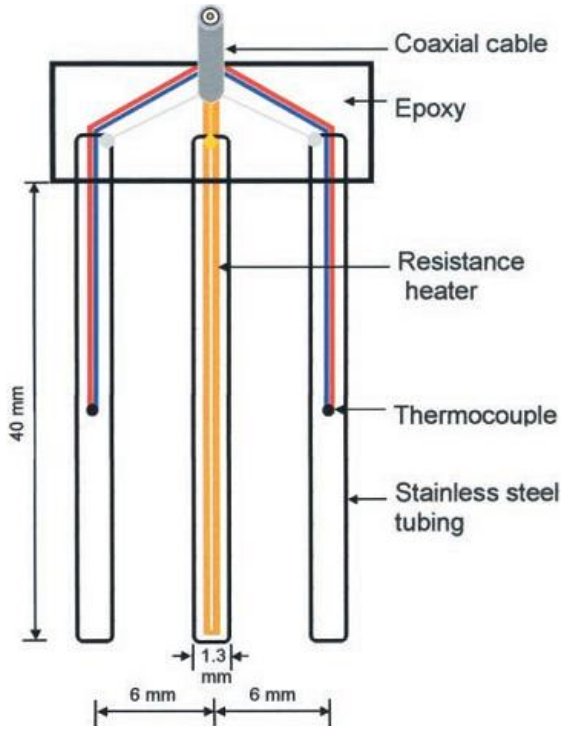

Figure 2-19 The schematic view of thermo-time domain reflectometry probe (units: mm) (Ren et al., 2003)

Ren et al. (2003) studied the developed thermo-TDR probe for vadose zone measurements. Based on the comparison between the measured results and the theoretical model predictions, he demonstrated that the probe can determine soil water content, electrical conductivity, and thermal properties, as well as other physical parameters, such as bulk density, porosity, and degree of saturation.

Liu et al. (2008) investigated the soil bulk density by using the thermo-TDR probe. He also compared the performance of the probes with four different designs and concluded that the thermo-TDR probe of 2 mm in diameter, 40 mm in probe length and 8 mm in probe-to-probe spacing showed the highest accuracy in estimating soil bulk density. Figure 2-20 shows the schematic of the probes with two different designs in his study. Figure 2-21 and 2-22 show the comparison of measured bulk density from the probe and gravimetrically measured results in laboratory and in the fields, respectively. In terms of relative error, the sensor 2 (i.e., the best design mentioned above) is generally within 5% accuracy under laboratory conditions and within 10% accuracy under field conditions. Although the measurement accuracy of soil thermal properties and moisture content was not evaluated for the above four different designs, the thermo-TDR probe is a promising and valuable tool.

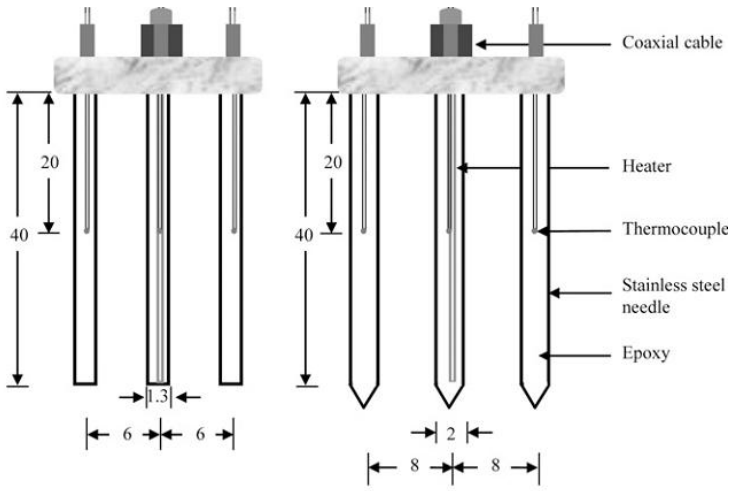

Figure 2-20 Schematic view of two different thermo-TDR probes (Liu et al., 2008)

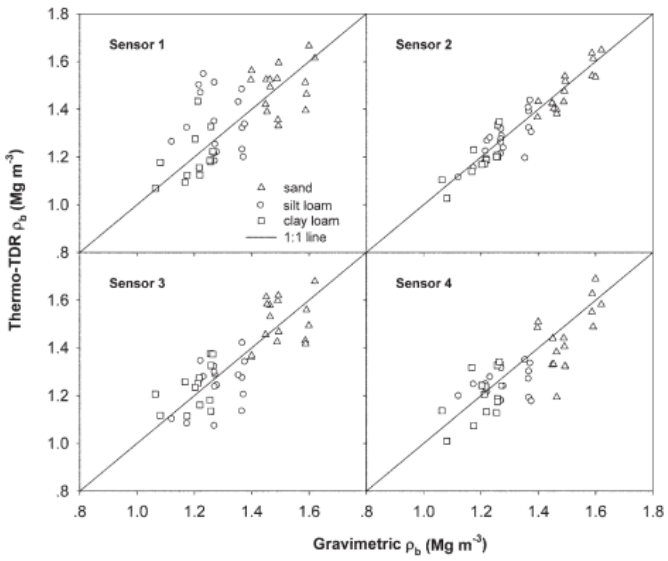

Figure 2-21 Thermo-TDR probe estimated bulk density against gravimetrically measured results in laboratory (Liu et al., 2008)

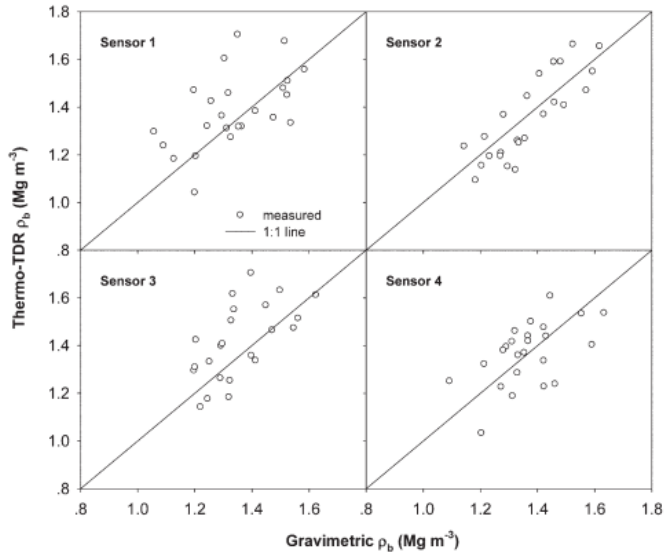

Figure 2-22 Thermo-TDR probe estimated bulk density against gravimetrically measured results in the field (Liu et al., 2008)

2.5 Measurement of Soil Matric Suction

Soil suctions can be found in all the ground that lies above the water table, and it is one of the most important parameters to use in describing the moisture stress condition of unsaturated soils. Laboratory measurements of suction can be very useful for assessing the quality of the soil samples, estimating the in situ effective stress, and realistic applications of unsaturated soil mechanics (Pan et al., 2010).

In terms of soil matric suction measurement methodology, there are two broad categories: direct measurement techniques (axis-translation technique, and tensiometer and suction probe) and indirect measurements (TDR technique, thermal conductivity sensor, and in-contact filter paper method). Squeezing technique and saturation extract method are usually used as indirect osmotic suction measurement methods. In addition, indirect total suction measurement techniques are sometime used, including psychrometer technique, relative humidity method, chilled-mirror hygrometer method, and non-contact filter paper method. Table 2-3 shows the summary of methods for measuring total and matric suction (Fredlund and Rahardjo, 1993; Ridley and Wray, 1996).

This section will describe four main measurement techniques of soil suction: filter paper technique, pressure plate device, Tempe pressure cells, and TDR probe method.

Table 2-3 The summary of methods for measuring total and matric suction (Fredlund and Rahardjo, 1993; Ridley and Wray, 1996)

Device	Method (Property Measured)	Suction Measured	Range (kPa)	Principle constraints
Thermocouple psychrometers	Indirect (Relative Humidity)	Total	100 to 7500	Affect by temperature fluctuations and gradients. Sensitivity deteriorates with time.
Thermistor psychrometers	Indirect (Relative Humidity)	Total	100 to 10000	Poor sensitivity in the low suction range. Frequent re-calibration is required.
Transistor psychrometers	Indirect (Relative Humidity)	Total	100 to 71000	Frequent re-calibration is required. Specimens must be tested in order of increasing suction to avoid hysteresis.
Filter paper (non-contact)	Indirect (Water content)	Total	400 to 30000	Calibration is sensitive to the equilibrium time.
Filter paper (in-contact)	Direct	Matric	Entire range	Automation of the procedure is difficult.
Pressure plate (Null technique)	Direct	Matric	0 to 1500	Range of suction limited by the air-entry value of the plate (Laboratory usage)
Standard tensiometer	Direct	Matric	0 to 90	Requires daily maintenance. Temperature fluctuations affect readings.
Osmotic tensiometer	Direct	Matric	0 to 1500	Reference pressure can deteriorate with time. Temperature dependent.
Imperial College tensiometer	Direct	Matric	0 to 1800	Range in suction is limited by the air-entry value of the ceramic. Cavitation problems with time.
Porous block (Gypsum, nylon, fiber glass)	Indirect (Electrical resistance)	Matric	30 to 3000	Observations need to be corrected fir temperature. Blocks are subject to hysteresis and changes in calibration due to salt. Response to suction can be slow.
Original heat dissipation sensors	Indirect (Thermal conductivity)	Matric	0 to 1000+	High failure rate. Fragile ceramic.
Fredlund Thermal Conductivity Sensor	Indirect (Thermal conductivity)	Matric	0 to 1500+	Range in suction is controlled by the pore-size distribution of the ceramic.

2.5.1 Filter Paper Technique

The filter paper technique was developed and employed to measure soil suction by soil scientist and agronomists (Al-Khafaf and Hanks, 1974; Deka et al., 1995; Fawcett and Collis-George, 1967; Gardner, 1937; Greacen et al., 1987; and Hamblin, 1981). Many scholars have also used this method in geotechnical engineering (Chandler et al., 1992; Chandler and Gutierrez, 1986; Fredlund et al., 1995; Houston et al., 1994; Leong et al., 2002; and Ridley et al., 1995). It has been proven to be a simple and economical method for soil suction measurement, and it consists of the in-contact filter paper method for matric suction measurement and non-contact method for total suction measurement. Moreover, both of the two methods have been standardized in ASTM D5298-94 (ASTM, 2010). Figure 2-23 shows the general testing configurations for filter paper testing: (a) non-contact method; (b) in-contact method (Hoyos, 1998).

The methodologies of both methods for estimating soil suction are by measuring the amount of water transferred from an unsaturated soil specimen to an initially dry filter paper. The moisture content of the filter paper at equilibrium is measured gravimetrically and related to soil suction through a predetermined calibration curve for the particular type of paper used (Hoyos, 1998; and Lu and Likos, 2004). The calibration curve for the filter paper matric suction measurement is commonly established using a pressure plate apparatus (Al-Khafaf and Hanks, 1974; Deka et al., 1995; Greacen et al., 1987; Hamblin, 1981; Leong et al., 2002).

The in-contact method filter paper method is not very accurate at high total suction ranges, whereas sensitivity of the non-contact filter paper method is decreased at low total suction levels. Ridley and Wray (1996) found that the non-contact filter paper technique is insensitive when used for measuring low total suctions due to possible vapor and temperature non-equilibrium during the measurements. Pan et al. (2010) stated that

the similar filter papers, as used in the in-contact filter paper method, can be used in the non-contact filter paper technique. But the limitation is the long equilibrium time and the need for strict protocol in the experiments.

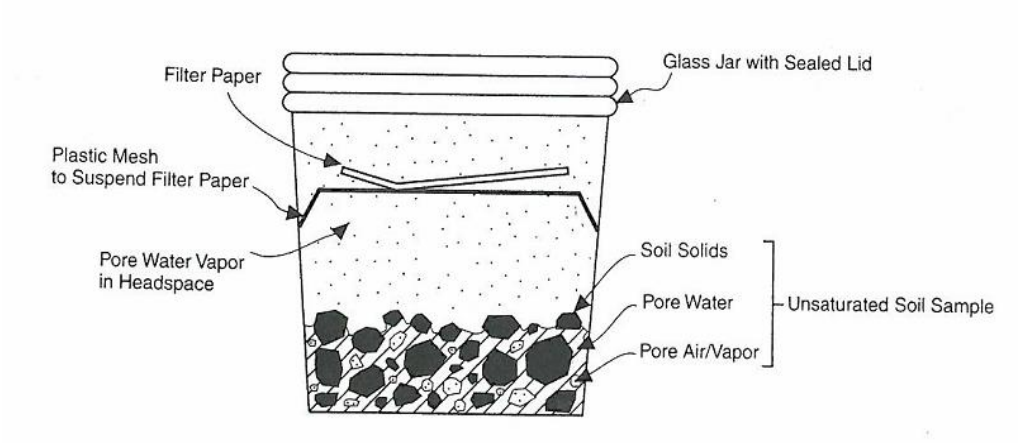

(a)

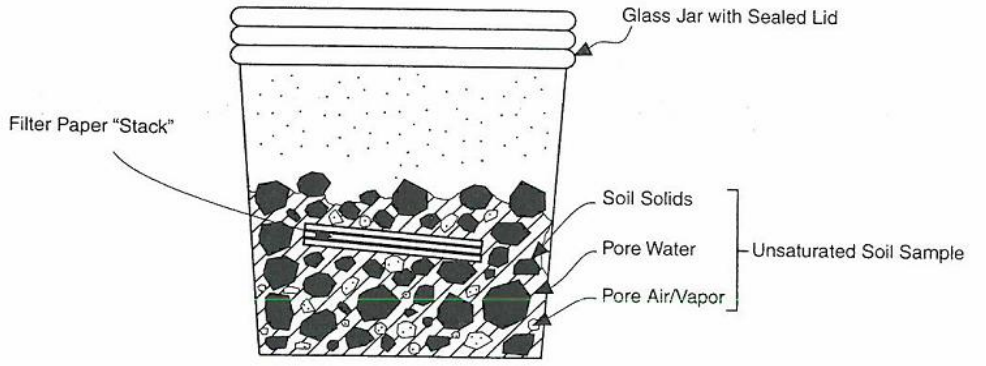

(b)

Figure 2-23 General testing configurations for filter paper testing: (a) non-contact method; (b) in-contact method (Hoyos, 1998)

2.5.2 Pressure Plate Device

The pressure plate device consists of a steel pressure vessel and a saturated high air entry value ceramic plate or cellulose membrane, and a small water reservoir

under the plate, using an internal screen and a neoprene diaphragm. The water reservoir is vented to the atmosphere through an outflow tube located on top of the ceramic plate, thereby allowing the air pressure in the chamber and the water pressure in the reservoir to be separated across the air-water interfaces bridging the saturated pores of the high air entry materials. Figure 2-24 shows the schematic of pressure plate axis translation apparatus.

The test procedures are described as follows: (1) Several identical soil samples are prepared at same conditions (i.e., same dry density and moisture content) and placed on top of the ceramic plate; (2) The samples are initially saturated by applying a partial vacuum to the air chamber and allowing the samples to imbibe water from the underlying reservoir through the ceramic plate; (3) Air pressure is applied in the chamber to the desired level and the water in the specimen is drained out through the outflow tube until the equilibrium is attained; (4) The outflow of water is monitored until it ceases, then the pressure chamber is opened, and the actual moisture content is measured by the oven-drying method. Thus, one point in the SWCC curve can be obtained; (5) Then, the air pressure is increased to the next suction level to generate additional points on the curve, using other specimens.

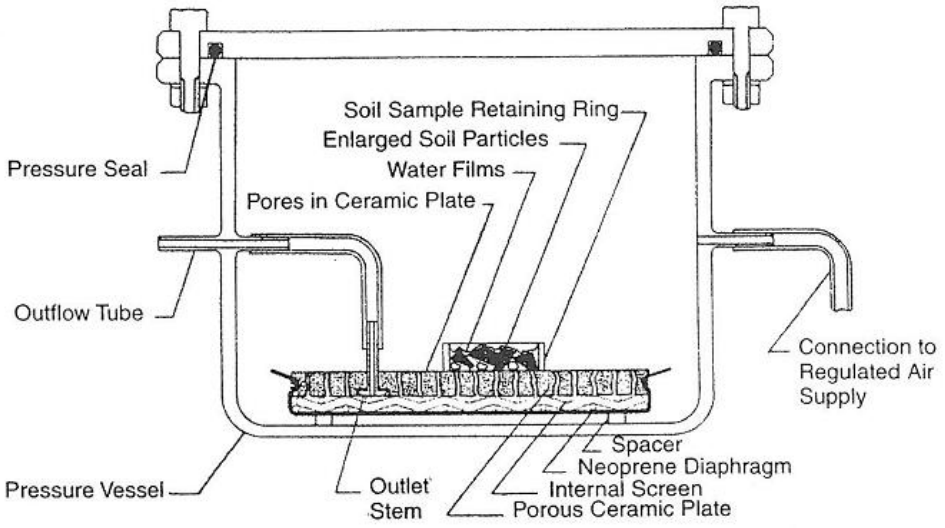

Figure 2-24 Schematic of pressure plate axis translation apparatus (Soil Moisture Equipment Corp., 2003)

2.5.3 Tempe Pressure Cell Device

Figure 2-25 shows the cross section of a Tempe pressure cell apparatus. It consists of a saturated high-air-entry-value ceramic disk separating air and water chambers in a closed vessel. Differing from the pressure plate device as mentioned above, a single soil sample is placed in the cell so that several pairs of data points comprising the SWCC may be determined by applying increasing increments in air pressure. The water content of soil samples at equilibrium is measured for each air pressure increment by weighting the entire apparatus and noting the amount of mass lost because of pore water drainage. The cell is disassembled once the highest desired level of matric suction is attained, and the final moisture content of soil samples can be determined gravimetrically. The final water content may then be considered in light of the incremental changes in mass to back-calculate water content values corresponding to the preceding levels of matric suction.

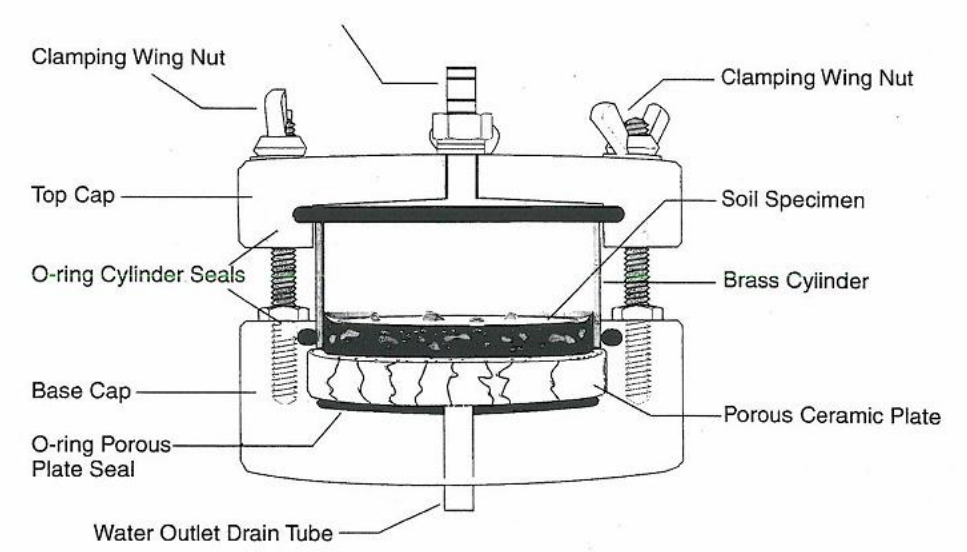

Figure 2-25 Schematic cross section of Tempe pressure cell apparatus (Soil Moisture Equipment Corp., 2003)

Figure 2-26 shows the Fredlund soil water characteristic curve device. This device is the one that can obtain continuous water or volume changes of soil specimen. The overburden pressure can also be simulated by applying a vertical load on top of the specimen. It uses the axis-translation technique, and usually has a matric suction measurement range of 0-1500 kPa. In the experiments, the soil sample sits on top of the ceramic disk and the water drained out from the soils is continuously monitored by the two-volume indicator water tubes on the pressure panel, which are connected to the chamber below the ceramic disk through the flexible plastic tubes.

Flushing can be conducted to remove the air bubbles from the entire system at least once per day. The desorption curve is obtained by testing fully saturated soil samples and applying air pressure increasingly, while the wetting curve is obtained by decreasing air pressure. Either only one specimen can be used to get all the data points

on SWCC or obtaining only one point from one specimen and repeating the test on other samples for other points.

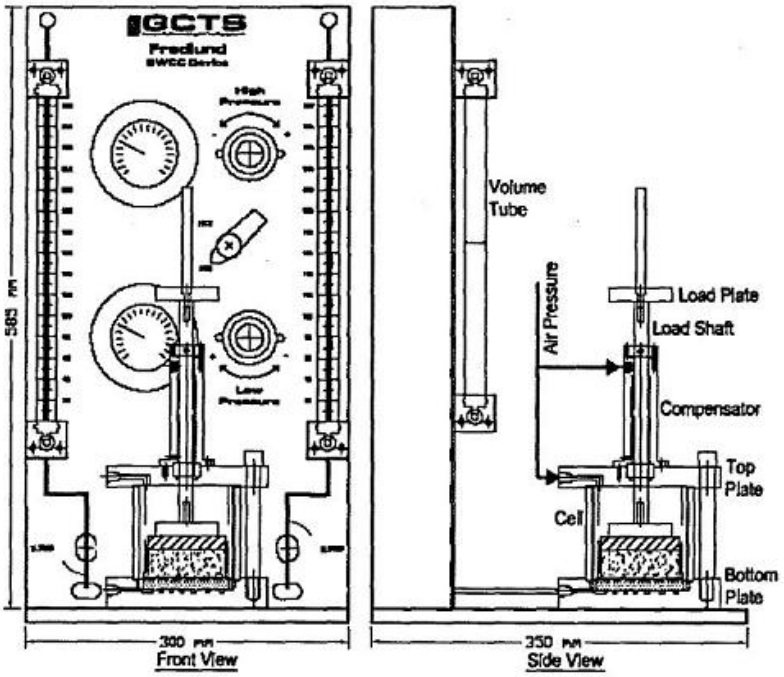

Figure 2-26 Fredlund soil water characteristic curve (Perera et al., 2005)

2.5.4 Time Domain Reflectometry Probe Method

As described in the previous sections, the TDR technique has been demonstrated successfully as a promising tool for measuring soil moisture content. Noborio et al. (1999) attached a gypsum block at the end of the two steel rods (i.e., transmission lines) to measure the soil matric suction. The schematic of the TDR probe is shown in Figure 2-27. Since the gypsum block has a certain pore size distribution, the soil matric suction was measured indirectly by linking the suction of gypsum block to the suction of soils. In addition, the suction of the gypsum block is related to the moisture content, which determines its dielectric constant (K_a). Since the K_a of the gypsum block can be calculated from the TDR waveforms, the soil suction is finally estimated from the

calibration between K_a and suction of gypsum. The probe calibration was conducted by the pressure plate test, and the typical TDR waveforms, under different suction levels, are shown in Figure 2-28.

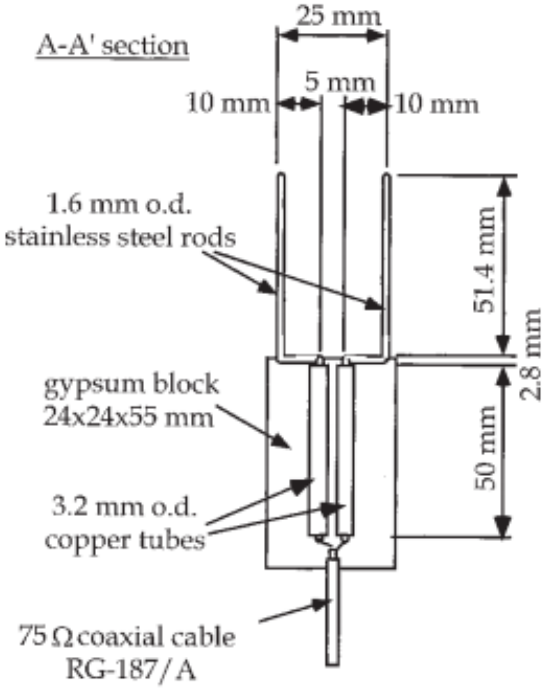

Figure 2-27 Schematic of TDR probe (Noborio et al., 1999)

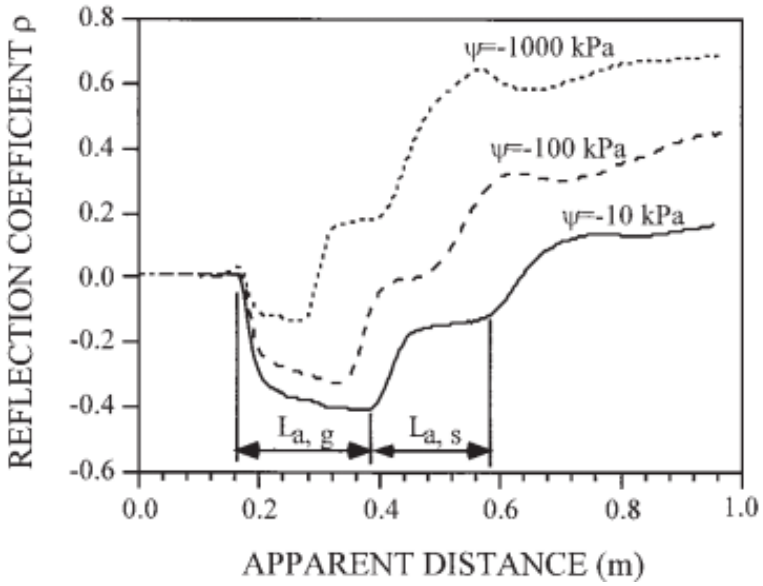

Figure 2-28 Typical reflected TDR waveforms of the TDR probe (Noborio et al., 1999)

2.6 Soil Thermal Conductivity Prediction Models

Although many researchers did a lot of experimental studies on soil thermal properties in the laboratory and in the field, an accurate prediction of soil thermal conductivity is still very important in many engineering applications. In accordance with the previous experimental studies, moisture content, dry density, and soil mineral components are considered as the three main influencing factors of soil thermal conductivity. They were also selected as the variables in the existing soil thermal conductivity models.

Dong et al. (2015) presented a critical review of thermal conductivity models for unsaturated soils. Generally, soil thermal conductivity models can be divided into three categories: (1) empirical models, (2) theoretical models, (3) other models. This section will present the origin and the development of some classical soil thermal conductivity models which have been widely used in soil science, agronomy, and geotechnical

engineering. The applicability, advantages, and disadvantages of each model will also be discussed in the following subsections.

2.6.1 Empirical Models

2.6.1.1 Kersten (1949) Model

Kersten (1949) measured thermal properties of 19 different soils by using a line heat source in the laboratory. The test soils included five sands or gravel; six materials of heavier texture, varying from sandy loam to clay; seven minerals or crushed rocks; and one organic soil. The effects of temperature, dry density, moisture content, degree of saturation, and soil texture on thermal conductivity were analyzed, then the empirical thermal conductivity models were proposed as follows,

For silts and clay,

$$k = 0.1442 \times [0.9 \log w - 0.2] \times 10^{0.6243\gamma_d} \tag{2.17}$$

For sands and sandy soils,

$$k = 0.1442 \times [0.7 \log w + 0.4] \times 10^{0.6243\gamma_d} \tag{2.18}$$

where k is the thermal conductivity of soils, W $m^{-1}K^{-1}$; w is the moisture content, %; γ_d is the dry density, lb/ft^3.

Because all the soil samples were not tested at saturated condition, the model was proposed by extrapolating the experimental data to high degree of saturation. Thus, the model prediction of soil thermal conductivity might not be accurate at high degree of saturation.

2.6.1.2 Johansen (1977) Model

Johansen (1977) first proposed the concept of normalized thermal conductivity (k_r). He stated that the relationship between k_r and degree of saturation (S_r) can reflect the effects of soil types, porosity, moisture content, and soil mineralogy on soil thermal conductivity in a unique way. The k_r can be expressed by,

$$k_r = \frac{k - k_{dry}}{k_{sat} - k_{dry}} \tag{2.19}$$

where k_r is the normalized thermal conductivity, k_{sat} and k_{dry} are the soil thermal conductivities at fully saturated and dry conditions, respectively. It is found that k_r=0 when soil is at dry condition since k=k_{dry}; and k_r=1 when soil is at fully saturated condition since k=k_{sat}; Figure 2-29 shows the thermal conductivity of unfrozen granular pavement materials for usual form and normalized form (Cote and Konrad, 2005).

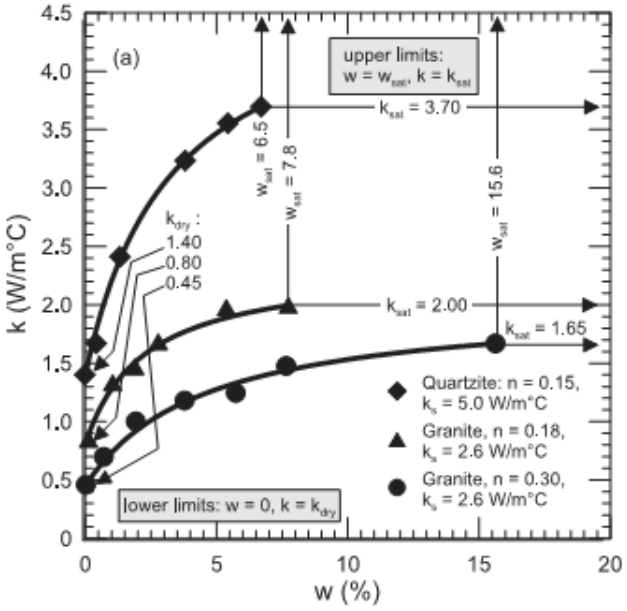

(a)

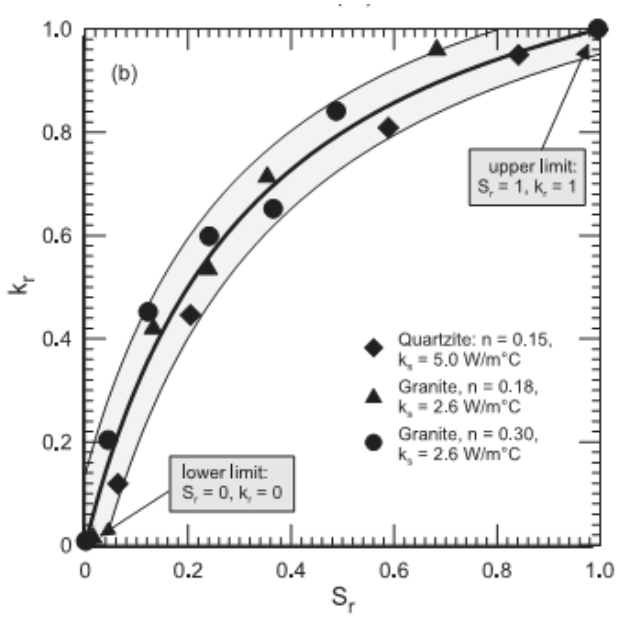

(b)

Figure 2-29 The thermal conductivity of unfrozen granular pavement materials, (a) usual form, (b) normalized form (Côté and Konrad, 2005)

The thermal conductivity of soils at saturated condition can be calculated by Sass et al. (1971) equation,

$$k_{sat} = k_{water}^{n} k_{solid}^{1-n} \tag{2.20}$$

where k_{water} and k_{solid} are thermal conductivity of water and solid, respectively, W $m^{-1}K^{-1}$; n is the porosity.

Johansen (1977) modified De Vries (1963) model and proposed a calculation model for thermal conductivity of dry soils,

$$k_{dry} = \frac{0.137\rho_d + 64.7}{2650 - 0.947\rho_d} \tag{2.21}$$

where ρ_d is the dry density of soils, kg/m^3.

By fitting the experimental data provided by Kersten (1949), Johansen (1977) also presented several different k_r-S_r relationships for different soil types:

For medium and fine sands,

$$k_r = 0.7\log(S_r) + 1 \tag{2.22}$$

For fine grained soils,

$$k_r = \log(S_r) + 1 \tag{2.23}$$

For frozen medium, fine sands and fine grained soils,

$$k_r = S_r \tag{2.24}$$

According to the Equation 2.19, 2.20 and 2.21, the soil thermal conductivity model proposed by Johansen (1977) is expressed as follows,

$$k = \left(k_{water}^{n} k_{solid}^{1-n} - \frac{0.137\rho_d + 64.7}{2650 - 0.947\rho_d} \right) k_r + \frac{0.137\rho_d + 64.7}{2650 - 0.947\rho_d} \tag{2.25}$$

Johansen (1977) adopted the geometric mean method to calculate soil thermal conductivity, and compared the results with experimental data from Kersten's (1949) study. He found that the thermal conductivity of solids predicted by his model was around 5 W $m^{-1}K^{-1}$ for sandy soils, and 3 W $m^{-1}K^{-1}$ for silts and silty soils. Hence, his model may underestimate the thermal conductivity of some sandy soils containing relatively high quartz content, and overestimate clayey soils or clay. Moreover, his model does not consider the effect of quartz content on soil thermal conductivity, which cannot be ignored in some cases. However, the calculation model for thermal conductivity of dry soils, which was obtained from the modified De Vries (1963) model and experimental data from Kersten (1949) study, shows high prediction accuracy. More importantly, the normalized thermal conductivity concept he proposed has initiated an innovative idea to establish a soil thermal conductivity model and has been widely used by many other researchers (Lu et al., 2007; Zhang et al., 2015a).

2.6.1.3 Cote and Konrad (2005) Model

Côté and Konrad (2005) established a new k_r-S_r relationship, incorporating κ as a variable to consider the effect of soil type on k_r-S_r relationship. The k_r-S_r relationship they proposed is given below,

$$k_r = \frac{\kappa S_r}{1+(\kappa-1)S_r} \tag{2.26}$$

where κ is the coefficient accounting for soil type effect on k_r-S_r relationship and they suggested that values for gravel, coarse sands; medium and fine sands; silts, clayed soil and clay, are 4.5, 3.55 and 1.9, respectively.

On the other hand, they also analyzed the relationship between thermal conductivity of dry soils and porosity based on a large dataset of previous thermal

conductivity measurements in the literature, and presented a new equation to calculate the thermal conductivity of dry soils,

$$k_{dry} = \chi 10^{-\eta n} \tag{2.27}$$

where χ and η are material parameters accounting for the particle shape effect; and n is the porosity of soils. The values of χ and η are 1.7 W $m^{-1}K^{-1}$ and 1.8 for crushed rocks, 0.75 W $m^{-1}K^{-1}$ and 1.2 for natural mineral soils, and 0.3 W $m^{-1}K^{-1}$ and 0.87 for organic fibrous soils or peat. The influence of soil type on thermal conductivity of dry soils is illustrated in Figure 2-30.

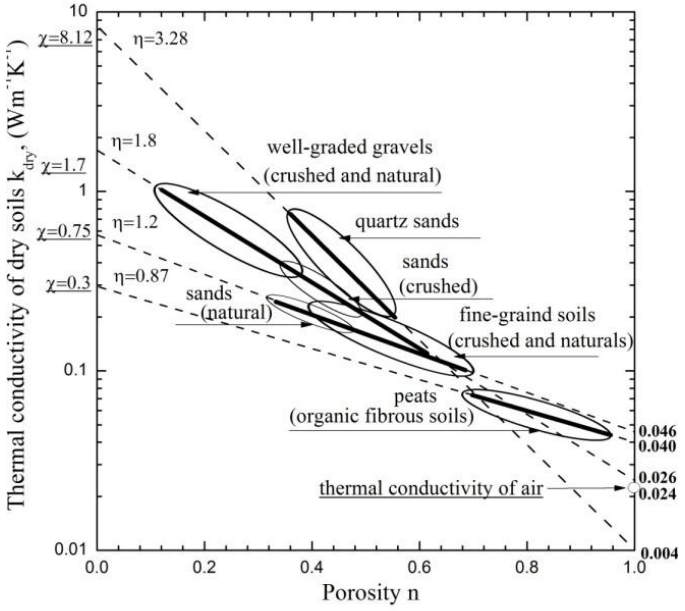

Figure 2-30 Influence of soil type on k_{dry} (Côté and Konrad, 2005)

The soil thermal conductivity model Côté and Konrad (2005) proposed considers the effects of soil type, porosity, degree of saturation, soil mineralogy, soil particle size and shape simultaneously, and the mathematical expression is as follows,

$$k = \left(k_{water}^{n} k_{solid}^{1-n} - \chi 10^{-\eta n}\right)\left[\frac{\kappa S_r}{1+(\kappa-1)S_r}\right] + \chi 10^{-\eta n} \tag{2.28}$$

On the basis of the normalized thermal conductivity concept and a large dataset of previous thermal conductivity measurements, Côté's and Konrad's (2005) model exhibited a reasonably high prediction accuracy for different soil types. But it still needs to be improved to study the limit value of κ between any two neighboring soil types for providing continuous thermal conductivity prediction over the entire soil type range.

2.6.1.4 Balland and Arp (2005) Model

Balland and Arp (2005) considered the effect of organic material on soil thermal conductivity and proposed a thermal conductivity model for solid material,

$$k_s = k_{om}^{V_{om,s}} k_{quartz}^{V_{quartz,s}} k_{\min}^{1-V_{om,s}-V_{quartz,s}} \tag{2.29}$$

where k_{om}, k_{quartz} and k_{min} are thermal conductivities of organic matter, quartz and other soil minerals, respectively. $V_{om,s}$ and $V_{quartz,s}$ are the volume fraction of organic matter and quartz in solids.

The thermal conductivity of dry soils can be calculated by,

$$k_{dry} = \frac{(ak_s - k_a)\times\rho_d + k_a G_s}{G_s - (1-a)\times\rho_d} \tag{2.30}$$

where k_a is the thermal conductivity of air, W $m^{-1}K^{-1}$. The suggested value of a is 0.053. It should be noted that Equation 2.30 is the same as Equation 2.21 when k_s=3.0 W $m^{-1}K^{-1}$ and k_a=0.024 W $m^{-1}K^{-1}$.

The k_r-S_r relationship he proposed is,

$$k_r = S_r^{0.5\times(1+V_{om,s}-\alpha V_{sand,s}-V_{cf,s})} \times \left[\left(\frac{1}{1+\exp(-\beta S_r)}\right)^3 - \left(\frac{1-S_r}{2}\right)^3\right]^{1-V_{om,s}} \tag{2.31}$$

where α and β are coordinate coefficients, $V_{sand,s}$ and $V_{cf,s}$ are volume fractions of sands and coarse grains in solids. The thermal conductivity model can be derived from Equation 2.29, 2.30 and 2.31 based on the normalized thermal conductivity concept.

It is noted that this model originated from the normalized thermal conductivity concept, but the calculation model for thermal conductivity of dry soils was modified to account for the organic matter effect. The new k_r-S_r relationship can be used both at low moisture content and extreme high degree of saturation. It provides a continuous thermal conductivity prediction curve over the entire range of soil moisture content and particle size. However, the quantitative estimation for the contents of quartz and other soil minerals in the calculation of thermal conductivity of solids will have an effect on the predicted soil thermal conductivity.

2.6.1.5 Lu et al. (2007) Model

Lu et al. (2007) used a thermo-TDR probe to measure the thermal conductivity of twelve different soils at different moisture content conditions. He stated that the k_r-S_r relationship is dependent on the soil type, particularly for fine grained soils. In addition, he obtained a more simplified linear relationship between thermal conductivity of dry soils and porosity through the curve fitting in experimental data. In accordance to the normalized thermal conductivity concept, he also proposed an empirical soil thermal conductivity model,

$$k = \left[k_{water}^{n} k_{solid}^{1-n} - (b - an) \right] \times \exp\left[\alpha (1 - S_r^{\alpha - 1.33}) \right] + (b - an) \tag{2.32}$$

where a and b are the parameters that determine thermal conductivity of dry soils, the suggested values are 0.56 and 0.51, respectively. α accounts for the soil type effect on k_r-S_r relationship, and the suggested values for coarse soils and fine grained soils are 0.96 and 0.27, respectively.

The laboratory experiments in the Lu et al. (2007) study covered many different types of soils, ranging from sand and sandy soils to clay and clayed soils. The thermo-TDR probe is a more reliable and accurate measuring technique for thermal conductivity measurements (Ren et al., 1999; and Zhang et al., 2015a), but the quartz content in the test soil samples was assumed to be the same as the sand content in the calculation of thermal conductivity of solids and soils at saturated condition, which resulted in overestimating the soil thermal conductivity. Furthermore, the soil type effect on thermal conductivity of dry soils was not taken into account in the model prediction, which also affected the prediction accuracy of soil thermal conductivity.

2.6.1.6 Chen (2008) Model

Chen (2008) used the thermal probe method to the test thermal conductivity of four quartz sands with different particle size distributions. It was found that the thermal conductivity of sands was linearly distributed with porosity in semilogrithmic scale, and it was only affected by the degree of saturation. Consequently, Chen selected the power exponential function to establish a thermal conductivity model for sands,

$$k = k_{water}^{n} k_{solid}^{1-n} \left[(1-b)S_r + b\right]^{cn} \tag{2.33}$$

where b and c are empirical coefficients, and the suggest values for them are 0.0022 and 0.78, respectively.

The Chen (2008) model exhibited very high accuracy when predicting thermal conductivity of sands with high quartz content, since the model was obtained through the curve fitting to experimental data of quartz sands. Another advantage was that the model was expressed in a simple form, and it had fewer model parameters than most of other models. However, the shortcoming was that his model may not be applicable to other soil types.

2.6.2 Theoretical Models

2.6.2.1 Wiener (1912) Model

Wiener (1912) presented that the thermal conductivity of porous media had two bounds: the upper bound and the lower bound, depending upon the arrangement of the three phases in media and the heat flow direction. The effective thermal conductivities of porous media arranged in serial and in parallel connections are expressed respectively as,

$$k = k_W^L = \left[\sum \frac{\phi_\alpha}{k_\alpha} \right]^{-1} \qquad \text{(serial)} \qquad (2.34a)$$

$$k = k_W^U = \sum \phi_\alpha k_\alpha \qquad \text{(parallel)} \qquad (2.34b)$$

where k_W^L and k_W^U are the lower bound and the upper bound of thermal conductivity of porous media, respectively. Φ_a is the volume fraction of each phase in media and k_a is the thermal conductivity of this phrase, W $m^{-1}K^{-1}$. Figure 2-31 shows the Wiener bounds of thermal conductivity of porous media under multiphase conditions. Series and parallel connection models correspond to the lower and upper Wiener bounds.

From the aspect of a theoretical soil thermal conductivity model, the Wiener (1912) model is the most classic one that has been obtained under idealized conditions for porous media. It forms the foundation of the heat conduction process in porous media, and has been widely used or modified, for many years, by numerous researchers to develop soil thermal conductivity models.

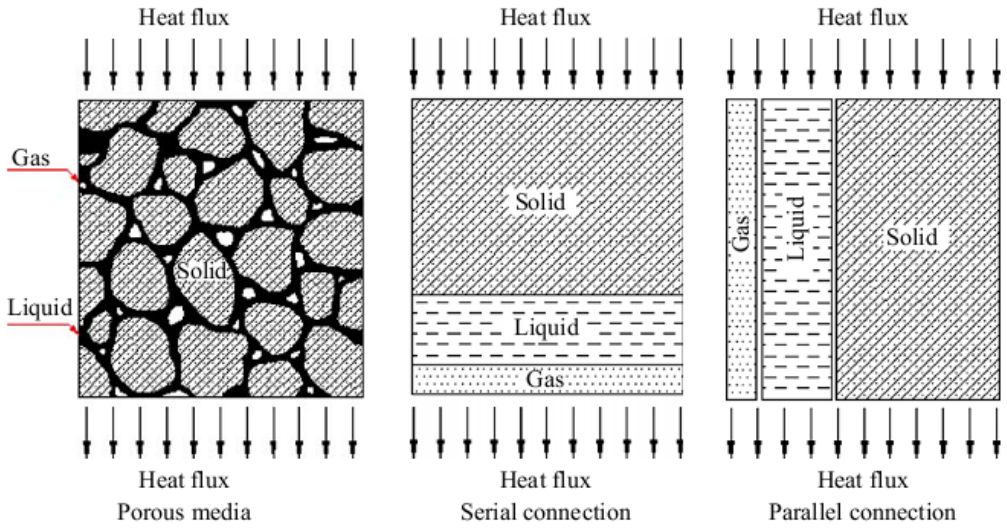

Figure 2-31 Wiener bounds of thermal conductivity of porous media under multiphase conditions (Tong et al., 2009)

2.6.2.2 De Vries (1963) Model

Based on Maxwell's equation, which is mostly used in the fields of classical electrodynamics, classical optics, and electric circuits, De Vries (1963) assumed that soil particles are distributed uniformly in continuous pore fluid in soils, and proposed a theoretical soil thermal conductivity model,

$$k = \frac{\sum_{i=0}^{N} K_i x_i k_i}{\sum_{i=0}^{N} K_i x_i} \tag{2.35}$$

where k_i is the thermal conductivity of each phase, W $m^{-1}K^{-1}$. x_i is the volume fraction of each phase, K_i is the ratio of the average temperature gradient in the granules and the corresponding quantity in the medium,

$$K_i = \frac{\left(\overline{dT/dz}\right)_1}{\left(\overline{dT/dz}\right)_0} \tag{2.36}$$

Considering the several possible influence factors of K_i (e.g., the ratio of thermal conductivity of one phase to that of continuous pore fluid in soils, particle size, shape, and relative position), De Vries (1963) presented an equation to calculate K_i,

$$K_i = \frac{1}{3}\sum_{a,b,c}\left[1+\left(\frac{k_i}{k_0}-1\right)g_a\right]^{-1} \tag{2.37}$$

where g_a , g_b and g_c are the coefficients accounting for particle shape. The suggested value for round particles is 1/3.

Due to the randomness of soil particle shape in practice, it is difficult to determine values of g_a , g_b and g_c in the model. In addition, the field capacity of soils, which is used to distinguish whether water or air is considered as continuous pore fluid in soils, is affected by many factors, such as soil particle size, gradation, soil mineralogy, etc. It should be emphasized that the model always provides lower thermal conductivity values for dry soils.Thus, a correction coefficient of 1.0-1.25 is introduced in the model prediction, especially for dry soils.

2.6.2.3 Gori (1983) Model

Gori (1983) proposed a thermal conductivity model of soil unit. He grouped soil moisture into four different ranges: $0<w<W_c$, $W_c<w<W_p$, $W_p<w<W_F$, and $w>W_F$. W_c, W_p and W_F are absorbed moisture content, wilting point and field capacity of soils, respectively. The schematic of Gori (1983) model in above four moisture ranges is shown in Figure 2-32.

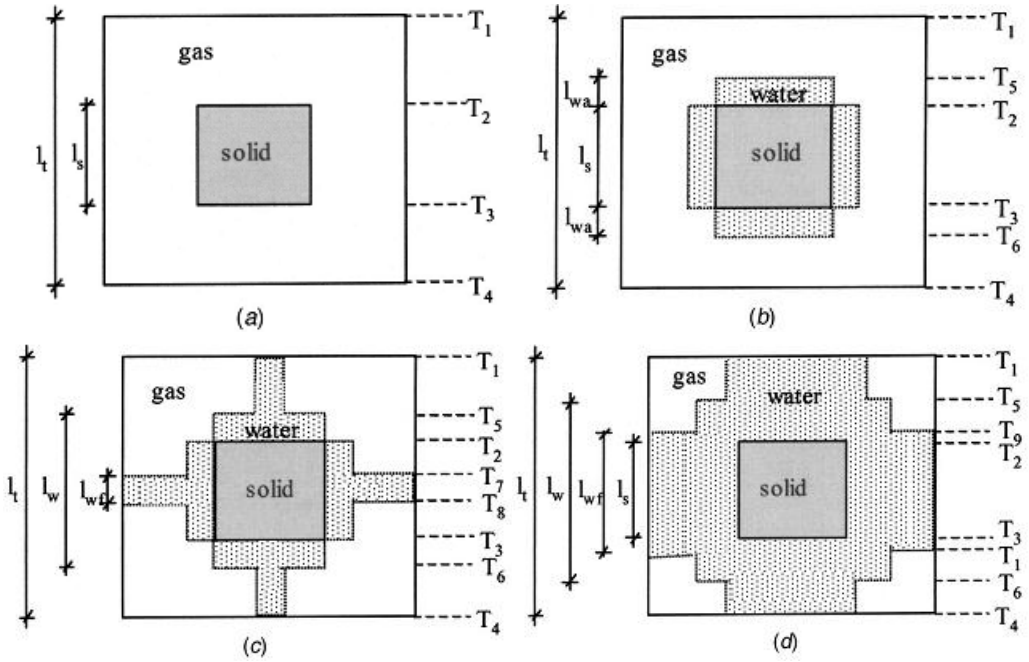

Figure 2-32 Schematic of 2D soil thermal conductivity model in different water content ranges (Gori and Corasaniti, 2002)

This model can effectively reproduce the soil thermal behavior, with the assumption that the water bridge is being formed at moisture content equal to the wilting point. In addition, the model prediction of thermal conductivity is not continuous with moisture content or degree of saturation, which is not consistent with experimental results in other studies. This is mainly because the change in geometry of soil pore fluid is not continuous among different moisture content ranges during the calculation of moisture content or degree of saturation. Compared with other models, the mathematical expression of the model is complicated and difficult to use for future applications. Moreover, the uncertainty of wilting point of soil is another disadvantage of this model.

2.6.2.4 Tong et al. (2009) Model

Tong et al. (2009) proposed a thermal conductivity model on the basis of Wiener's (1912) theory for porous media. The model accounts for the effects of moisture

content, porosity, degree of saturation, temperature, and pressure on soil thermal conductivity. The mathematical expression is given below,

$$k = \eta_1(1-\phi)k_s + (1-\eta_2)\left[1-\eta_1(1-\phi)\right]^2 \times \left[\frac{(1-\phi)(1-\eta_1)}{k_s} + \frac{\phi S_r}{k_w} + \frac{\phi(1-S_r)}{k_g}\right]^{-1} + \eta_2\left[(1-\phi)(1-\eta_1)k_s + \phi S_r k_w + \phi(1-S_r)k_g\right] \quad (2.38)$$

where k_s, k_w and k_g are thermal conductivities of solid, liquid and gas in porous media, respectively, W $m^{-1}K^{-1}$. Φ is the porosity, η_1 is the coefficient which is related to the pore structure of solid-liquid mixture, $0<\eta_1(\Phi)<1$. η_2 is a function of pore structure, degree of saturation and temperature, $0< \eta_2 (\Phi,S,T)<1$.

The Tong et al. (2009) model incorporated almost all the influence factors of soil thermal conductivity, but the coefficients η_1 and η_2 are not unique which might be affected by soil types. In the Tong et al. (2009) study, laboratory experiments on MX-80 bentonite were used to determine η_1 and η_2. The applicability of this model is to other soil types still needs to be verified.

2.6.2.5 Haigh (2012) Model

Haigh (2012) presented a simple soil unit element model and derived a soil thermal conductivity model theoretically. The model clearly describes the heat conduction behavior among soil's three phases in the unit, while retaining a physical origin. The model expression is shown below,

$$\frac{k}{k_s} = 2(1+\xi)^2\left\{\begin{array}{l}\dfrac{\alpha_w}{(1-\alpha_w)^2}\ln\left[\dfrac{(1+\xi)+(\alpha_w-1)x}{\xi+\alpha_w}\right] \\ +\dfrac{\alpha_a}{(1-\alpha_a)^2}\ln\left[\dfrac{(1+\xi)}{(1+\xi)+(\alpha_a-1)x}\right]\end{array}\right\} + \frac{2(1+\xi)}{(1-\alpha_w)(1-\alpha_a)}\left[(\alpha_w-\alpha_a)x-(1-\alpha_a)\alpha_w\right] \quad (2.39)$$

where $\alpha_w=k_w/k_s$, $\alpha_a=k_a/k_s$; ξ and x are the parameters which are related to thickness of water films, and degree of saturation. β (shown in Figure 2.33) is related to the width of water films.

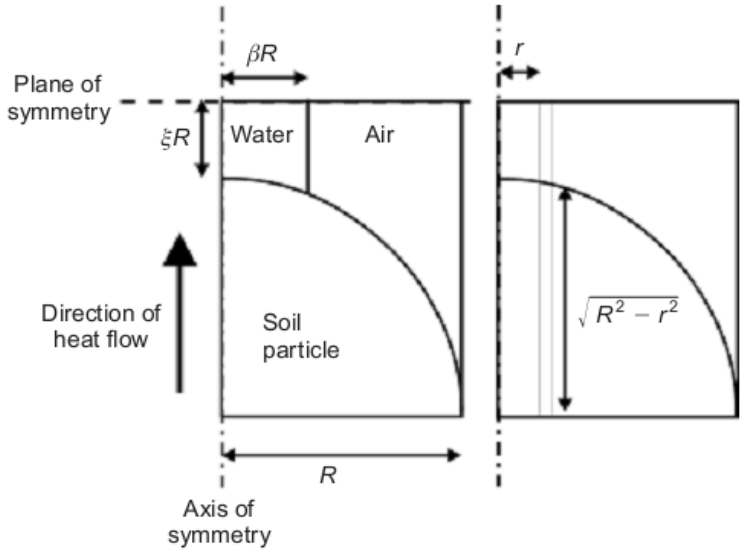

Figure 2-33 Geometry of axisymmetric contact model (Haigh, 2012)

The Haigh (2012) model was validated by comparing predicted results with experimental data of sands provided by Chen (2008). Because the model does not account for the effect of neighboring particles on the effective thermal conductivity in the unit, a correction factor of 1.58 was introduced through the comparison mentioned above. It should be noted that this correction factor is only suitable for sands and might be inaccurate for other soils. Moreover, the model cannot be applied to soils when porosity is less than 0.33 because of the limitation of the geometry of soil unit itself.

2.6.3 Other Models

2.6.3.1 Donazzi (1979) Model

As is known, thermal resistivity is the reciprocal of thermal conductivity. Donazzi et al. (1979) proposed a soil thermal conductivity model from the thermal resistivity measurements of soils in laboratory. The model expression is as follows,

$$k = k_{water}^{n} k_{solid}^{1-n} \exp\left[-3.08n(1-S_r)^2\right] \tag{2.40}$$

The model does not have other coefficients except for porosity and degree of saturation;

Therefore, it might not be applied over the entire range of soil type.

2.6.3.2 Gangadhara Rao and Singh (1999) Model

Gangadhara Rao and Singh (1999) adopted a thermal probe method to measure thermal resistivity of four soils in the laboratory and presented an empirical relationship among thermal resistivity and moisture content and dry density. The thermal conductivity can be calculated by,

$$k = 10^{0.01\gamma_d - 1}(1.07 \log w + b) \tag{2.41}$$

where γ_d is the dry density, lb/ft^3; b is dependent on soil type as presented in Table 2-4.

Table 2-4 b value in Equation 2.41 (Gangadhara Rao and Singh, 1999)

Soil type	b
Black cotton soil	-0.73
Silts	-0.54
Silty sand	0.12
Fine sand	0.70
Coarse sand	0.73

The model development was based on the curve fitting to thermal resistivity measurements of four different soils at different moisture contents and dry density conditions. The prediction accuracy was much higher when the degree of saturation was less than 0.3; it decreased incrementally with the increase of the degree of saturation. This is probably because all the degrees of saturation of test soils were less than 0.5 in the experiments.

2.7 Summary

This chapter presents the relevant research background of this study, including the time domain reflectometry (TDR) technique; soil thermal properties, their influence factors, and applications; the measurement techniques of soil thermal properties; the

measurement methods of soil suction; and the development of soil thermal conductivity models.

Chapter 3

Design and Evaluation of a Thermo-TDR Probe

3.1 Introduction

The study of soil thermal properties has drawn more attention recently because of the rapid development of the field of geothermal energy. Soil thermal properties have many engineering applications such as borehole thermal energy storage (BTES), geothermal energy piles (GSP), the ground source heat pump (GSHP) system, and high level radioactive nuclear waste disposal (HLWD). All of these applications involve the heat transfer process governed by soil thermal properties. Therefore, it is important to study the soil thermal properties, including thermal conductivity, diffusivity, and heat capacity, as well as their influence factors such as moisture content and dry density. It is advantageous, for the above applications, to be able to measure soil thermal properties, moisture, content and dry density simultaneously.

The transient state method is the most commonly used method today to measure soil thermal properties, and like the dual-heat probe methods is based on the development of the heat pulse theory (Jaeger, 1965; Larson, 1988; Lubimova et al., 1961). The dual probe heat pulse (DPHP) device has been widely used by many researchers (Bristow et al., 1994a; Bristow et al., 1994b; Campbell et al., 1991; Kluitenberg et al., 1995; Kluitenberg et al., 1993) to measure thermal conductivity, diffusivity, and heat capacity. The TDR technique has been demonstrated to be a rapid and reliable method for monitoring and measuring soil moisture content, both in the lab and in-situ (Baker and Allmaras, 1990; Benson and Bosscher, 1999; Dalton et al., 1984; Noborio, 2001; Topp et al., 1988; Yu and Drnevich, 2004). The thermo-TDR probe was first designed by the integration of a dual heat pulse probe with a TDR moisture probe (Ren et al., 1999). Liu et al. (2008) studied the effect of probe configurations such as

probe length, diameter and probe-to-probe spacing on the accuracy of measured soil bulk density and thermal properties. However, there are still some disadvantages of previous probes that affect the measured results. For example, the diameter of Ren's (1999) probe was only 1.3 mm, which may cause probe deflection during the insertion process. Another problem is that the flat end of this probe may cause much disturbance and affect the measured results. The probe length and probe-to-probe spacing need to be designed very carefully for an accurate measurement of soil thermal properties and the precise predictions of moisture content and dry density by the TDR moisture sensor. There is a lack of comprehensive analyses and evaluations of the use of thermo-TDR probes for geothermal applications, which require measurements of gravimetric water content and dry density.

This chapter presents the design and fabrication of a new thermo-TDR probe for simultaneous measurements of soil thermal properties, moisture content, and dry density. This probe has point tips which can minimize the insertion disturbance. The sensor calibration for dielectric constant (K_a) was completed by testing five different chemicals with known K_a values. NaCl and KCl solutions with different concentrations were used for the calibration of electrical conductivity (EC_b). Laboratory tests on three sands and kaolin clay were performed for the comprehensive evaluation of the thermo-TDR probe. The accuracy of the thermal properties measurement was evaluated by comparing the test results from the thermo-TDR probe with those obtained from the standard KD2 probes (Decagon Device, 2011). Based on the K_a and EC_b obtained from the TDR waveforms analyses, the predicted soil moisture content and dry density by Topp's equation, the heat capacity method, and the "One-Step Method" were compared with actual moisture content from the oven drying method and calculated dry density.

3.2 Design and Fabrication of Thermo-TDR Probe

3.2.1 Design of Thermo-TDR Probe

There are several different types of TDR probes reported in previous literatures, including unbalanced coaxial cells (Topp et al., 1980; Zegelin et al., 1989), balanced two-rod probes with a balun (Baker and Lascano, 1989; Topp et al., 1982) and without a balun (Malicki and Skierucha, 1989), and symmetric multi-rod probes (Heimovaara, 1993). The TDR probe usually works based on the transmission line theory, but there is little information regarding its specific design criteria. The dual probe heat pulse device is based on the theory of radial heat conduction of short heat pulse away from an infinite line heat source. The thermo-TDR probe is a integration of the TDR probe with the dual probe heat pulse device that can measure soil thermal properties, moisture content, and dry density simultaneously. Several different kinds of thermo-TDR probes, such as single probe, dual probe, and multiple probes, can be found in previous studies (Bilskie et al., 1998; Bristow et al., 1993; Mortensen et al., 2006; Ren et al., 1999).

The errors in measurement and calculation of soil thermal properties, moisture content, and dry density might be attributed to the inappropriate design in dimensions or assumptions of the infinite line source heater. For instance, assuming the probe has an infinite length leads to less than 2% of errors in the evaluation of soil thermal properties since the probe should have a finite length (Campbell et al., 1991; Bristow et al., 1994a). When considering the cylindrically-shaped heater as a line heat source, it may cause errors of less than 0.6% in the calculated soil thermal properties (Kluitenberg et al., 1993, 1995). Moreover, the axial heat flow error may become significant if the length and the diameter of the probe are not properly designed. Blackwell (1956) suggested that the ratio of probe length to diameter should be greater than 25 in order to limit the axial heat flow error to within 1%. A typical dual probe heat pulse device developed by Bristow et al.

(1994a) had a probe length of 0.028 m, probe diameter of 0.008 m, and probe-to-probe spacing of 0.006 m. Noborio et al. (1996) indicated that considerable errors were generated in measured thermal conductivity and heat capacity when the probe length was increased to 0.075 m and the probe-to-probe spacing was increased to 0.01 m.

The major design constraints of the TDR probes are the signal attenuation, sampling area, and sensor installation. The probe length is supposed to be determined by the source voltage of the pulse generator, resolution of recorded signals, and signal loss which is dominated by soil electrical conductivity (Ren et al., 1999). The length of TDR probes is limited by several factors, such as the strength and attenuation of the TDR signals and the resolution of the reading equipment. Otherwise, the minimum length is supposed to be determined by the dielectric constant of soil, the voltage step rise, and the resolution of the TDR equipment (Ren et al., 1999; Blackwell, 1956). Relatively small probe-to-probe spacing leads to a small measurement region and reduces the representative sample volume. However, a large spacing will affect the rising time of the propagated signal and cause the change of spacing during the insertion process. Knight (1992) suggested that the diameter of the probes should be as large as possible if there is no significant compaction or disturbance in the soils. Hence, there are many factors to be considered simultaneously in the design of the thermo-TDR probe. The design should satisfy the requirements of both the dual probe heat pulse device and the TDR probe. According to the above discussion, the design constraint of the thermo-TDR probe is defined by Equations 3.1, 3.2 and 3.3,

$$\frac{L}{2r} > 2.2 \tag{3.1}$$

$$\frac{L}{d} > 25 \tag{3.2}$$

$$\frac{d}{2r} < 0.13 \tag{3.3}$$

where L and d are the probe length and diameter, respectively; r is the probe-to-probe spacing between the center probe and the outer probe. The schematic of a new design of a thermo-TDR probe in this study is shown in Figure 3-1, with probe length of 40.5 mm, probe diameter of 2 mm, and probe-to-probe spacing of 6 mm. Compared with the optimized design recommended by Liu et al. (2008), smaller spacing and a little longer probe length were adopted in this new design to reduce the spacing change during the insertion process. The pointed tip was also used to reduce the soil disturbance as much as possible in order to minimize the measurement errors.

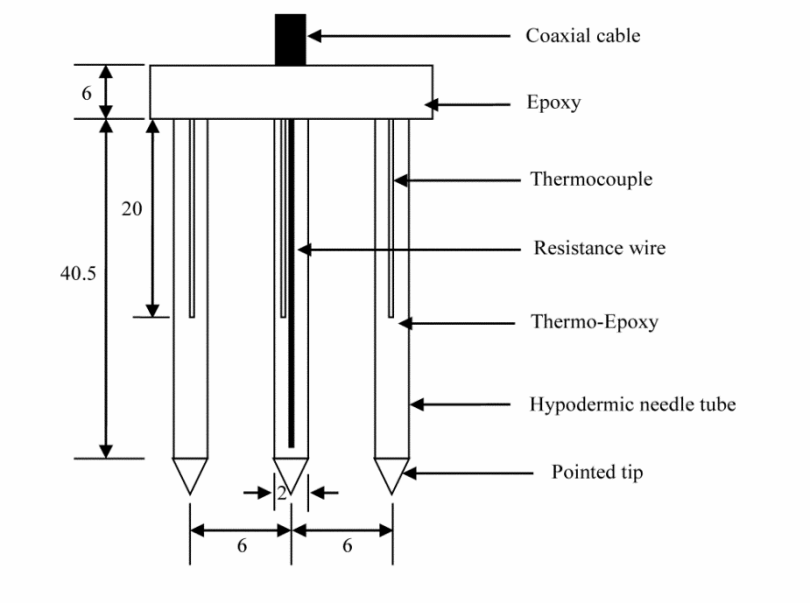

Figure 3-1 Schematic of thermo-TDR probe (unit: mm)

3.2.2 Fabrication of Thermo-TDR Probe

According to above design criteria, the fabrication processes were as follows: (1) Three hypodermic needle tubes (shown Figure 3-2) were used, with inside and outside diameters of 1.7 mm and 2 mm, respectively. The length of the tubes was 46.5 mm, and

the length extending beyond the head of the thermo-TDR probe was 40.5 mm. (2) The tubes were filled with a mixture of thermal epoxy OMEGABOND 200 RESIN and OMEGABOND 200 catalyst, with a weight ratio of 10 to 1. They remained in liquid state at room temperature. (3) Three thermocouples (shown in Figure 3-4) with a wire diameter of 0.076 mm and two loops of 38 gauge Nichrome 80 resistance wire (shown in Figure 3-3), with total length of 80 mm were coated with the thermal epoxy mixture and transferred into the muffler furnace at a temperature of 204 ^{o}C for 2 hours to cure the insulation between them. (4) The three thermocouples were inserted into three tubes, with the sensing unit extending to the mid-height of the tubes. The resistance wire was inserted into the center tube, extending the full length of the tube. (5) The three tubes, with thermal couples and resistance wire, were transferred into the muffler furnace again at the same temperature for another 2 hours. The thermal epoxy was solidified and the thermocouples and the resistance wire were fixed (shown in Figure 3-5). (6) A multimeter was used to check the wired outputs to ensure that the resistance wire, thermocouples, and the tubes were perfectly electrically insulated from each other. (7) The three completed tubes were clamped into a prefabricated mold, which held them in place with a probe-to-probe distance between the tubes of 6 mm. (8) The RG-58 coaxial cable (shown in Figure 3-6) was connected to the corresponding tubes by soldering, as shown in Figure 3-7. (9) The CR-600 casting resin was poured into the mold (as shown in Figure 3-8), and the head was removed from the mold after 24 hours. (10) Three pointed tips were attached by soldering at the probes' ends to reduce soil disturbance during the insertion process. The completed thermo-TDR probe is shown in Figure 3-9.

Figure 3-2 Picture of three hypodermic needle tubes

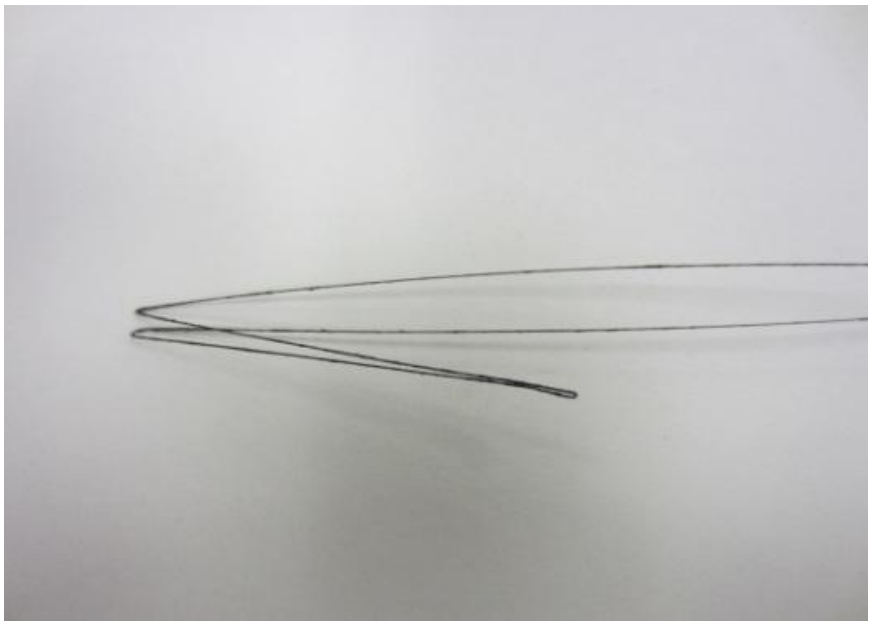

Figure 3-3 Nichrome 80 resistance wire

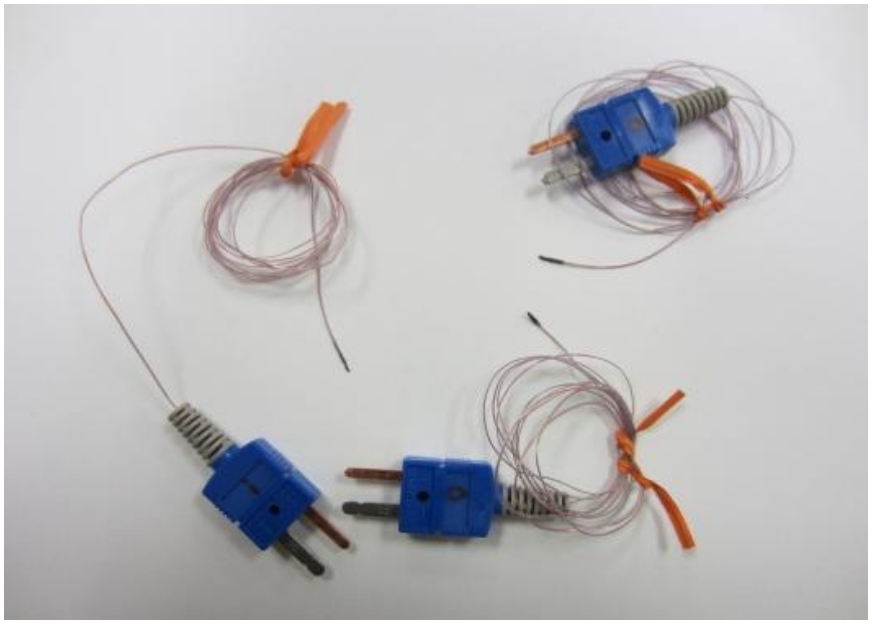

Figure 3-4 Three thermocouples

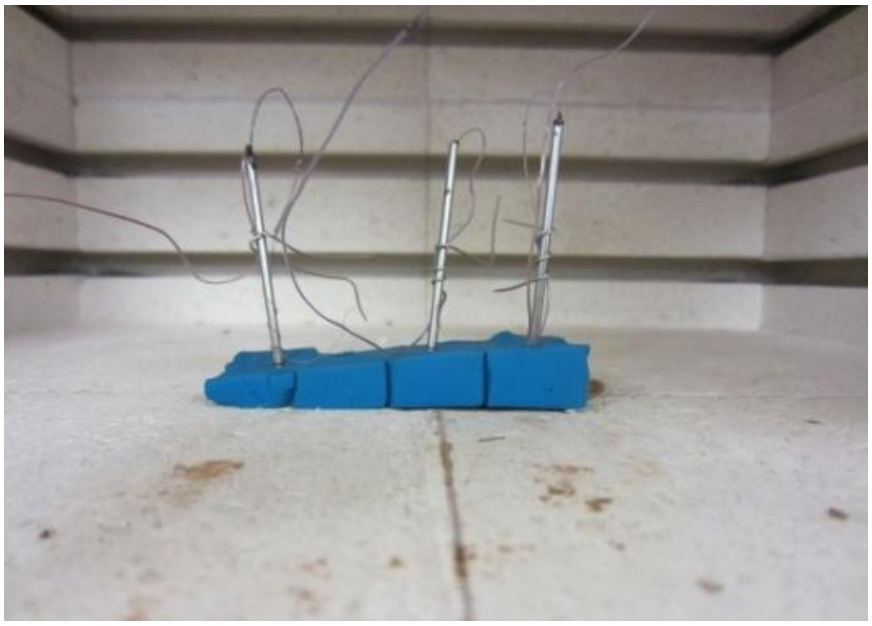

Figure 3-5 Completed probe with resistance wire, thermocouples and thermal epoxy

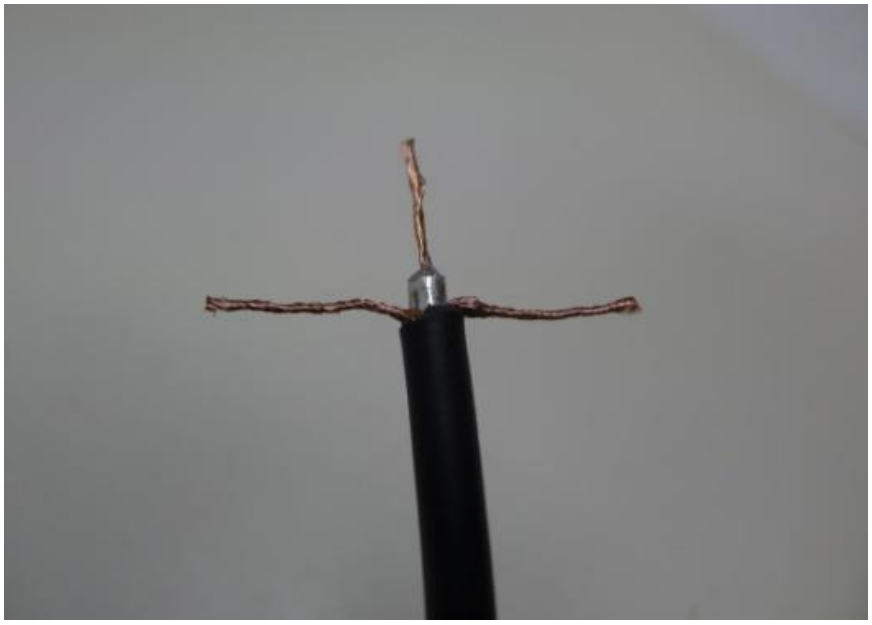

Figure 3-6 The RG-58 coaxial cable

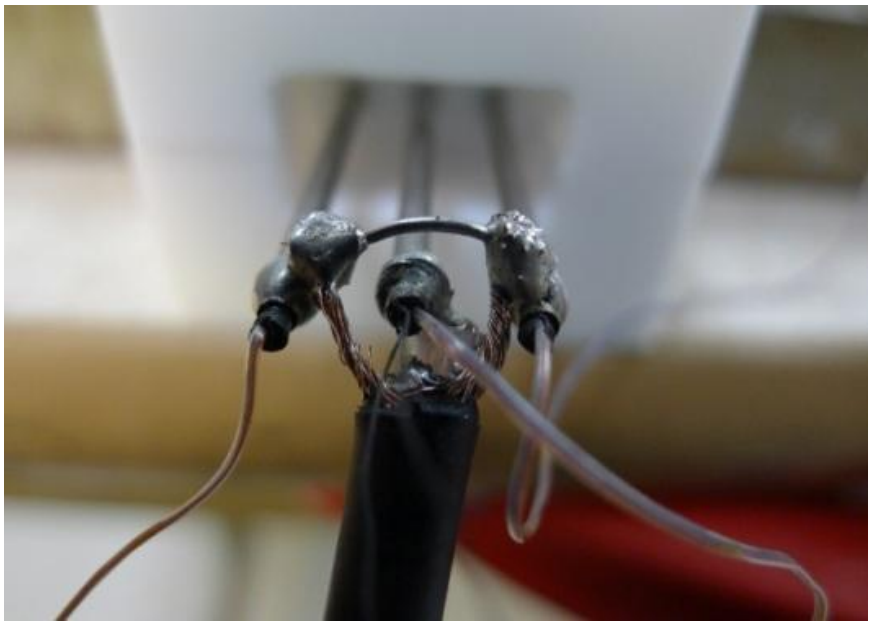

Figure 3-7 Connections between coaxial cable and the probe by soldering

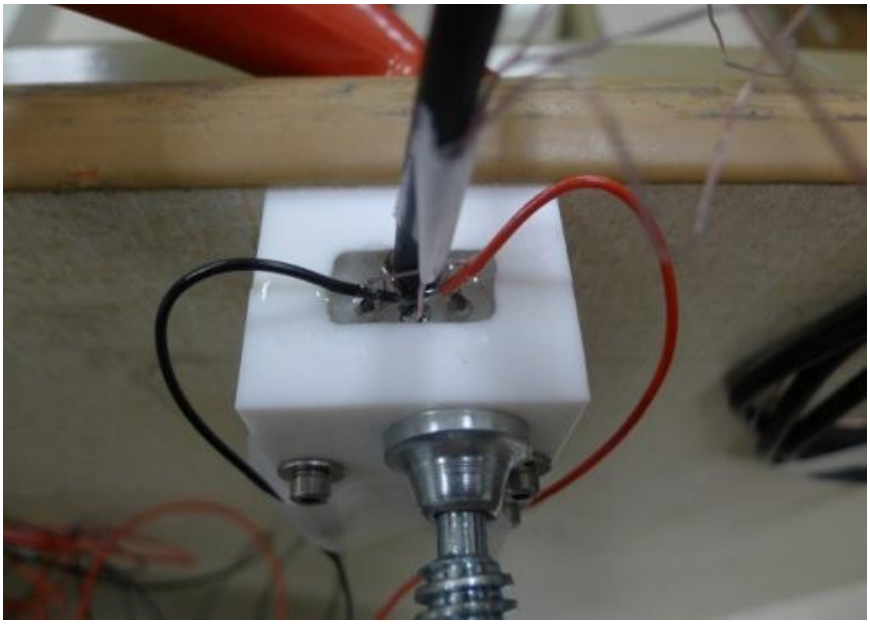

Figure 3-8 Casting the head of thermo-TDR probe

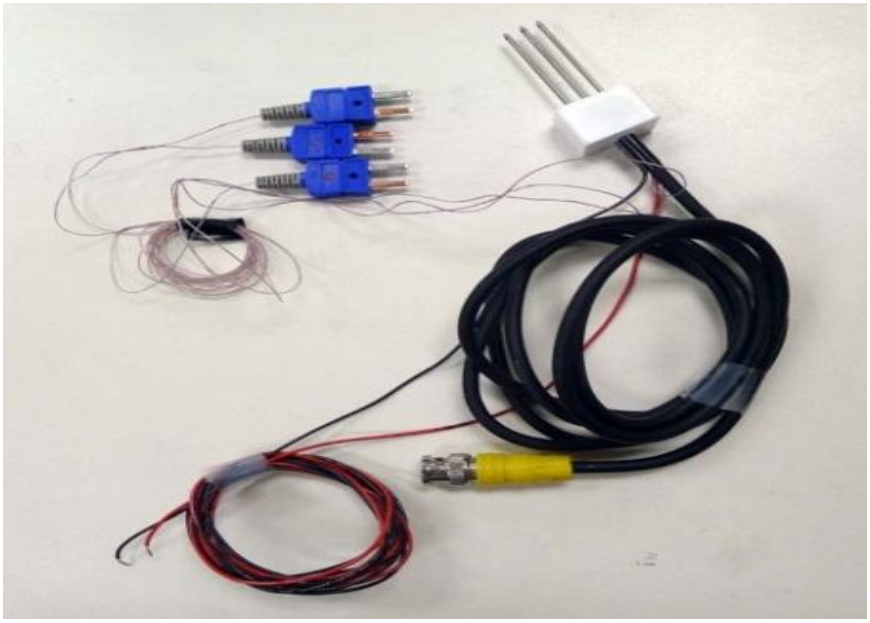

Figure 3-9 Completed thermo-TDR probe

3.3 Calibration of Thermo-TDR Probe

3.3.1 Signal Analyses for TDR Waveforms

Soil dielectric constant is an important property that can be determined from TDR-reflected waveforms analyses. Topp et al. (1980) indicated that dielectric constant from TDR waveforms was known as apparent dielectric constant. A typical TDR waveform of NaCl solution, with concentration of 500 ppm, is shown in Figure 3-10. An apparent dielectric constant from TDR waveforms can be determined by the following equation,

$$K_a = (L_a / L_p)^2 \tag{3.4}$$

where K_a is the apparent dielectric constant; L_p is the physical length of probe in testing materials (L_p=0.0405 m); L_a is the apparent length (length on the waveform) of probe in the testing materials. The apparent length from the TDR waveforms can be determined by locating the electromagnetic wave reflection points at the probe head and at the probe end (shown in Figure 2-4). The single tangent method proposed by Baker and Allmaras (1990) was used to determine the position of the first and second reflection points. This method was chosen because it leads to more reliable and accurate results than other available analysis methods (Chung and Lin, 2009).

Dalton et al. (1984) first demonstrated that the TDR technique can be utilized to measure the apparent bulk soil electrical conductivity. The potential accuracy and precision of TDR measurement was demonstrated by the comparison between electrical conductivity measured in solutions using both TDR and standard methods (Heimovaara et al., 1995; Reece, 1998; Spaans and Baker, 1993). The original equation for calculating electrical conductivity from TDR waveforms was proposed by (Giese and Tiemann, 1975),

$$EC_b(\mathrm{Sm}^{-1}) = \frac{\varepsilon_o c Z_o}{L_p Z_c}\left(\frac{2V_o}{V_f} - 1\right) \tag{3.5}$$

where EC_b is the electrical conductivity, Sm^{-1}; V_o is the source voltage (V_o=1.0 V) and V_f is the long term voltage level of reflected signal (shown in Figure 3-10); ε_o is the dielectric permittivity of free space (ε_o=8.9×10^{12} Fm^{-1}); c is the speed of light in vacuum (c=3×10^8 m/s); L_p is the probe length (L_p=0.0405 m); Z_o is the characteristic probe impedance which is 138.7 Ω for the thermo-TDR probe calculated from the equation proposed by (Huisman et al., 2008); Z_c is the TDR cable tester output impedance (Z_c=50 Ω).

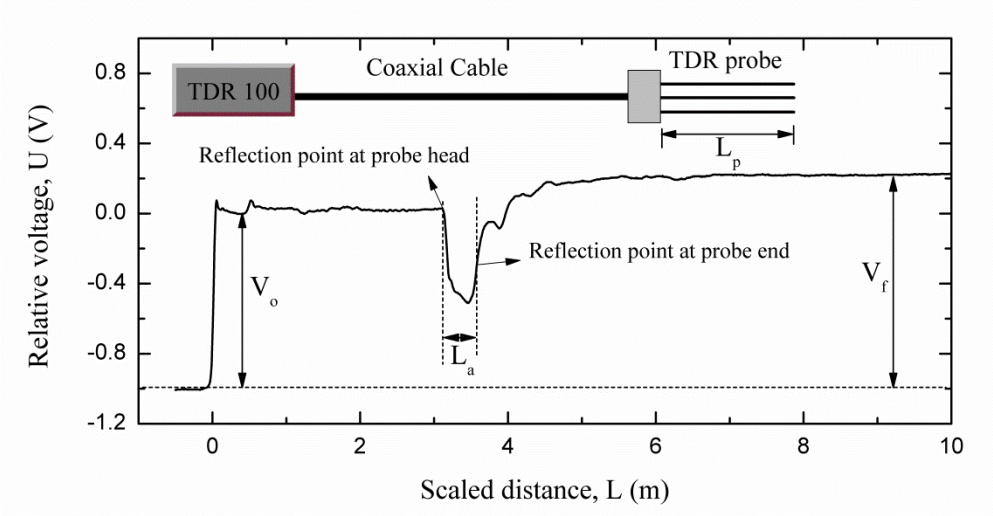

Figure 3-10 TDR waveform of NaCl solution with 500 ppm

3.3.2 Probe Calibration for K_a and EC_b

The sensor calibration of the thermo-TDR probe for K_a was conducted by testing five different chemicals with known K_a values, i.e., cyclohexane (2.0), methylene chloride (8.8), acetone (20.8), methanol (32.6), and deionized water (79.9). Figure 3-11 shows the TDR waveforms and measured K_a values of these five chemicals. The calibration for EC_b was performed by testing twelve NaCl and KCl solutions with different concentrations, ranging from 50-750 ppm, using both the thermo-TDR probe and the electrical

conductivity meter (EC meter). The EC meter is a commonly-used standard method to monitor nutrients, salts, and impurities in liquids. The TDR waveforms of NaCl and KCl solutions are shown in Figure 3-13. The comparison between measured and actual values, with two calibration equations for K_a and EC_b are shown in Figures 3-12 and 3-14. The calibration results showed that the thermo-TDR probe can satisfactorily and simultaneously measure both the apparent dielectric constant and electrical conductivity.

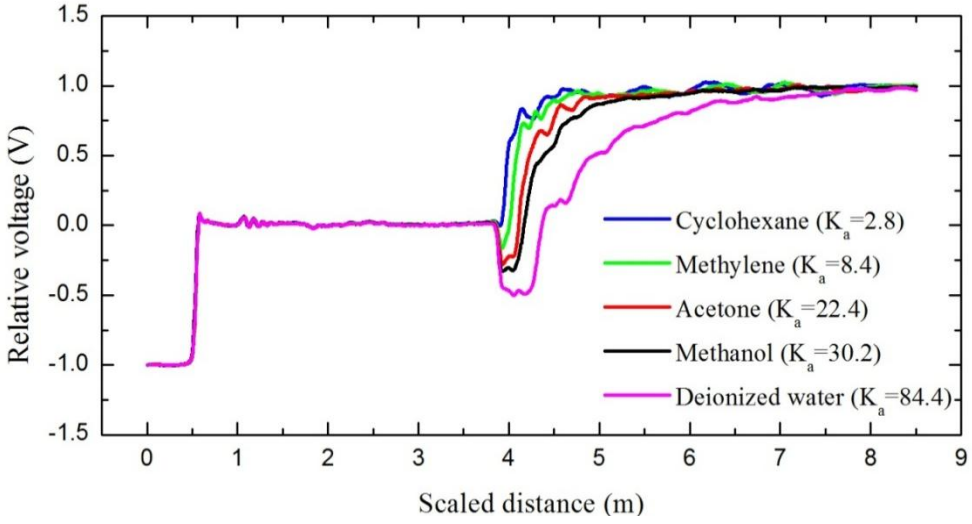

Figure 3-11 Reflected TDR waveforms of five different chemicals with measured K_a values

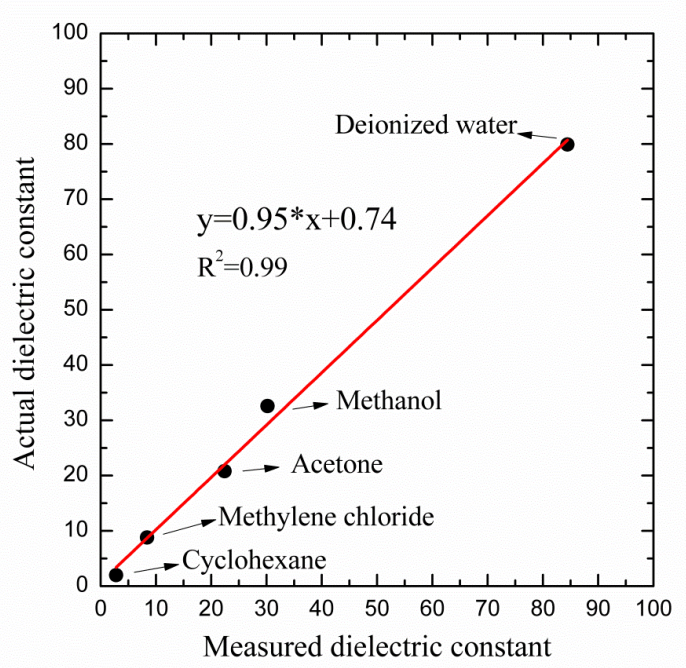

Figure 3-12 Probe calibration for dielectric constant (K_a)

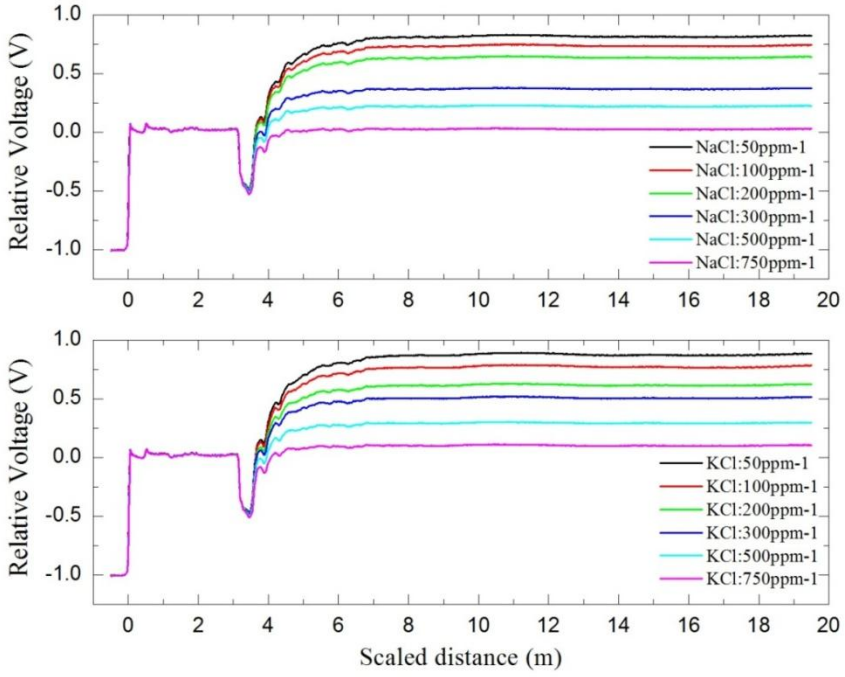

Figure 3-13 TDR waveforms of NaCl and KCl solutions with different concentrations

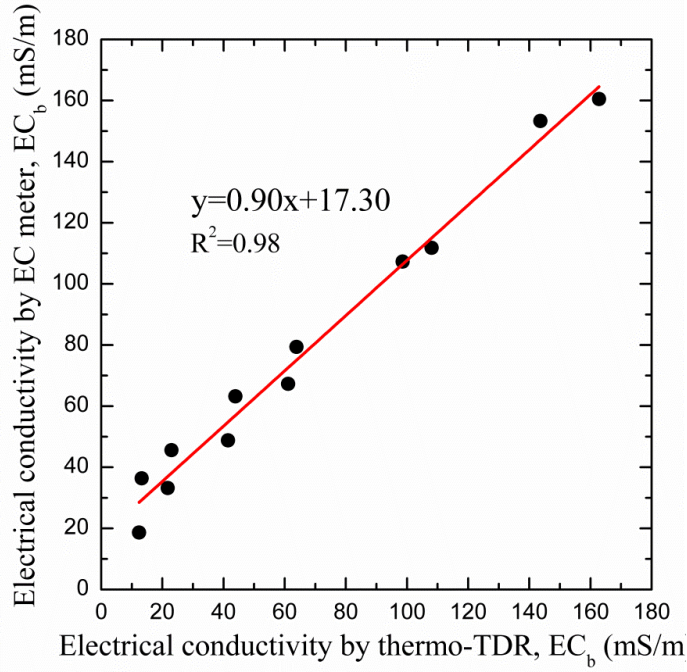

Figure 3-14 Probe calibration for electrical conductivity (EC_b)

3.4 Evaluation of Thermo-TDR Probe for Thermal Properties Measurements

3.4.1 Materials and Methods

For evaluating the performance of the new thermo-TDR probe, three sands, including ASTM-graded sand, brown sand, and Ottawa 20/30 sand, were tested in the experiments. Kaolin clay, which is mainly composed of anhydrous aluminum silicate from US Silica, was also tested by the thermo-TDR probe in the laboratory. Both ASTM-graded sand and Ottawa 20/30 sand are Ottawa-type silica sands, manufactured by US Silica,with white color and round-to-sub-rounded shape, complying with the requirement of ASTM standard C778. The brown sand is common construction sand for concrete cement, passing through a U.S. No. 40 sieve. Figure 3-15 shows the particle size distributions of these four testing materials. ASTM-graded sand is slightly finer than the

brown sand; Ottawa 20/30 sand is poorly graded, primarily with diameters of 20/30 sieve. The physical properties of test material are listed in Table 3-1.

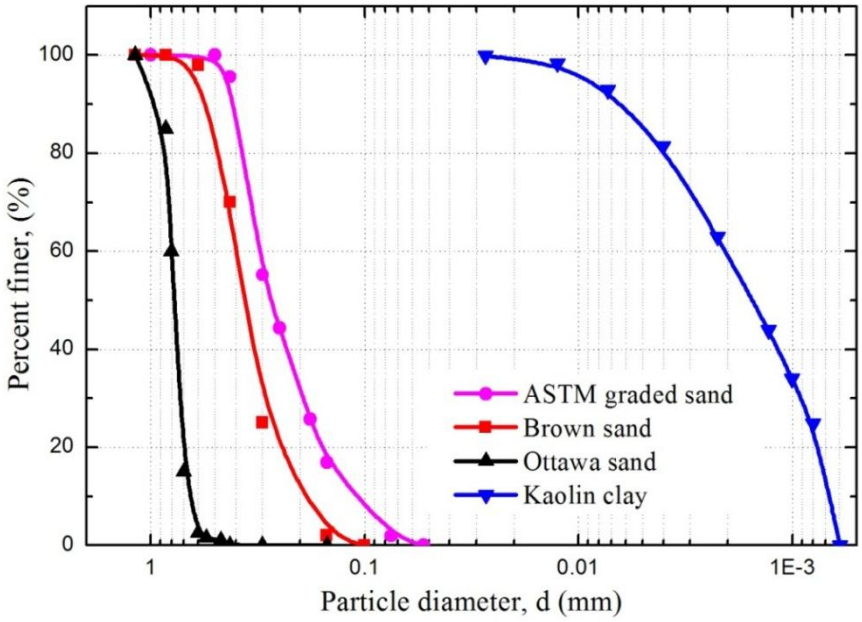

Figure 3-15 Particle size distributions of test materials

A mineral component analysis of the three tested sands was performed by the Energy Dispersive Spectrometer (EDS) test, with results shown in Table 3-2. It can be seen that the major mineral in the three sands is quartz. Moreover, ASTM-graded sand has the highest quartz content of 97.15%, while the Ottawa 20/30 sand has the lowest value of 92.00%. The photos of four test materials are shown in Figure 3-16 (a)-(d).

Table 3-1 Physical properties of test materials

Name	Color	Roundness	Specific Gravity
ASTM graded sand	white	0.9+	2.65
Brown sand	brown	unknown	
Ottawa 20/30 sand	white	0.9+	
Kaolin clay	white	0.9+	2.58

Table 3-2 Percentage of mineral components in sands

Mineral	ASTM graded sand (%)	Brown sand (%)	Ottawa sand (%)
SiO_2(Quartz)	97.15	93.52	92.00
Al_2O_3	1.73	4.12	6.45
MgO	1.05	1.85	1.06
Fe_2O_3	<0.1	<0.1	<0.1
CaO	<0.1	<0.5	<0.1
TiO_2	<0.1	<0.1	<0.1

Soil specimens were prepared by employing the following procedures. The dry soil with known weight was thoroughly mixed with deionized water to make moist specimens with different target moisture contents. The ASTM-graded sand, brown sand, and clay samples were compacted, using a steel rod with a specified number of drops in a PVC plastic mold with an inner height of 136 mm and a diameter of 101 mm. The number of drops was varied to make three different dry densities at targeted moisture contents. Only one specimen density was prepared for the Ottawa 20/30 sand at the targeted moisture content due to the relatively large particle size and high roundness; hence the difficulty encountered in preparing samples with different dry densities at the same moisture content. The specimens were wrapped with plastic and left for 24 hours at room temperature to obtain uniformly distributed moisture. The target moisture contents and the actual dry density ranges of sands and clay in the experiment are given in Table 3-3.

Table 3-3 Target moisture contents of test materials in the experiment

	ASTM graded sand	Brown sand	Ottawa 20/30 sand	Kaolin clay
Target moisture content (%)	2, 5, 8, 11, 14	2, 5, 8, 11	1, 2, 3, 4, 5	10, 20, 30, 40, 50
Actual density range (g/cm^3)	1.53-1.67	1.46-1.66	1.46-1.52	0.65-0.72

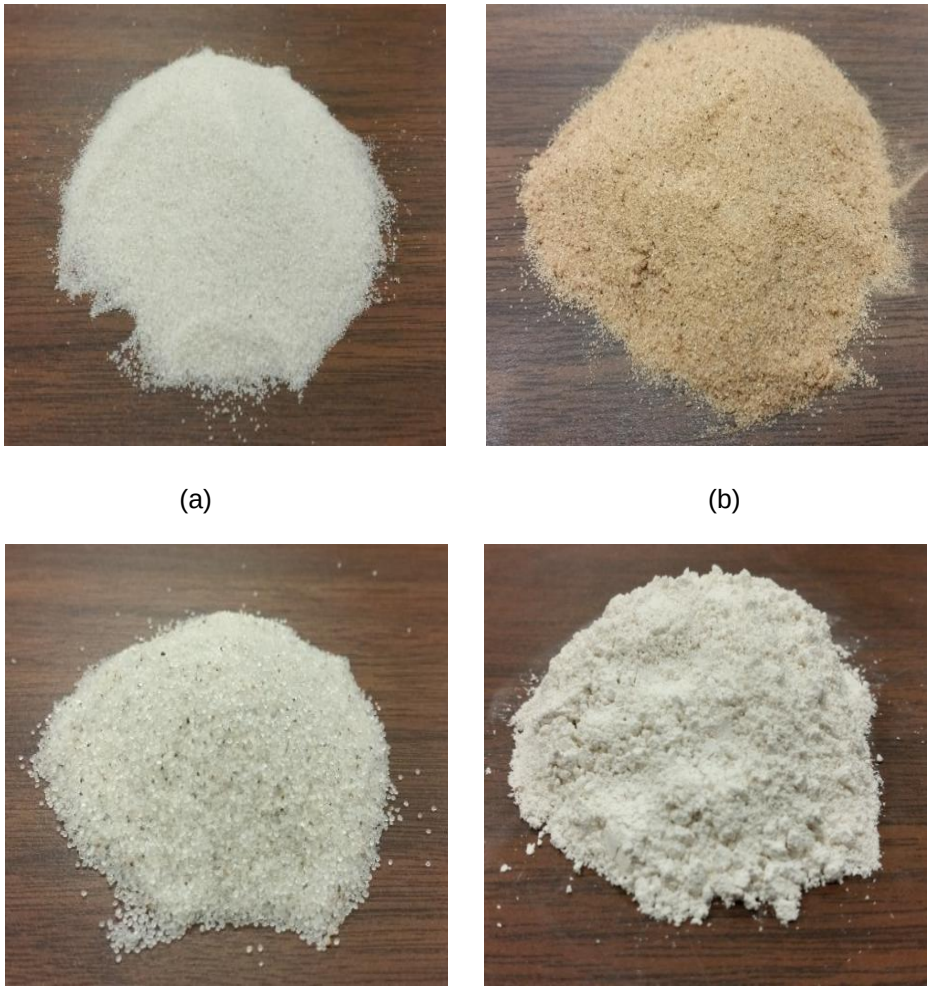

(a) (b)

(c) (d)

Figure 3-16 Photos of four test materials: (a) ASTM graded sand; (b) Brown sand; (c) Ottawa sand; (d) Kaolin clay

3.4.2 Experimental Setup

Figure 3-17 shows the schematic of the experimental setup of the thermo-TDR system. The thermo-TDR probe was connected to the Campbell Scientific TDR 100 through a coaxial cable to obtain TDR waveforms. The resistance wire was connected to the DC current generator BK Precision 17850B to heat the soil specimens. In addition, three thermal couples were connected to the temperature readout unit TC-08 to record temperature variations at the center probe and the two outer probes every second. All the experimental data was recorded automatically in the computer. Figure 3-17 shows the photo of the experimental setup.

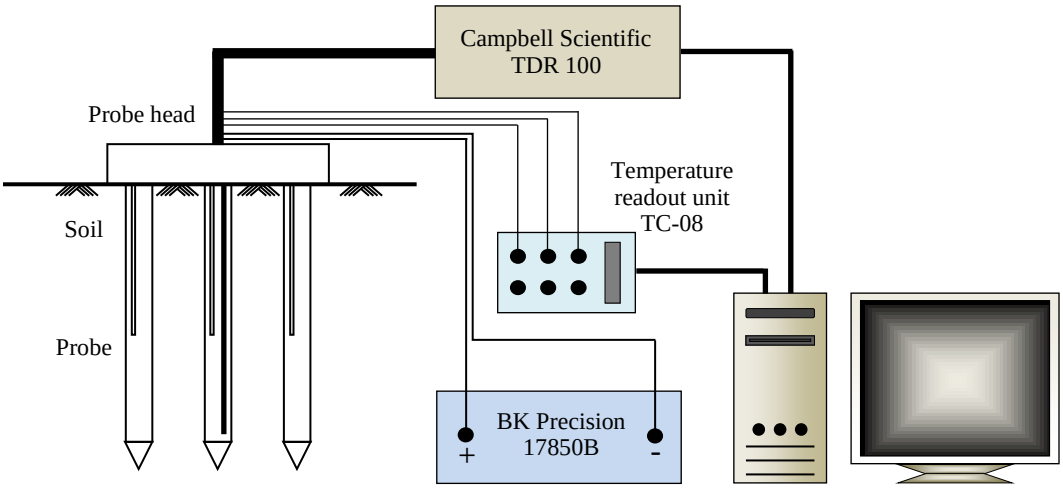

Figure 3-17 Schematic of experimental setup: thermo-TDR system

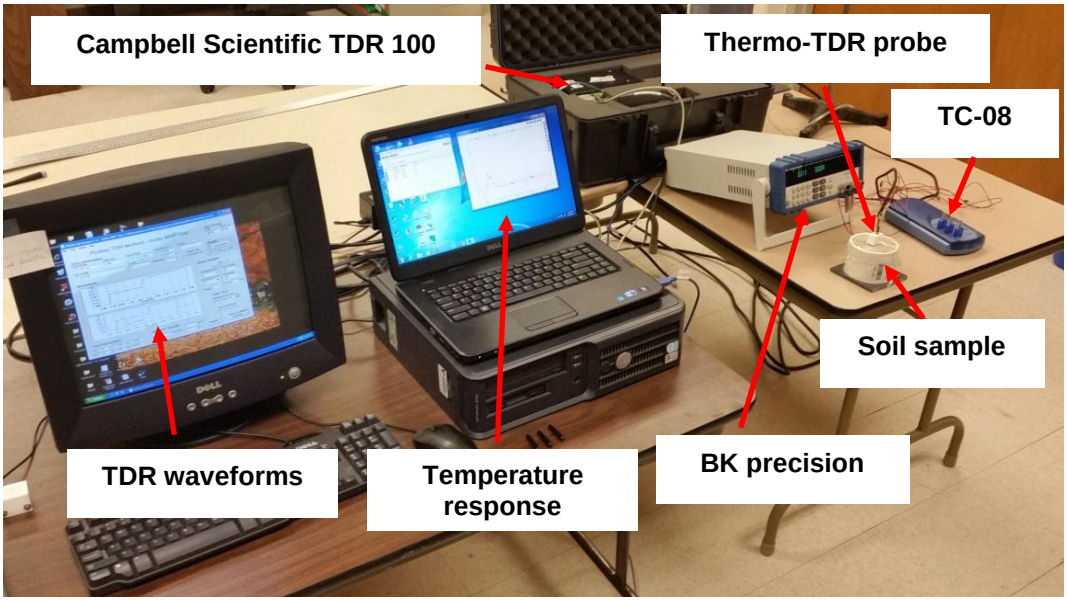

Figure 3-18 Photo of experimental setup

Figure 3-19 shows the KD2 probe system. The KD2 probe consists of a KS-1 single probe, a TR1 single probe, a SH-1 dual probe, and a RK-1 single needle. The TR-1 single probe and the SH-1 dual probe were used in the experiments to measure soil thermal properties. The TR-1 probe has a length of 100 mm, a diameter of 2.4 mm and it can provide thermal conductivity measurement with accuracy of 10 % from 0.2-4.0 W $m^{-1}K^{-1}$ and $\pm$0.02 W $m^{-1}K^{-1}$ from 0.1-0.2 W $m^{-1}K^{-1}$. The SH-1 probe has a length of 30 mm, a diameter of 1.3 mm and a probe-to-probe spacing of 6 mm. It can give thermal conductivity values with accuracy of $\pm$0.01 W $m^{-1}K^{-1}$ from 0.02-0.2 W $m^{-1}K^{-1}$ and $\pm$10% from 0.2-2.0 W $m^{-1}K^{-1}$.

Furthermore, the measurement error was also provided to validate the accuracy and reliability of measured thermal conductivities, and it can be evaluated by considering a dimensionless error provided as an output from the probe. The equation used to calculate the error is as follows (Decagon Devices, 2011),

$$Error = \lambda S_{yx} \tag{3.6}$$

where λ is the thermal conductivity, S_{yx} is the standard error calculated by the following equation:

$$S_{yx} = \sqrt{\frac{SSE}{n}} \tag{3.7}$$

where n is the number of temperature measurements, and SSE is the sum of squares of error in the form:

$$SSE = \sum \left(T_i^* - M_i^* \right)^2 \tag{3.8}$$

where T_i^* and M_i^* are the measured and modeled variables, respectively. A good data set will give error values below 0.01, except at very low thermal conductivity, e.g,. insulation materials (Decagon Devices, 2011).

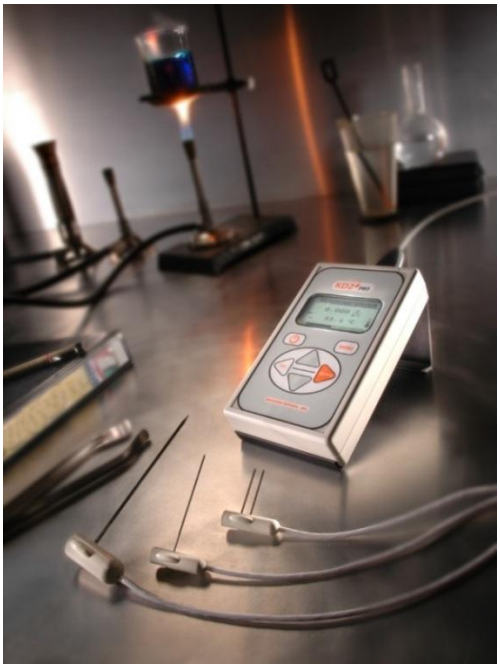

Figure 3-19 Photo of KD2 probe (Decagon Devices, 2011)

The testing procedures for measuring soil thermal properties, moisture content, and dry density properties in the laboratory are as follows: The plastic cover was removed, and the thermo-TDR probe was inserted vertically into the specimen at the center of the top surface. The distance between the center probe and the outer boundary (i.e., plastic wall) was about 44.5 mm, which was 7.41 times the probe-to-probe spacing. Comparing this value with the 2.37 recommended by Campbell et al. (1991), this distance was large enough to avoid any boundary effect. The reflected TDR waveforms were obtained from the signal generator, Campbell TDR100 and PMTDR data-acquiring software. Then, the soil specimens were heated for 15 seconds by applying the current sent from the current generator BK Precision 17850B. The current was then cut off and the specimens were allowed to cool down to the room temperature. During the heating and cooling process, the temperature variations of the center probe and outer probes were recorded by the readout unit TC-08 from Pico Technologies. The thermo-TDR probe was taken out of the specimen and the standard KD2 single probe was inserted into the specimen at a nearby location to measure the thermal conductivity. The KD2 dual probe was then inserted into the specimens to measure the thermal diffusivity and the volumetric heat capacity. Finally, the actual moisture content and dry density of specimens were determined by the oven drying method at 105 ^{o}C.

3.4.3 Determination of Soil Thermal Properties

The resistance wire embedded in the thermo-TDR center probe was connected to the DC current supply equipment, which is the heat source that generates the heat pulse in the heating process. Temperature variations at the center and outer probes were recorded for soil thermal properties analyses by means of the infinite line heat source theory. Theoretically, the temperature change is a function of time and radial distance

away from the line heat source (Kluitenberg et al. 1993; De Vries 1952). The mathematic expression of temperature variations is given by,

$$T(r,t)=\frac{Q}{4\pi\alpha}\left[Ei\left(\frac{-r^2}{4\alpha(t-t_o)}\right)-Ei(\frac{-r^2}{4\alpha t})\right] \tag{3.9}$$

where Q is the strength of line heat source, defined as $Q=q/\rho_c$,q is the quantity of line heat source, W/m; ρ_c is the volumetric heat capacity, MJ $m^{-3}K^{-1}$; T is the temperature change, ^oC; t is the time, s; t_o=15s, which is the duration of the heat pulse; α is the soil thermal diffusivity, mm^2/s; r is the radial distance, m; Ei(x) is the exponential integral.

Once the temperature variations are obtained, Equation 3.9 can be used to calculate the thermal properties of soils by means of nonlinear regression (Bristow et al., 1995; Welch et al., 1996). By differentiating Equation 3.9 with respect to time and setting, the results are equal to zero, Bristow et al. (1994a) proposed a following solution to determine ρ_c and α, as given below,

$$\rho_c=\frac{q}{4\pi\alpha T_m}[Ei(\frac{-r^2}{4\alpha(t_m-t_0)})-Ei(\frac{-r^2}{4\alpha t_m})] \tag{3.10}$$

$$\alpha=\frac{r^2}{4}[\frac{1}{(t_m-t_0)}-\frac{1}{t_m}]/\ln[\frac{t_m}{(t_m-t_0)}] \tag{3.11}$$

According to the relationship among thermal conductivity, thermal diffusivity, and volumetric heat capacity, $k=\rho_c\times\alpha$ the thermal conductivity can be expressed as,

$$k=\frac{q}{4\pi T_m}[Ei(\frac{-\ln[t_m/(t_m-t_0)]}{t_0/t_m})-Ei(\frac{-\ln[t_m/(t_m-t_0)]}{t_0/(t_m-t_0)})] \tag{3.12}$$

where r=6 mm, which is the radial distance between the center probe and outer probes (shown in Figure 3-1); t_m is the time when the maximum temperature at outer probes occurred, s; T_m is the maximum temperature increase at outer probes, ^oC. In order to

ensure that heat conduction is the main mechanism of heat transfer in soils, the heating power should be selected very carefully. With very low heating power, temperature rise is not obvious and the recorded temperature curve is greatly affected by electrical noise. Too much heat, however, will induce moisture migration. Figure 3-19 shows the different temperature variations between the applied current of 0.15 A and 0.05 A and the method to determine the value of t_m and T_m. The temperature variation of the other outer probe is not shown in the figure because two outer probes had almost the same temperature variation from the experiments. The thermal conductivity of soil was calculated by the average value of above two outer probes.

It is noted that the temperature rise was too small at I=0.05 A, and it was difficult to accurately determine the rise peak. However, the maximum temperature change at the center probe was about 5 ^{o}C, and the corresponding T_m value was around 0.5 ^{o}C at outer probe if the current was increased up to 0.15 A. On the other hand, the resistance of heating wire can be calculated from the manufacturer, which is R=22.23 Ω. Consequently, the heating power in Equations 3.10 and 3.12 is calculated as follows,

$$q = I^2 R / L = 0.15^2 \times 22.23 / 0.0405 = 12.35 W / m \qquad (3.13)$$

According to Ren et al.'s (1999) study, this heating power can minimize the convective heat flow and the effect of vapor movement on soil thermal property measurements. It should be emphasized that the selected heating power of thermo-TDR probe is not unique, while the effect of it on measure thermal properties needs to be further examined.

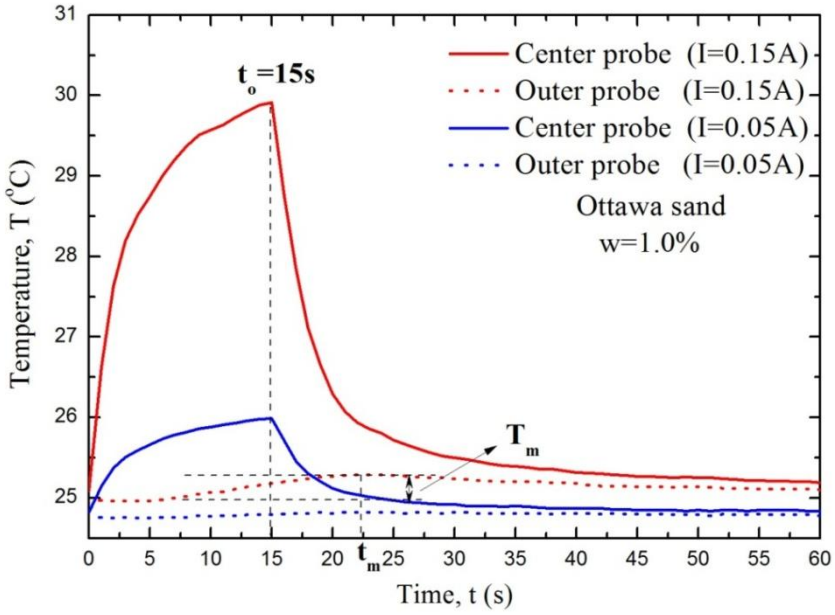

Figure 3-20 Temperature variations of Ottawa sand with different heating powers (Zhang et al. 2015a)

3.4.4 Results and Discussion

A comparison of measured thermal conductivity, thermal diffusivity, and volumetric heat capacity between the thermo-TDR probe and the KD2 probe are shown in Figures 3-20, 3-21 and 3-22. It is noted that the measured thermal conductivities in Figure 3-20 were obtained from a KD2 TR-1 single probe, because they were expected to exceed the measuring range of the SH-2 dual probe. The measured thermal diffusivities and volumetric heat capacities in Figures 3-21 and 3-22 were from the KD2 SH-2 dual probe.

For the three sands under moist or saturated conditions, measured thermal conductivity ranged from 1.4-3.0 W/m*K; thermal diffusivity was between 0.8-1.4 mm^2/s; and volumetric heat capacity ranged from 1.3-2.5 MJ/ (m^3*K). The thermal conductivity of kaolin clay was relatively low, ranging from 0-0.7 W/m*K; thermal diffusivity was between

0.1 and 0.3 mm^2/s; and volumetric heat capacity had a larger range, between 0.9-2.8 $MJ/(m^3*K)$.

Thermal conductivity measured by the thermo-TDR probe was in close agreement with the results of those of the KD2 probes when compared with the other two thermal properties. It is obvious that the relative deviation was within 10% for thermal conductivity, but 20% for thermal diffusivity, and 25% for volumetric heat capacity. Due to the difference in configurations such as probe length, probe diameter, probe-to-probe spacing, and measuring range, and even the analytical method used to determine the thermal properties, it is reasonable to assume that there were small errors in the test results. Another possible reason is that it is difficult to determine t_m in Equations 3.12 for some samples under dry or low moisture content conditions because the low rate of heat dissipation will keep T_m constant for several seconds.

According to the dual probe algorithm in the KD2 User Manual (Decagon Device, 2011), thermal conductivity and diffusivity are first calculated from the curve fitting method. Volumetric heat capacity is then calculated based on the relationship $k= \rho_c \times \alpha$. Due to the smaller measured conductivity values and higher diffusivity values measured from the KD2 dual probe, the calculated heat capacities were much smaller than those from the thermo-TDR probe. This is the reason why the deviation was 25%, as shown in Figure 3-22. However, the thermo-TDR probe still exhibited a high degree of accuracy and excellent performance in the thermal properties measurement in this study.

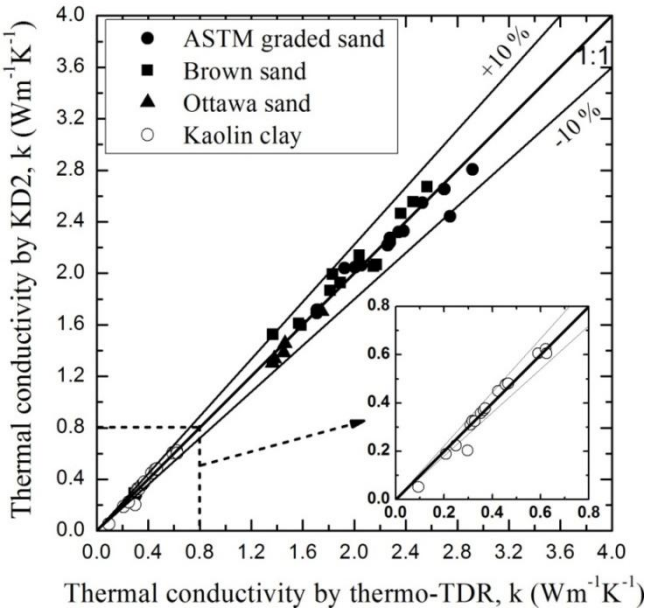

Figure 3-21 Comparison of thermal conductivity measurements between thermo-TDR probe and KD2 TR-1 single probe

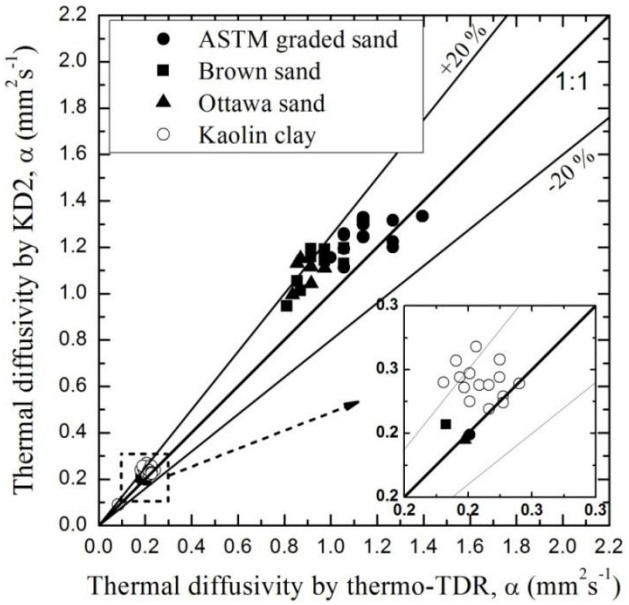

Figure 3-22 Comparison between thermo-TDR probe and KD2 SH-1 dual probe for thermal diffusivity

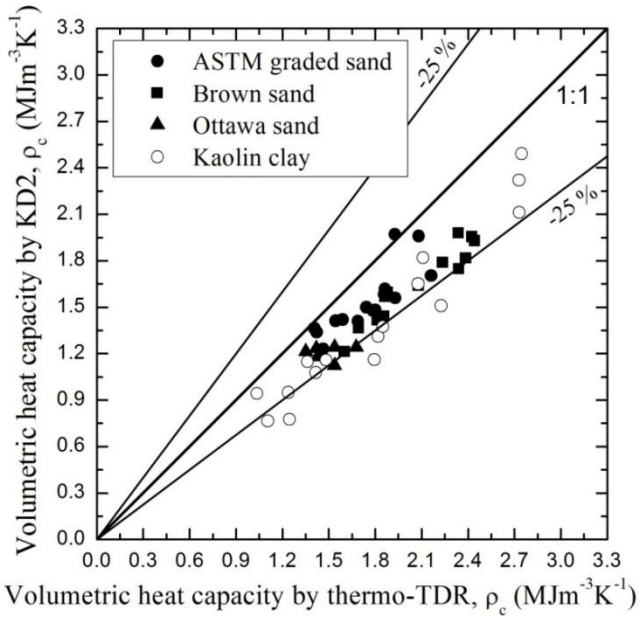

Figure 3-23 Comparison between thermo-TDR probe and KD2 SH-1 dual probe for volumetric heat capacity

3.5 Evaluation of Thermo-TDR Probe for Moisture Content and Dry Density Predictions

Soil moisture content and dry density are very important parameters in geotechnical engineering. It is possible to measure soil moisture content by the oven drying method in the laboratory and dry density by the sand replacement method in the field. However, the thermo-TDR probe is becoming a more accurate, rapid, and reliable tool for predicting the moisture content and dry density simultaneously (Topp et al., 1980, 1988; Dalton et al., 1984; Baker and Allmaras, 1990; Yu and Drnevich, 2004; Ren et al., 1999; Ren et al., 2003). There are three methods included in this section to evaluate the performance of the thermo-TDR probe for the predictions of soil moisture content and dry density: Topp's equation method, heat capacity method. and one-step method.

3.5.1 Topp et al. (1980) Equation Method

Due to the large difference in dielectric constant (K_a) among soil solids (around 3-5), water (around 81 at 20 ^{o}C) and air (around 0), the soil overall dielectric constant is

strongly dependent on its moisture content. Topp et al. (1980) studied the dependency of the dielectric constant on the volumetric moisture content at frequencies between 1 MHz and 1 GHz in the laboratory through experiments on four mineral soils with a wide range of textures, from sandy loam to clay. An empirical relationship between the apparent dielectric constant and volumetric moisture content, which was independent of soil type, density, temperature, and soluble salt content, was obtained and is widely used as follows,

$$\theta = 4.3\times10^{-6}K_a^3 - 5.5\times10^{-4}K_a^2 + 2.92\times10^{-2}K_a - 5.3\times10^{-2} \quad (3.14)$$

where θ is the volumetric moisture content, m^3/m^3. In this study, moisture content of soil specimens can be evaluated by Topp's equation based on measured apparent dielectric constant from the reflected TDR waveforms. Predicted moisture content was also compared with the actual moisture from the oven drying method.

3.5.2 Heat Capacity Method

The volumetric heat capacity of soil can be calculated by summing up the heat capacities of the three different soil constituents including solid, water, and air (De Vries, 1963), which is expressed as follows,

$$\rho_c = \rho_s c_s \theta_s + \rho_w c_w \theta_w + \rho_a c_a \theta_a \quad (3.15)$$

where ρ is the density, kg/m^3; c is the specific heat capacity, kJ $kg^{-1}K^{-1}$; θ is the volumetric fraction; m^3/m^3; s, w and a denote solid, water, and air, respectively. The contribution of air to the soil volumetric heat capacity can be ignored because of the small density and the heat capacity of air compared with the other two phases (Campbell et al., 1991). Equation 3.15 can be simplified as,

$$\rho_c = \rho_d c_s + \rho_w c_w \theta_w \quad (3.16)$$

where ρ_d is the dry density of soil ($\rho_d = \rho_s \times \theta$), kg/m^3. Then, ρ_d can be calculated by,

$$\rho_d = \frac{\rho_c - \rho_w c_w \theta_w}{c_s} \tag{3.17}$$

where c_s is the specific heat capacity of solid particles, kJ $kg^{-1}K^{-1}$. Since this parameter is related to the soil textures, mineral component, and organic matter content, the accuracy of ρ_d can be improved using specific ρ_c values measured by the thermo-TDR probe on dry soils (Ren et al., 2003). In this study, c_s was obtained from the thermal properties measurements of dry soil specimens.

3.5.3 One Step Method

For organic soils, fine-textured soils, and clays, the dependency of K_a on θ differs from Topp's equation (Dasberg and Hopmans, 1992; Dirksen and Dasberg, 1993; Dobson et al., 1985) because it does not consider the effects of soil density and texture on its K_a (Abdulla et al., 1988; Ponizovsky et al., 1999). Another limitation is that gravimetric moisture content is more likely to be used, compared with volumetric moisture content in Topp's equation, in geotechnical engineering. Thus, Siddiqui and Drnevich (1995) and Siddiqui et al. (2000) used gravimetric moisture content and soil dry density to establish the relationship between apparent dielectric constant and gravimetric moisture content, as given below,

$$\sqrt{K_a}\,\frac{\rho_w}{\rho_d} = a + bw \tag{3.18}$$

where *a* and *b* are specific calibration constants; ρ_d is the dry density of soil, kg/m^3; ρ_w is the density of water, kg/m^3; w is the gravimetric moisture content, %.

The overall dielectric constant of soils is dominated by the dielectric constant of water. Similarly, the electrical conductivity of pore fluid in soil has a significant effect on the overall electrical conductivity (Sihvola, 1999). Yu and Drnevich (2004) proposed a

calibration relationship between electrical conductivity and moisture content, incorporating soil dry density and gravimetric moisture content, as given below,

$$\sqrt{EC_b}\,\frac{\rho_w}{\rho_d} = c + dw \tag{3.19}$$

where *c* and *d* are two specific calibration constants. Thus, gravimetric moisture content and dry density can be evaluated by solving Equations 3.18 and 3.19,

$$w = \frac{c\sqrt{K_a} - a\sqrt{EC_b}}{b\sqrt{EC_b} - d\sqrt{K_a}} \tag{3.20}$$

$$\rho_d = \frac{d\sqrt{K_a} - b\sqrt{EC_b}}{ad - cb}\rho_w \tag{3.21}$$

The accuracy of Equations 3.20 and 3.21 is affected by electrical conductivity of pore-fluid of soils and temperature. It has been reported that the calibration for K_a is insensitive to pore-fluid conductivity encountered in common geotechnical soils for both sandy and clayey soils (Topp et al., 1980; Yu and Drnevich, 2004; Zegelin, 1989). However, the electrical conductivity of pore-fluid has a considerable effect on EC_b calibration and soil-specific calibration constants c and d. In this study, the effects of temperature and electrical conductivity of pore fluid were not considered since deionized water was used as pore fluid in the soil specimens, and all the experiments were conducted at room temperature of 24-25^{o} C.

3.5.4 Calibration Relationships for K_a and EC_b

According to Equations 3.18 and 3.19, the calibration relationships for K_a were plotted in Figures 3-23 and 3-24 for sands and clay, respectively. It is evident that $\sqrt{K_a}\rho_w / \rho_d$ increased as the moisture content increased, and excellent linear relationships existed between them from curve fitting for sands and clay. It should be

noted that the specific calibration constant a was almost the same for the three sands, which confirms the test results in Yu's and Drnevich's (2004) study. The b value of Ottawa sand was 6.47. However, both the ASTM-graded sand and brown sand showed a relatively low value of parameter *b*, as shown in Figure 3-23, which was probably because of the dry density effect. The compaction method used in this study was different from the standard compaction mold method used in Yu's and Drnevich's (2004) study. K_a is most affected by the amount of water existing in the soil pores because water has a higher K_a value than solids and air. Therefore, the higher dry density at each target moisture content reduced the $\sqrt{K_a}\rho_w / \rho_d$ value and lowered the slope (i.e., b value) of fitting curve for ASTM-graded sand and brown sand. However, calibration relationships of these two sands took the dry density effect into account and can be applied to a wide dry density range in the future.

Similarly, calibration relationships for EC_b, based on Equation 3.19 for sands and clay, were plotted in Figures 3-25 and 3-26. It is noted that $\sqrt{EC_b}\rho_w / \rho_d$ is increased with moisture content for all three sands, and the d value of Ottawa sand is greater than that of the other two sands. This is also because of the dry density effect, which is similar to that for the apparent dielectric constant. For kaolin clay, the opposite trend of $\sqrt{EC_b}\rho_w / \rho_d$ with gravimetric moisture content showed that $\sqrt{EC_b}\rho_w / \rho_d$ decreased with gravimetric moisture content. The reason is that surface conductivity of clay particles plays an important role in electrical conduction at dry or low moisture content because of the existence of large numbers of physical contacts between clay particles. As moisture increases, some particlesdissolve in deionized water and lose contacts between them. In addition, deionized water, containing very few ions, has a very low EC_b value that cannot contribute significantly to soil electrical conductivity.

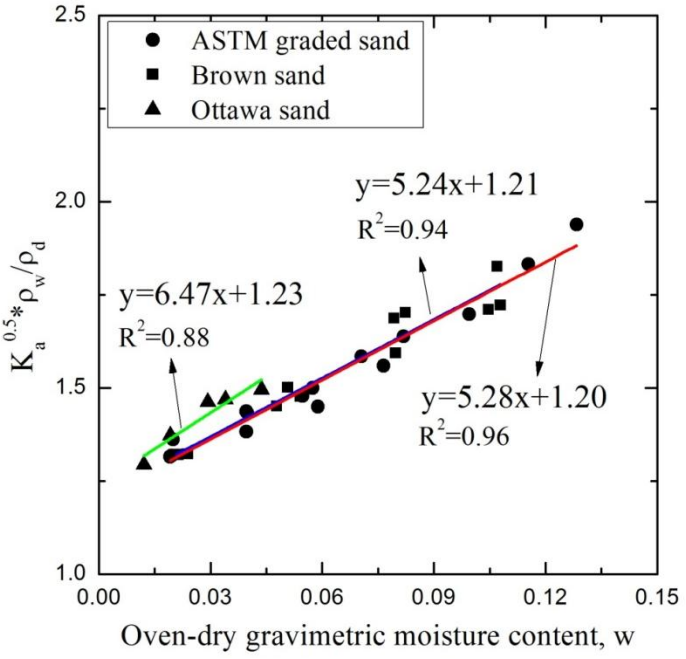

Figure 3-24 Calibration relationships of sands for dielectric constant

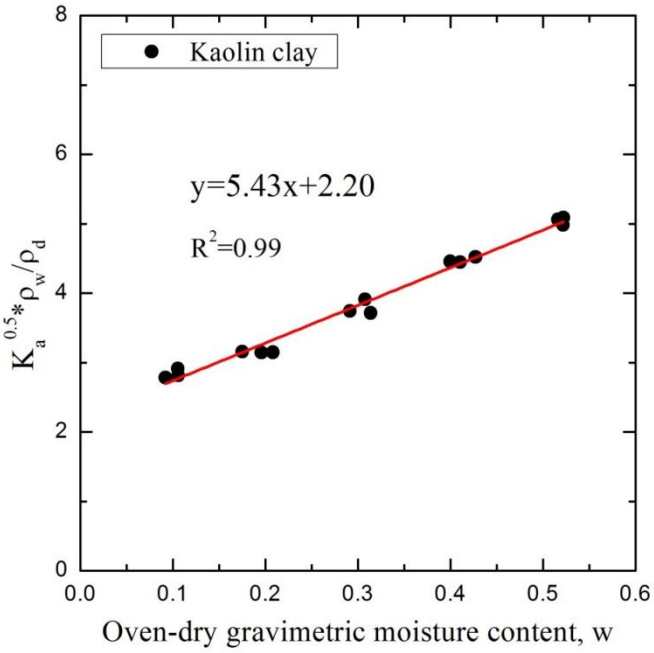

Figure 3-25 Calibration relationships of kaolin clay for dielectric constant

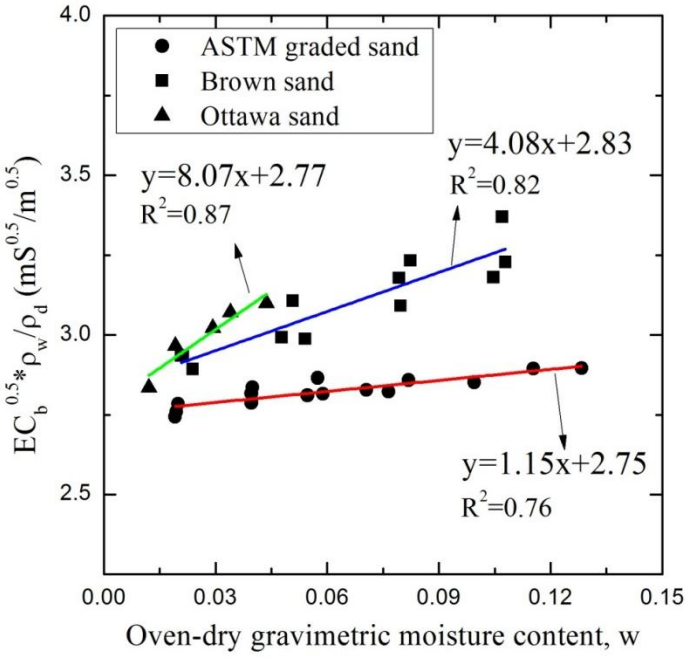

Figure 3-26 Calibration relationships of sands for electrical conductivity

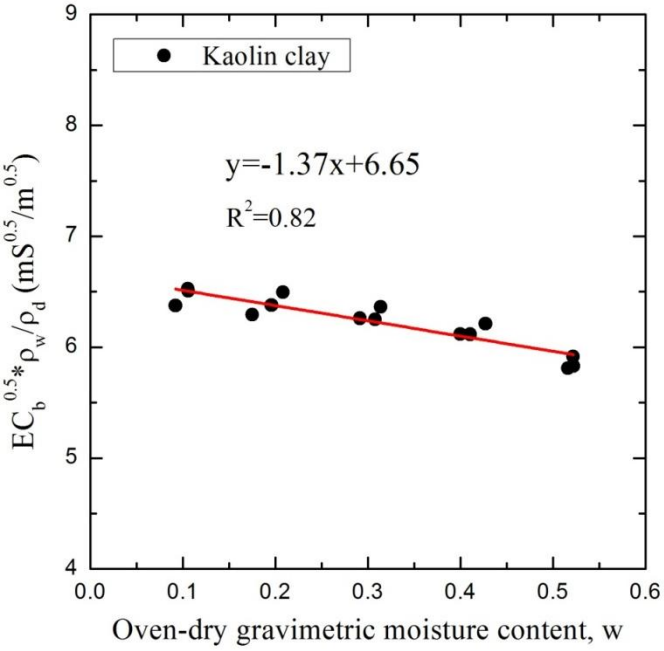

Figure 3-27 Calibration relationships of kaolin clay for electrical conductivity

3.5.5 Results and Discussion

Figure 3-27 shows the actual volumetric moisture content by the oven drying method and predicted value by Topp's equation. The relationship between volumetric moisture content and the apparent dielectric constant by the thermo-TDR probe is depicted in Figure 3-28. A slight discrepancy existed between the measured volumetric moisture and the predicted value by Topp's equation for sands. However, there was a large difference between measured and predicted values for clay specimens. This deviation can probably be attributed to the effect of particle size, mineral component, soil texture, and bound water on the dependency of apparent dielectric constant on volumetric moisture content (Dobson et al., 1985; Dasberg et al., 1992; Roth et al., 1992; Dirksen and Dasberg, 1993; Abdulla et al., 1988; Ponizovsky et al., 1999). Dirksen and Dasberg (1993) also indicated that the deviation from Topp's equation appears more due to the density than the texture effect. Jacobsen and Schjønning (1993) presented that the improved accuracy of their moisture prediction equation is primarily due to the incorporation of dry density. Moreover, the differences in probe dimensions and methods in TDR waveforms analyses may also account for the different relationship between the volumetric moisture content and apparent dielectric constant. In Figure 3-28, it is shown that θ-K_a relationships for both sands and clays differed from Topp's equation. The new fitted relationships for sands and clays can be expressed as below,

Sands: $\theta = -6.62\times10^{-4}K_a^3 + 9.93\times10^{-3}K_a^2 - 6.49\times10^{-3}K_a - 5.46\times10^{-2}$ (3.22)

Clay: $\theta = 2.29\times10^{-4}K_a^3 - 8.11\times10^{-3}K_a^2 + 11.19\times10^{-2}K_a - 24.33\times10^{-2}$ (3.23)

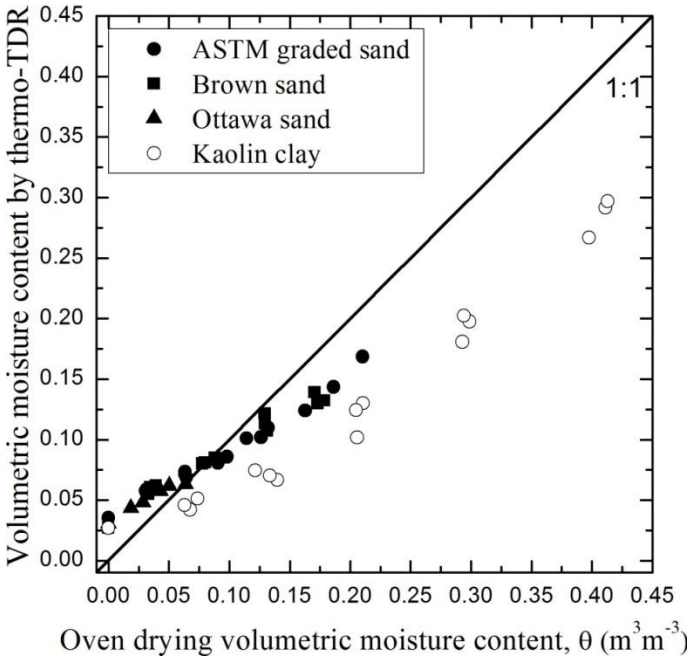

Figure 3-28 Actual volumetric moisture content and predicted value by Topp's equation

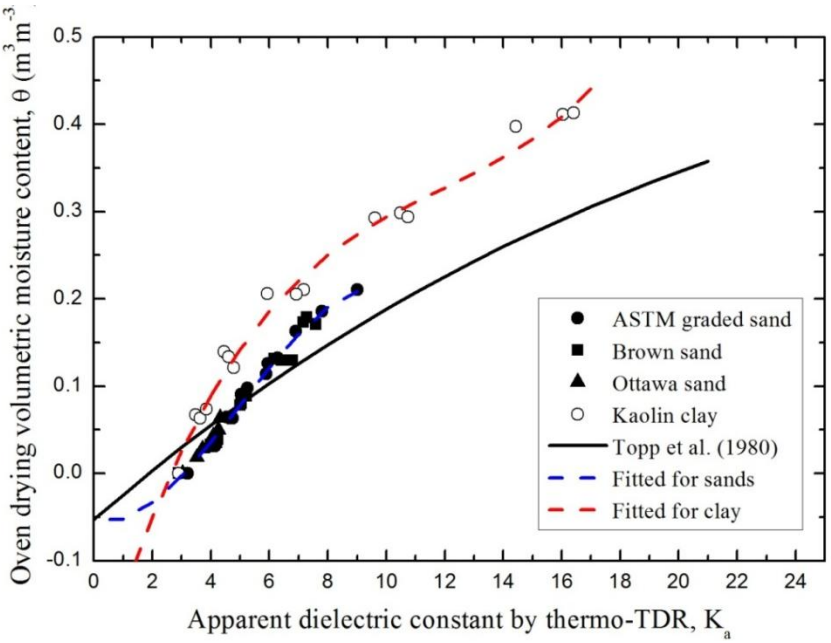

Figure 3-29 Relationship between apparent dielectric constant and volumetric moisture content

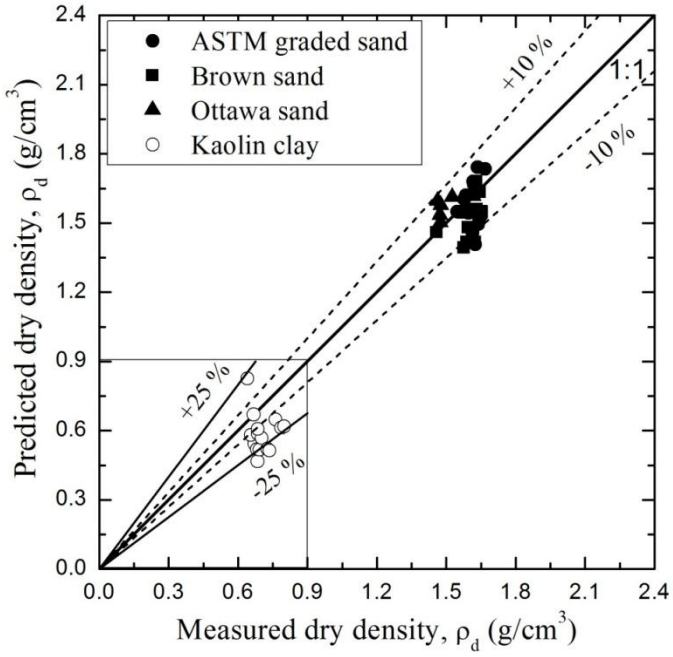

Figure 3-30 Measured dry density and predicted value by heat capacity method

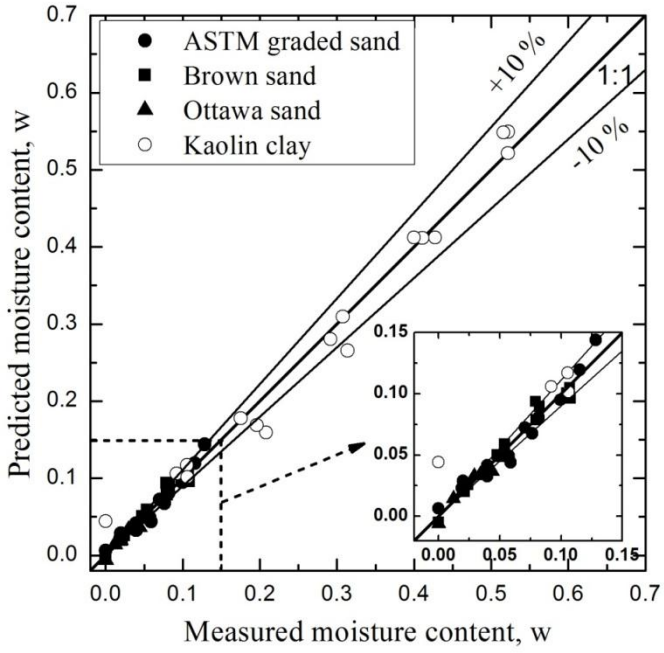

Figure 3-31 Measured gravimetric moisture content predicted value by one step method

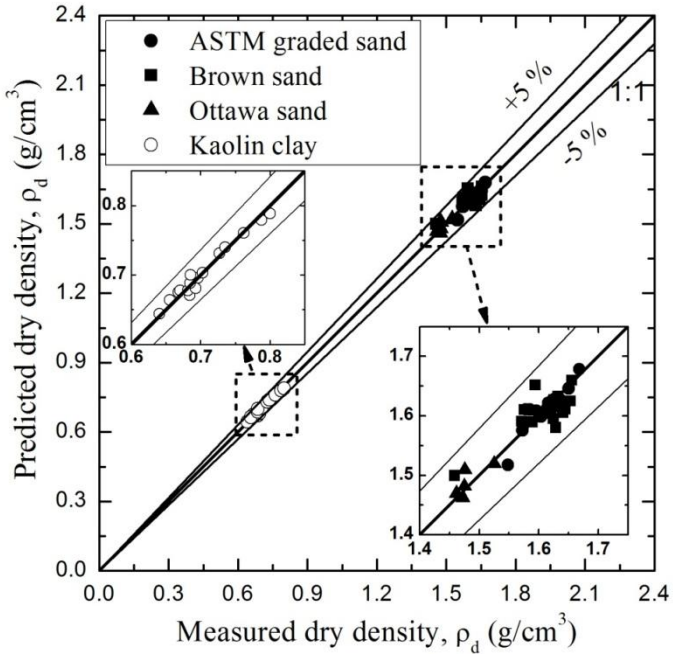

Figure 3-32 Measured dry density and predicted value by one step method

Measured dry density and predicted values by the heat capacity method are shown in Figure 3-29, illustrating that the relative deviation between measured and predicted value is within 25% for clay and even much lower, within 10%, for sands. According to Equation 3.17, the accuracy of ρ_c and c_s data is the major factor for determining the soil dry density. Liu et al. (2008) examined all the measured ρ_c values and the corresponding theoretical values from Equation 3.16. He also did heat-pulse measurements and evaluated the specific heat capacity (c_s) of dry sands, which was about 0.791 kJ $kg^{-1}K^{-1}$. In this study, the thermo-TDR probe was adopted to measure the specific heat capacity (c_s) of dry samples, which were 0.969, 1.097 and 0.884 $kg^{-1}K^{-1}$ for ASTM-graded sand, brown sand, and Ottawa sand, respectively. Thus, the measured values of specific heat capacity (c_s) almost concur with previous study. The errors occurring in the experiment may be caused by the change in probe-to-probe spacing

during the insertion process in the measurement of volumetric heat capacity c by the thermo-TDR technique (Ham and Benson, 2004; Ren et al., 2003).

According to the calibration relationships of apparent dielectric constant (K_a) and electrical conductivity (EC_b) obtained from the thermo-TDR test results, Equations 3.20 and 3.21 were used to predict soil moisture content and dry density by the one-step method. A comparison between the measured and predicted value of moisture content and dry density for both sands and clay is shown in Figures 3-30 and 3-31.

It is observed that the agreement between predicted and measured values for moisture content and dry density was better than those of the previous two methods. The relative deviations for moisture content and dry density prediction wee within 10% and 5%, respectively. Because Equations 3.20 and 3.21 were actually derived from the two calibration equations for dielectric constant (K_a) and electrical conductivity (EC_b), the excellent linear relationship in the two calibration equations resulted in the high degree of accuracy of the prediction of soil moisture content and dry density. Hence, the excellent performance of the thermo-TDR probe in measuring dielectric constant (K_a) and electrical conductivity (EC_b) was noted.

3.6 Summary

The thermo-TDR probe is a promising tool which can measure soil thermal properties, moisture content, and dry density simultaneously in the laboratory and in the field. In this study, a new thermo-TDR probe, integrating the dual heating probe with the TDR moisture probe, was designed and fabricated with the optimized dimensions and pointed tips. The sensor calibration results revealed that the thermo-TDR probe can measure both dielectric constant (K_a) and electrical conductivity (EC_b) reasonably well from TDR waveforms analyses, using the Baker and Allmaras (1990) method.

Three sands and one Kaolin clay were used to perform the laboratory tests to evaluate the performance of the thermo-TDR probe in the measurements of soil thermal properties and predictions of soil moisture content, and dry density. The excellent performance in the thermal properties measurement by the thermo-TDR probe was corroborated by comparing the test results with those obtained from the standard KD2 TR-1 single probe and the SH-1 dual probe. The relative deviations for measurements of thermal conductivity, thermal diffusivity, and volumetric heat capacity were within 10%, 20%, and 25%, respectively. The prediction of soil moisture content and dry density by the thermo-TDR probe was also conducted by using three different approaches: the Topp's equation, the heat capacity method, and the one-step method. The new relationships between the dielectric constant and volumetric moisture content for sands and clay were proposed from the tests results by the thermo-TDR probe. The heat capacity method showed reasonably well-predicted results for soil dry density. The one-step method exhibited the highest accuracy in the prediction of both soil moisture content and dry density through the comparison of predicted values with actual measured results. The deviations for moisture content and dry density were only within 10% and 5%, respectively. However, before the thermo-TDR probe can be used in other geotechnical engineering applications, it needs to be further evaluated on other types of soils.

Chapter 4

Laboratory Experimental Program on Thermal Conductivity

4.1 Introduction

The heat transfer process in soils depends on its thermal conductivity property and is affected by soil compositional and environmental factors, such as soil gradation, mineralogy components, compaction moisture content, and dry unit weight conditions. The soil thermal conductivity property has many geothermal applications, such as geothermal energy piles (GEP), ground source heat pump (GSHP), and borehole thermal energy storage (BTES), etc.

This chapter presents three laboratory experimental studies on quartz sands, sand-sand mixtures, and sand-clay mixtures, respectively, using the thermo-TDR probe. The effects of quartz content, moisture content, dry density, and clay content on soil thermal conductivity were studied. An improved soil thermal conductivity model for quartz sand was proposed based on the normalized thermal conductivity concept and experimental results. A model prediction was also conducted to predict thermal conductivity of sand-sand and sand-clay mixtures, using existing thermal conductivity models.

4.2 Laboratory Experiment on Quartz Sands

Knowledge of soil thermal conductivity is fundamental to understanding the heat transfer process in soils, which is also critical for many applications such as active geothermal structures. Brandl (2006) presented the importance of soil thermal properties in the behavior of thermo-active ground structures, such as geothermal energy piles (GEP) and other ground-source heat pump (GSHP) systems. When heat-carrying fluid is circulated in pipes underground, heat transfer and exchange occur between the fluid and he soils, which determines the entire working efficiency of the structures. The thermal

property of soils is critical to governing the heat transfer process and enabling more efficient design of geothermal foundation systems.

Thermal conductivity is the most frequently used soil thermal property and is affected by several factors, such as moisture content, degree of saturation, dry density, and mineral components. Such effects have been studied by many researchers (Kersten, 1949; Johansen, 1977; Farouki, 1981; and Cote and Konrad, 2005). Lu et al. (2007) used a thermo-TDR probe to investigate the relationships between thermal conductivity and volumetric moisture content properties of different soils ranging from sand, sandy loam, and silt loam, to clay loam. Chen (2008) later performed a series of thermal probe tests on four quartz sands with various particle size distributions to study the effects of porosity and the degree of saturation on their thermal conductivity properties.

Model prediction of soil thermal conductivity has been conducted by several researchers (De Vries, 1963; Johansen, 1977; Donazzi et al., 1979; Gangadhera, Rao and Singh, 1999; Gori and Corasaniti, 1983, 2002; Cote and Konrad, 2005; Lu et al., 2007; Chen, 2008; and Haigh, 2012). De Vries (1963) proposed a thermal conductivity model derived from Maxwell's equations. Weighted average thermal conductivity of each phase of the soil matrix was taken into account for the overall thermal conductivity of soil. Johansen (1977) introduced the concept of normalized thermal conductivity by using experimental data provided by Kersten (1949) to predict soil thermal conductivity. In accordance with this concept, Cote and Konrad (2005) presented a generalized thermal conductivity model for soils and construction materials. These models cannot be applied to quartz sands, however, due to the effect of high quartz content on the thermal conductivity prediction.

This section mainly focuses on the thermal conductivity of three quartz sands by using the newly developed thermo-TDR probe. The effects of moisture content, dry

density, quartz content, and particle size on thermal conductivity is also discussed, based on the measured experiment results. An improved thermal conductivity model, based on the normalized thermal conductivity concept and experimental data, was later developed for the quartz sands. The performance of this model was compared with other five existing thermal conductivity models through a statistical regression analysis and root mean square error analysis.

4.2.1 Materials and Methods

A laboratory test program was conducted to test the thermal conductivity of three selected sands by using the developed thermo-TDR probe. The test variables considered were moisture content, dry density, quartz content, and particle size. The selected test sands were ASTM-graded sand, brown sand, and Ottawa 20/30 sand, which are the same as those in Chapter 3. The physical properties of the sands are shown in Table 3-1. The mineral component analyses are given in Table 3-2. The target moisture content and actual dry density range of sand samples in the experiments are presented in Table 3-3. The experimental setup (shown in Figure 3-17) and specific testing procedures were described in Chapter 3.

4.2.2 Results and Discussion

Two thermal conductivities can be calculated from the recorded temperature variations at two outer probes by using Equation 3.12. Figure 4-1 shows the relationship between the average values of the above two calculated thermal conductivities and gravimetric moisture content. It is indicated that the thermal conductivity of quartz sands increased with gravimetric moisture content, and power function can be used to describe their relationships, as shown in Figure 4-1. Another noticeable feature is that the thermal conductivity increased rapidly at low moisture content, then became more gradual at high moisture content range. This is also consistent with previous thermal conductivity studies

on other soil types (Johansen, 1977; Cote and Konrad, 2005; Lu et al., 2007; Chen, 2008). At low moisture content, small amounts of water films and water bridges formed, and a small portion of the air in the void was replaced by the moisture content. These water bridges facilitated the heat transfer process in sands and improved the effective thermal conductivity of sands due to the relatively high thermal conductivity of water compared with that of air. After all sand particles were connected through the water bridges, the thermal conductivity increased slightly.

Figure 4-1 also indicates that the thermal conductivity of ASTM-graded sand was greater than that of brown sand and Ottawa 20/30 sand. This is because of the effect of the particle size on thermal conductivity of sands. The smaller the particle size is, the greater the specific surface area is. Smaller particle sizes in soils have larger amounts of water film and water bridge formations, resulting in higher thermal conductivity. In addition, quartz has the highest thermal conductivity (i.e. 7.7-8.4 W $m^{-1}K^{-1}$) of all the soil minerals (De Vries, 1963). According to the equation provided by Johansen (1977) for calculating the thermal conductivity of solid fractions in soils, higher quartz content leads to higher thermal conductivity of solid particles in sands. Since the greatest contribution to effective thermal conductivity of soils comes from solid fraction, the thermal conductivity of sands will be increased due to the higher quartz content.

Figures 4-2 and 4-3 show the relationships between thermal conductivity and dry density of ASTM-graded sand and brown sand, respectively. It is noted that thermal conductivity increased with dry density at each target moisture content for these two sands. However, the effect of dry density on thermal conductivity is not very significant in this study. Theoretically, the increase in dry density in sand samples will increase the number of physical contact points between sand particles, reducing the thermal resistance at contact points and increasing sand thermal conductivity. Compared

with the moisture content effect, dry density is the secondary influence factor on thermal conductivity of quartz sands.

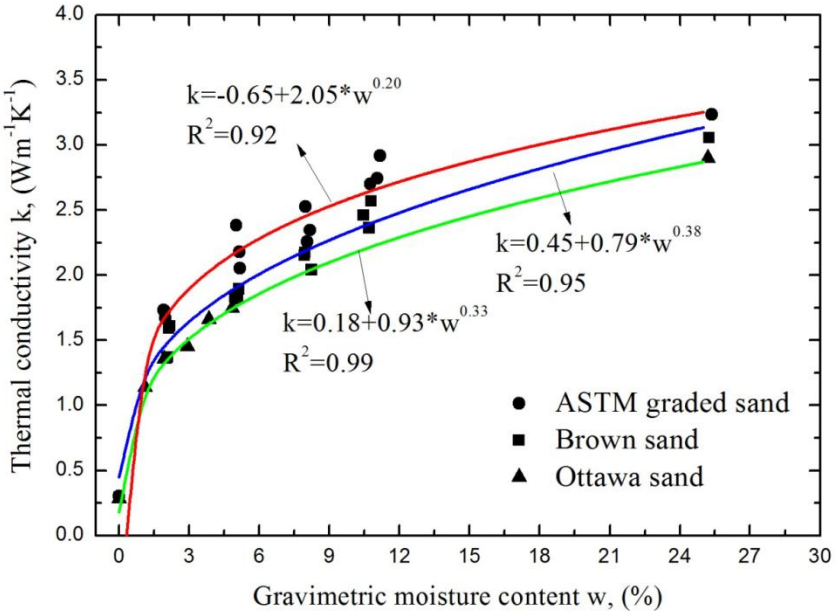

Figure 4-1 Thermal conductivity and gravimetric moisture content of quartz sands

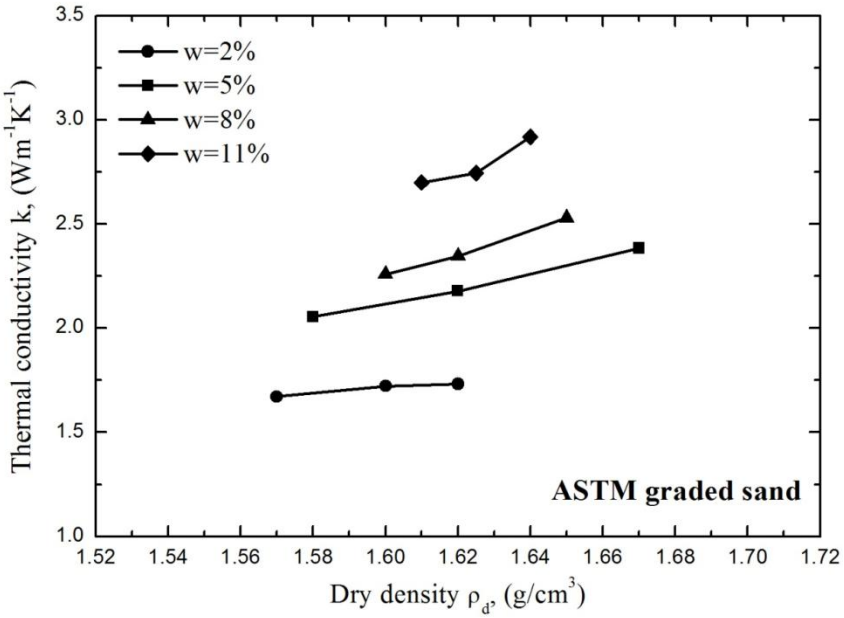

Figure 4-2 Thermal conductivity and dry density of ASTM graded sand

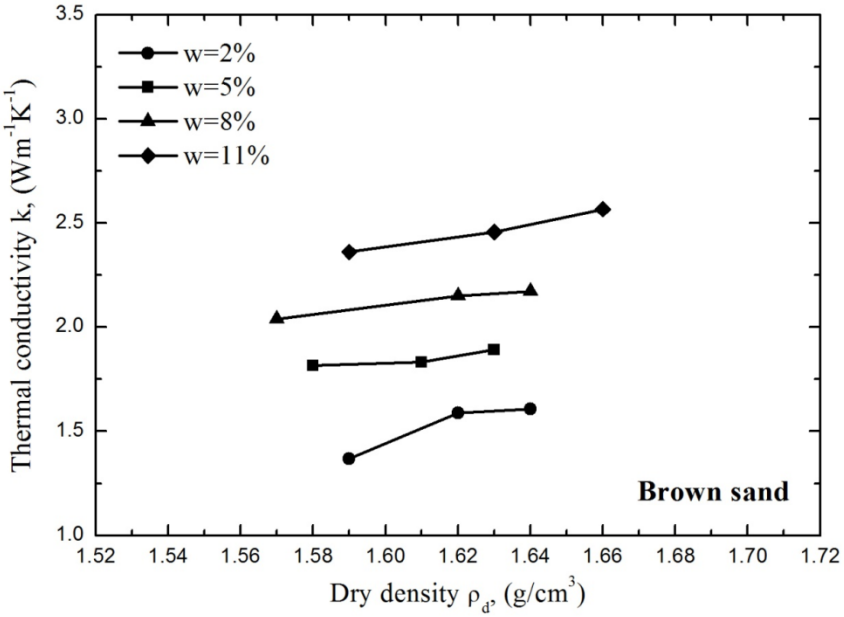

Figure 4-3 Thermal conductivity and dry density of brown sand

4.2.3 Model Prediction

The normalized thermal conductivity concept has been adopted by many researchers to develop thermal conductivity prediction models (Johansen, 1977; Cote and Konrad, 2005). More importantly, this concept can also be applied to various soil types for thermal conductivity predictions. Thus, an improved model is proposed by fitting experimental data to predict thermal conductivity of quartz sands.

The thermal conductivity equations obtained for various soils can be expressed by the normalized thermal conductivity concept proposed by Johansen (1977):

$$k_r = \frac{k - k_{dry}}{k_{sat} - k_{dry}} \tag{4.1}$$

where k_r is the normalized thermal conductivity, k_{dry} and k_{sat} are the thermal conductivity of soils at dry and fully saturated conditions, respectively, W $m^{-1}K^{-1}$,

Then, establishing the k_r-S_r relationship, the effects of porosity, moisture content, and mineral component on the thermal conductivity can be studied in a unique way because of the diverse relationships for given types of soil (Cote and Konrad, 2005). The lower and upper bounds of this relationship are as follows:

Lower limit condition: $S_r = 0 \rightarrow k_r = 0$

Upper limit condition: $S_r = 1 \rightarrow k_r = 1$

Johansen (1977) also proposed the following empirical k_r-S_r relationships for soils studied by Kersten (1949):

$k_r = 0.7\log(S_r) + 1$ unfrozen medium and fine sands (4.2)

$k_r = \log(S_r) + 1$ unfrozen fine-grained soils (4.3)

The generalized thermal conductivity model can be derived from Equation 4.1, as given below,

$$k = k_r \times (k_{sat} - k_{dry}) + k_{dry} \quad (4.4)$$

The simplest expression for calculating the thermal conductivity of saturated soils is given below (Sass et al., 1971):

$$k_{sat} = k_{water}^{n} k_{solid}^{1-n} \quad (4.5)$$

Cote and Konrad (2005) proposed a generalized thermal conductivity model for soils and construction materials with a wide range of soil types, porosity, and degree of saturation. The generalized k_r-S_r relationship he provided is as follows:

$$k_r = \frac{\kappa S_r}{1 + (\kappa - 1) S_r} \quad (4.6)$$

The relationship between thermal conductivity and porosity of dry soils they proposed is given as follows:

$$k_{dry} = \chi 10^{-\eta n} \quad (4.7)$$

Substituting Equations 4.5, 4.6, and 4.7 into Equation 4.4, the thermal conductivity prediction model can be obtained, which is the same as the Cote and Konrad (2005) model. Although this model was developed based on a large dataset from a wide range of types of soils, the effect of high content quartz on the thermal conductivity of sands was not clarified in his study. Therefore, the parameters κ, χ and η in Equations 4.6 and 4.7 need to be determined from the thermo-TDR test results in this study.

Experimental data obtained from the thermo-TDR probe were collected to plot the k_r-S_r relationship, as shown in Figure 4-4, for the purpose of determining the κ value of quartz sands. k_r-S_r relationships from the Johansen (1977) study, which are Equations 4.2 and 4.3, were also plotted in the same figure. It was shown that Equations 4.2 and 4.3 deviated significantly from the k_r-S_r relationship of quartz sands, and the best data fitting with Equation 4.6 can be achieved at κ=6 for three quartz sands, which is almost

twice the suggested values of 3.55 for fine and medium sands mentioned previously (Cote and Konrad, 2005). The higher κ value represents the higher k_r value at the same saturation degree, as shown in Figure 4-4. Furthermore, thermal conductivity k increased with k_r from Equation 4.4. Consequently, thermal conductivity k increases as κ increases. It also means thermal conductivity of quartz sands is greater than that of other types of soils with the degree of saturation, which is mainly attributed to a higher quartz content compared with other soils.

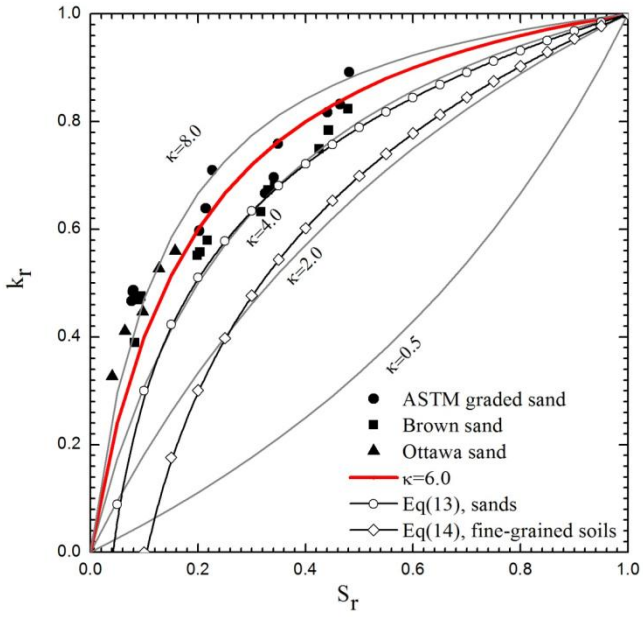

Figure 4-4 k_r-S_r relationship of sands and determination of κ value for quartz sands

Chen (2008) performed many thermal probe tests on four quartz sands with different particle size distributions to measure their thermal conductivities under dry, moist, and fully saturated conditions. In order to study the effect of quartz content on k_{dry}, some data provided by Chen (2008) was used to determine the relationship between k_{dry} and the porosity of dry quartz sands, which is shown in Figure 4-5. The several typical

relationships between k_{dry} and porosity provided by Cote and Konrad (2005), Smith (1942), Kersten (1949), and Johansen (1977) for other soil types, including crushed sands, natural mineral soils, and peat, were also plotted in the same figure. It should be noted that k_{dry} values provided by Kersten (1949) were extrapolated from k_r-S_r relationships, because completely dry soils were not tested in his study.

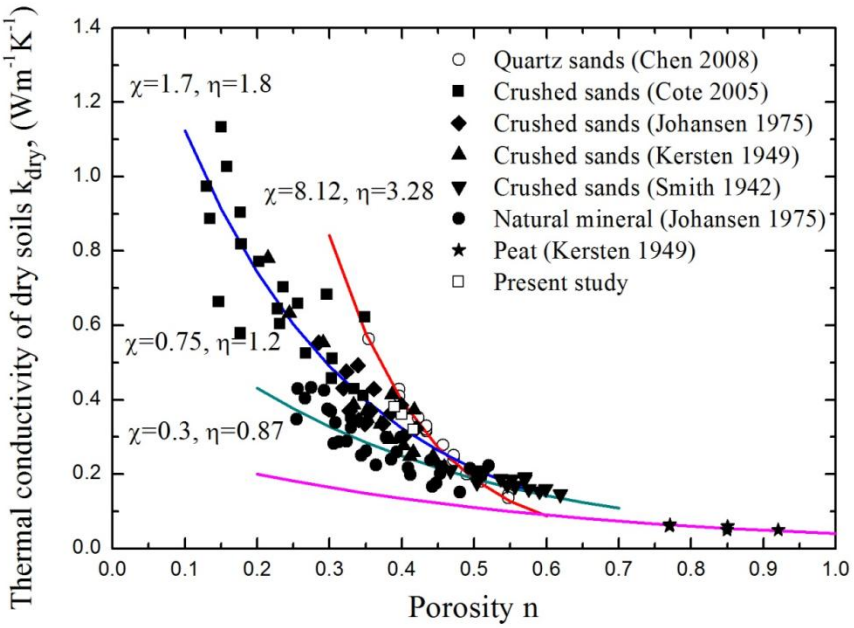

Figure 4-5 k_{dry}-n relationship and determination of χ and η values for quartz sands

Figure 4-5 also shows four different fitting curves and χ and η values with Equation 4.7 for four different soil types. It can be found that all the measured thermal conductivities of dry soils decreased as porosity increased. Heat conduction through physical contacts between solid particles is the main heat transfer mechanism in dry soils. As porosity decreases, more contact is formed, and the thermal conductivity of dry soils becomes higher. For quartz sands, k_{dry} ranges from 0.14-0.56 W $m^{-1}K^{-1}$ for porosities between 0.35 and 0.55. For crushed sands, k_{dry} ranges from about 0.13-1.13 W $m^{-1}K^{-1}$ for porosities between 0.13 and 0.62. For natural mineral soils, k_{dry} is between

0.15 and 0.43 W $m^{-1}K^{-1}$, with porosity ranges from 0.27-0.48. The thermal conductivity of dry peat ranges from about 0.04-0.06 W $m^{-1}K^{-1}$, with porosity ranges from 0.77-0.92. Similar to the k_r-S_r relationship in Figure 4-4, dry quartz sand always has the highest thermal conductivity when compared with other soils within the porosities of 0.35 and 0.55. The best fitting curve for quartz sands was obtained with χ and η values of 8.12 and 3.28, with Equation 4.7. These two values are higher than the suggested values proposed by Cote and Konrad (2005) for fine and medium sands, even much higher than others for silty soils, clayey soils, silts, and clays, as given in Figure 4-5.

Cote and Konrad (2005) collected a large set of data on thermal conductivity of dry soils and grouped them according to the type of dry soil, such as crushed rocks and gravels, natural mineral soils, and organic fibrous soils (i.e., peat). Through the relationship between thermal conductivity of dry soils and porosity, an empirical approach was used to analyze the thermal conductivity data for dry soils. It was concluded that thermal conductivity of dry quartz sands is always much higher than that of other soil types within a range of porosity between 0.35 and 0.55.

This can be explained by the fact that all the sands tested in this study have an extremely high quartz content. Moreover, the thermal conductivity of solid particles in sands, (k_s was about 7.7-8.4 W $m^{-1}K^{-1}$ for quartz sands), is the highest among all soil minerals (De Vries, 1963). k_s was between 1.6-3.4 W $m^{-1}K^{-1}$, as reported by Cote and Konrad (2005), and ranged from 2.5-3.0 W $m^{-1}K^{-1}$, as reported by Smith (1942) for crushed sands. In Kersten (1949) and Johansen (1977) studies, k_s was calculated from the mineral component, which is between 2.7 and 4.3 W $m^{-1}K^{-1}$. For natural mineral soils, Johansen (1977) reported that the estimated value of k_s equals 2.7-5.9 W $m^{-1}K^{-1}$. An average thermal conductivity value of 0.25 W $m^{-1}K^{-1}$ is generally assigned to peat solid particles.

Based on the previous discussion, new values of 6.0, 8.12, and 3.28 for κ, χ and η, respectively, were adopted in the improved thermal conductivity prediction model for quartz sands. Figure 4-6 shows the relationship between measured thermal conductivity and the degree of saturation. Predicted thermal conductivity from the improved model and other models was also depicted in the same figure. Material properties used in the models are given in Table 4-1. It was noted that were some variations in values quoted for the thermal conductivity of quartz. This value ranged between 4 W $m^{-1}K^{-1}$ (Donazzi et al., 1979) and 8.4 W $m^{-1}K^{-1}$ (De Vries, 1963). Considering the large amount of quartz existing in the three test sands, 7.5 W $m^{-1}K^{-1}$ (Chen, 2008) was used as the thermal conductivity of solid particles in all of the models. The average porosities of ASTM-graded sand, brown sand, and Ottawa 20/30 sand samples are 0.43, 0.39, and 0.39, respectively. Thus, the average porosity of 0.40 was used in all the model predictions. It is obvious that all of the other models underestimated the thermal conductivity when compared with experimental data, because the effect of the high quartz content on thermal conductivity is significant and results in the relatively high overall thermal conductivity. The improved model can certainly show the best agreement with the experimental data.

Table 4-1 Materials properties used in the model prediction

Material	Thermal conductivity W $m^{-1}K^{-1}$	References
Soil solid (quartz)	7.5	Chen (2008)
Water (1bar, 300K)	0.61	
Air (1 bar, 300K)	0.026	Stephan and Laesecke (1985)

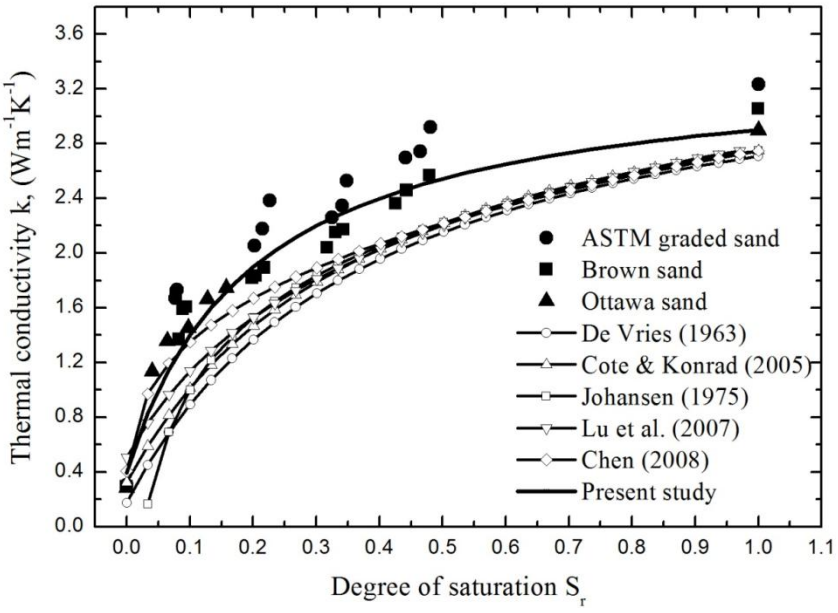

Figure 4-6 Comparison of prediction models with experimental data for n=0.40

A comparison between experimental data and predicted values of thermal conductivity of quartz sands is shown in Figure 4-7. By the linear regression analysis passing through the original point, all of the models provided a reasonable fit to the trend of data. However, the improved model gave the maximum gradient of 0.95, the largest R^2 value of 0.99, and the smallest standard error of 0.012, as given in Table 4-2. In order to evaluate the performance of the improved model on other soil types, measured thermal conductivity of clay loams, silt loams, and sandy soils provided by Lu et al. (2007) and quartz sands from Chen (2008) study were also collected and plotted against predicted values from the improved model, as shown in Figure 4-8. The improved model predicted the thermal conductivity of quartz sands within a reasonable deviation of 15%, but overestimated thermal conductivity of other types of soils containing less quartz content.

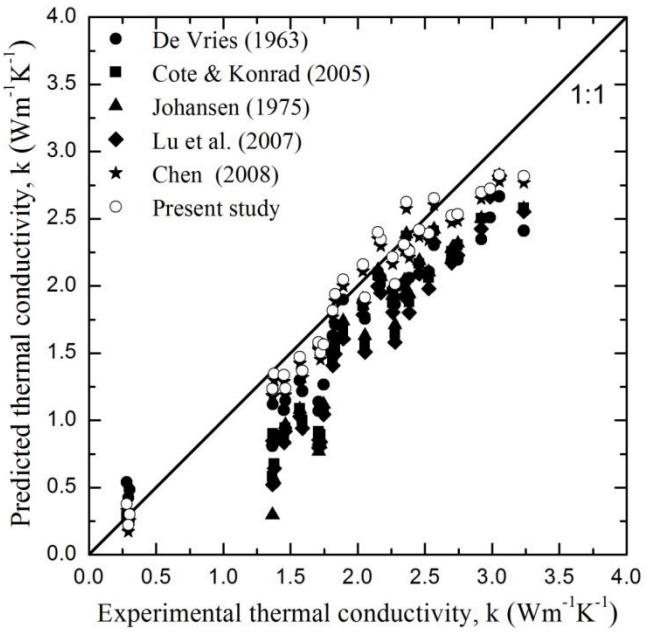

Figure 4-7 Comparison between experimental data and predicted values

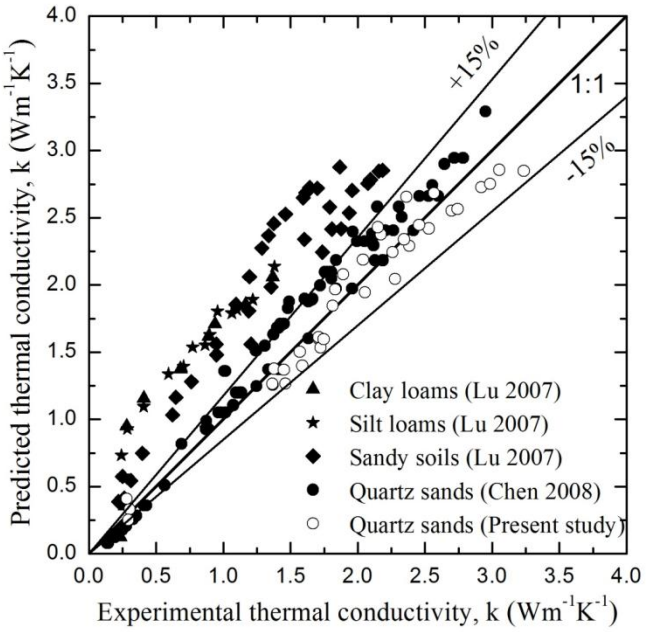

Figure 4-8 Comparison between published experimental data and predicted values

Table 4-2 Summary of linear regression analysis (Zhang et al., 2015a)

Model	Gradient	R^2	Standard error $W\ m^{-1}K^{-1}$
De Vries (1963)	0.82	0.98	0.019
Cote and Konrad (2005)	0.80	0.97	0.024
Johansen (1977)	0.80	0.96	0.028
Lu et al. (2007)	0.75	0.97	0.025
Chen (2008)	0.89	0.99	0.017
Present study	0.93	0.99	0.015

In order to further compare the performance of these thermal conductivity prediction models, root mean square error analysis (RMSE) was also performed in this study. The equation is as follows:

$$RMSE = \sqrt{\frac{1}{n}\sum_{1}^{n}\left[\frac{k_{\exp} - k_{model}}{k_{\exp}}\right]^2} \tag{4.8}$$

where k_{exp} is the measured thermal conductivity from the thermo-TDR method, k_{model} is the corresponding thermal conductivity from prediction model, and n is the number of sand samples. The RMSE analysis was separated by the sand type and degree of saturation including dry, moist, and fully saturated conditions. The summary of the RMSE analysis is given in Table 4-3.

From the RMSE analysis, the prediction accuracy of thermal conductivity for quartz sands was significantly increased by using the improved model rather than the other models, except for the Chen (2008) model which also performed well for quartz sands under moist conditions. This is probably because Chen (2008) also used similar quartz sands and the thermal probe method to perform the experiment, and he developed the model based on the curve fitting to test data. Cote and Konrad (2005)

model exhibited the best performance for dry sands, and the improved model showed the highest prediction accuracy for saturated sands (Zhang et al., 2015a).

Table 4-3 Summary of RMSE analyses (Zhang et al., 2015a)

Name	Degree of saturation S_r	De Vries (1963)	Cote and Konrad (2005)	Johansen (1977)	Lu et al. (2007)	Chen (2008)	Improved model
ASTM graded sand	$S_r=0$	0.788	0.023			0.289	0.178
	$0<S_r<1$	0.232	0.297	0.305	0.331	0.166	0.162
	$S_r=1$	0.259	0.195	0.220	0.218	0.217	0.187
Brown sand	$S_r=0$	0.635	0.119			0.042	0.091
	$0<S_r<1$	0.119	0.192	0.199	0.217	0.109	0.061
	$S_r=1$	0.132	0.081	0.081	0.081	0.079	0.078
Ottawa sand	$S_r=0$	1.109	0.209			0.662	0.534
	$0<S_r<1$	0.288	0.440	0.588	0.462	0.273	0.248
	$S_r=1$	0.162	0.103	0.115	0.131	0.111	0.091

Notes: Johansen (1977) and Lu et al. (2007) model cannot be applied to dry soils

4.3 Laboratory Experiment on Sand-Sand Mixtures

The particle size and particle size distribution of soils are important factors controlling soil thermal conductivity property (Beziat et al., 1992; Brigaud et al., 1990; Griffiths et al., 1992; Jones and Pascal, 1994; and McKenna et al., 1996). Midttømme and Roaldset (1998) proposed that the particle size effect is a much more prominent on thermal conductivity property for fine-grained soils than for coarse-grained soils. The effect of particle size on thermal conductivity is mainly related to the change in number of physical contact points among soil particles (McGaw, 1969). Incropera (2011) found that the thermal resistance of soils comes more from the particle contact area than from particles themselves. Therefore, the reduction of particles size, resulting in more contact area, leads to a decrease in thermal conductivity. McGaw (1969) and Griffiths et al.

(1992) explained this by attributing the reduction in heat flow to an increased number of particle contact points by thin fluid films among particles.

The thermal conductivity of sand-sand mixtures was measured by the thermo-TDR probe. Mixed sand samples were prepared and tested for analyzing and addressing the effects of both particle size and the fines content on the sand thermal conductivity property.

4.3.1 Materials and Methods

The laboratory tests were performed on three typical sands with extremely high quartz contents. They include Silica 12/20 sand, Ottawa 20/30 sand, and ASTM-graded sand. Silica 12/20 sand is a coarse sand with brown color; both Ottawa 20/30 sand and ASTM-graded sand are the same sands as those described in Chapter 3. Figure 4-9 shows the particle size distributions of the three test sands. Figure 4-10 shows the photo of Silica 12/20 sand. The d_{50} of the Silica sand, Ottawa 20/30 sand and ASTM-graded sand are 1.029 mm, 0.783 mm and 0.362 mm, respectively. Thus, it can be stated that the ASTM-graded sand is the finest sand, Silica 12/20 sand is the coarsest sand, and Ottawa 20/30 sand is the medium one between them.

Laboratory tests were conducted on both pure sands and mixed sands as per the experimental program that is presented in Table 4-4. Nos. 1-3 refer to the thermal conductivity tests on pure Silica 12/20 sand, Ottawa 20/30 sand, and ASTM-graded sand, respectively. There were three different combinations for mixed sands, which are characterized as No. 4-6 (i.e., Silica-Ottawa mixtures), No. 7-9 (i.e., Ottawa-ASTM mixtures) and No. 10-12 (i.e., Silica-ASTM mixtures). For each mixed sand, the fine sand was mixed at a fraction of 30%, 50% to 70% by weight. The target moisture contents for all sand samples were prepared at 0%, 1%, 2%, 3%, 4% and 5%, respectively. The following procedures were followed for specimen preparation: (1) Dry sands with known

weight were mixed thoroughly with deionized water and poured into a plastic cylinder mold with a diameter of 67.7 mm and height of 47.5 mm. (2) Sand samples were compacted to obtain uniform moisture distribution. (3) The thermo-TDR probe was then inserted into the center of the sand samples from the top surface. (4) A current of 0.15 amps was applied for 15 s to heat the sands, and the temperatures at center probe and outer probe were recorded during this heating and following cooling process. (5) A few sand samples were tested with oven drying for moisture content measurements. (6) Thermal conductivities of sand samples were analyzed and calculated from the above mentioned recorded temperature records (Zhang et al., 2015b). The experimental setup and the method to determine soil thermal conductivity were introduced in Chapter 3, as shown in Figure 3-17.

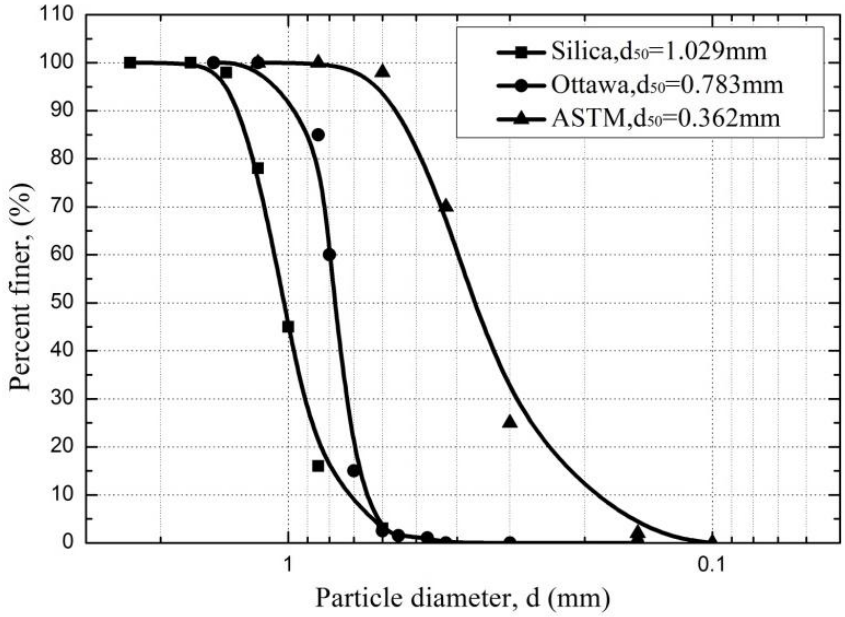

Figure 4-9 Particle size distribution of the three test sands

Figure 4-10 Photo of Silica 12/20 sand

Table 4-4 Experimental program of sand-sand mixtures

No	Content by weight, %			e_{max}	e_{min}	e_{test}
	Silica 12/20	Ottawa 20/30	ASTM graded			
1	100	0	0	0.690	0.572	0.619
2	0	100	0	0.712	0.534	0.682
3	0	0	100	0.717	0.551	0.695
4	70	30	0	0.666	0.527	0.659
5	50	50	0	0.671	0.531	0.665
6	30	70	0	0.678	0.538	0.674
7	0	70	30	0.624	0.484	0.621
8	0	50	50	0.628	0.486	0.610
9	0	30	70	0.626	0.485	0.612
10	70	0	30	0.561	0.434	0.553
11	50	0	50	0.573	0.419	0.571
12	30	0	70	0.581	0.421	0.578

4.3.2 Results and Discussion

4.3.2.1 Thermal Conductivity and Gravimetric Moisture Content

Tthermal conductivity and gravimetric moisture content of three pure sands are shown in Figure 4-11. It was found that thermal conductivity of sands was much higher at moist conditions than at dry conditions, and it increased with moisture content for all sand samples. A slight difference in measured thermal conductivities of the three pure sands at moist conditions can be observed. ASTM-graded sand showed the highest, and Silica 12/20 sand showed the lowest thermal conductivity at all target moisture contents. ASTM-graded sand had the smallest particle size, resulting in the largest specific surface area, thereby the water films and water bridges formed much more easily among sand particles compared with other two coarse sands. The specific surface area effect can be explained by the heat flow barrier arising from the water film coating the water-wet mineral grains (Middttømme et al., 1998). However, the water films and water bridges facilitated the heat transfer process and increased the thermal conductivity. This is because water has higher thermal conductivity than air; therefore, thermal resistance generated at solid-water interface is less than that at solid-air interface, and the existence of water in sands reduces the overall thermal resistance at low moisture conditions. In Figures 4-12, 4-13 and 4-14, it is obvious that the different mixing ratios of fine sands led to different thermal conductivities of mixed sands in the experiments. But the thermal conductivity of Ottawa 20/30-ASTM-graded sand was almost unchanged with fine sands' mixing ratio. This is probably because of the coupling effects of particle size, grain shape, and fines content on thermal conductivity, as will be discussed later.

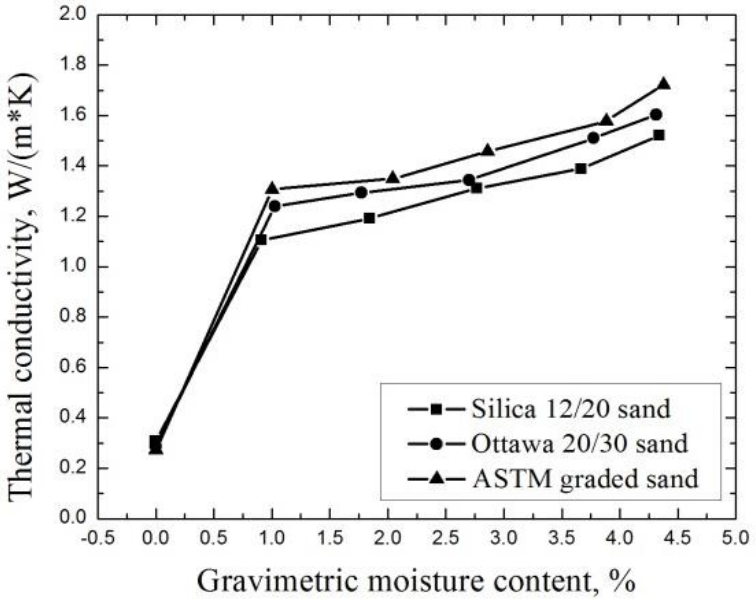

Figure 4-11 Thermal conductivity and moisture content of pure sands

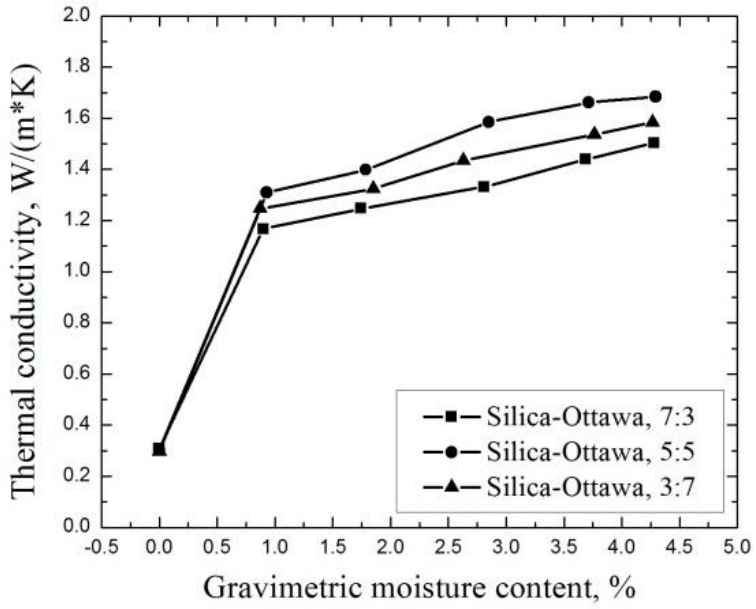

Figure 4-12 Thermal conductivity and moisture content of Silica-Ottawa mixtures

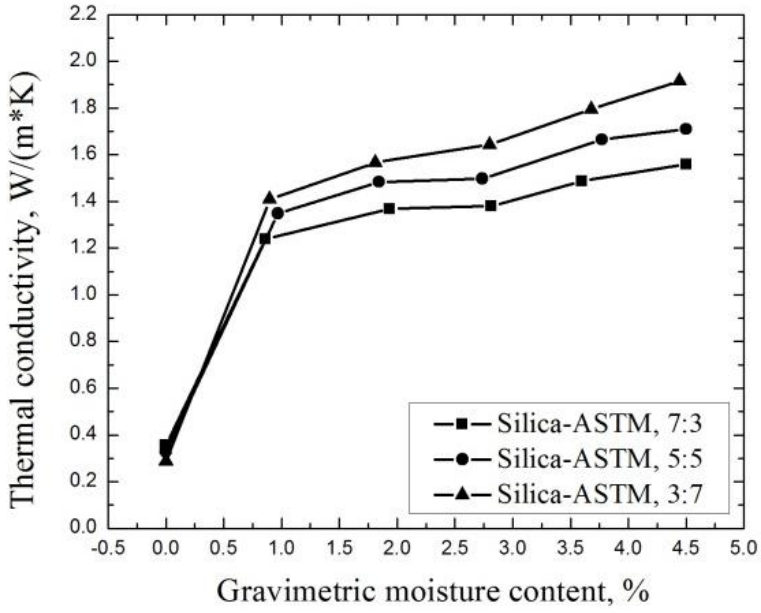

Figure 4-13 Thermal conductivity and moisture content of Silica-ASTM mixtures

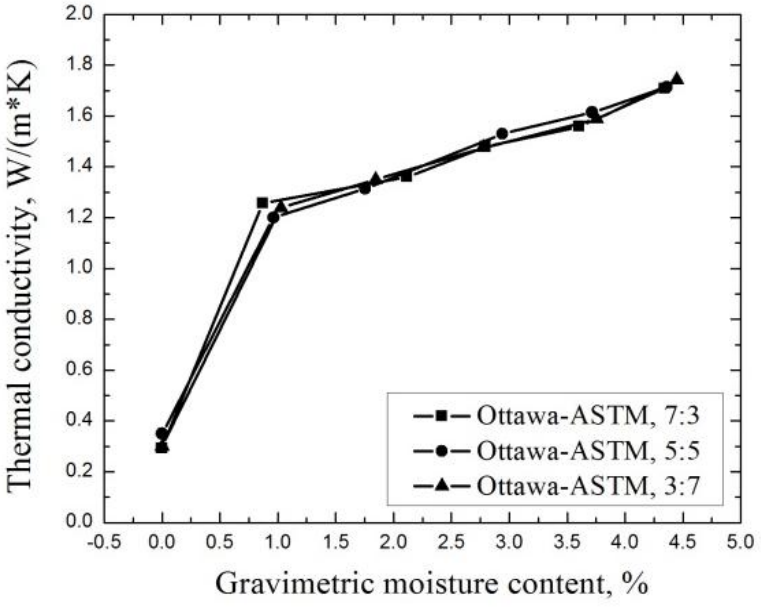

Figure 4-14 Thermal conductivity and moisture content of Ottawa-ASTM mixtures

4.3.2.2 Thermal Conductivity of Dry Sands

Figure 4-15 presents the relationship of thermal conductivity of dry sands and porosity, as derived from this study and from the experimental data provided by Chen (2008). As shown in previous studies, (Chen, 2008; De Vries, 1963, Farouki, 1981; Lu et al., 2007; and Cote and Konrad, 2005), thermal conductivity decreases with increased porosity. Moreover, coarse sands showed lower porosity than fine sands in the experiments. Comparing this study with Chen's (2008) data, it was demonstrated that although the differences in both thermal conductivity and porosity among the three pure sands were very small, thermal conductivity decreases as soil particle size decrease, due to an increase in the number of physical contact points leading to more thermal resistance between soil particles. In addition, using the equation $k_{dry}=\chi 10^{-\eta n}$ provided by Cote and Konrad (2005) to fit all the data as shown in Figure 4-15, it is shown that the best agreement is attained at $\chi=7.7$ and $\eta=3.4$. When porosity equals to zero, the sands are considered as solid material, mainly composed of quartz, and the thermal conductivity of 7.7 W $m^{-1}K^{-1}$ obtained from above equation is almost the same as the actual value of thermal conductivity of pure quartz.

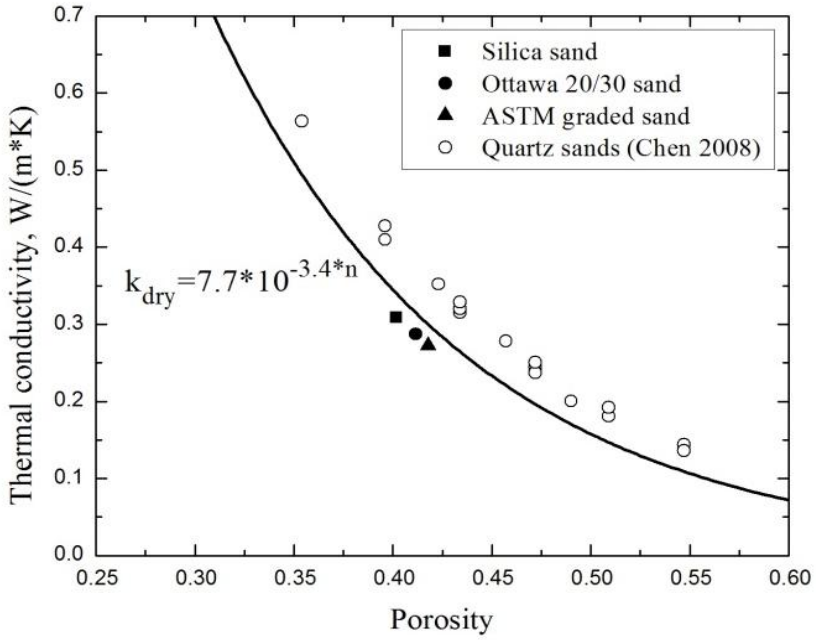

Figure 4-15 Thermal conductivity and porosity of dry sands

Figure 4-16 shows the relationship between porosity, thermal conductivity, and fines content of mixed sands at dry condition. It was found that the thermal conductivity and porosity were almost constant for Silica-Ottawa mixtures because of their relatively large and almost identical particle size, whereas the other two mixed sands showed the obvious maximum thermal conductivity, which corresponds to the minimum porosity. The maximum thermal conductivity was at 30 % fines content for Silica-ASTM mixtures and 50% fines content for Ottawa-ASTM mixtures. Theoretically, the number of physical contact points is supposed to be increased if coarse sands are mixed with fine sands. It also means that the thermal conductivity will be reduced because of the increasing thermal resistance described previously. However, thermal conductivity of mixed sands may be increased at dry condition since the thermal resistance at solid-solid interface (i.e., new physical contact points) is less than that at the original solid-air interface. For example, newly-formed physical contact points provide some new heat flow paths

between sand particles and lower thermal resistance, improving sand thermal conductivity.

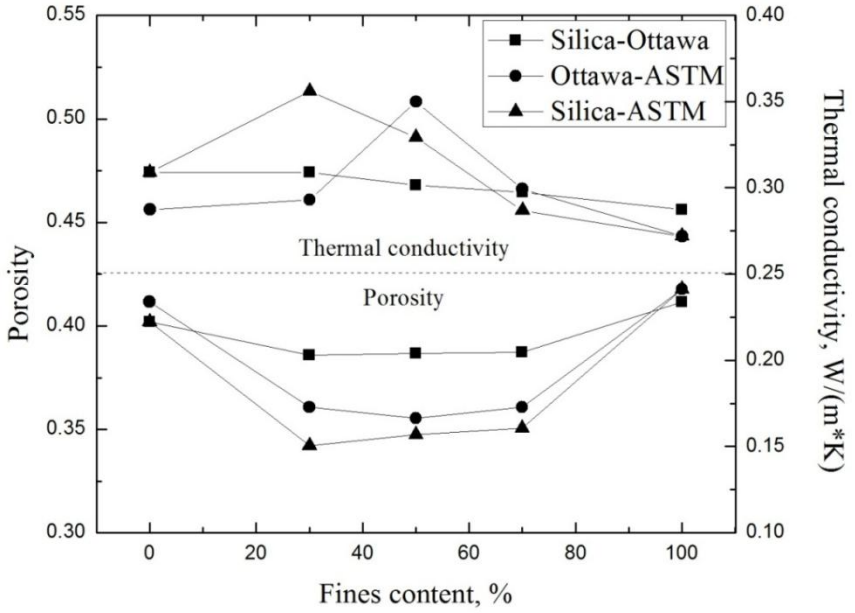

Figure 4-16 Porosity, thermal conductivity of mixed sands and fines content

The schematic of the heat flow path in dry sands was depicted in Figure 4-17 to further explain the heat transfer mechanism in dry sands, considering the particle size effect. There are two horizontal heat flow paths between sand particles, and there is only one physical contact point in heat flow direction, as shown in Figure 4-17 (a). The number of physical contacts is increased continuously, as particle size decreases, and thermal resistance must increase because the contact area is so limited at contact points. In Figure 4-17 (b), the number of horizontal heat flow paths is increased to four if one small particle is embedded into the initial pore. Two more possible inclined heat flow paths passing through this particle may also work to improve the overall thermal conductivity. These four horizontal flow paths are assumed to be unchanged if the small particle is replaced by four even smaller particles; however , more inclined flow paths are formed

and the thermal conductivity should increase further since more physical contact points are generated in this process. Consequently, the particle size effect on thermal conductivity of sands can be classified into two categories: the thermal conductivity decreases as particle size decreases for uniform sands; the thermal conductivity increases due to the occupation of fine particles in sand pores for non-uniform sands.

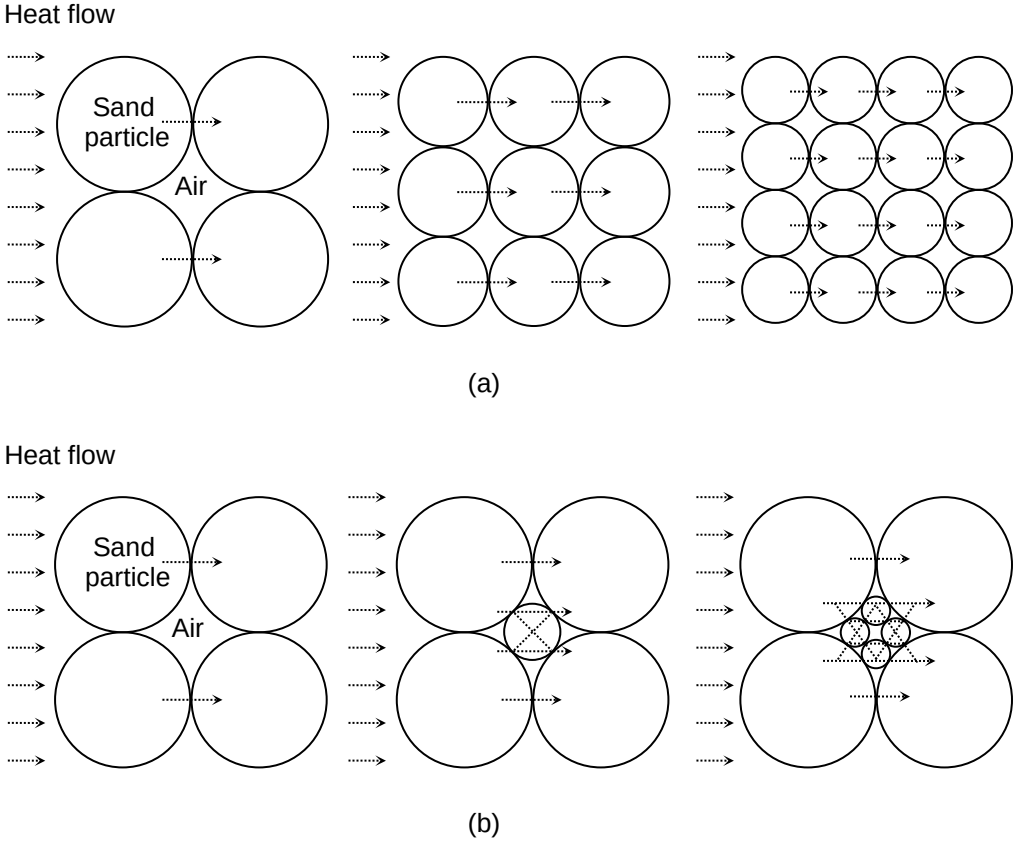

Figure 4-17 Particle size effect on heat flow path in dry sands: (a) pure sands; (b) mixed sands (Zhang et al., 2015b)

4.3.2.3. Fines Content Effect on Thermal Conductivity of Mixed Sands

Figures 4-18, 4-19 and 4-20 show the relationships between thermal conductivity and fines content at different moisture contents for three mixed sands. In Figure 4-18, Ottawa 20/30 sand was considered as fine sand, and thermal conductivity of this mixed

sand increased with fines content up to 50%, but decreased after that. In Figure 4-19, Silica 12/20 sand (the coarsest sand) was mixed with ASTM-graded sand (the finest sand), and the thermal conductivity increased with fines content. The maximum thermal conductivity was attained at 70% fines content. In Figure 4-20, two highly rounded sands, Ottawa 20/30 and ASTM-graded sand, were mixed. The thermal conductivity of this mixed sand did not change too much at different moisture contents. The maximum thermal conductivity of the Ottawa-ASTM mixture appeared at fines content between 50%-70%. It is also obvious that the maximum thermal conductivity appeared at the same fines content for all the moisture contents, leading to the conclusion that the optimum mixing ratio for the maximum thermal conductivity is unique for each mixed sand.

Adding fine sands to coarse sands leads to the recognition that some original pores in coarse sands are occupied by some fine sand particles, and the porosity of the mixture can be reduced to some extent. In the meantime, the number of heat transfer paths passing through sand particles, contact points, and water bridges formed at moist conditions increases. Thus, the real conductivity of mixed sands should increase with fines content and reach the maximum value at the critical fines content (F_{cr}). F_{cr} increased as d_f/d_c (the mean grain size ratio of fine sands to coarse sands) decreased in the experiment, as shown in the figure. The value of F_{cr} is affected by several factors such as d_f/d_c ratio and grain shape. For example, comparing Silica-Ottawa mixtures with Silica-ASTM mixtures, the mixing ratio corresponding to the maximum thermal conductivity increased from 50% to 70%. Since ASTM-graded sand is finer than Ottawa 20/30 sand because of the fines content in the mixture, more fine sands need to fill sand pores to achieve the highest overall thermal conductivity. The reason for almost the same measured thermal conductivity in Ottawa-ASTM mixtures is that both of these two sands

are very fine sands, with extremely high roundness of 0.9+ (shown in Table 3-1). Therefore, mixing Ottawa 20/30 sand with fine sands, i.e., ASTM-graded sand, at different fractions may not influence the overall thermal conductivity very much.

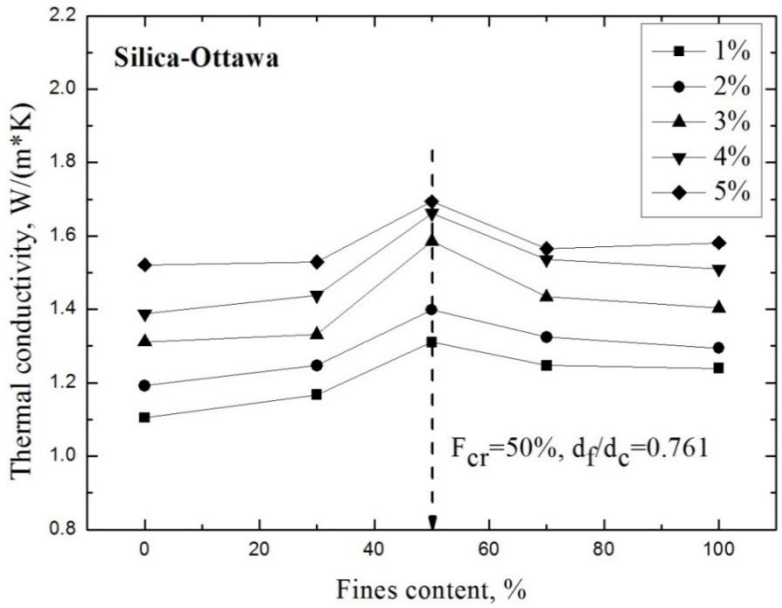

Figure 4-18 Thermal conductivity and fines content of Silica-Ottawa mixtures

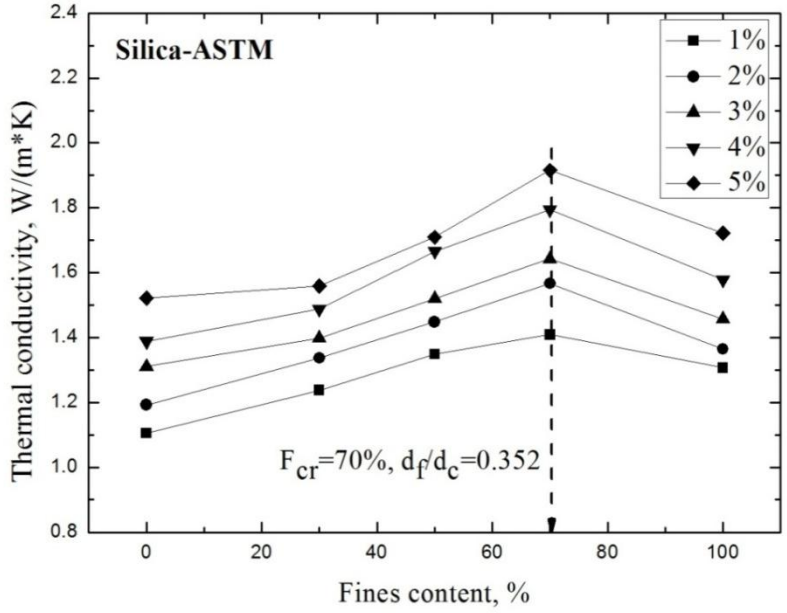

Figure 4-19 Thermal conductivity and fines content of Silica-ASTM mixtures

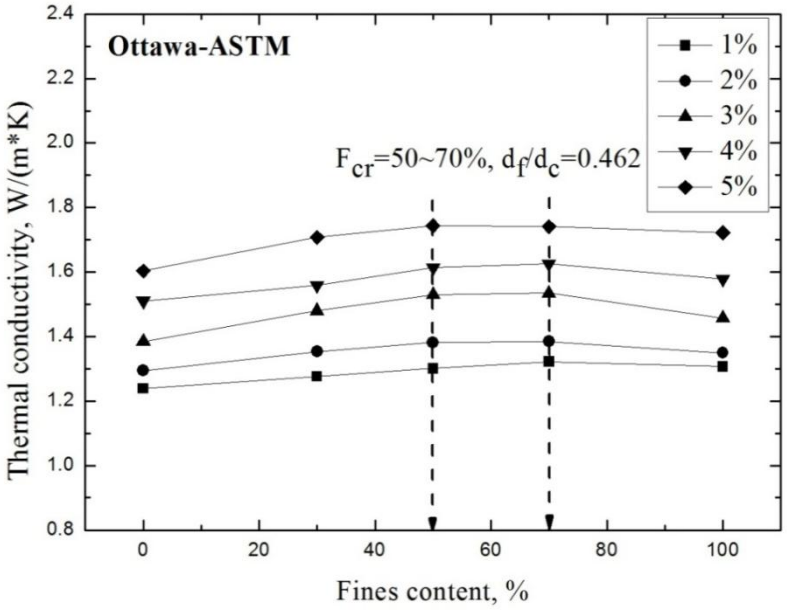

Figure 4-20 Thermal conductivity and fines content of Ottawa-ASTM mixtures

4.4 Laboratory Experiment on Sand-Clay Mixtures

Many studies have been reported regarding the physical and mechanical properties of sand-clay mixtures (Abiodun and Edwin, 2014; Boutin et al., 2011; Chen, 2010; Chiu and Shackelford, 1998; and Marion et al., 1992), but it's difficult to find research on its thermal properties, such as thermal conductivity, diffusivity and heat capacity. In the case of high-level radioactive waste disposal in a deep geological site, highly compacted clay is usually placed in between the containers and the surrounding rock as engineered barriers or buffers to remove the heat coming from the thermal power generated by the radioactive decay of the nuclear waste. The aim of employing engineered barriers is to isolate the waste from the biosphere, contain the radionuclides associated with the waste, and prevent them from being released to the surface environment that could harm to life and the environment.

The influence factors of soil thermal conductivity can be divided into two categories: environmental factors, i.e., compaction moisture contents and dry density; and compositional factors, i.e., mineralogy components, soil fabric, and gradation. As reported in published literatures (De Vries, 1963; Johansen, 1977; Farouki, 1981; and Cote and Konrad, 2005), soil thermal conductivity increases with moisture content because of the higher thermal conductivity of water compared with that of air as soil pore fluid. In addition, the elevated soil dry density leads to an increase in the number of interparticle physical contact points and a reduction of thermal resistance among soil particles, thereby increasing the thermal conductivity. The effect of mineralogy components on soil thermal conductivity has not been studied systematically in the past several decades. Tarnawski et al. (2009) assessed the impact of quartz content on the prediction of soil thermal conductivity. The thermal conductivity of quartz is around 7.7-8.4 W $m^{-1}K^{-1}$, which is the highest among all the soil minerals. Thus, sand or sandy soils

which are composed of quartz always have higher thermal conductivity than clayed soils or clay. It is also necessary to study the effect of clay content on soil thermal conductivity because such effect must be considered in some geothermal applications, such as borehole thermal energy storage (BTES) and deep geological repository of high-level radioactive waste (HLRW), which require engineering soils with relatively low thermal conductivity values.

This section will present the laboratory experimental study, using the thermo-TDR probe, on thermal conductivity of sand-kaolin clay mixtures. Five alternative soil thermal conductivity models (Johansen, 1977; Cote and Konrad, 2005; Lu et al., 2007; Chen, 2008, and Zhang et al., 2015a) were selected to predict thermal conductivity of sand-kaolin clay mixtures and to provide a comparison with experiment results. Improved models were also presented to consider the continuous change of thermal conductivity of mixtures as clay content varies.

4.4.1 Materials and Methods

Laboratory experiments were performed on pure quartz sand, kaolin clay, and sand-kaolin clay mixtures. The sand was the ASTM-graded sand as described in Chapter 3. The sand content was assumed to be the same as the quartz content in soil samples because it contained over 99% quartz. The kaolin clay was mainly composed of anhydrous aluminum silicate, and its thermal conductivity was around 2.9 W $m^{-1}K^{-1}$ (Lee et al., 2012). The sand was mixed with kaolin clay in different proportions, with clay content ranging from 5%, 10%, 20% to 30% by dry weight, as is presented in Table 4-5. Pure quartz sand and kaolin clay were also tested in the experiments to determine the upper and lower bounds of thermal conductivity of sand-kaolin clay mixtures. The gradation curves of sand (S), kaolin clay (K), and sand-kaolin clay mixtures are shown in Figure 4-21. The photos of sand and kaolin clay are shown in Figure 4.22.

Table 4-5 Experimental program of sand-clay mixtures

	No	1	2	3	4	G_s
Content by dry weight, (%)	Sand	100	95	90	0	2.65
	Kaolin	0	5	10	20	2.58
Target moisture content (%)		0, 3, 5, 7				
Target dry density (g/cm^3)		1.55, 1.60, 1.65				

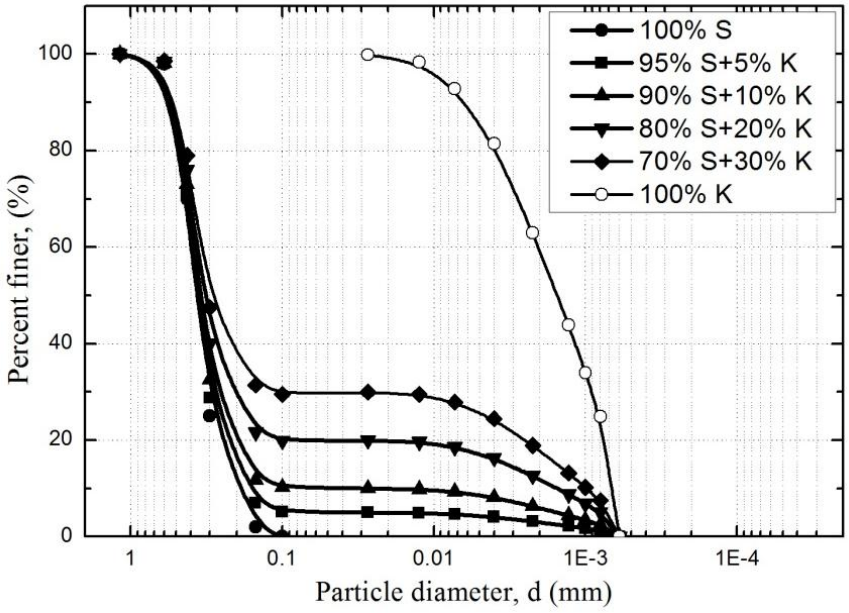

Figure 4-21 Gradation curves of sand (S), kaolin clay (K), and sand-kaolin clay mixtures

(a) (b)

Figure 4-22 The photos of sand and kaolin clay: (a) Sand, (b) Kaolin clay

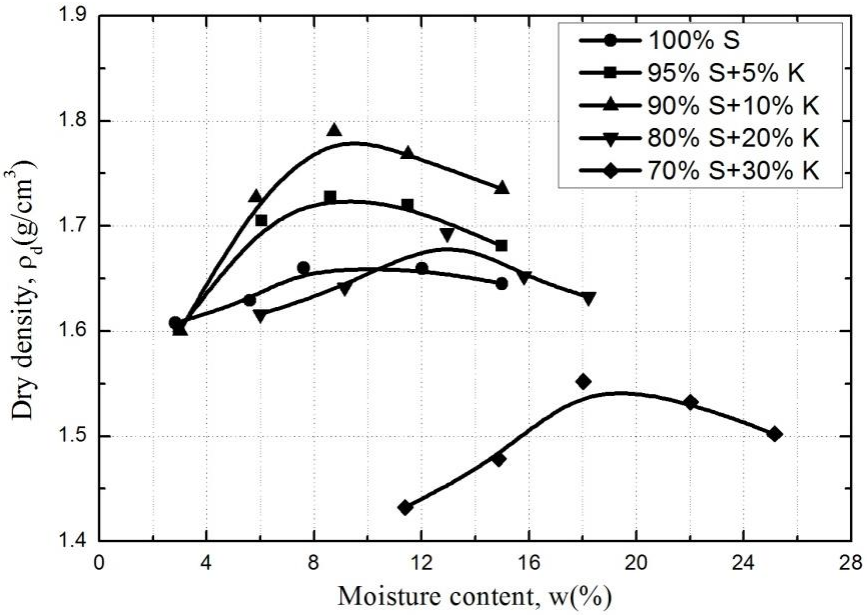

Figure 4-23 Compaction curves of sand (S) and sand-kaolin clay mixtures (ASTM D698)

Soil samples were prepared at different porosities and degrees of saturation according to the corresponding compaction curves (shown in Figure 4-23) obtained from standard compaction tests (ASTM D698). From Figure 4-23, it is found that the maximum

dry density increased with an increase in clay content from 0 % to 10 % and decreased when clay content was greater than 10 %. For 70% (S)+30% (K) mixture, the maximum dry density reached the lowest level, and the corresponding optimum moisture content reached the highest level compared with other mixtures. Accordingly, the target dry density and degree of saturation in the experiments are presented in Table 4-6. Test methods and sample preparation procedures will be presented in the following section.

The following procedures were followed for sample preparation: (1) Dry sand and kaolin clay with known weight were mixed thoroughly with deionized water and poured into a PVC mold with a diameter of 67.7 mm and height of 47.5 mm. (2) Soil samples were compacted to obtain the target dry densities and degrees of saturation. (3) The thermo-TDR probe was then inserted into the center of the samples, from the top surface. (4) A current of 0.15 amps was applied for 15 s to heat the samples, and temperatures at the center probe and two outer probes were recorded during this heating and following cooling processes, (5) A few soil samples were tested by the oven drying method for actual moisture content measurements. (6) Thermal conductivity of soil samples was analyzed and calculated from the above recorded temperature records. The experimental setup and the method to determine soil thermal conductivity were described in Chapter 3.

4.4.2 Results and Discussion

Figures 4-24, 4-25, 4-26, and 4-27 show the thermal conductivity and gravimetric moisture content at different dry densities for different clay contents. Clay content is denoted by “c” in the figure. It is indicated that the thermal conductivity of sand-kaolin clay mixtures increased with moisture content for all the soil specimens. This is mainly because of the higher thermal conductivity of water, compared with that of air, as soil pore fluid. The elevated dry density leads to an increase in number of interparticle physical contact points, a reduction of thermal resistance among soil particles, and then

an improvement of soil thermal conductivity. Comparing with moisture content, dry density effect on thermal conductivity is not dominant. Another feature is that the increments of thermal conductivity at low moisture content (i.e., from 0% to 3%) for pure sand (i.e., c=0%) was much greater than those for c=5%, 10% and 20%. In addition, thermal conductivity of mixtures was almost linearly increased with moisture content for both c=10% and 20%.

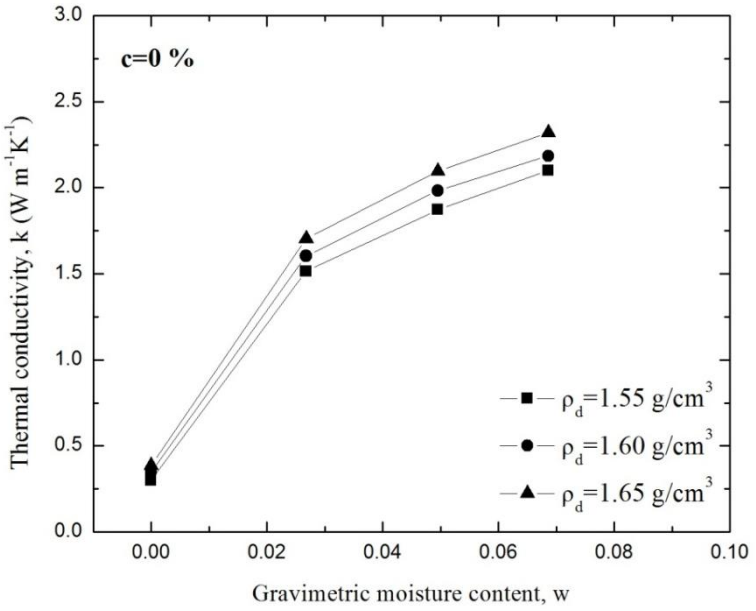

Figure 4-24 Thermal conductivity and moisture content at c=0%

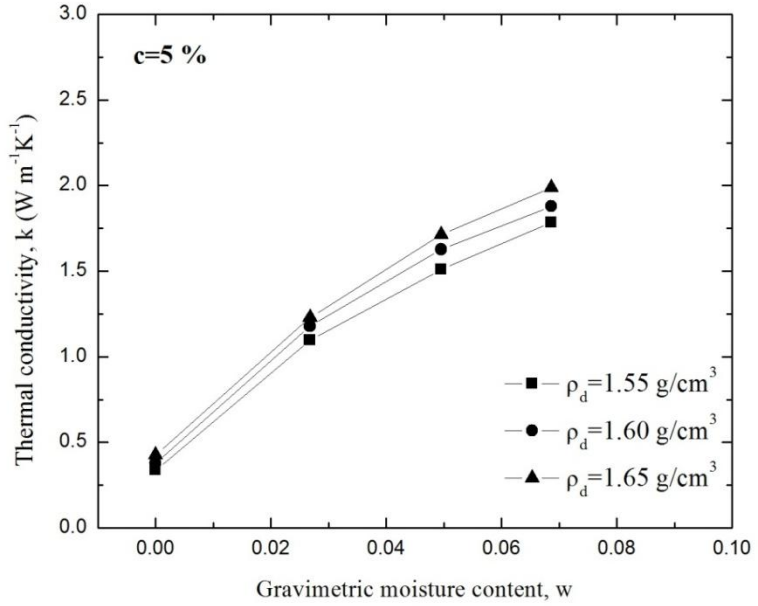

Figure 4-25 Thermal conductivity and moisture content at c=5%

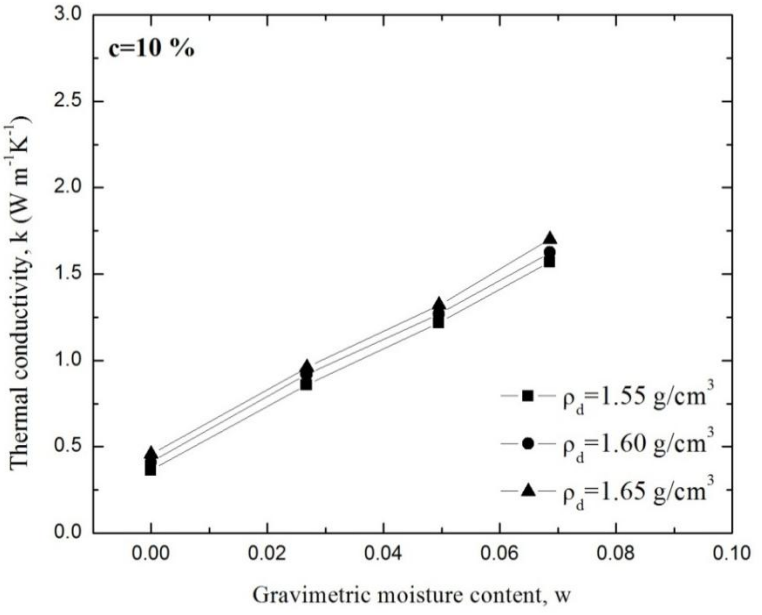

Figure 4-26 Thermal conductivity and moisture content at c=10%

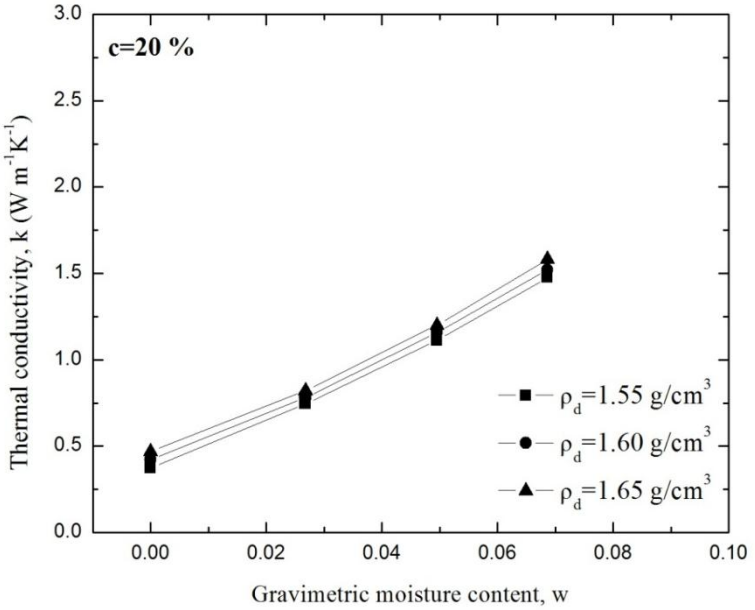

Figure 4-27 Thermal conductivity and moisture content at c=20%

Figure 4-28 shows the relationships between thermal conductivity and clay content under dry condition. It was found that thermal conductivity of sand-kaolin clay mixtures increased with clay content under dry condition by three bilinear relationships, with inflection points observed at c=10%. It is also indicated that the increase in thermal conductivity in the first stage, from c=0% to c=10%, was about 0.08 W $m^{-1}K^{-1}$ for all dry density conditions, and this increment was slightly greater than that in the second stage, which was around 0.01 W $m^{-1}K^{-1}$ from c=10% to c=20%. Furthermore, the thermal conductivity also increased with dry density at each clay content, but the increment was only 0.05 W $m^{-1}K^{-1}$ between any two neighboring target dry densities.

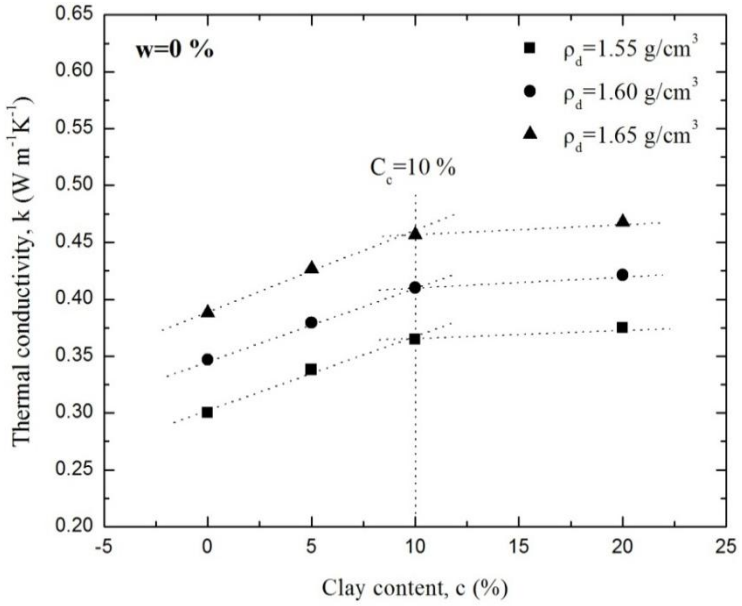

Figure 4-28 Thermal conductivity and clay content of dry mixtures

Figures 4-29, 4-30 and 4-31 show the relationships between thermal conductivity and clay content under moist conditions. It is obvious that thermal conductivity decreased with clay content under experimental moisture conditions. Similarly, the variations of thermal conductivity with clay content also had two different stages, with a limited clay content of 10%, which is the same as that under dry condition, shown in Figure 4-28. In both of two stages, thermal conductivities were linearly changed with clay content. However, the reduction of thermal conductivity in the first stage (i.e., c<10%) was much greater than that in the second stage (i.e. c>10%).

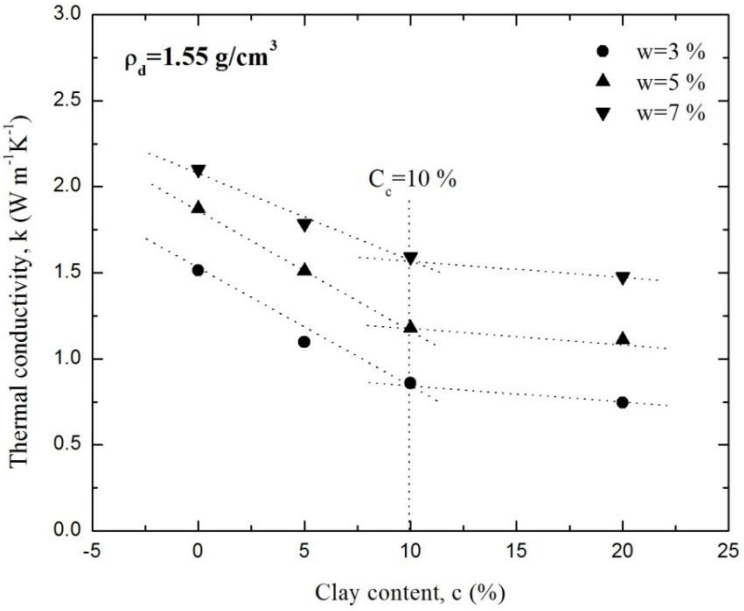

Figure 4-29 Thermal conductivity and clay content at ρ_d=1.55 g/cm^3

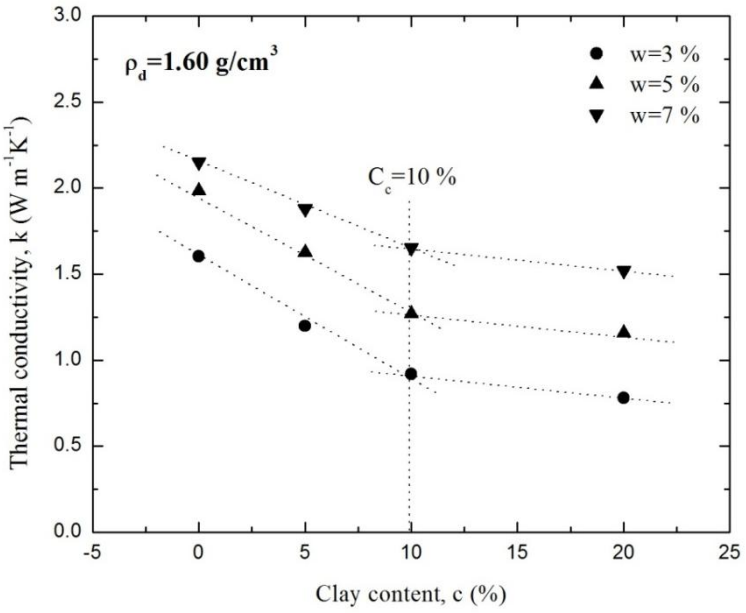

Figure 4-30 Thermal conductivity and clay content at ρ_d=1.60 g/cm^3

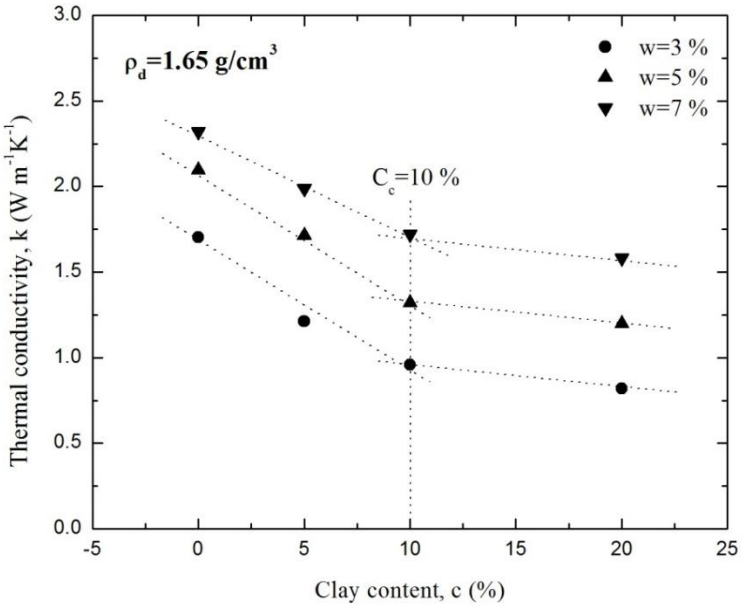

Figure 4-31 Thermal conductivity and clay content at ρ_d=1.65 g/cm^3

The micro-geometrical arrangement of sand, clay, and sand-clay mixtures with different clay contents and dry densities (i.e., degree of compaction) was studied by (Knoll and Knight, 1994). At low clay contents, clay particles fit the pore space of a sand pack. This sort of geometry naturally occurs when the volume fraction of porous clay (C_p) is less than the inherent porosity of the sand pack (n_s). The porosity of sand-clay mixtures decreases as the clay content increases, to fill the pore space of sands. However, at high clay contents, when C_p is greater than n_s, the micro-geometrical arrangement changes. Clay particles form a new soil matrix, and sand particles are disconnected from each other. In this clay content range (i.e., C_p>n_s), the porosity of sand-clay mixtures increases as clay content increases since microporous packets of clay are replacing zero-porosity sand grains (Knoll and Knight, 1994; Marion et al., 1992). Thus, there is a limit to the clay content existing in sand-clay mixtures that can distinguish above two different micro-

geometrical arrangements (i.e., $C_p<n_s$ and $C_p>n_s$) and it is defined as "critical clay content (C_c)," which equals 10% in this study, as discussed previously.

4.4.2.1 Microstructure of Sand-clay Mixtures and Critical Clay Content (C_c)

Figure 4-32 shows the micro-geometrical arrangement of components assumed in sand, clay, and sand-clay mixtures with different clay contents and dry densities (i.e., degree of compaction). At low clay contents, clay particles fit the pore space of a sand pack. This sort of geometry naturally occurs when the volume fraction of porous clay is less than the inherent porosity of the sand pack. The porosity of sand-clay mixtures decreases as the clay content increases to fill the pore space of sands, and the porosity is calculated according to the equation given below:

$$n = n_s - C_p(1-n_c) \qquad \text{for} \quad C_p < n_s \tag{4.9}$$

where n_s is the inherent porosity of sand pack; C_p is the volume fraction of porous clay; n_s is the inherent porosity of clay at a given level of compaction.

As clay content increases, when C_p equals n_s, the porosity is calculated by,

$$n = n_s n_c = C_p n_c \qquad \text{for} \quad C_p = n_s \tag{4.10}$$

At high clay contents, when C_p is greater than n_s, the micro-geometrical arrangement will be changed in the mixtures. Clay particles form a new soil matrix, and sand particles are disconnected from each other. In this clay content range (i.e., $C_p>n_s$), the porosity of sand-clay mixtures increases as the clay content increases since microporous packets of clay are replacing zero-porosity sand grains (Marion et al., 1992; and Knoll and Knight, 1994). The porosity is calculated by,

$$n = C_p n_c \qquad \text{for} \quad C_p > n_s \tag{4.11}$$

Thus, there is a limit clay content existing in sand-clay mixtures that can distinguish the two different micro-geometrical arrangements (i.e., $C_p<n_s$ and $C_p>n_s$), and it is defined as "critical clay content (C_c)" in this study.

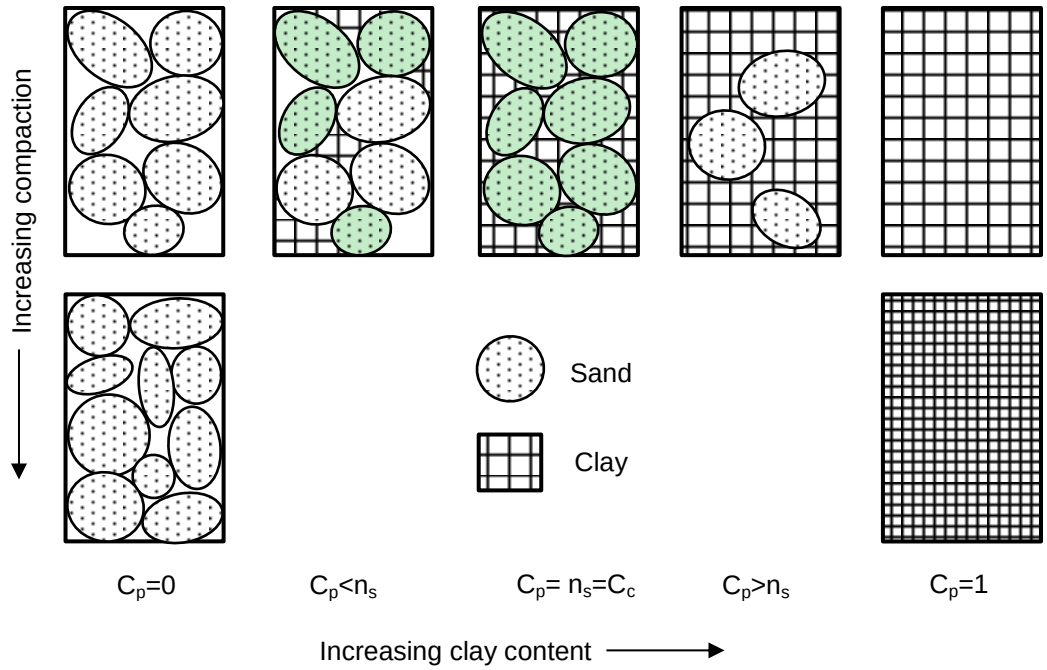

Figure 4-32 Conceptual diagram of packing geometries for sand, clay, and sand-clay mixtures in terms of experimental parameters: dry density (or degree of compaction); porous clay fraction (C_p) and sand porosity (n_s)

Calculate the values of C_p and n_s of sand-clay mixtures at each clay content and dry density to plot the relationships between C_p/n_s and clay content, as shown in Figure 4-33. In the calculation, the bulk density of clay was assumed as 0.368 g/cm^3, which was provided by the manufacturer, and it was found that the degree of saturation of sand-clay mixtures had no effect on the calculated C_p and n_s values. In Figure 4-33, it is indicated that C_p/n_s was almost linearly increased with clay content. At all clay contents, higher dry density led to higher C_p/n_s values, because C_p increases but n_s decreases with an increase in dry density of mixtures. Moreover, three C_p/n_s values at c=10% were very

close to unit, which also means that the volume fraction of porous clay was almost equal to the sand porosity at this clay content and exactly matched the limit clay content (i.e., c=10%) described in the previous sections. As a result, the limit clay content (i.e. c=10%) is identical to the critical clay content C_c in Figure 4-22, which equals 10 % for sand-clay mixtures in this study.

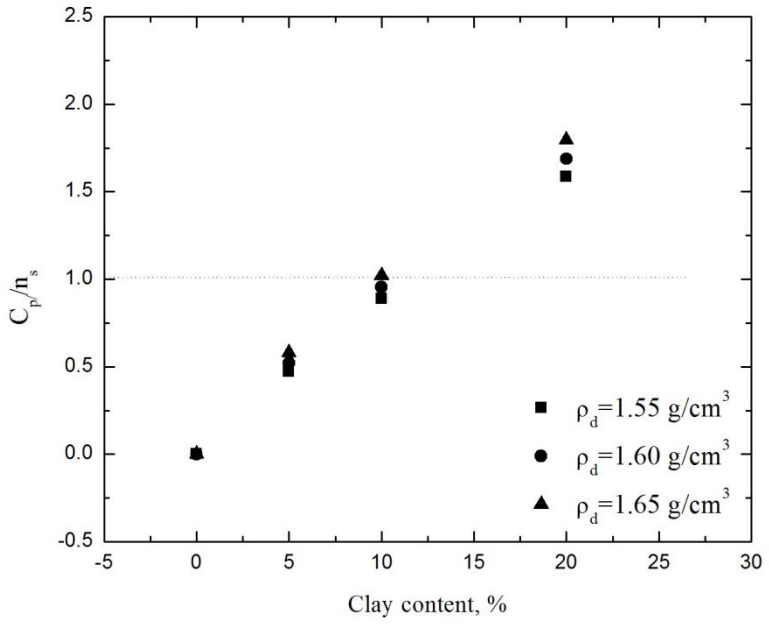

Figure 4-33 Relationships between C_p/n_s and clay content at different dry densities

4.4.2.2 Porosity of Sand-Clay Mixtures

Pore volume of a mixture of coarse and fine particles has been quantified by many authors, including McGeary, 1961, and there are numerous notations that have generally not been used in geophysics. Marion et al. (1992) performed a series of experiments on sand-clay mixtures to investigate the porosity of mixtures and proposed a porosity model. In accordance with his study, the volume fraction of porous clay must be converted into clay weight fraction in order to compare the model with experimental data. Clay weight fraction w_c is defined as the ratio of the mass of the dry clay to the mass of

the dry sand-clay mixture, which ranges from 0%, 5%, 10%, 15% to 20% in this study. w_c is calculated by the following equations,

$$w_c = \frac{C_p(1-n_c)\rho_c}{C_p(1-n_c)\rho_c + (1-n_s)\rho_s} \quad \text{for} \quad C_p < n_s \qquad (4.12)$$

$$w_c = \frac{C_p(1-n_c)\rho_c}{C_p(1-n_c)\rho_c + (1-C_p)\rho_s} \quad \text{for} \quad C_p > n_s \qquad (4.13)$$

where ρ_c and ρ_s are the specific gravity of clay and sands, respectively. It should be noted that n_s and n_c in Equations 4.9-4.13 are dependent on the dry density (i.e., degree of compaction) of sand-clay mixtures. According to the relation: $n=1-\rho_d/\rho_s$ (ρ_s is the specific gravity of soils), the theoretical values of n_s and n_c at different experimental dry densities, i.e., 1.55 g/cm^3, 1.60 g/cm^3, 1.65 g/cm^3 are presented in Table 4-6.

Table 4-6 Theoretical values of n_s and n_c at different dry densities

ρ_d (g/cm^3)	n_s	n_c
1.55	0.415	0.399
1.60	0.396	0.380
1.65	0.377	0.360

Thus, the porosities of sand-clay mixtures can be predicted based on Equations (6)-(10) and theoretical values of n_s and n_c in Table 4-6. The prediction of porosity from Marion's 1992 model and experimental data from dry sand-clay mixtures are shown in Figure 4-34. It is indicated that the porosities were decreased to minimum values (i.e., 0.403 at ρ_d=1.55 g/cm^3, 0.380 at ρ_d=1.60 g/cm^3 and 0.354 at ρ_d=1.65 g/cm^3) at c=10% and then increased after that with clay content. As discussed in the previous sections, the porosity is supposed to be at the lowest level at critical clay content (i.e. C_c=10%); thereby, the relationships between the porosity and clay content from experiments were

also consistent with previous theoretical analyses, as shown in Figure 4-32 and experimental results as shown in Figure 4-33. In contrast, the predicted porosities exhibited the same trend with clay content, but the lowest porosities (i.e., 0.166 at ρ_d=1.55 g/cm^3, 0.151 at ρ_d=1.60 g/cm^3 and 0.136 at ρ_d=1.65 g/cm^3) were much smaller and the corresponding critical contents (i.e., 29.3%, 28.4% and 27.4%) were much higher than the experimental values. Another feature is that the model always underestimated the porosity in the experimental clay content range.

The differences between the predicted results and the experimental data in Figure 4-34 are attributed primarily to the following reasons. (1) In the model prediction, the assumption is made that the addition of clay particles to sand packing will not disturb the original sand lattice. However, this assumption is not valid for either very low or very high clay content (Marion et al., 1992). In addition, each component is expected to disturb the original packing of other components to some extent for intermediate clay contents (McGeary, 1961). (2) The expansion of clay particles located between sand grains will induce an increase in porosity of sand-clay mixtures. (3) The theoretical values of inherent porosity of clay n_c in the model prediction are much smaller than the actual values in the experiments due to the considerable expansion of clay particles in practice, particularly at high clay contents. This also explains the fact that the difference between the model prediction and the experimental data increased as clay content increased, as shown in the Figure 4-34.

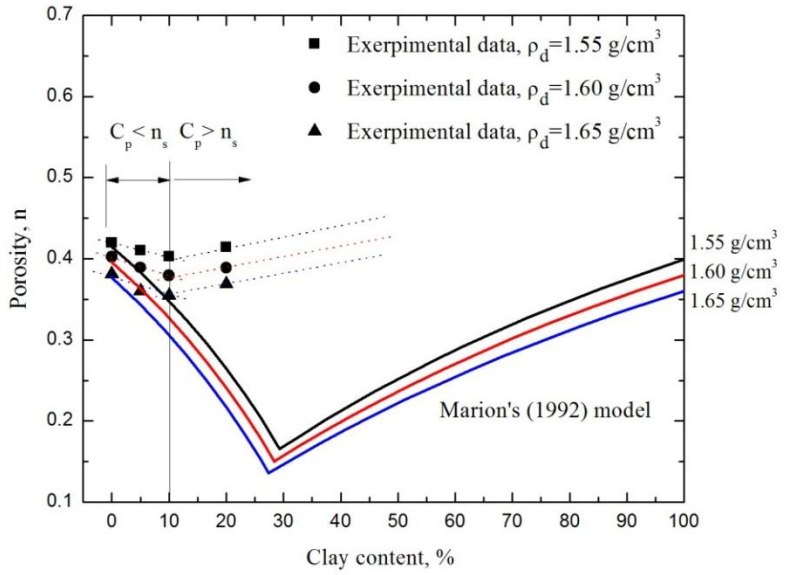

Figure 4-34 Relationships between porosity and clay content from Marion (1992) model and experimental data

4.4.2.3 Heat Conduction in Sand-Cay Mixtures

Soil is a complex substance that consists of three phases which are solid, liquid (i.e., water), and gas (i.e., air). The heat conduction in soils is mainly governed by soil overall thermal conductivity, which is affected by the thermal conductivity of each constituent and its relative volume fraction. In addition, some environmental factors (i.e., moisture content and dry density) and compositional factors (i.e., soil mineral components and particle size distribution) will also affect soil thermal conductivity. Based on the above discussion, the change in microstructure influences the porosity of sand-clay mixtures and fundamentally affects the heat conduction process in mixtures. Accordingly, the thermal conductivity of mixtures will be changed.

The mechanism of heat conduction in sand-clay mixtures can be divided into two categories with respect to dry condition and moist condition. For the sand-clay mixtures under dry condition, heat is conducted primarily through the soil particles and the

interparticle physical contact points among soil particles, but the air in mixtures has little contribution to the heat transfer process since the thermal conductivity of air is quite small (i.e., 0.026 W $m^{-1}K^{-1}$). Thus, the thermal conductivity of solids has the effect on overall thermal conductivity of mixtures. In this study, thermal conductivity of sand (99% quartz) is much higher than kaolin clay (93% anhydrous aluminum silicate and 7% quartz) due to the quartz content effect (Zhang et al. 2015a). Thus, the thermal conductivity of solids decreases as clay content increases, leading to a reduction of thermal conductivity of mixtures. But such effect is not prominent when the clay content is less than the critical clay content (i.e., c=10%) according to the geometric mean model (Johansen, 1977). However, the number of interparticle physical contact points will increase considerably as the clay content increases and before it reaches the critical clay content because the clay particles are filling the sand pores in the first stage (i.e., c<10%). As a result, the number of heat paths in mixtures increases and the thermal conductivity is expected to be elevated. When the clay content is greater than the critical clay content, the number of physical contact points which are formed among soil particles is not as great as in the first stage, and the decrease in thermal conductivity of solids is more pronounced. Thus, the increase in the thermal conductivity of mixtures is reduced in the second stage. In addition, the elevated dry density induces more physical contact points in the mixtures, and increases the thermal conductivity to some extent. But this effect on thermal conductivity is not significant in this study.

For the sand-clay mixtures under moist condition, air, which is considered as pore fluid, is partially or totally replaced by water in mixtures, as shown in Figure 4-35. As reported, thermal conductivity of water is 0.59 W $m^{-1}K^{-1}$, which is around 22 times that of air (De Vries, 1963; and Horai, 1971). Thus, the thermal conductivity of mixtures is supposed to increase dramatically compared with dry condition. But it decreases with an

increase in clay content. The existence of water promotes the formation of water films and water bridges that reduce the original thermal resistance among soil particles under dry condition, facilitates the heat conduction process, and then increases the thermal conductivity of mixtures. But the hydration is the dominating water-retention mode when clay soil is under high matric suction or low moisture content conditions (Lu and Dong, 2015). Most of the hydrated water is located on the soil particle surface or inside the mineral crystal structures surrounding the exchangeable cations (Revil and Lu, 2013). Therefore, the thermal conductivity of sand-clay mixtures decreases with increasing clay content. Moreover, such decrease in thermal conductivity is more pronounced as the addition of clay particles increases in the first stage (i.e., c<10%) than in the second stage (i.e. c>10%).

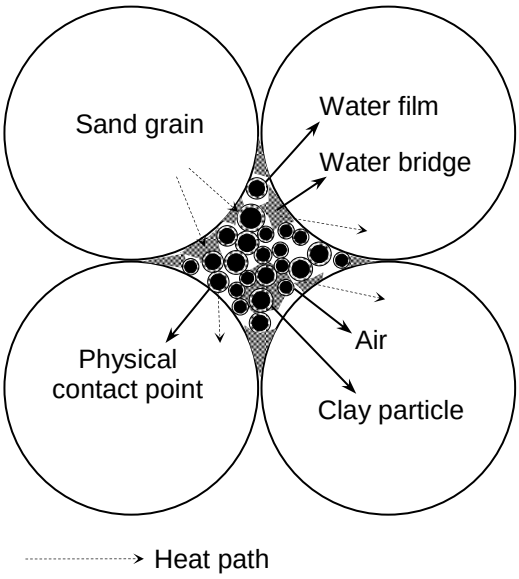

Figure 4-35 Diagram of heat conduction in sand-kaolin clay mixtures under moist condition

4.4.3 Model Prediction

Johansen (1977) proposed an empirical relationship to predict soil thermal conductivity,

$$k = \left(k_{water}^{n} k_{solid}^{1-n} - \frac{0.137\rho_d + 64.7}{2650 - 0.947\rho_d} \right)\left(0.7 \log S_r + 1\right) + \frac{0.137\rho_d + 64.7}{2650 - 0.947\rho_d} \quad (4.14)$$

where k_{water} and k_{solid} are thermal conductivities of water and solid, respectively; n is the porosity; S_r is the degree of saturation; ρ_d is the dry density, kg/m^3. This model is valid only for degrees of saturation greater than 5%; it provides negative thermal conductivity values below this level.

Cote and Konrad (2005) modified Johansen's (1977) model in order to eliminate the logarithmic dependence on degree of saturation, and proposed a new empirical equation,

$$k = (k_{water}^{n} k_{solid}^{1-n} - \chi 10^{-\eta n})\left[\frac{\kappa S_r}{1 + (\kappa - 1)S_r} \right] + \chi 10^{-\eta n} \quad (4.15)$$

where χ and η account for particle shape effect, and κ accounts for soil texture effect. For fine and medium sands, the suggested values provided by Cote and Konrad (2005) were 1.7 W m^{-1}K^{-1} for χ, 1.8 for η and 3.55 for κ, and these values were adopted in the model prediction.

Lu et al. (2007) also proposed a modified relationship based on Johansen's (1977) model,

$$k = \left[k_{water}^{n} k_{solid}^{1-n} - (b - an) \right] \exp\left[\alpha (1 - S_r^{\alpha - 1.33}) \right] + (b - an) \quad (4.16)$$

Where a , b and α are empirical parameters. The suggested values are 0.56 for a, 0.51 for b, and 0.96 for α for coarse soils, and these values were employed in the model prediction.

Chen (2008) proposed an empirical equation given by,

$$k = k_{water}^{n} k_{solid}^{1-n} \left[(1-0.0022)S_r + 0.0022\right]^{0.78n} \quad (4.17)$$

This equation is an empirical relationship based on laboratory experiments on four quartz sands with different particles sizes, shapes, and gradations. It probably shows relatively high prediction accuracy for sands or sandy soils.

Zhang et al. (2015a) measured the thermal conductivity of three sands with extreme high quartz content by using the thermo-TDR probe and modified Cote and Konrad (2005) model in order to account for the effect that high quartz content has on soil thermal conductivity. The formula remained the same, but model parameters were modified as 8.12 W $m^{-1}K^{-1}$ for χ, 3.18 for η and 8.0 for κ for quartz sands.

In the model prediction, k_{solid} can be estimated by generalized geometric mean method as given by,

$$k_s = \prod_j k_{m_j}^{x_j} \qquad with \qquad \sum_j x_j = 1 \quad (4.18)$$

where k_{mj} is the thermal conductivity of rock-forming mineral j; and x_j is the volumetric proportion of the mineral j. In this study, thermal conductivity of quartz and kaolin clay were assumed to be 7.5 W $m^{-1}K^{-1}$ (Chen, 2008) and 2.9 W $m^{-1}K^{-1}$ (Lee et al., 2012). According to Equation 4.18, k_{solid} of sand-kaolin clay mixtures were calculated and shown in Table 4-7. Thermal conductivity of water was assumed to be 0.61 W $m^{-1}K^{-1}$ (Chen, 2008).

Table 4-7 Thermal conductivities of solid and water in model prediction

Clay content (%)	k_{solid} (W $m^{-1}K^{-1}$)	k_{water} (W $m^{-1}K^{-1}$)
0	7.50	0.61
5	7.15	
10	6.82	
20	6.20	

Figures 4-36, 4-37, 4-38, and 4-39 show the comparison of experimental data and model prediction for different clay contents at dry density of 1.60 g/cm^3. In Figure 4-36, it is shown that all of the predicted curves underestimated the thermal conductivity of pure sand. However, the Zhang et al. (2015a) model showed the best agreement with experimental data, compared with other models, because the effect of high quartz content was taken into account in the model. The difference between measured and predicted results from the Chen (2008) model at high moisture contents might be due to the underestimation of the thermal conductivity of solids. The other three models could not accurately predict thermal conductivity of quartz sands since the natural soils, tested in their studies for model development, had relatively low quartz content. Predicted thermal conductivity from the Zhang et al. (2015a) model became higher than measured values for sand-kaolin clay mixtures, and the deviation increased with the increase in clay content.

For the other four models, the model prediction slightly underestimated soil thermal conductivities at c=5%, as shown in Figure 4-37, and the predicted thermal conductivities agreed with the measured values at c=10%, except for Chen's (2008) model, as shown in Figure 4-38. In contrast, the predicted results were slightly higher than the measured values at c=20%, as shown in Figure 4-39. It should be noted that the Chen (2008) model always predicts relatively high thermal conductivity values at low

moisture content level, and it comes close to the other three models as moisture content increases. As reported in literatures (Lu et al., 2007; and Haigh, 2012), thermal conductivity of sands increases dramatically at low moisture contents because the formation of water films around soil particles and water bridges among soil particles reduces the thermal resistance and increases number of heat paths during heat transfer process in sands.

As clay content increases, thermal conductivity of solids decreases because of the reduction of quartz content, i.e., sand content. Thermal resistance among soil particles also increases because sand grains are covered by fine clay particles with very low thermal conductivity. Moreover, the formation of water films and bridges which facilitates the heat transfer process, as occurs in sands, are not prominent. This is because hydration is the dominating water-retention mode when clay soil is under high matric suction or low moisture content conditions (Lu and Dong, 2015). The hydrated water is located mostly on the soil particle surface or inside the mineral crystal structures surrounding the exchangeable cations (Revil and Lu, 2013). Consequently, thermal conductivity of sand-kaolin clay mixtures decreases gradually with an increase in clay content, and the change of thermal conductivity should be continuous as the clay content varies.

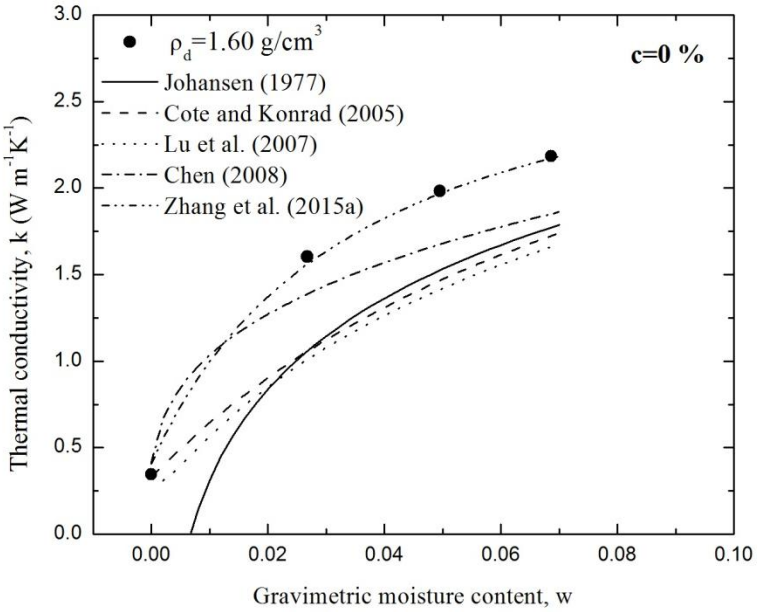

Figure 4-36 Comparison between experimental data and model prediction at c=0%

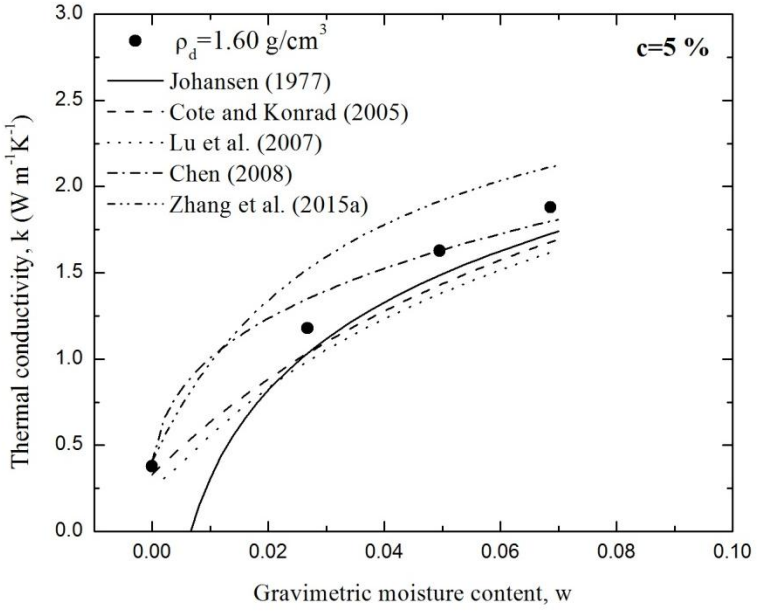

Figure 4-37 Comparison between experimental data and model prediction at c=5%

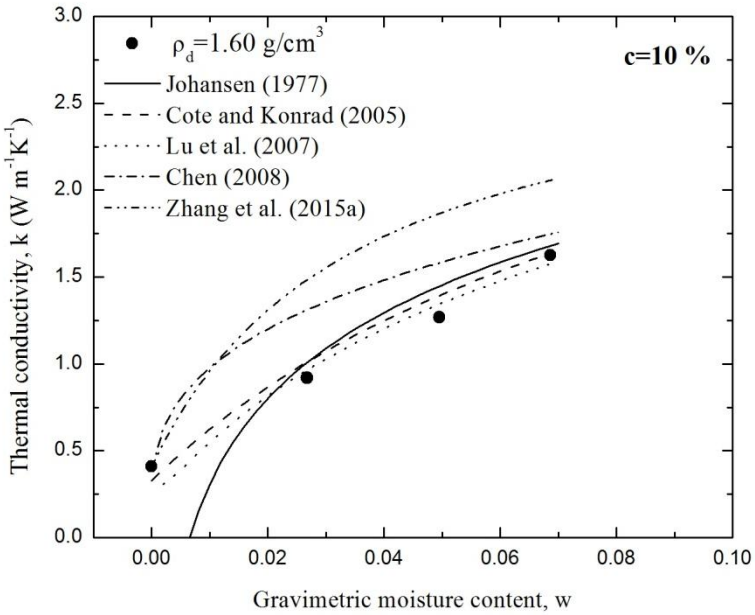

Figure 4-38 Comparison between experimental data and model prediction at c=10%

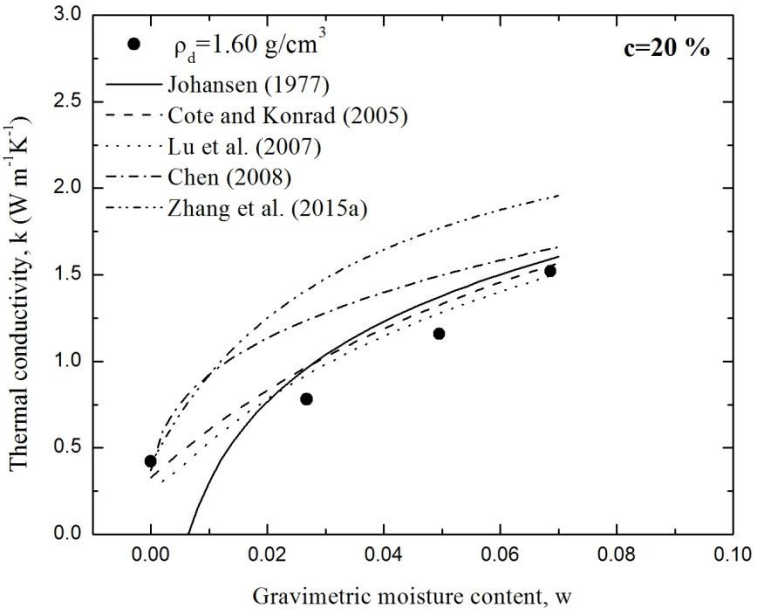

Figure 4-39 Comparison between experimental data and model prediction at c=20%

In order to consider the continuous change of thermal conductivity with clay content, model parameters κ in Cote's and Konrad's (2005) model and α in Lu's et al. (2007) model were modified. The comparisons between experimental data and predicted thermal conductivities from the modified Cote and Konrad (2005) model and the Lu et al. (2007) model are shown in Figures 4-40 and 4-41, respectively.

In Figure 4-40, the best agreements between measured and predicted values were attained when κ equaled to 8, 5, 3 and 2.5 for c=0%, 5%, 10% and 20%, respectively. The suggested values of κ are 4.5 for gravels and coarse sands; 3.55 for fine and medium sands; 1.9 for silty soils, clayey soils, silts, and clays; and 0.6 for organic fibrous soils, as provided by Cote and Konrad (2005). It was increased up to 8 for quartz sands to account for the extremely high quartz content's effect on soil thermal conductivity. In Figure 4-40, the predicted thermal conductivities agreed with measured values very well when α equals 1.15, 1.05, 0.95, 0.90 for c=0%, 5%, 10% and 20%, respectively. Lu et al. suggested that the value of α is 0.95 for coarse soils and 0.27 for fine-grained soils. Because the maximum fraction of kaolin clay was only 20% in this study, the modified values of parameter α were very close to the above suggested value (0.95) for coarse soils.

Furthermore, two identical exponential functions were employed to describe the relationships between clay content and κ and α, as depicted in Figures 4-42 and 4-43. It was found that both κ and α decrease with clay content, and the fitting curves were able capture the continuous change of values of κ and α, as well as the thermal conductivity of sand-kaolin mixtures with clay content.

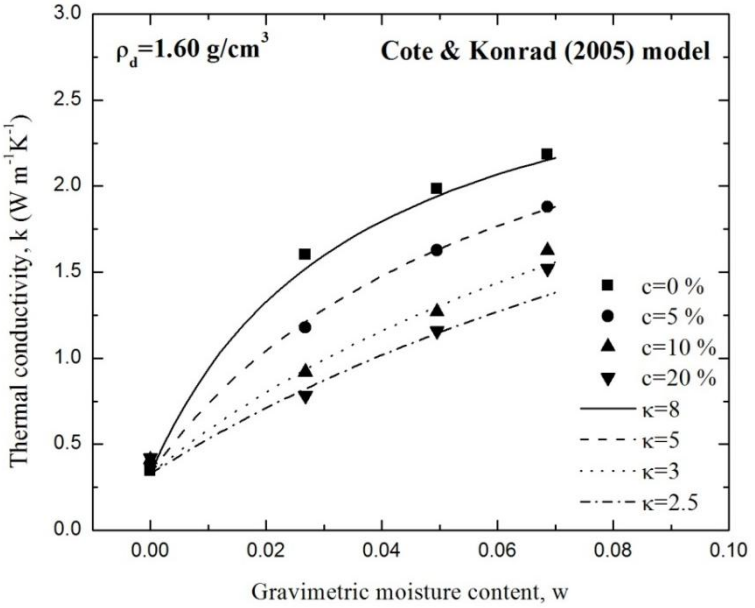

Figure 4-40 Comparison between experimental data and predicted thermal conductivities from modified Cote and Konrad (2005) model

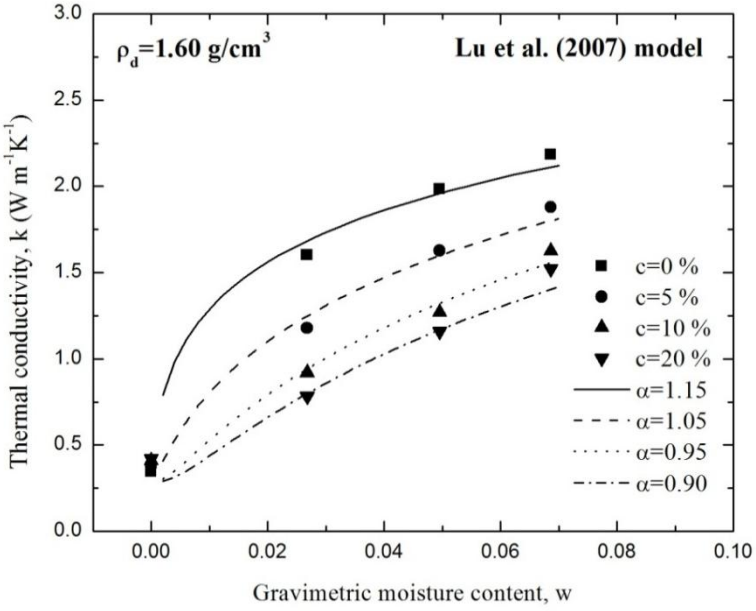

Figure 4-41 Comparison between experimental data and predicted thermal conductivities from modified Lu et al. (2007) model

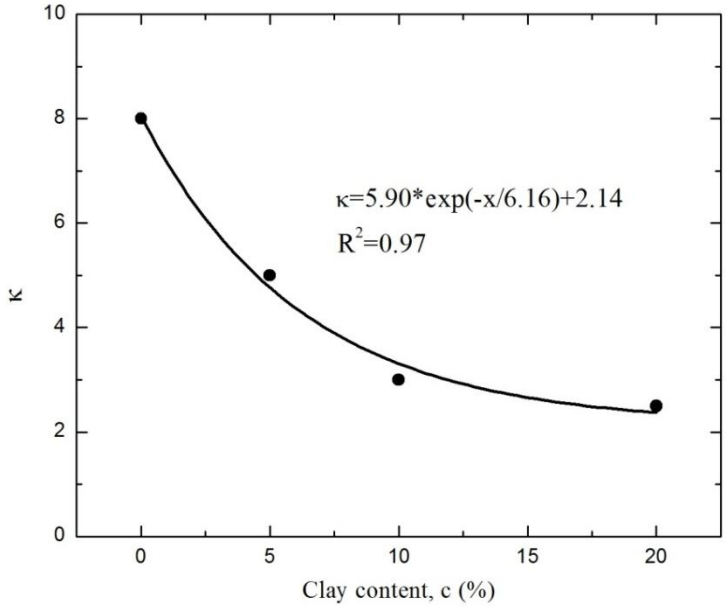

Figure 4-42 Relationship between clay content and model parameter κ

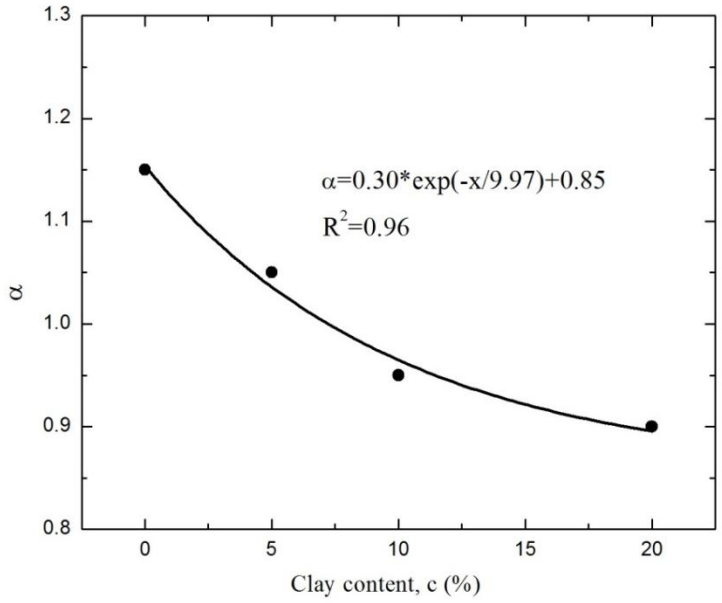

Figure 4-43 Relationship between clay content and model parameter α

4.5 Summary

Thermal conductivity is a fundamental physical property governing the heat transfer process in soils. It is affected by both environmental and compositional factors, such as moisture content, dry density, and the soil mineralogy component. This chapter covers the thermal conductivity of quartz sands, sand-sand mixtures, and sand-kaolin clay mixtures that were measured at different conditions.

Thermal conductivity of quartz sands increases with moisture content and dry density, but the dry density effect is not very significant in this study. Higher quartz content leads to higher thermal conductivity since, of all the soil minerals, quartz has the highest thermal conductivity, Thermal conductivity is also affected by the water films and water bridges formed between sand particles. The finer the sand particle is, the easier the water films and water bridges form and the higher the thermal conductivity is. The improved model (Zhang et al., 2015a) exhibits a high degree of accuracy in predicting thermal conductivity of quartz sands.

From the study of sand-sand mixtures, it is concluded that, compared with coarse sands, fine sands have lower thermal conductivity at dry conditions, but higher thermal conductivity at low moisture content conditions because of the particle size effect. The thermal conductivity of moist sands is much greater than dry sands, and it increases with moisture content. The thermal conductivity of coarse sands increases to peak value by increasing the fine sand content to critical fines content (F_{cr}). F_{cr} is increased with a decrease in d_f/d_c value in the experiments, and it is also affected by the grain shape.

From the study on sand-kaolin clay mixtures, it's apparent that the thermal conductivity of mixtures increases with both moisture content and dry density, but it decreases as clay content increases in the mixtures. The critical clay content (C_c) is found to be equal to 10%. Five alternative soil thermal conductivity prediction models

were also selected to predict thermal conductivity of mixtures. All the model predictions exhibited either overestimation or underestimation for measured thermal conductivities as the clay content varied. The Zhang et al. (2015a) model showed the highest prediction accuracy for pure sands compared with other models. The Modified Cote and Konrad (2005) model and Lu et al. (2007) model, which account for a continuous change of model parameters κ and α with clay content, can accurately predict thermal conductivity of sand-kaolin clay mixtures and effectively guide the design of geothermal-related structures.

Chapter 5

Development of a Continuum Soil Thermal Conductivity Model

5.1 Introduction

As reported in previous literatures (Kersten, 1949; Johansen, 1977; Donazzi et al., 1979; Gangadhara Rao and Singh, 1999; Cote and Konrad, 2005; Lu et al., 2007; Chen, 2008; and Zhang et al., 2015a), many researchers have developed soil thermal conductivity prediction models which were primarily based on the empirical fits to experimental data of natural soils. For example, Kersten (1949) performed a series of laboratory experiments to measure the thermal conductivity of 19 different types of soils and proposed the empirical relationships between thermal conductivity and moisture content and dry density. Johansen (1977) proposed the unique normalized thermal conductivity concept that can be used to study the effects of soil types, porosity, degrees of saturation, and mineral components on soil thermal conductivity through the k_r-S_r relationship. He also presented some different k_r-S_r relationships for different soil types and developed a new thermal conductivity model based on this concept. Côté and Konrad (2005) further studied the thermal conductivity of soils and construction materials and established a new k_r-S_r relationship, incorporating variable κ and accounting for the soil type effect. In addition, variables χ and η, accounting for particle shape effect, were also incorporated to calculate the thermal conductivity of dry soils. Lu et al. (2007) conducted the thermal-TDR tests on 12 different natural soils ranging from sand, silts, to loam or clay loam and proposed another k_r-S_r relationship across the entire range of soil moisture content to develop a thermal conductivity model.

There are also other empirical thermal conductivity models. Chen (2008) developed a thermal conductivity model for sands with high quartz content. Zhang et al. (2015a) improved Cote's and Konrad's (2005) model to provide more accurate thermal

conductivity predictions for pure quartz sands. Donazzi et al. (1979) and Gangadhara Rao, and Singh (1999) established the relationships between thermal resistivity and porosity, degree of saturation, dry density, and moisture content, based on laboratory experiments and resulting in a thermal conductivity model that can be derived according to the reciprocal correlation between thermal conductivity and resistivity.

Due to the unavoidable gaps in measured thermal conductivities between any two neighboring soil types in previous studies, the model prediction of soil thermal conductivity may not agree with the actual values for some other types of soils, or soils which lie in between two neighboring soil types. Moreover, the predicted thermal conductivity might be discontinuous over the entire range of soil type. Another problem is that the sand content was usually assumed to be the same as the quartz content, and was used to calculate the thermal conductivity of solids, resulting in an overestimation of soil thermal conductivity (Lu et al., 2007). Thus, a lack of data for quartz content is another critical issue, hindering the successful application of the above models (Furmanski 2013; Tarnawski et al., 2009).

On the other hand, various theoretical models for soil thermal conductivity predictions are summarized as follows: Gemant (1950) attempted to derive an analytical solution using finite-element method to determine thermal conductivity of lattice, but this does not appear to have been widely used since. De Vries' (1963) model was derived from Maxwell's equations, and the weighted average thermal conductivity of each constituent in the soil matrix was introduced into the model development. The disadvantage of this model is the uncertainty of the soil field capacity, which is the limit moisture content in determining whether water or air is the continuous media in soils. Gori (1983) proposed a soil cubic model, considering the effects of water films and bridges around soil particles on the heat transfer process, but the complexity of the

formula limits future applications. Tong et al. (2009) studied the heat transfer process in porous media and proposed a generalized thermal conductivity model, accounting for many effects, but the dependence of parameters η_1 and η_2 on soil types was not clarified. Haigh (2012) presented a thermal conductivity model for sands, based on three-phase soil contact element. The model showed higher prediction accuracy than other models, particularly for sands, but the applicability for other soil types still needs to be studied.

This chapter presents the development and validation of a new continuum soil thermal conductivity model, considering the effects of porosity, degree of saturation, quartz content, and soil types simultaneously. Laboratory experiments were performed on pure quartz sand (> 99 % quartz content), kaolin clay, and sand-kaolin clay mixtures in different proportions at different porosities and degrees of saturation, using the thermo-TDR probe. The model was developed based on the normalized thermal conductivity concept proposed by Johansen (1977), followed by the model validation for k_{dry}-n (thermal conductivity of dry soils and porosity) and k_r-S_r relationships. The model performance was also evaluated through the comparison of predicted thermal conductivity with experimental data both from this study and other thermal conductivity measurements from published literatures (Lu et al., 2007; and Chen, 2008).

5.2 Laboratory Experiments

The laboratory experiments were performed on sand, kaolin clay, and sand-kaolin clay mixtures. ATSM-graded sand and kaolin clay were selected in the study according to the physical properties of test materials presented in Chapter 4. The experimental program is presented in Table 5-1, and the target dry density and degree of saturation in the experiment were determined (shown in Table 5-2) based on compaction curves of sand-kaolin clay mixtures with different mixing ratios (shown in Figure 4-23).

The experimental setup is shown in Figure 3-17, and the method to determine soil thermal conductivity was described in Chapter 3.

Table 5-1 Experimental program of sand, kaolin clay, and sand-kaolin clay mixtures

	No	1	2	3	4	5	6	G_s
Content by dry weight, (%)	Sand	100	95	90	80	70	0	2.65
	Kaolin	0	5	10	20	30	100	2.58

Table 5-2 Target dry density and degree of saturation in the experiment

Name	Sand	Sand-kaolin mixtures				Clay
No	1	2	3	4	5	6
ρ_d (g/cm^3)	1.55	1.55	1.55	1.55	1.40	0.65
	1.60	1.60	1.60	1.60	1.45	0.68
	1.65	1.65	1.65	1.65	1.50	0.71
		1.70	1.75			
S_r	0	0	0	0	0	0
	0.1	0.1	0.1	0.1	0.3	0.3
	0.2	0.2	0.2	0.25	0.4	0.4
	0.25	0.25	0.3	0.5	0.5	0.6
	1	1	1	1	1	1

5.3 Experimental Results and Discussion

5.3.1 Measurements of Thermal Conductivity and Porosity

Figure 5-1, 5-2 and 5-3 show the relationships between thermal conductivity and porosity for sand, kaolin clay and sand-kaolin clay mixtures. It is evident that thermal conductivity increased with a decrease in porosity at each degree of saturation level. Moreover, the excellent linear trends between thermal conductivity and porosity in semi logarithmic scale were found for all the soil samples, which is consistent with Chen's (2008) study. Another feature is that thermal conductivity converged to a unique value at y axis as porosity decreased to zero, and such value was different for different clay mixing ratios. This is because thermal conductivity of soils is actually the thermal conductivity of solids when the soil porosity equals zero, and it is strongly dependent on quartz content (i.e., sand content) in mixtures due to the highest thermal conductivity of quartz compared with all the other soil minerals.

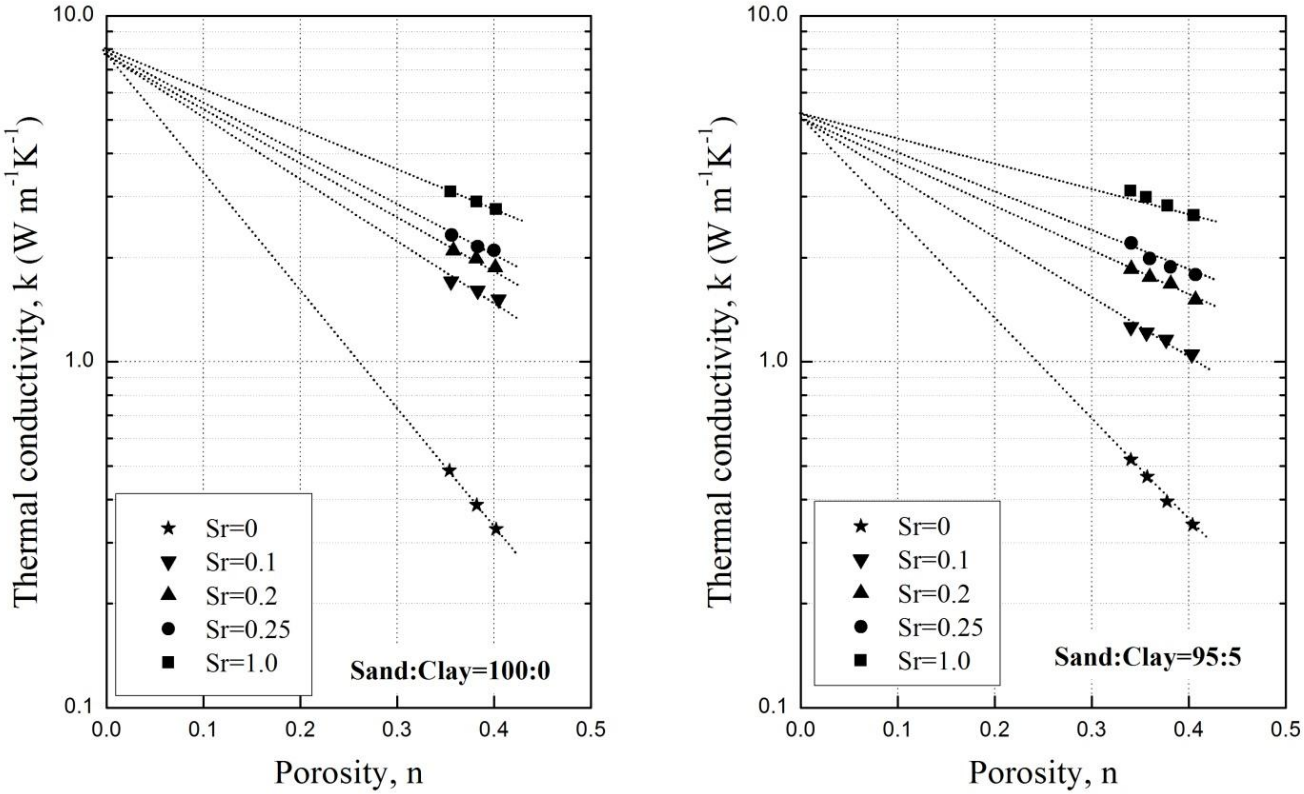

Figure 5-1 Thermal conductivity and porosity at c=0% and c=5%

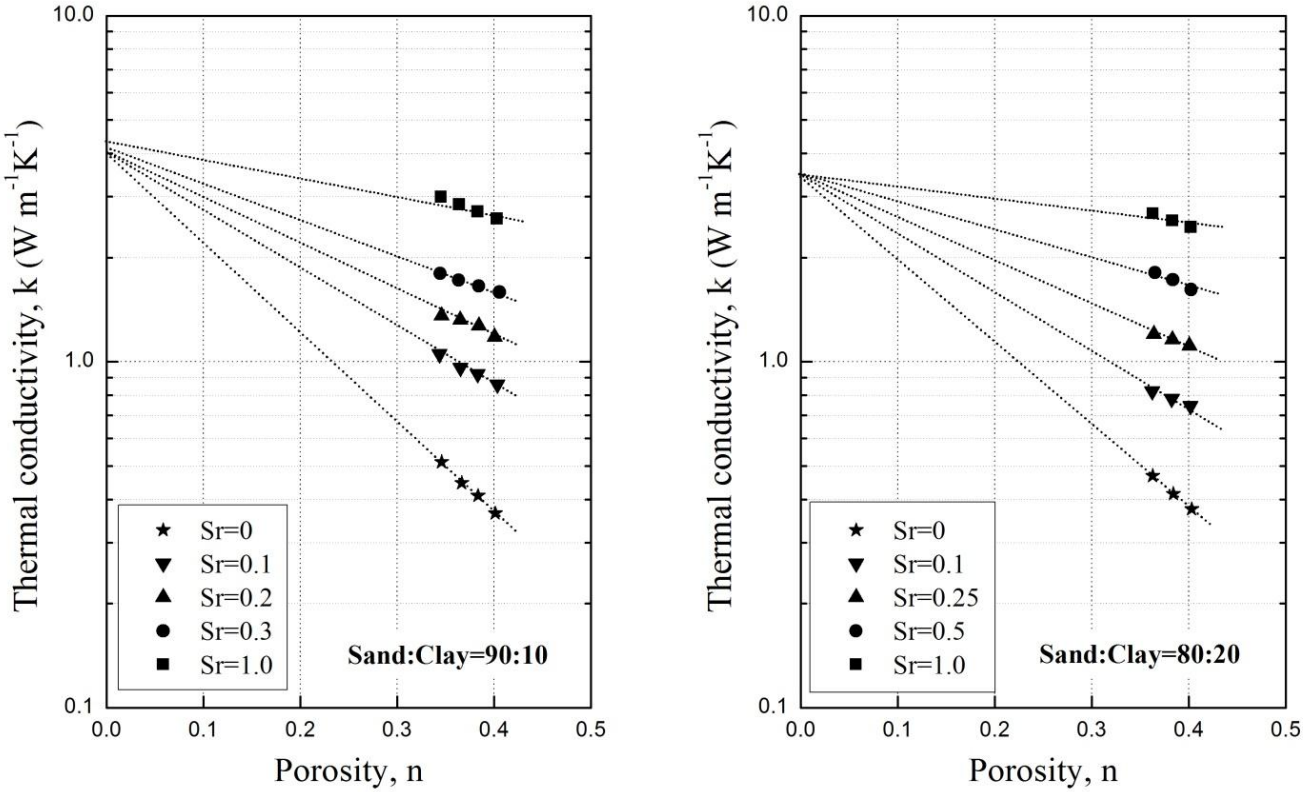

Figure 5-2 Thermal conductivity and porosity at c=10% and c=20%

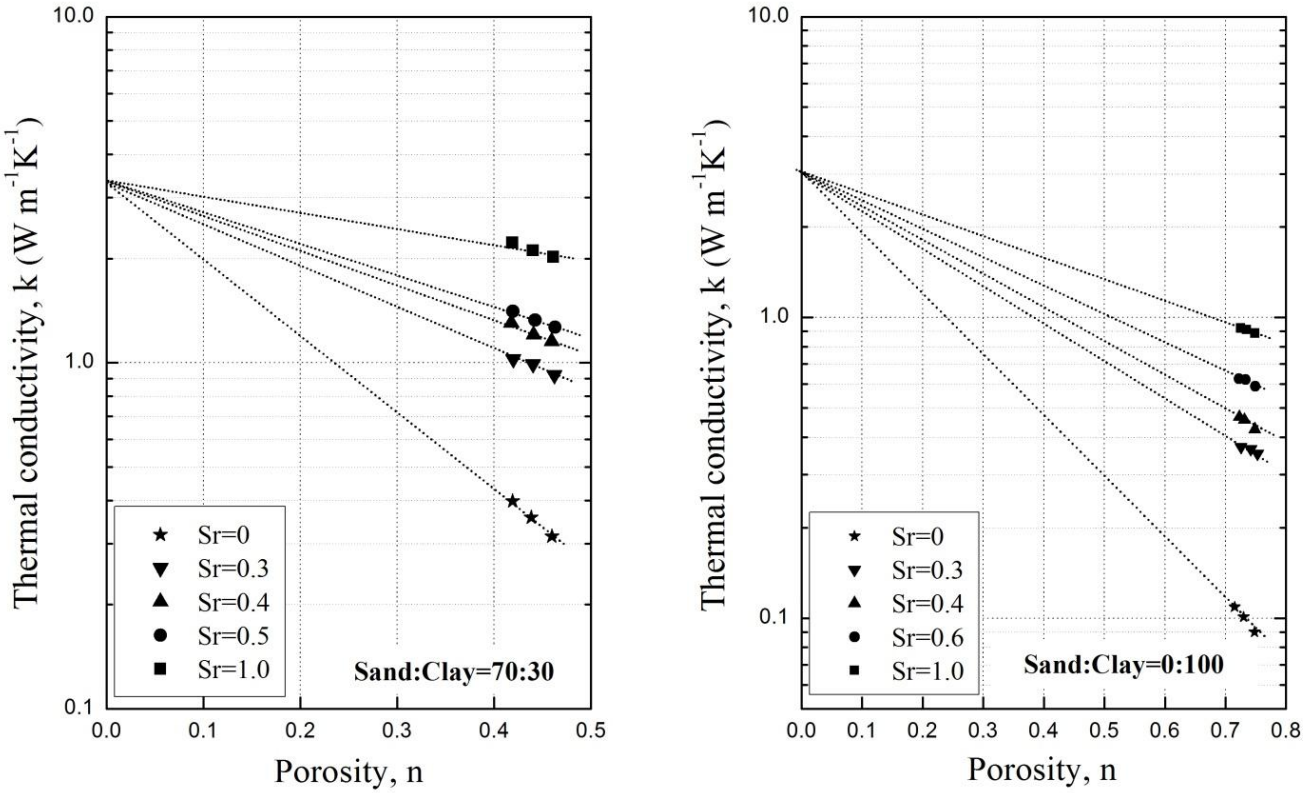

Figure 5-3 Thermal conductivity and porosity at c=30% and c=100%

5.3.2 Measurements of Thermal Conductivity and Degree of Saturation

Figures 5-4, 5-5, 5-6, 5-7, 5-8, and 5-9 show the relationships between thermal conductivity and degree of saturation. It is indicated that thermal conductivity increases with an increase in degree of saturation at each porosity level. The thermal conductivity increase was greater at a low degree of saturation in pure sand than in other samples. However, this increment decreased gradually, as the clay content increased. Furthermore, there was a linear increase of thermal conductivity with degree of saturation when clay content increased up to 30%. This is mainly attributed to the effects of particle size and quartz content on thermal conductivity. In sand, water films and bridges are more likely to be formed among soil particles to facilitate the heat transfer process and improve the thermal conductivity at low degrees of saturation. The subsequent slight increase in thermal conductivity of sand is due to the increase in thermal conductivity of pore fluid as more voids are replaced by water. In contrast, the moisture is distributed more uniformly as the clay content increases in mixtures, and the `effects of water films and bridges on thermal conductivity do not extend over the entire range of degree of saturation. This is also because hydration is the dominating water-retention mode when clay soil is under high matric suction or low moisture content conditions (Lu and Dong, 2015). The hydrated water is located on the soil particle surface or inside the mineral crystal structures surrounding the exchangeable cations (Revil and Lu, 2013). Another reason is that the decrease in quartz content results in a reduction of thermal conductivity of solids and then the thermal conductivity of soils. For pure clay, the linear trend between thermal conductivity and the degree of saturation was also very obvious, but the thermal conductivity decreased dramatically more than the other samples because of the relatively low thermal conductivity of solid phase (i.e.,. kaolin clay) and high porosity of clay samples.

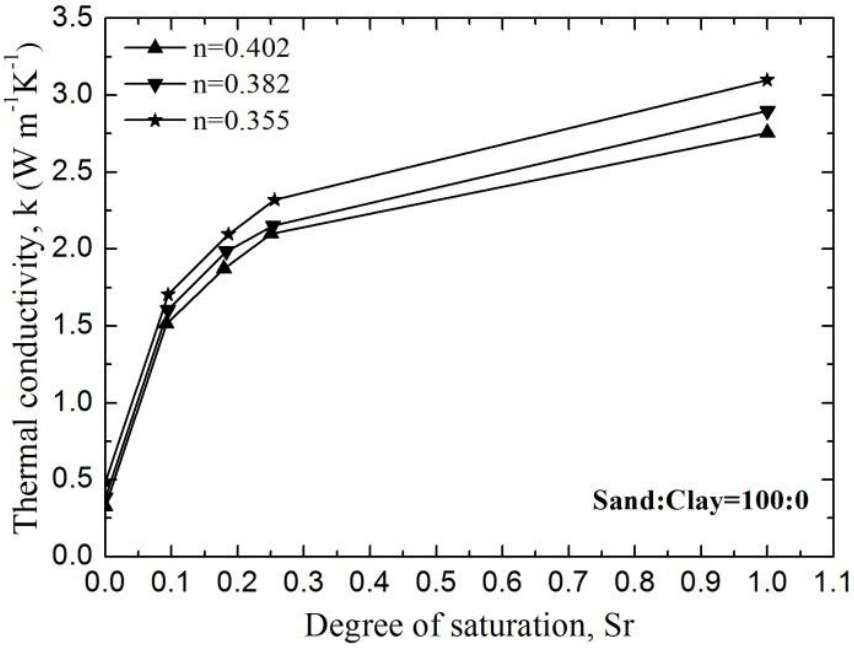

Figure 5-4 Thermal conductivity and degree of saturation at c=0%

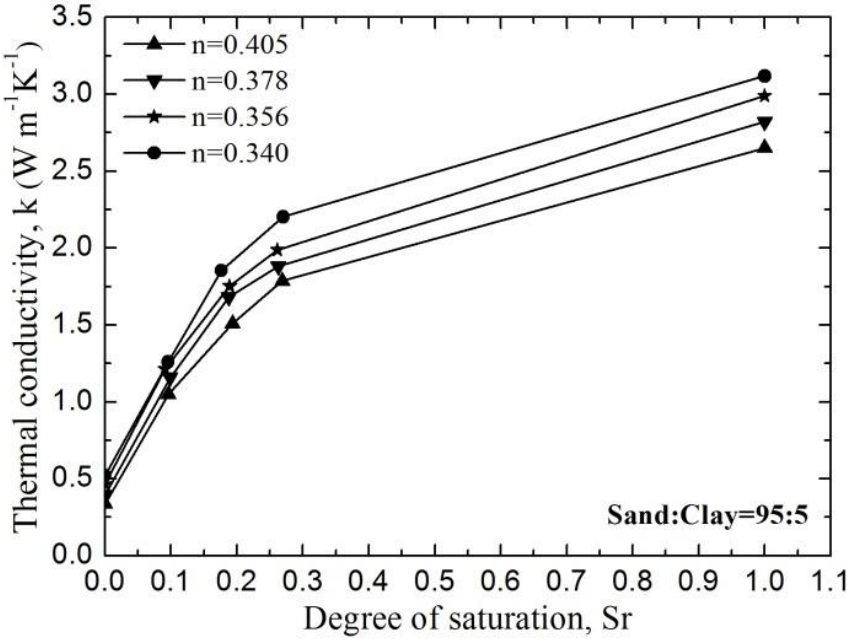

Figure 5-5 Thermal conductivity and degree of saturation at c=5%

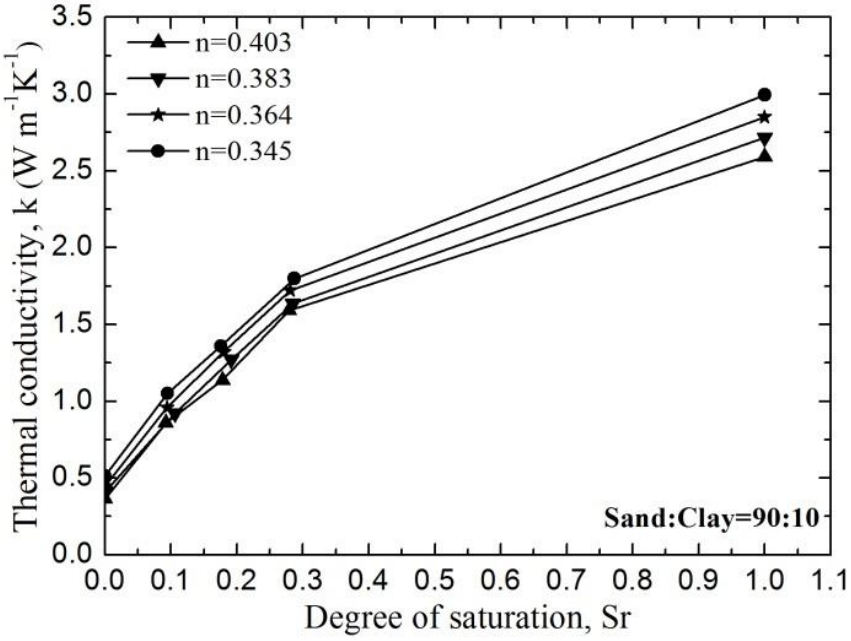

Figure 5-6 Thermal conductivity and degree of saturation at c=10%

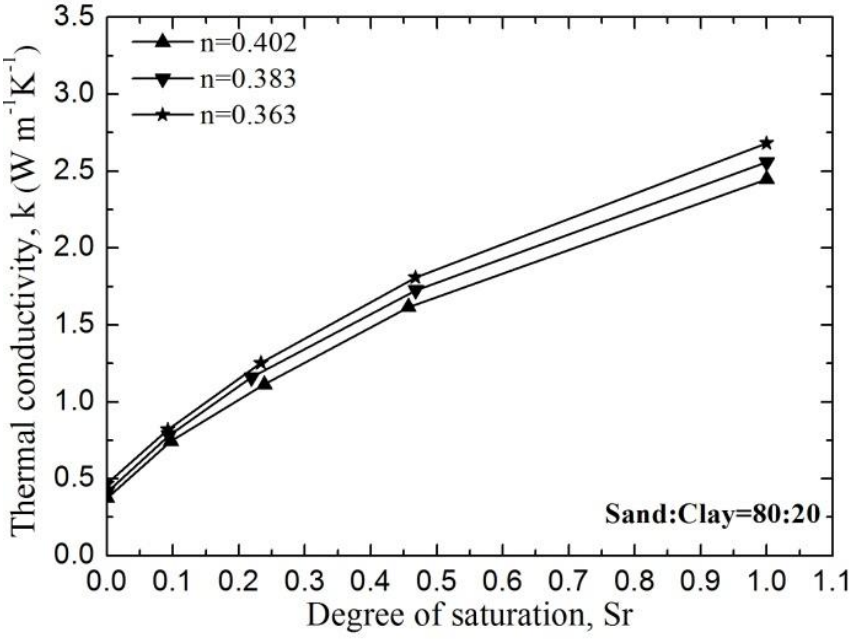

Figure 5-7 Thermal conductivity and degree of saturation at c=20%

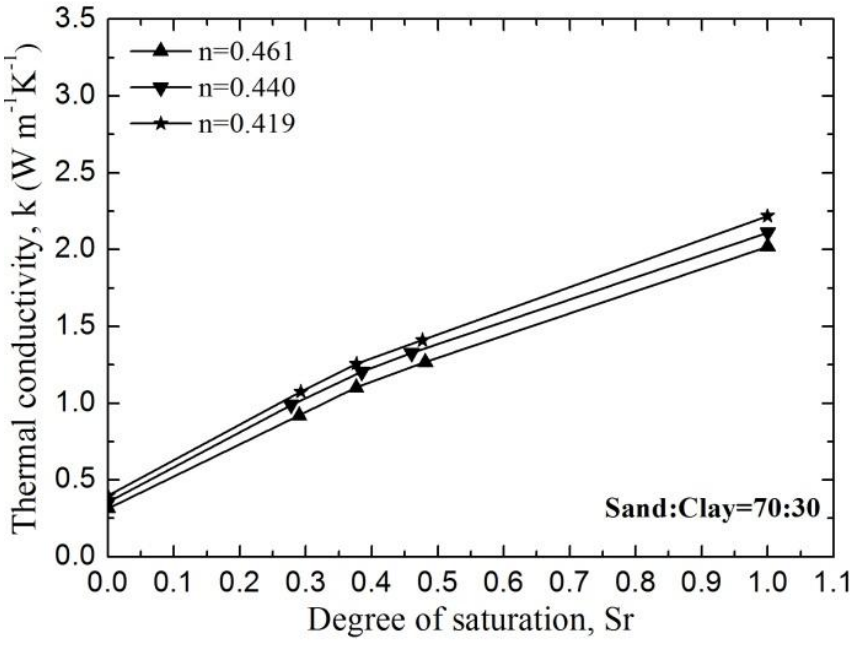

Figure 5-8 Thermal conductivity and degree of saturation at c=30%

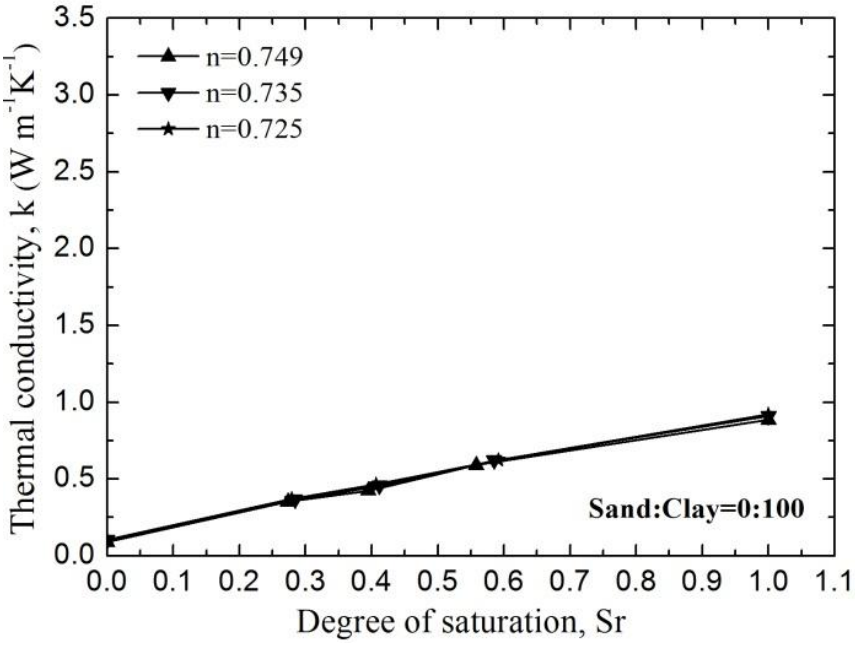

Figure 5-9 Thermal conductivity and degree of saturation at c=100%

5.4 Model Development

5.4.1 Framework of Normalized Thermal Conductivity

The normalized thermal conductivity proposed by Johansen (1977) can be expressed as follows,

$$k_r = \frac{k - k_{dry}}{k_{sat} - k_{dry}} \tag{5.1}$$

where k_r is the normalized thermal conductivity, k_{dry} and k_{sat} are the thermal conductivities of soils at dry and fully saturated conditions, respectively, W $m^{-1}K^{-1}$. Then, establishing a k_r-S_r relationship enables the study of the effects of porosity, moisture content, and soil mineral component on thermal conductivity in a unique way because of the unique relationship for a given type of soil (Côté and Konrad, 2005). The lower and upper bounds of this relationship are given as follows,

Lower limit condition: $S_r = 0 \rightarrow k_r = 0$

Upper limit condition: $S_r = 1 \rightarrow k_r = 1$

Thus, soil thermal conductivity can be calculated from Equation 5.1, as given below,

$$k = k_r \times (k_{sat} - k_{dry}) + k_{dry} \tag{5.2}$$

The simplest expression for calculating the thermal conductivity of saturated soils had been widely used as follows, (Sass et al., 1971),

$$k_{sat} = k_{water}^{n} k_{solid}^{1-n} \tag{5.3}$$

Cote and Konrad (2005) proposed a generalized thermal conductivity model for soils and construction materials in a wide range of soil types, porosity, and degree of saturation. The generalize k_r-S_r relationship they provided is as follows,

$$k_r = \frac{\kappa S_r}{1+(\kappa-1)S_r} \tag{5.4}$$

where κ is an empirical parameter accounting for the soil type effect in the unfrozen and the frozen states. The values of κ are 4.7 and 1.8 for the unfrozen and the frozen state, respectively. The relationship between thermal conductivity of dry soils and porosity in the Cote and Konrad (2005) study is given as follows,

$$k_{dry} = \chi 10^{-\eta n} \tag{5.5}$$

where χ and η are material parameters accounting for the particle shape effect; and n is the porosity of dry soils.

5.4.2 Model Formulation

Figure 5-10 shows the normalized thermal conductivity and degree of saturation for sand, kaolin, and sand-kaolin clay mixtures. According to Equation 5.4, different κ values were obtained for different quartz (sand) contents by fitting the experimental data. It was found that κ was equal to 8 and 1.2 for pure sand and pure kaolin clay, respectively, and it was in between the above two values for sand-kaolin clay mixtures with κ increased as quartz (sand) content increased. Moreover, according to Equations 5.1 and 5.2, a higher κ value leads to higher soil thermal conductivity, with k_{dry} and k_{sat} remaining constant for any given soil at certain porosity level. Thus, soil thermal conductivity increased with quartz (sand) content, which also conformed to the previous experimental results. Considering the dependence of κ on quartz (sand) content, an exponential function was adopted to describe the relation between κ and quartz (sand) content, which is shown in Figure 5-11. Substituting this relation into Equation 5.4, a new k_r-S_r relationship was proposed as follows,

$$k_r = \frac{(2.168\times10^{-5}\times\exp(x/7.903)+1.252)S_r}{1+(2.168\times10^{-5}\times\exp(x/7.903)+0.252)S_r} \quad (5.6)$$

where x is the quartz (sand) content, %.

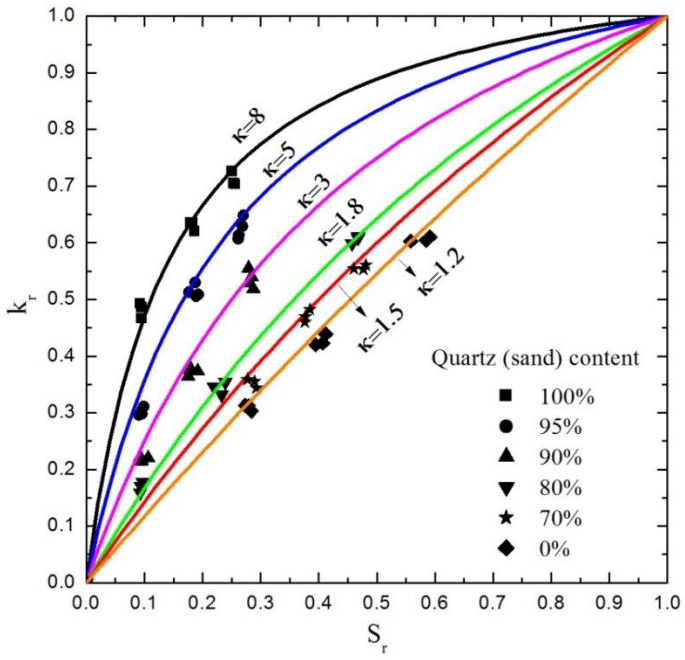

Figure 5-10 Normalized thermal conductivity (k_r) and degree of saturation (S_r)

Based on the collection of the experimental data of soil samples, the thermal conductivity and porosity of sand, kaolin clay, and sand-kaolin mixtures under dry condition is shown in Figure 5-12. The slope (k) and intercept (c) of the linear trends between thermal conductivity and porosity in semi logarithmic scale were changed with quartz (sand) content. Pure sand showed the highest intercept and the lowest slope, whereas pure clay showed the lowest intercept and the highest slope.

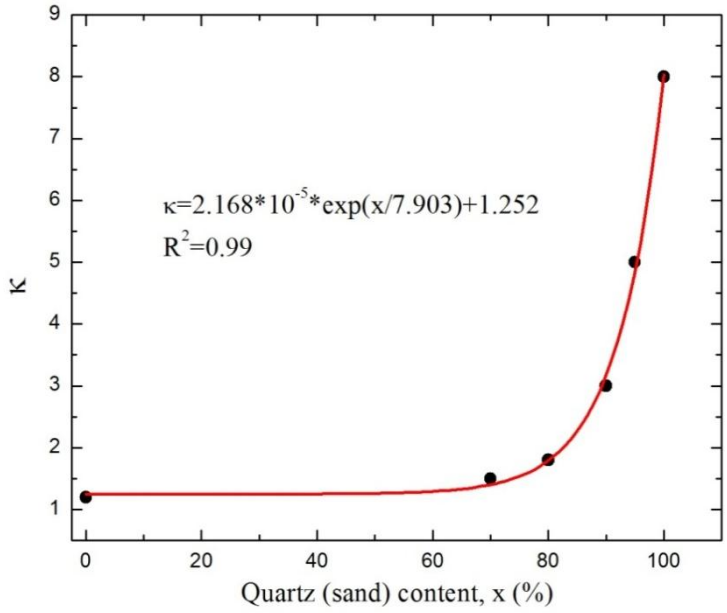

Figure 5-11 Relationship between κ and quartz (sand) content

All the other thermal conductivity measurements of sand-kaolin clay mixtures were in between the two linear lines depicted above. Comparing Equation 5.5 with experimental results, as shown in Figure 5-12, it is inferred that the absolute value of k is equal to η, and c is equal to χ. In Figure 5-13, the relationships between slope (k), intercept (c), and quartz (sand) content were shown, and two identical exponential functions were used to describe these relationships, with both R^2 values were very close to unit. Therefore, thermal conductivity of dry soils can be formulated according to Equation 5.5, which is expressed as follows,

$$k_{dry} = \left(1.216\times10^{-6}\times\exp(x/6.599)+3.034\right)\times10^{\left(-0.003\times\exp(x/16.452)-1.840\right)\times n} \quad (5.7)$$

According to Equation 5.3, thermal conductivity of saturated soils can be calculated as,

$$k_{sat} = k_{water}^{n}\left(k_{quartz}^{x/100}k_{kaolin}^{1-x/100}\right)^{1-n} \quad (5.8)$$

where k_{quartz} is assumed as 7.5 W $m^{-1}K^{-1}$ (Chen, 2008); and k_{kaolin} is assumed as 2.9 W $m^{-1}K^{-1}$ (Lee et al., 2012).

A continuum thermal conductivity model can be formulated.by substituting Equation 5.6, 5.7, and 5.8 with Equation 5.2, introducing a new variable x to consider the effects of quartz (sand) content and soil types on soil thermal conductivity. Model predictions and validations will be presented in the following sections.

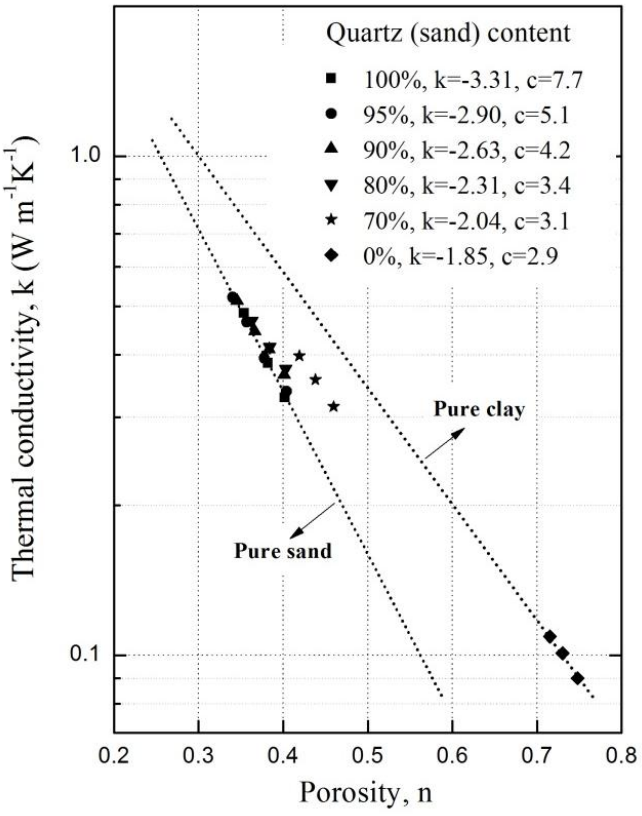

Figure 5-12 Thermal conductivity and porosity of sand, kaolin clay, and sand-kaolin clay mixtures under dry condition

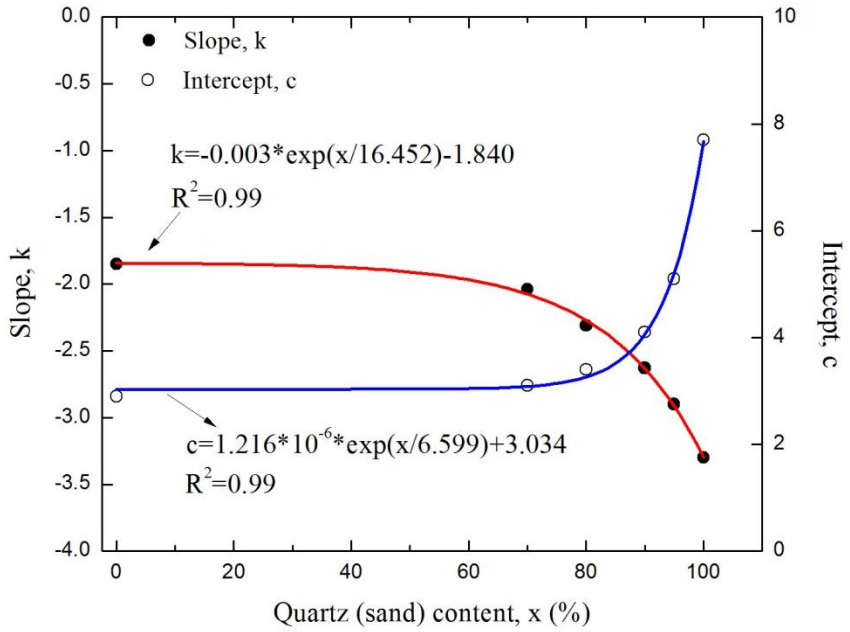

Figure 5-13 Relationships between slope (k), intercept (c), and quartz (sand) content

5.4.3 Model Prediction

Figure 5-14 shows the predicted thermal conductivity with degree of saturation for different porosities at 90% quartz (sand) content. The model predictions matched the experimental results (i.e., Figures 5-4 to 5-9) reasonably well. Lower porosity leads to a higher thermal conductivity at each degree of saturation because the heat transfer process is facilitated by an increase in the number of interparticle physical contact points in soils, as porosity reduces. Figure 5-15 shows the predicted thermal conductivity with degree of saturation for different quartz (sand) contents at porosity equal to 0.4. It is observed that thermal conductivity increased as quartz (sand) content decreased under dry condition, which also conformed to the experimental results shown in Figure 5-12. This can be explained by the fact that more voids in soils are occupied by fine clay particles to form more interparticle contacts as clay content increases, resulting in an increase of thermal conductivity of soils. Moreover, although the thermal conductivity of

clay particles is smaller than sand grains, it is still greater than that of air, and such newly-formed interparticle contacts will reduce the thermal resistance at original interfaces between sand grains and air, and will improve soil thermal conductivity. Conversely, , the thermal conductivity increased as the quartz (sand) content increased under moist conditions because of the quartz content's effect on soil thermal conductivity. In Figures 5-14 and 5-15, the model predictions not only matched the experimental results, but also accurately reproduced the characteristics of thermal conductivity variations with degrees of saturation for different porosities of quartz (sand) contents over the entire range of soil moisture content.

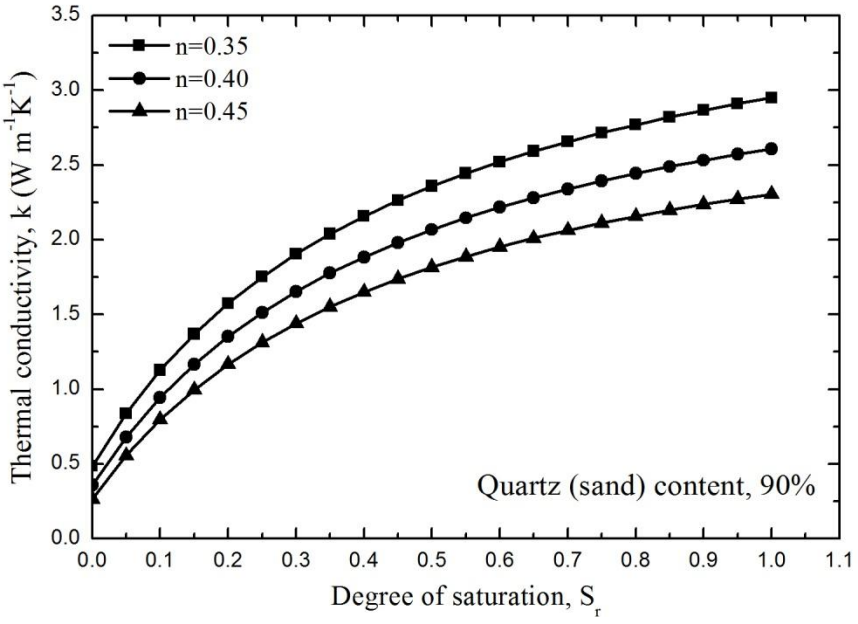

Figure 5-14 Predicted thermal conductivity with degree of saturation for different porosities at x=90%

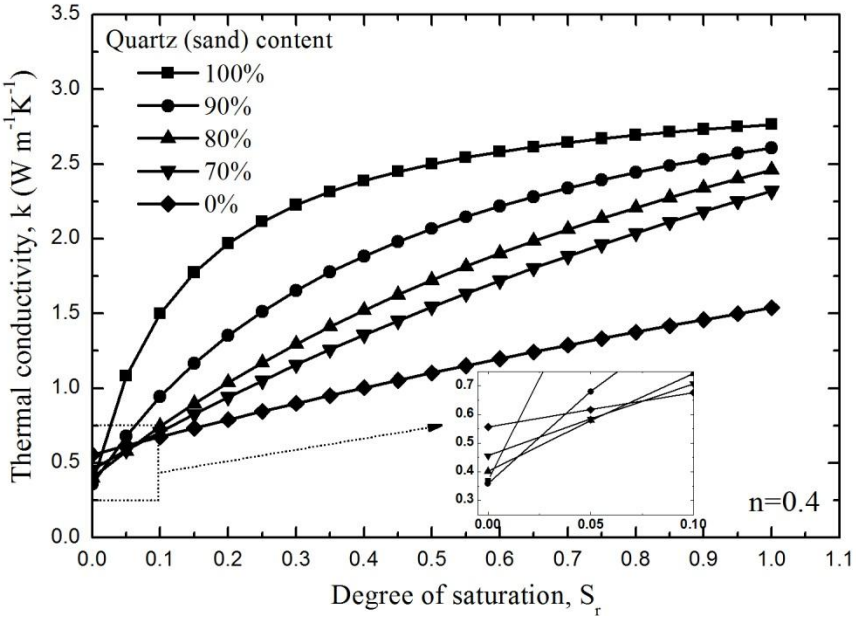

Figure 5-15 Predicted thermal conductivity with degree of saturation for different quartz (sand) contents at n=0.4

5.4.4 Model Validation

5.4.4.1 Validation for k_{dry}-n Relationships

Figure 5-16 shows the comparisons of predicted thermal conductivity of dry soils for different quartz (sand) contents with experimental data from published literatures (Côté and Konrad, 2005; Johansen, 1977; Kersten, 1949; Smith and Byers, 1938; and Smith, 1942). Since the exact quartz contents of soil samples in the literatures were not clarified, the model predictions did not agree with experimental data very well. It was observed that the predicted thermal conductivities were slightly higher than the measured values for crushed rocks and natural mineral soils. This is mainly because of the extremely high quartz content of sands in this study. Assuming the quartz content in peat equals zero, the predicted thermal conductivities were still greater than the measured values because of the differences in mineral components between kaolin clay and peat.

Peat consists of a large amount of organic matter that has lower thermal conductivity than the anhydrous aluminum silicate in kaolin clay. However, the model prediction of thermal conductivity variations with porosity and quartz (sand) contents under dry condition still agreed with experimental data.

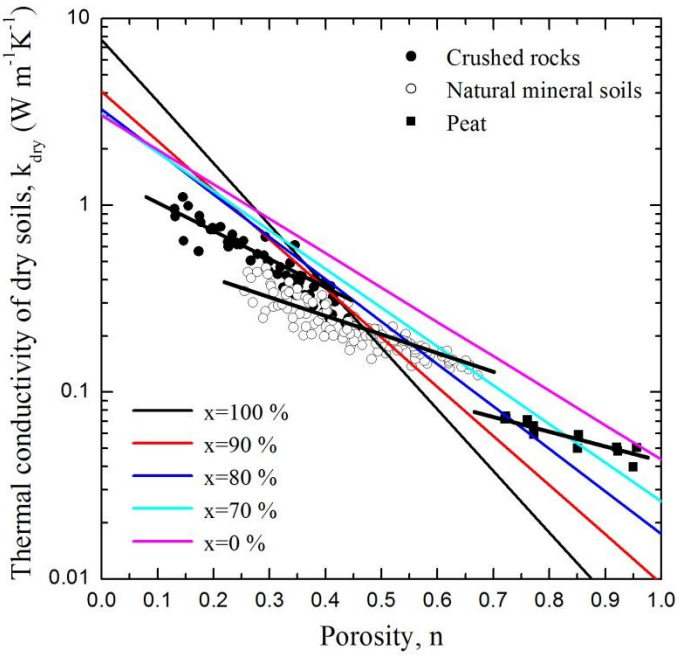

Figure 5-16 Comparison of predicted thermal conductivity of dry soils for different quartz (sand) contents with experimental data (Smith and Byers, 1938; Smith, 1942; Kersten, 1949; Johansen, 1977; and Cote and Konrad, 2005)

5.4.4.2 Validation for k_r-S_r Relationships

Figures 5-17 and 5-18 show the comparison of k_r-S_r relationships between the present model and Kersten (1949) data from different soil types. In Figure 5-17, the k_r-S_r relationship was depicted at quartz (sand) content equal to 100%, according to Equation 5.6, and it showed very good agreement with Ottawa sand and crushed quartz at low degrees of saturation. But the model overestimated the k_r value for the other three sands (i.e., Northway fine sand, Norway sand and Lowell sand) at high degree of saturation.

This is because these sands have different quartz contents: Ottawa sand and crushed quartz have the highest quartz content of 90%-100%, which is close to the quartz content (i.e., 100%) in the model prediction; whereas Lowell sand has quartz content of 43%-72%; and Northway sand and Northway fine sand contain only 10% quartz. In Figure 5-18, two k_r-S_r relationships were depicted at quartz (sand) content equal to 85% and 0%, respectively. Although the exact quartz contents of silty soils, clayey soils, silts and clays in Kersten's (1949) study were not clarified, the k_r-S_r relationship at x=0% (i.e. pure clay) also defined a lower boundary through the comparison with the experimental data. In addition, the k_r-S_r relationship at x=85% defined an upper boundary for all the experimental data which laid in between x=0% and x=85%. Consequently, the k_r-S_r relationship proposed in this study can effectively capture soil characteristics with respect to normalized thermal conductivity concept over a wide range of soil types.

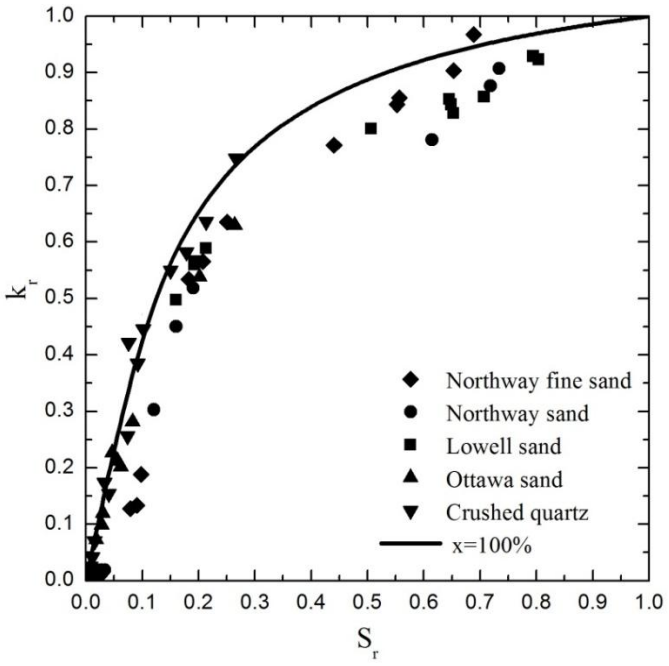

Figure 5-17 Comparison of k_r-S_r relationships between present model and 's (1949) data for medium and fine sands

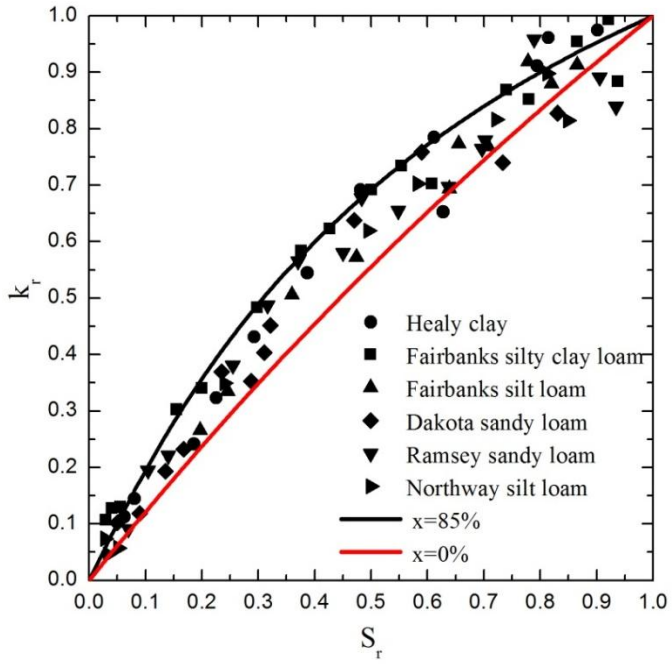

Figure 5-18 Comparison of k_r-S_r relationships between present model and Kersten's (1949) data for silty soils, clayey soils, silts, and clays

5.4.4.3 Validation for Thermal Conductivity Predictions

Figures 5-19, 5-20, and 5-21 show the comparisons of predicted thermal conductivity with measured values from the present study, Lu's et al. (2007) study, and Chen's (2008) study. In Figure 5-19, the predicted thermal conductivities were found to be in good agreement with the measured values from this study, with a difference of only 10%. Due to the uncertainty of quartz contents of soil samples in Lu's et al. (2007) study, the sand content was assumed to be identical to the quartz content in the model prediction. The predicted results did not match the measure values very well, and the deviation was around 15%, as shown in Figure 5-20. In Figure 5-21, the model prediction agreed with Chen's (2008) data with the deviation of 15%. All the soil samples in Chen's (2008) study were sands with quartz content of around 99%, and this value was used in the model prediction. Although the quartz contents of soil samples were determined

precisely in this case, the existence of a slight difference between predicted and measured values was probably because of the effects of particle size distribution and particle shape on sand thermal conductivity. However, the model can be used to predict soil thermal conductivity with at least an 85% confidence level.

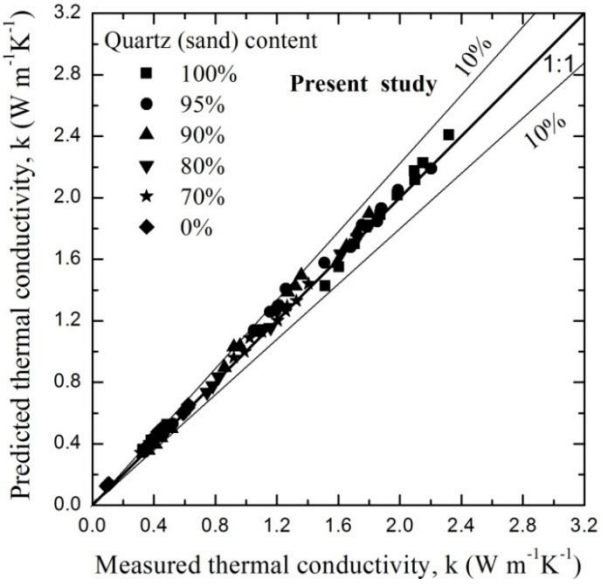

Figure 5-19 Comparison of predicted thermal conductivity with measured values from present study

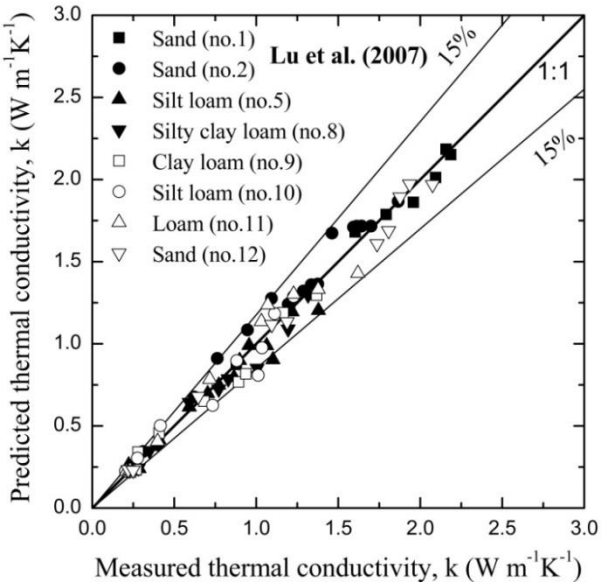

Figure 5-20 Comparison of predicted thermal conductivity with measured values from Lu et al. (2007) study

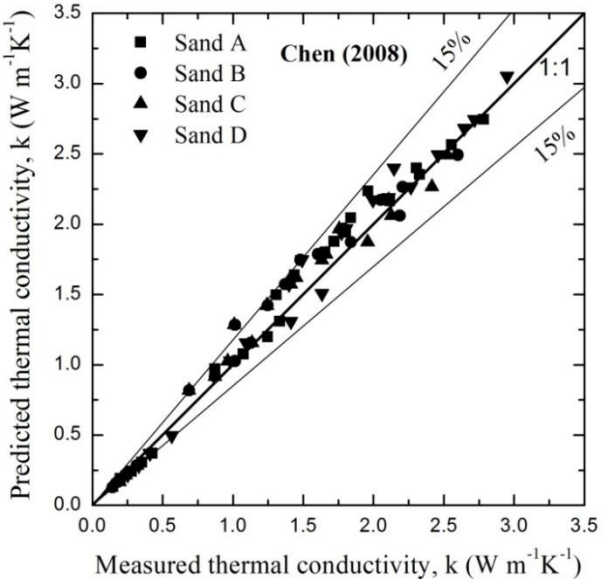

Figure 5-21 Comparison of predicted thermal conductivity with measured values from Chen's (2008) study

5.5 Summary

Soil thermal conductivity is of great importance in the exploitation and utilization of geothermal energy, as well as in the design of geothermal-related structures such as energy piles, ground source heat pumps (GSHP, and borehole thermal energy storage (BTES). In this chapter, a new continuum soil thermal conductivity model was proposed, based on a series of laboratory experiments on sand, kaolin clay, and sand-kaolin clay mixtures in different proportions, using the thermo-TDR probe. The major conclusions drawn in this chapter are detailed below.

Due to the considerable effect of quartz content on soil thermal conductivity, a fine-graded sand with known quartz content was selected to perform the laboratory experiments. The model proposed by empirical fits to experimental data incorporated quartz (sand) content as a variable and provided a precise prediction for thermal conductivity of solids in soils. It will further improve the prediction accuracy of overall thermal conductivity of soils, particularly when the quartz content of soils is known.

The effect of soil type on thermal conductivity was also taken into account from the change in sand (quartz) content in sand-kaolin clay mixtures. Since the sand content was assumed to be the same as quartz content in this study, there was no need to introduce other parameters. The model prediction of soil thermal conductivity was continuous over the entire soil type range, which filled the gaps of predicted soil thermal conductivity from other soil thermal conductivity models between any two neighboring soil types. It should be noted that the model validation for thermal conductivity prediction might not be adequate due to the lack of quartz content data of soil samples in previous literatures, but the predicted thermal conductivities were still found to be in good agreement with experimental data with at least 85% accuracy.

Chapter 6

Design and Evaluation of a Moisture/Suction TDR Probe

6.1 Introduction

Soil water characteristic curve (SWCC) is an important soil property under unsaturated conditions. It presents the relationship between the moisture content (i.e., w or θ) or degree of saturation (S_r) of soils and matric suction (ψ). As described in Chapter 2, several the of the most commonly used methods in the laboratory to obtain the SWCC of soils include filter paper method, pressure plate method, Tempe pressure cell method, and TDR probe method. However, in situ determination of SWCC is still difficult. Soil matric suction is often measured by a tensiometer in situ, but its measuring range is limited to ψ > -85 kPa (Cassel and Klute, 1986). Thermocouple psychrometry can be used to measure matric suction in a wide range, but it is very sensitive to temperature changes (Rawlins and Campbell, 1986). Thus, all previous methods may not be suitable for in situ measurements of matric suction and soil moisture content.

Noborio et al. (1999) indicated that measuring water, thermal, or electrical properties of a constructed porous medium equilibrated with surrounding soil is another attempt to indirectly measure soil matric suction. For specific ranges of water potential, the heat dissipation method, the filter paper method, or the gypsum block electrical-resistance method may be used in the laboratory and in the field (Campbell et al., 1986).

The TDR technique has been used successfully to measure soil moisture content, both in the laboratory and in situ (Yu and Drnevich, 2004). Baumgartner et al. (1994) and Whalley et al. (1994) attached porous materials functioning as tensiometers to the end of hollow electrodes of the TDR probe for simultaneous measurements of soil moisture content and matric suction. But the TDR probe has the same limitation as the

tensiometer does, which is the need to supply water to and the limited measuring range for ψ > -85 kPa.

Moreover, the TDR technique had been applied to a commercial product for estimating ψ values by measuring the dielectric constant (K_a) of an equilibrated porous medium (e.g. Equitensiometer, Delta-T Devices, Cambridge, England). Hence, an additional probe for moisture content measurement may be needed in order to measure a wider range of soil moisture contents and matric suctions simultaneously.

This chapter presents the design and evaluation of a moisture/suction TDR probe. The design and fabrication of the moisture/suction TDR probe was first introduced, then, the calibration of the probe was accomplished by a pressure plate test to establish the relationship between the matric suction and the dielectric constant (K_a) of a gypsum block. The evaluation of the probe was conducted by three tests: staged-drying test for validating the accuracy of measured soil moisture and matric suction by comparing it with other methods, and absorption and desorption tests for studying the response and equilibrium time of the gypsum block.

6.2 Design and Fabrication of Moisture/suction TDR Probe

6.2.1 Design of Moisture/suction TDR Probe

As described in Chapter 3, the impedance of a transmission line is a function of the spacing of the diameter of the probe in addition to the dielectric constant of the medium where the probe is installed. In addition, the location where a discontinuity is observed in a transmission line due to the change of spacing or diameter of the probe can be detected in reflected TDR waveforms (Davis, 1975). The impedance for a two-probe transmission line can be approximated by the following equation provided by Kraus (1984),

$$Z = (120 / K_a^{0.5}) \ln(s / d) \qquad (6.1)$$

where K_a is the dielectric constant of a material surrounding the transmission line, s is the spacing the two probes, and d is the diameter of the probes.

Figure 6-1 shows the schematic of the moisture/suction TDR probe in this research. There are two parts in the design. The two probes with a diameter of 2 mm and spacing of 25 mm in the top part are used to measure soil moisture, and the probes with the same diameter but smaller spacing of 5 mm, and covered by gypsum block of 25 mm × 25 mm × 50 mm in the bottom part, are for the matric suction measurement. It is noted that the design can distinguish reflections from the interface between different spacings of the two probes because the impedance is large enough in a full range of soil moisture contents. The gypsum block is made by the mixture of lab plaster and tap water in the laboratory. The fabrication of the probe will be introduced in the following section.

Knight (1992) and Petersen et al. (1995) suggested that a ratio of probe spacing to probe diameter should be greater than 0.02 to 0.1 to avoid concentrating the sensing volume in the surrounding space of the probe. The design of this probe meets the above requirements with ratios 0.08 and 0.4 for the top part and bottom part, respectively. Petersen et al. (1995) indicated that the distance between the TDR probe and the surface should be greater than 10, 15, and 20 mm for probes with spacing of 10, 20 and 50 mm, respectively, in order to avoid effects of incidents occurring on or near the soil surface on TR measurement. Moreover, the distance between the probe in the gypsum and the nearest gypsum surface is 10 mm, which is large enough to involve all the electromagnetic energy according to the recommendation in the Petersen et al. (1995) study. Consequently, the design can satisfy the main design criteria based on the previous studies.

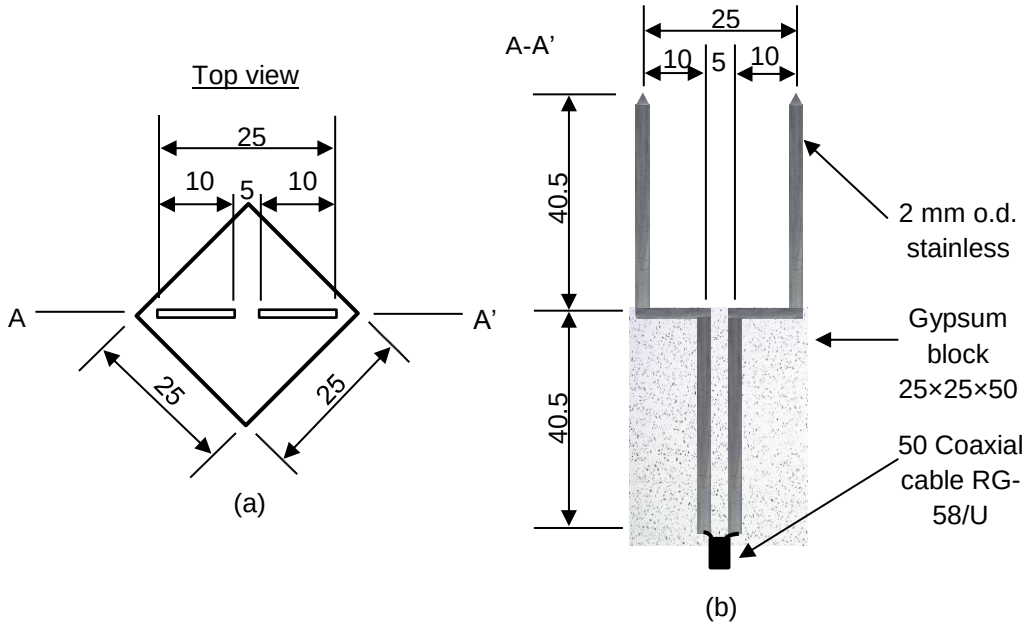

Figure 6-1 Schematic of moisture/suction TDR probe

6.2.2 Fabrication of Moisture/Suction TDR Probe

According to the design in Figure 6-1, the fabrication processes were as follows: (1) Two stainless probes with diameters of 2 mm were used. The total length of the probe was 82 mm, and it was bent in the shape shown in Figures 6-1 and 6-2. The pointed tip was also made for the two probes to disturb the soil as little as possible during the insertion process. (2) The two probes were clamped into a prefabricated Teflon mold, as shown in Figure 6-3. The probes were placed in the center of the mold and kept parallel to each other; (3) A Teflon spacer was used to clamp the probes outside the mold to fix the probe spacing (i.e., s = 25 mm), as shown in Figure 6-4. (4) One coaxial cable was taken, and the outer insulation layer was stripped to make the inner and outer wires exposed, with length of only 3 mm for both of them. The two wires were then soldered to the two probes at the top end by point contact, as shown in Figure 6-5. (5) The lab plaster was mixed with tap water in a ratio of 30 mL of water to 50 g of the lab plaster. The slurry of the lab plaster was then poured into the Teflon mold where the two probes were

placed in the center, as shown in Figure 6-6. The slurry was also stirred in the mold by a thin steel rod to remove as many air bubbles as possible. (6) The slurry was solidified and became hard with curing time. The Teflon mold and spacer were taken apart after 24 hours, and the moisture/suction TDR sensor was completed, as shown in Figure 6-7. (7) The surface of the gypsum block and the spacing between the two probes outside of the gypsum were examined. (8) The probe was left at room temperature (23-24^{o}C) for several days until the solidification process inside the gypsum block was completed.

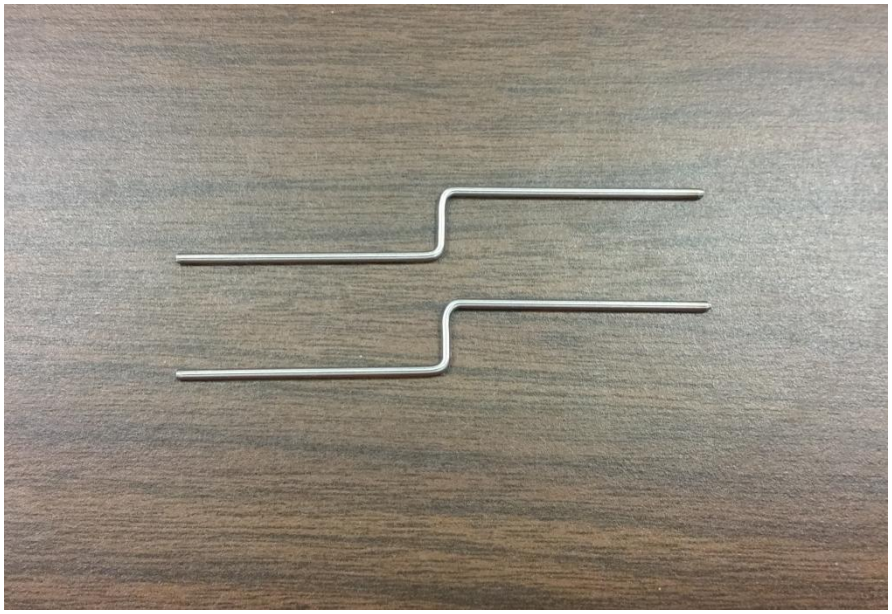

Figure 6-2 Photo of two steel stainless rods with diameter of 2 mm

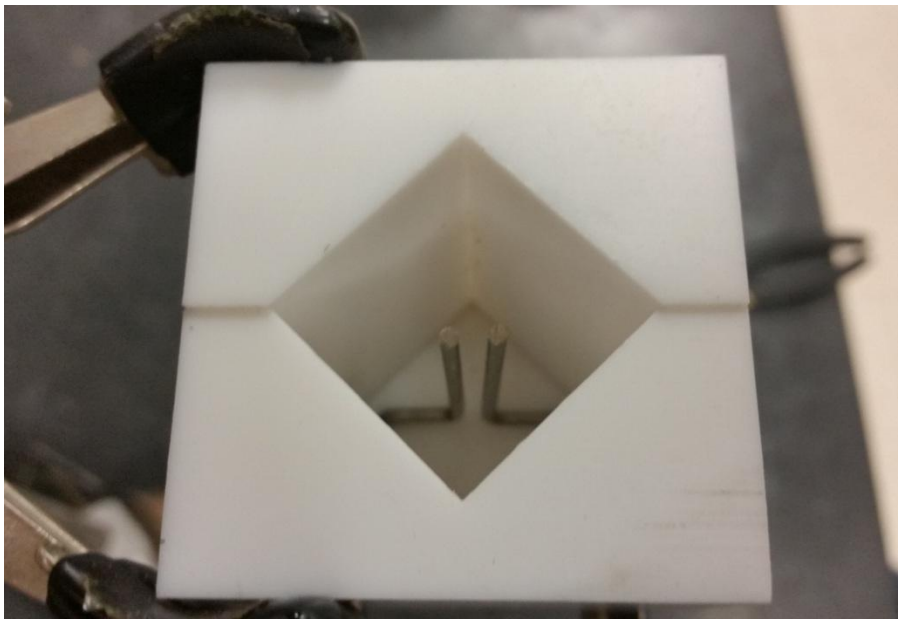

Figure 6-3 Photo of two rods clamped into a Teflon mode

Figure 6-4 Photo of the spacer at the probe end

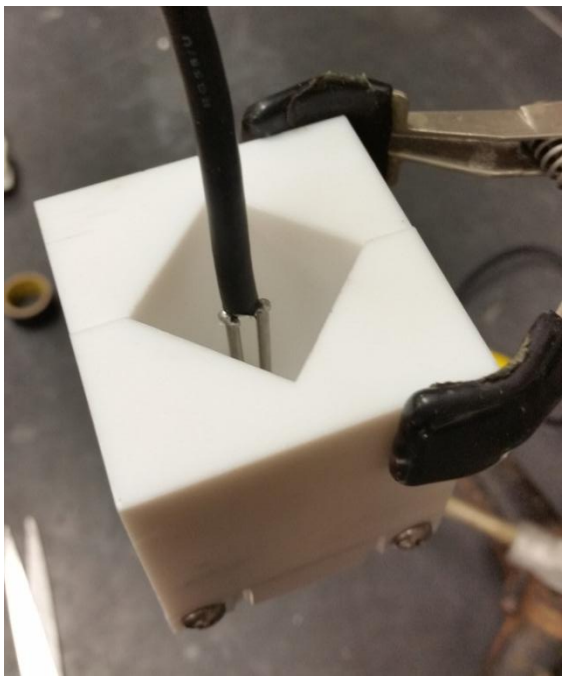

Figure 6-5 Coaxial cable was connected to the rods by soldering

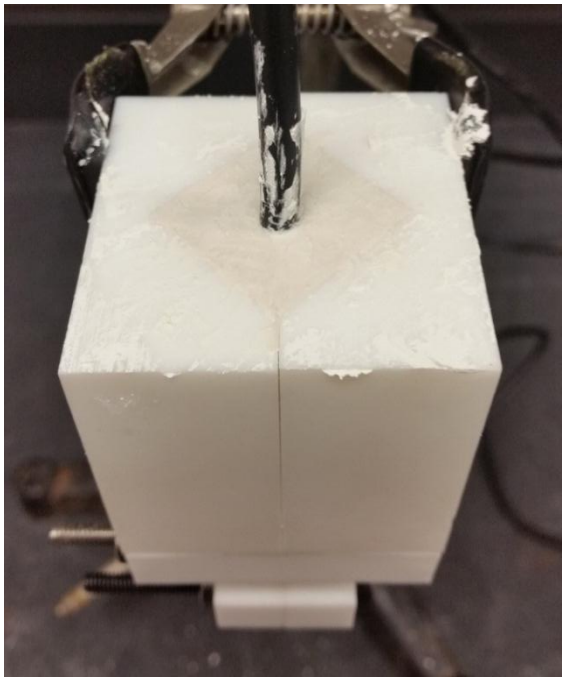

Figure 6-6 Casting of gypsum block

Figure 6-7 Completed moisture/suction TDR probe

6.3 Calibration of Moisture/Suction TDR Probe

The suction of gypsum was measured and assumed to be equal to the suction in the surrounding soils after the suction was equilibrated between the gypsum and the soils. As is well known, the suction is directly related to the moisture content, and the moisture content determines the dielectric constant (K_a), which can be estimated by the TDR technique with the help of the two probes embedded in the gypsum block. Thus, the goal of the calibration of the probe is to establish the relationship between K_a and the suction of the gypsum block for future suction measurements.

6.3.1 Determination of Reflection Points

Differing from the thermo-TDR probe, there are supposed to be three reflection points observed in the reflected TDR waveforms since the spacing of the two probes is suddenly changed at the interface between the gypsum block and the probes. However, the determination of the reflection points may become a little complicated for this

moisture/suction TDR probe. Hence, several simple tests were performed to illustrate the way to determine the locations of all the reflection points.

Two different types of experiments were conducted for the dry and saturated gypsum, respectively. The gypsum block was dried out at room temperature, and the TDR waveforms were collected under four scenarios: the probe was exposed in the air; only the probe was inserted into water, dry Ottawa 20/30 sand, and moist Ottawa 20/30 sand with moisture content of 1%, respectively. Then, the gypsum block was saturated in tap water for 24 hours, and the above tests were repeated. The reflected TDR waveforms of the dry and saturated gypsum are shown in Figures 6-8 and 6-9, respectively.

Figure 6-8 shows that the three reflection points were observed very clearly in water (i.e., red curve), but it was not easy to determine the second and the third reflection points for other scenarios. In addition, the K_a of water was around 79.8 from the calculation n, which was very close to the actual value (i.e., 81 at 20^{o}C). However, it was obvious that the signal was shifting to the right as the moisture content of the medium increased where the probe was inserted. Thus, the second and the third reflection points could eventually be determined through the comparison. In Figure 6-9, the similar pattern is also observed for the four scenarios. The location of the first reflection point was not changed for saturated gypsum, whereas both the second and the third reflection points shifted to the right, with the distance between the two points remaining constant (i.e., the calculated K_a of water was the same as shown in Figure 6-8). Moreover, the calculated K_a of gypsum was increased due to the increase in its moisture content. The two figures can be used as the reference to determine reflection points of the probe for future applications because the TDR waveforms under other conditions are supposed to lie in between that in air (i.e., black curve) and that in water (i.e., red curve).

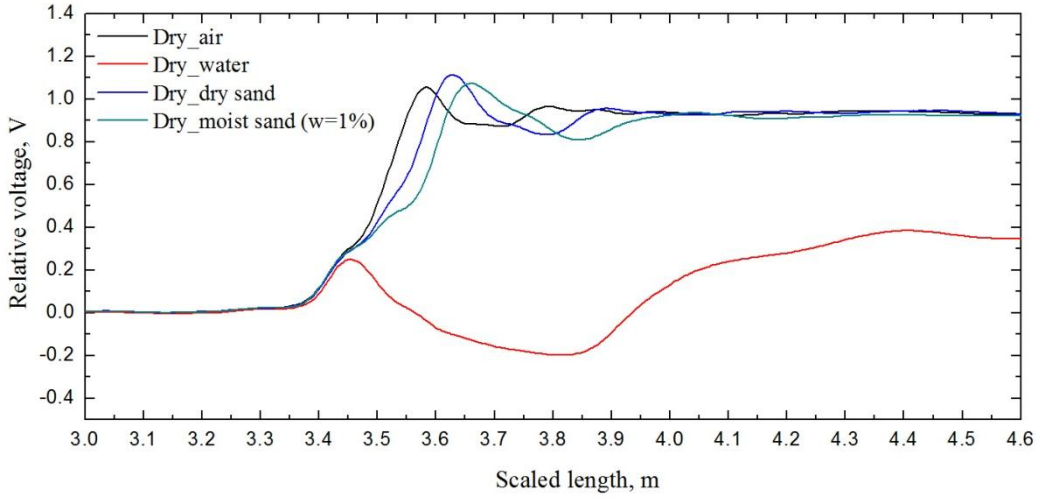

Figure 6-8 Typical reflected TDR waveforms of dry gypsum block

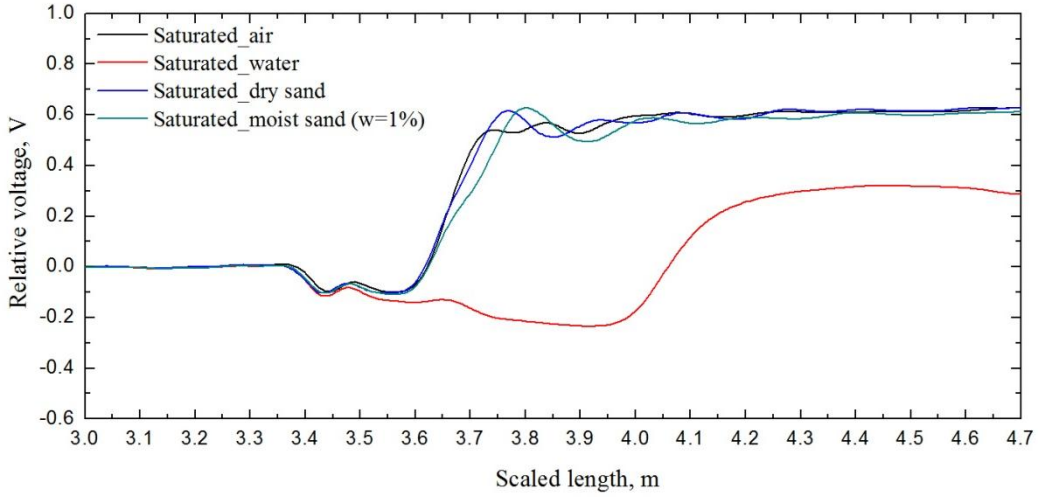

Figure 6-9 Typical reflected TDR waveforms of saturated gypsum block

6.3.2 Materials and Methods

The pressure plate test was employed to obtain the calibration relationship between K_a and the suction of gypsum block. The picture of the experimental setup is shown in Figure 6-10. The specific testing procedures were as follows. (1) The gypsum, along with the probe, was saturated in tap water for 24 hours, and the weight was

measured; The ceramic plate, with air entry value of 15 bars, was also saturated according to ASTM standard D6836. (2) The saturated gypsum block and ceramic plate were transferred into the pressure plate chamber, as shown in Figure 6-11. The effluent tube connected to a burette was filled with water and connected to the chamber, then the chamber was closed. (3) Air pressure of 7.5 bars was applied to the chamber, and the volume change of water in the gypsum block was monitored every day. (4) The effluent tube was removed when the volume change of water was less than one line per day, and the air supply was then stopped. (5) The chamber was opened, the probe was taken out and weighed again. The coaxial cable was connected to the Campbell Scientific TDR 100 to collect the reflected TDR waveform. (6) The above testing procedures were repeated under other air pressure levels, i.e., 4.0, 2.0, 1.0, 0.8, 0.5, 0.3, 0.1 bars.

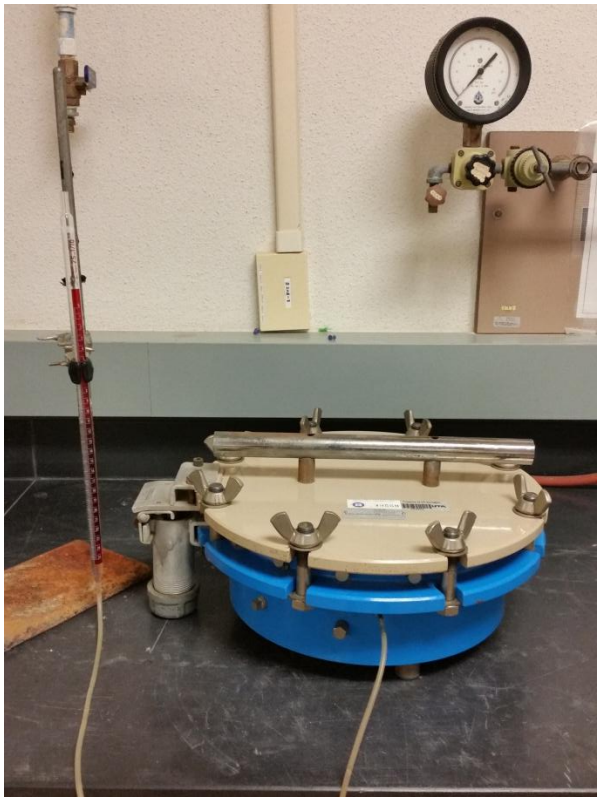

Figure 6-10 Photo of experimental setup of pressure plate test

Figure 6-11 Moisture/suction TDR probe in the chamber

6.3.3 Results and Discussion

The dielectric constant of gypsum and soil were determined (Baker and Allmaras, 1990) by,

$$K_{a,g} = (L_{a,g} / L)^2 \tag{6.2}$$

$$K_{a,s} = (L_{a,s} / L)^2 \tag{6.3}$$

where $K_{a,g}$ and $K_{a,s}$ are the dielectric constant of gypsum and soil, respectively; $L_{a,g}$ is the apparent length of gypsum, which is the distance between the first and the second reflection point in TDR waveforms; $L_{a,s}$ is the apparent length of soil, which is the distance between the second and the third reflection point in TDR waveforms; L is the probe length, i.e., 0.0405m.

Figure 6-12 depicts the reflected TDR waveforms under different suction levels from the pressure plate test. The symbol “Saturated” refers to the saturated gypsum block, and the corresponding TDR waveform was taken with the probe exposed in the air. It is evident that the signal was shifting to the right as the suction decreased, and the K_a of gypsum was increased as a result since the distance between the first and the second reflection point was increased. This is because the higher suction causes more moisture loss in the gypsum block; therefore, its K_a is going to be decreased.

Table 6-1 shows the summary of the pressure plate test, including the moisture loss, volumetric moisture content, the corresponding K_a of gypsum block at equilibrium, and the equilibrium time under each suction level. It should be noted that the initial volumetric moisture content of gypsum is 0.6, which was estimated by the change in weight under dry and fully saturated conditions. As suction increased, the moisture loss and the equilibrium time were increased, whereas the volumetric moisture and K_a of the gypsum block were decreased.

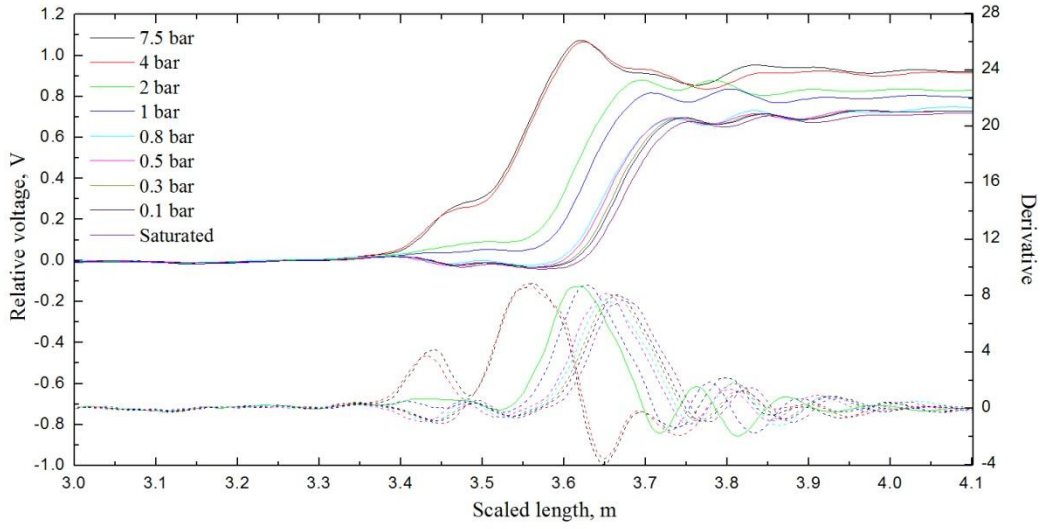

Figure 6-12 Reflected TDR waveforms in pressure plate test

Table 6-1 Summary of pressure plate test

Suction (bar)	Moisture loss (g)	Volumetric moisture content (θ)	Equilibrium time (day)	Dielectric constant (K_a)
0	0	0.600	0	24.25
0.1	0	0.600	1	23.26
0.3	0.02	0.599	2	22.83
0.5	0.08	0.597	2	21.78
0.8	0.11	0.596	2	19.75
1	1.26	0.560	6	16.01
2	3.35	0.493	8	11.11
4	8.60	0.325	9	7.12
7.5	9.50	0.296	10	5.98

Volumetric moisture content was plotted against matric suction, as shown in Figure 6-13. Similarly, the dielectric constant was plotted against the matric suction, as shown in Figure 6-14. Van Genuchten (1980) proposed a smooth, closed-form, three-parameter model for the soil-water characteristic curve in the form:

$$\theta = \theta_r + (\theta_s - \theta_r) \times \left[1/\left(1+\alpha\psi\right)^n \right]^m \tag{6.4}$$

where α, n, and m are fitting parameters. The mathematical form of the VG model accounts for an inflection point and allows greater flexibility than other models over a wider range of suction, and better captures the sigmoidal shape of typical curves. Moreover, the smooth transitions at the air-entry pressure and for suction approaching the residual condition are more effectively captured (Hoyos, 1998).

Using Equation 6.4 to fit the experimental data of volumetric moisture content and matric suction, as shown in Figure 6-10, it is found that the R^2 value was very close to the unity. The values of the fitted parameters are θ_s=0.603; θ_r=0.294; α=0.001;

n=2.111; m=12.969, respectively. Since the dielectric constant is directly related to the volumetric moisture content, the following equation, which is similar to van Genuchten's (1980) equation was used to fit the data of K_a and matric suction, as shown in Figure 6-14.

$$K_a = K_{ar} + (K_{as} - K_{ar}) \times \left[1/\left(1+\alpha\psi\right)^n \right]^m \tag{6.5}$$

where K_{as} and K_{ar} are dielectric constant at near saturation and residual water contents, respectively. The values of the fitted parameters are K_{as}=23.022; K_{ar}=3.648; α=0.015; n=4.524; m=0.198, respectively. It is obvious that the fitted curve can capture the characteristics of the relationship between K_a and matric suction very well, and it will be used as the calibration equation for future suction measurements. However, the measuring suction range of this probe is supposed to be limited from 10 to 750 kPa, which can be extended to a higher suction range by using other methods (e.g., filter paper method).

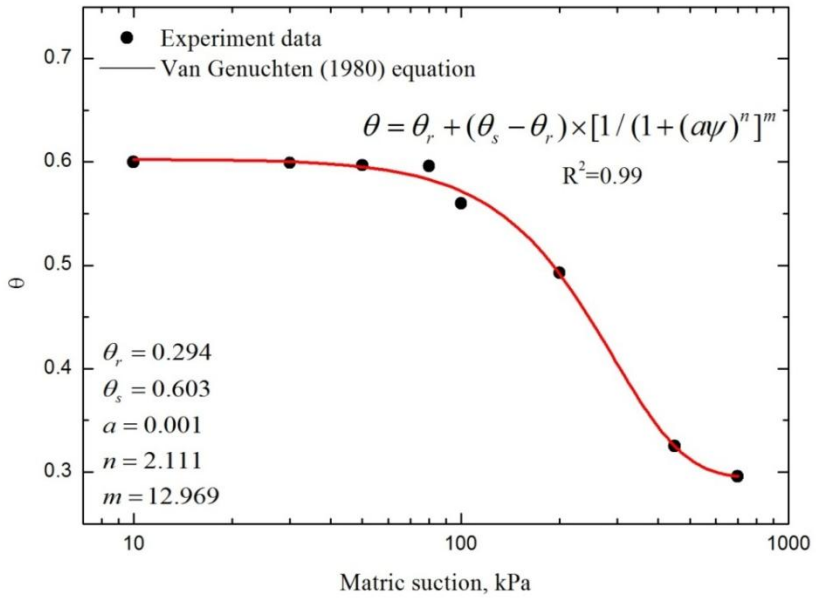

Figure 6-13 Volumetric moisture content and matric suction

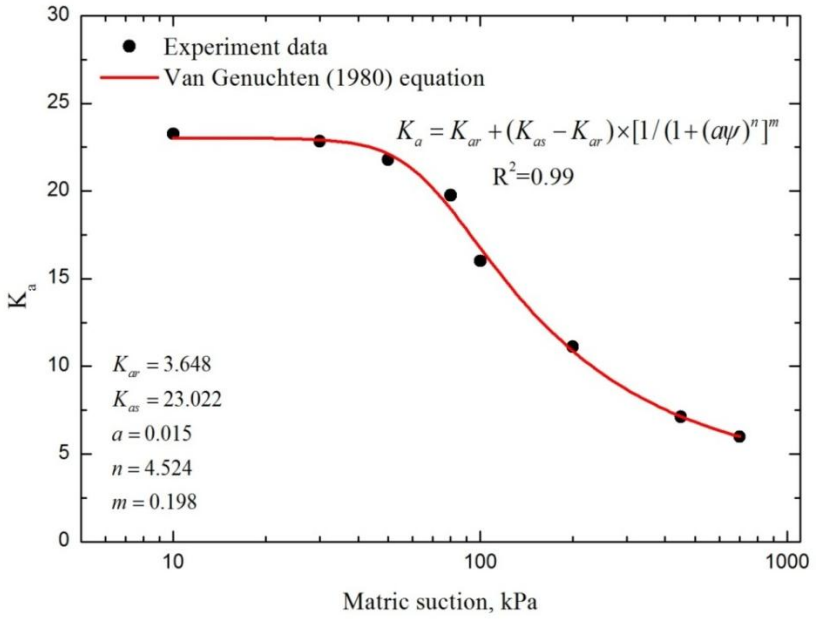

Figure 6-14 Dielectric constant and matric suction

6.4 Evaluation of Moisture/Suction TDR Probe

This section presents the evaluation of the moisture/suction TDR probe for soil moisture content and suction measurement. Three different experiments on silty sand were conducted, including staged-drying test, absorption test, and desorption test to evaluate the performance of the probe under low-to-medium matric suction range. The accuracy and reliability of the probe were validated against other suction measurements in previous studies.

6.4.1 Materials and Methods

The test soils were classified as silty sand (SM) according to the Unified Soil Classification System (USCS). The specific gravity test was conducted to obtain the specific gravity of the soil solids. Atterberg limit tests, conducted passing #4 fraction, classified the soil as non-plastic. The gradation curve of the silty sand is shown in Figure 6-15. The compaction curve obtained from standard proctor test (ASTM D698) is shown

in Figure 6-16.It was found that the maximum dry density of the silty sand was 1.875 g/cm^3, and corresponding optimum moisture content was 12.2%. The soil water characteristic curve (SWCC) of the silty sand was obtained by the Tempe cell test at maximum dry density, as shown in Figure 6-17. All the soil properties are listed in Table 6-2.

Table 6-2 Soil properties and grain sizes of silty sand (Patil, 2014)

Sand (%)	55
Silt (%)	37
Clay (%)	8
Specific gravity, G_s	2.67
USCS classification	Silty sand (SM)
Maximum dry unit weight, ρ_{dmax} (g/cm^3)	1.87
Optimum moisture content, w (%)	12.2

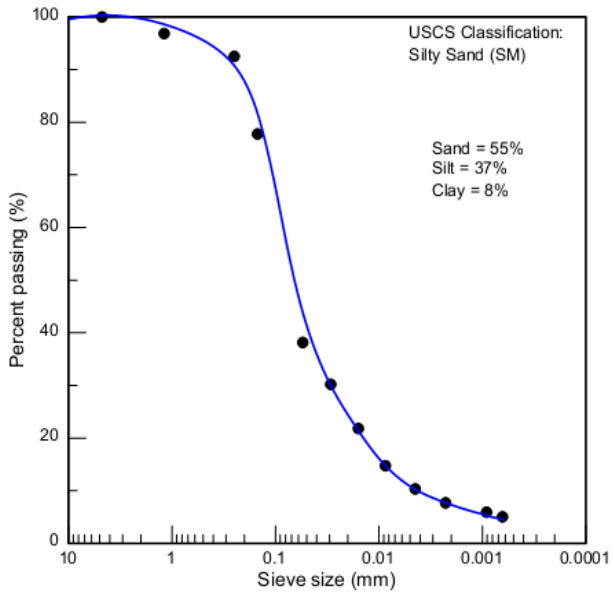

Figure 6-15 Gradation curve of silty sand (Patil, 2014)

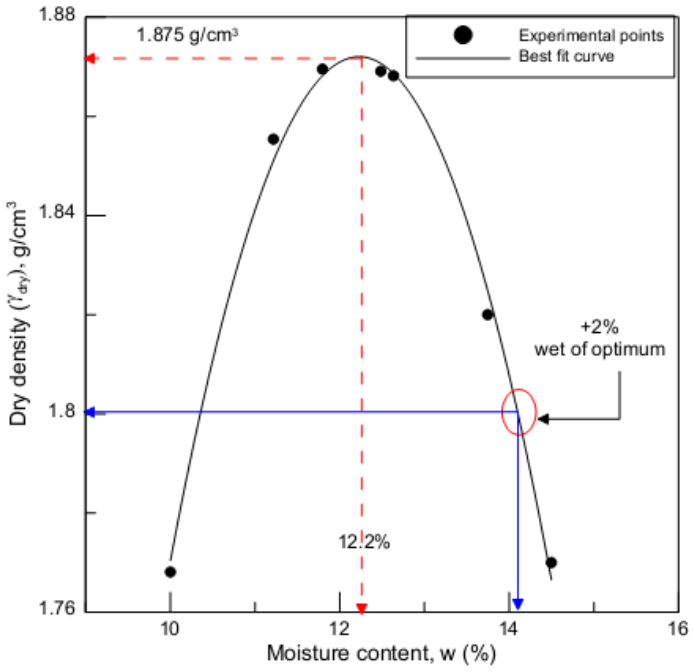

Figure 6-16 Standard proctor curve of silty sand (Patil, 2014)

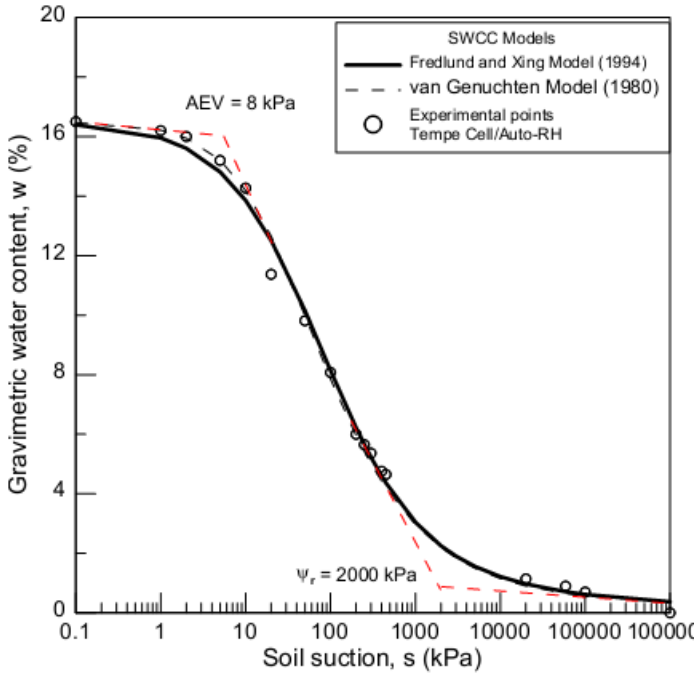

Figure 6-17 Soil-water characteristic curve for silty sand (Patil, 2014)

Three different tests can be conducted to evaluate the performance of the probe: staged-drying test, absorption test, and desorption test. The staged-drying test measures the soil suction at different moisture contents and compares the results with the suction measurements by the Tempe cell method in Patil's (2014) study. It is emphasized that the dry density of the sand specimen in this study is 1.875 g/cm^3, which is the maximum dry density of the silty sand and the same as that in Patil's (2014) study. In the meantime, the calibration relationship between K_a and the soil moisture content can be established for future moisture content measurement. The absorption and desorption tests can study the equilibrium time of the gypsum block in sand specimen for suction measurement. Figure 6-18 shows the schematic of the experimental setup. Figures 6-19 and 6-20 show the pictures of the sand specimen and the experimental setup.

The specific testing procedures of the staged-drying test are described as follows. A PVC mold with an inner diameter of 100 mm and height of 120 mm was prepared, and a hole with a diameter of 14.22 mm was drilled on the side wall of the PVC mold, 40 mm from the bottom. The height of the sand specimen in the mold was set as 80 mm (shown in Figure 6-18).

(1) The dry silty sand was thoroughly mixed with tap water. The target moisture content of the sand specimen was 12.2% (i.e., the optimum moisture content, as shown in Figure 6-16).

(2) The predetermined mass of moist silty sand was poured into the mold and compacted to form the first layer (i.e., 40 mm thick) of sand specimen with dry density equal to 1.875 g/cm^3.

(3) The moisture/suction TDR probe with the dry gypsum block was placed on the top surface of the sand specimen horizontally, and the coaxial cable was allowed to go through the hole on the side wall of PVC mold.

(4) The probe, along with the gypsum block, was covered by the second layer of 40 mm thick compacted silty sand.

(5) Heat and moisture insulation foam was used to seal the gap between the hole and coaxial cable to avoid moisture exchange between the atmosphere and sand specimen, as shown in Figure 6-19.

(6) A plastic cover was used to wrap the PVC mold at the top surface. Then, the TDR waveforms were collected continuously for 48 hours at moisture content of 12.2%.

(7) The plastic cover was removed, and the sand specimen was placed on an electronic scale. A mechanical fan was used to dry the specimen until the moisture content was reduced to 9%.

(8) The plastic cover was again used to cover the specimen, and the specimen was left for another 24 hours at room temperature.

(9) The TDR waveforms were again collected at w=9% for 48 hours, and the test was repeated at 6% and 3%.

The testing procedures of absorption and desorption test were as follows.

(1) After the staged-drying test, the total moisture loss of the sand specimen was 91.7 g. Then, the same amount of tap water was poured into the mold to start the absorption test, and the specimen was wrapped by the plastic cover.

(2) The TDR waveforms were then collected continuously for 90 hours.

(3) After the adsorption test, the mechanical fan was again used to dry the soil continuously for 400 hours, and the TDR waveforms and weight of the specimen were again collected at 1 hour to 150 hour intervals.

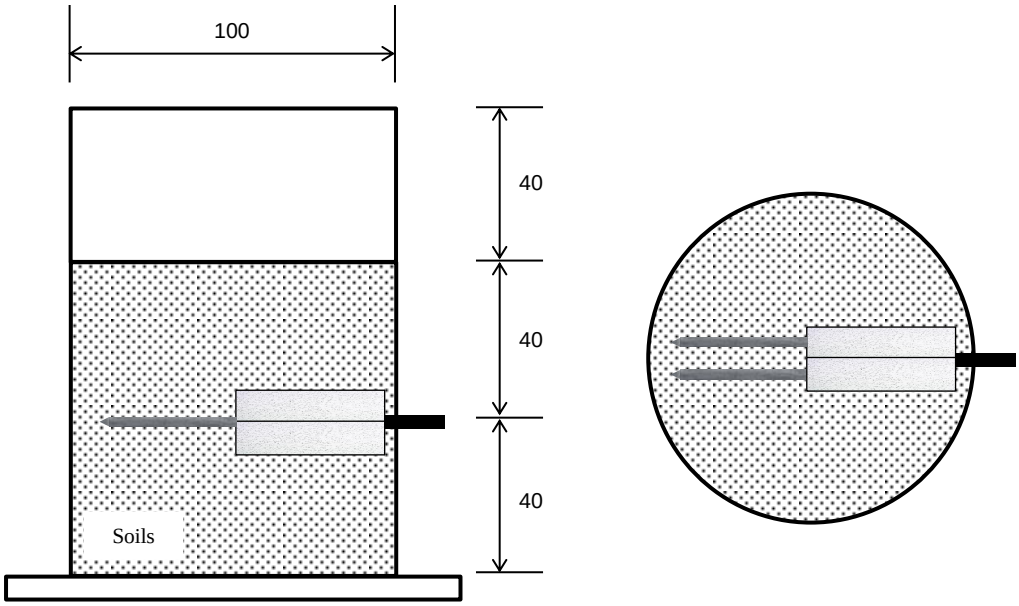

Figure 6-18 Schematic of experimental setup of staged-drying test, absorption and desorption tests

Figure 6-19 Photo of test silty sand in desorption test

Figure 6-20 Photo of experimental setup

6.4.2 Results and Discussion

6.4.2.1 Staged-Drying Test

Figures 6-21, 6-22, 6-23, and 6-24 show the reflected TDR waveforms in the staged-drying test at four different moisture contents (12.2%, 9%, 6%, and 3%). It was found that the signal did not vary with time at moisture content of 9%, 6%, or 3%. At moisture content of 12.2%, the first reflection point remained at the same location, but the second and the third reflection points shifted toward the right with time, as shown in Figure 6-21. At the beginning of the test, the dry gypsum block absorbed the moisture from the surrounding soils because of the large difference in moisture content between them. As a result, the TDR waveforms varied with time. After drying the specimen by the mechanical fan, the specimen was left for 24 hours, and then the TDR waveforms were collected. In Figures 6-22, 6-23, and 6-24, the unchanged TDR waveforms revealed that the moisture between the gypsum block and the surrounding soils was supposed to be

equilibrated all the time during the testing period of 48 hours. It is also inferred that the suction equilibrium between the gypsum block and soils had been attained before taking the TDR waveforms for moisture content of 9%, 6%, and 3%. In addition, the equilibrium time at w = 12.2% will be discussed in the following sections.

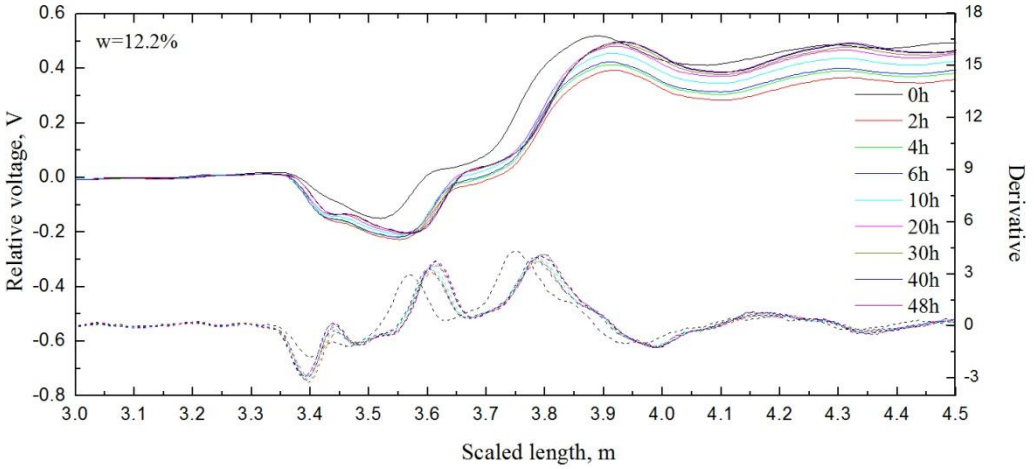

Figure 6-21 Reflected TDR waveforms at w = 12.2% in staged-drying test

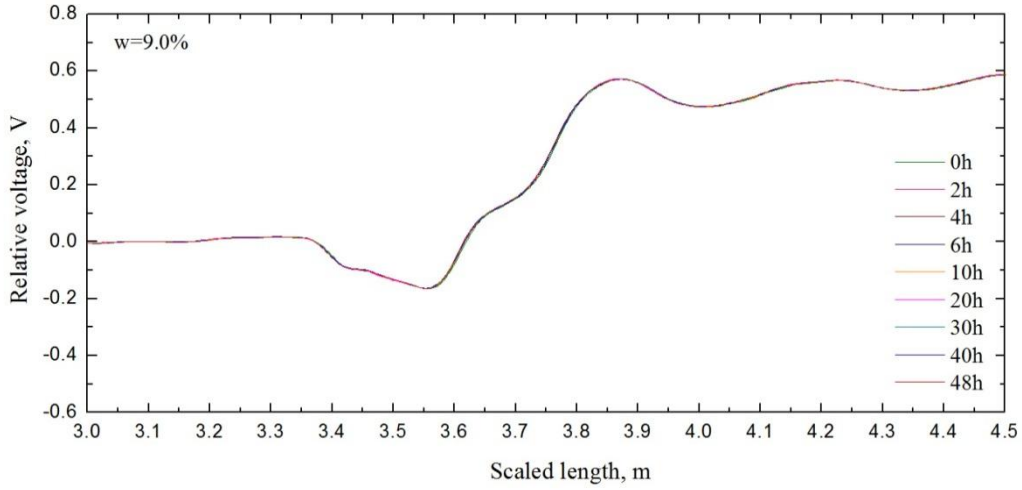

Figure 6-22 Reflected TDR waveforms at w = 9.0% in staged-drying test

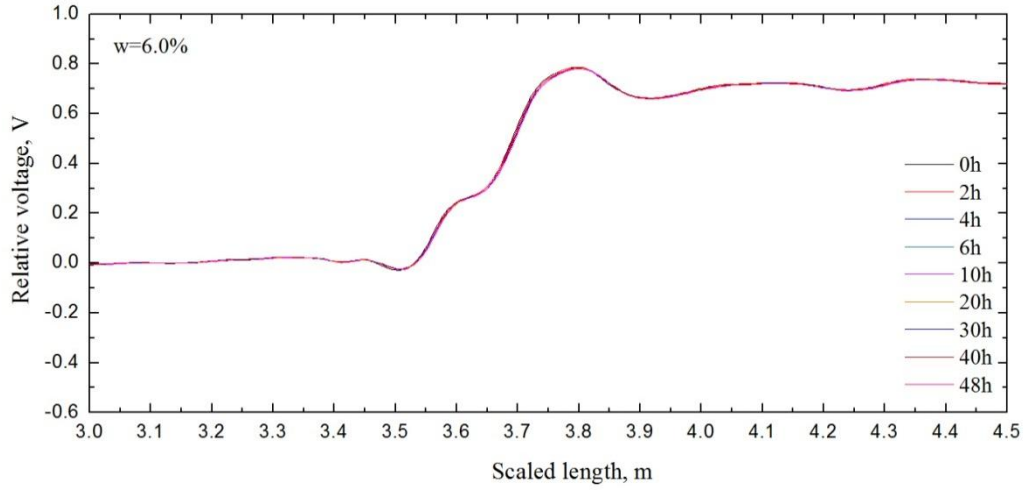

Figure 6-23 Reflected TDR waveforms at w = 6.0% in staged-drying test

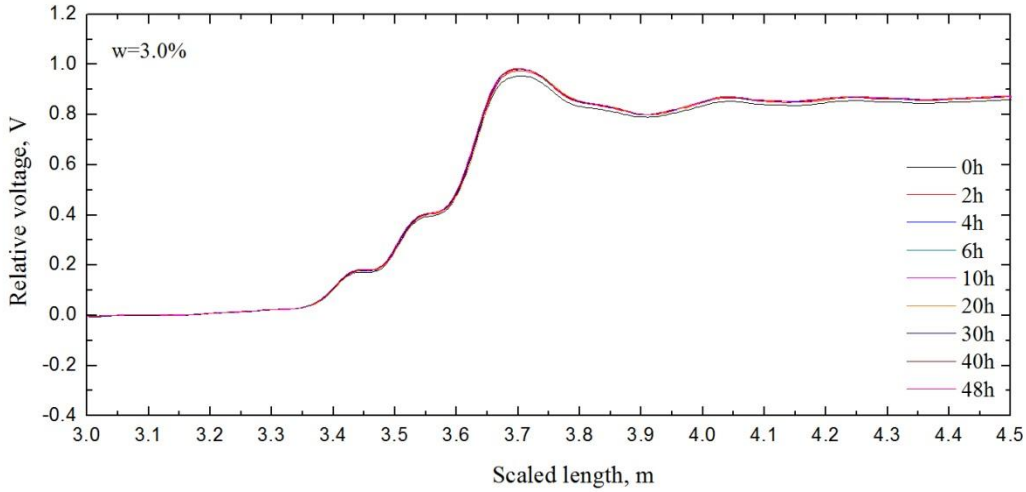

Figure 6-24 Reflected TDR waveforms at w = 3.0% in staged-drying test

According to Equations 6.2 and 6.3, the dielectric constants of gypsum block (i.e., K_{a1}) and soils (i.e., K_{a2}) can be calculated from the TDR waveforms. The variations of K_{a1} and K_{a2} with time are depicted in Figures 6-25 and 6-26. It is obvious that the increase in K_{a1} was significant in the first 7-8 hours, and then became gradual at w = 12.2%, while it was almost constant at w = 9%, 6%, and 3%. Another feature is that the

K_{a1} was not reduced considerably from 12.2% to 9%, but it dropped dramatically from 9% to 6%, as well as from 6% to 3%. This is probably because the higher matric suction, induced by the drying process, caused more moisture loss in the gypsum block, resulting in a big decrease in K_{a1} as well.

In Figure 6-26, K_{a2} did not vary too much for the whole testing period. A small fluctuation was observed in the beginning of the test, which was mainly caused by a disturbance from the environment. It was also proven that the moisture in the specimen at each target moisture content was uniformly distributed before collecting the TDR waveforms. The calculated K_{a2} and the actual moisture content can be used to establish the calibration relationship for future moisture content measurements for this silty sand.

According to the calibration equation shown in Figure 6-14, the suction of the gypsum block was calculated and plotted against time, as depicted in Figure 6-27. It is indicated that the suction continuously decreased with time at w = 12.2% because of the absorption of moisture of the gypsum block from the surrounding soils. The measured suction at the other three moisture contents was unchanged with time, which is consistent with previous results. Furthermore, it should be noted that the suction cannot be calculated based on the calibration equation if K_{a1} is greater than K_{as} (i.e., 23.022). In the experiment, the K_{a1} was increased to 23.000 at 48 hours at w = 12.2%, and it was assumed to be the actual value under the suction equilibrium. The equilibrium time at this moisture content was supposed to be around 48 hours as well.

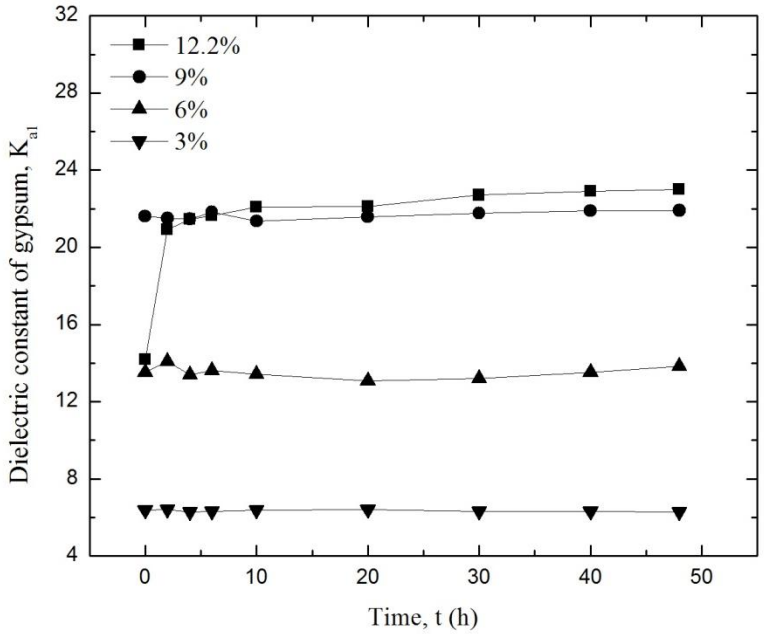

Figure 6-25 Variation of K_{a1} with time

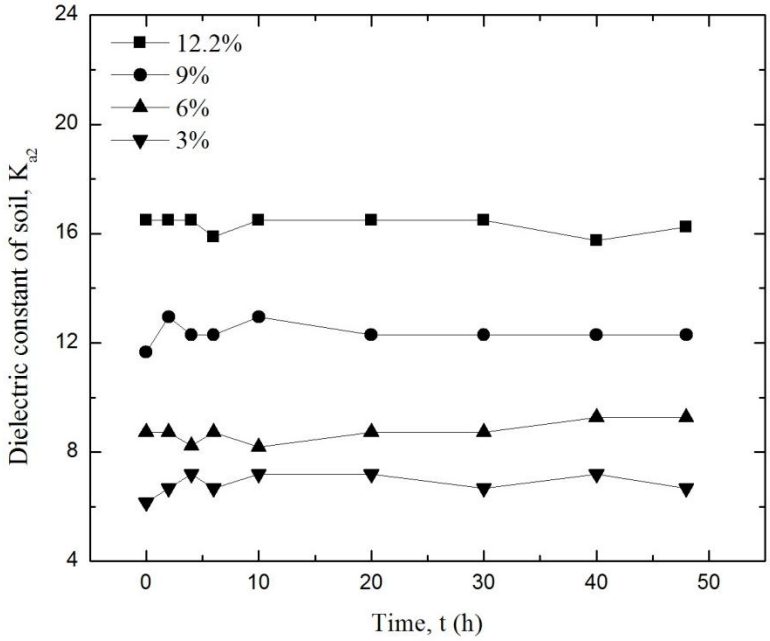

Figure 6-26 Variation of K_{a2} with time

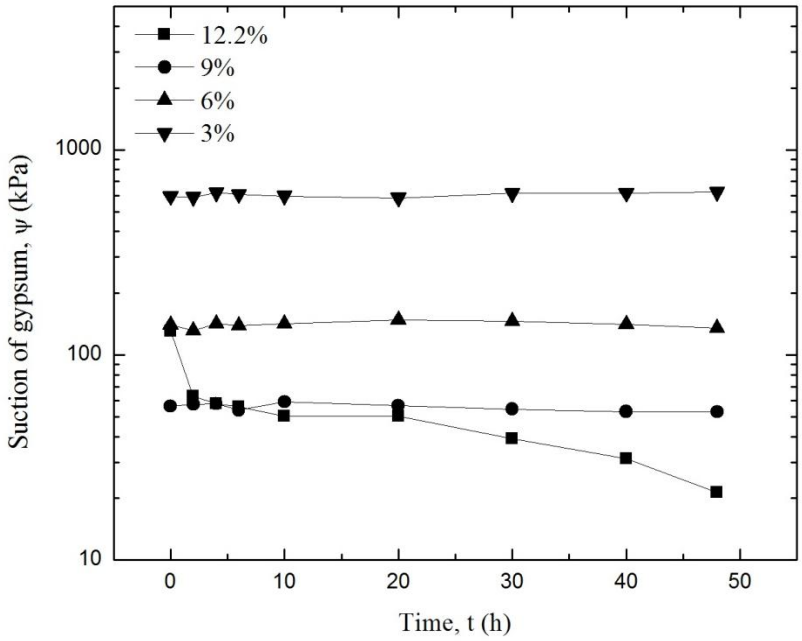

Figure 6-27 Variation of matric suction with time

Figure 6-28 shows the relationship between volumetric moisture content (θ) and dielectric constant (K_a). The comparison of experimental data with the Topp et al. (1980) equation is also presented in the figure. It should be noted that the TDR-measured K_a in Figure 6-28 was the average of the 48-hour measurement, as shown in Figure 6-26. It was found that the experimental data exhibited bias with Topp's et al. (1980) equation, but it followed a similar trend as the TDR-measured K_a was increased with volumetric moisture content. The difference between the experimental data and Topp's et al. (1980) equation can probably be attributed to the lack of considering the effect of dry density on K_a in Topp's et al. (1980) equation, as presented by Dirksen and Dasberg (1993). Jacobsen and Schjonning (1993) also noted that the improved accuracy of their moisture prediction equation was primarily due to the incorporation of dry density. In addition, the calibration equation for moisture content measurement was obtained by fitting the experimental data, using a power function, as shown in Figure 6-28.

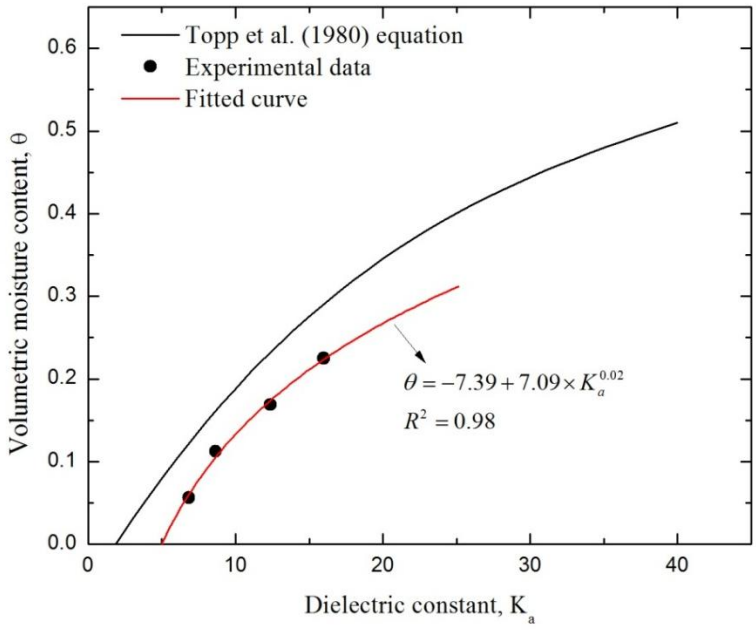

Figure 6-28 Volumetric moisture content and TDR-measured dielectric constant

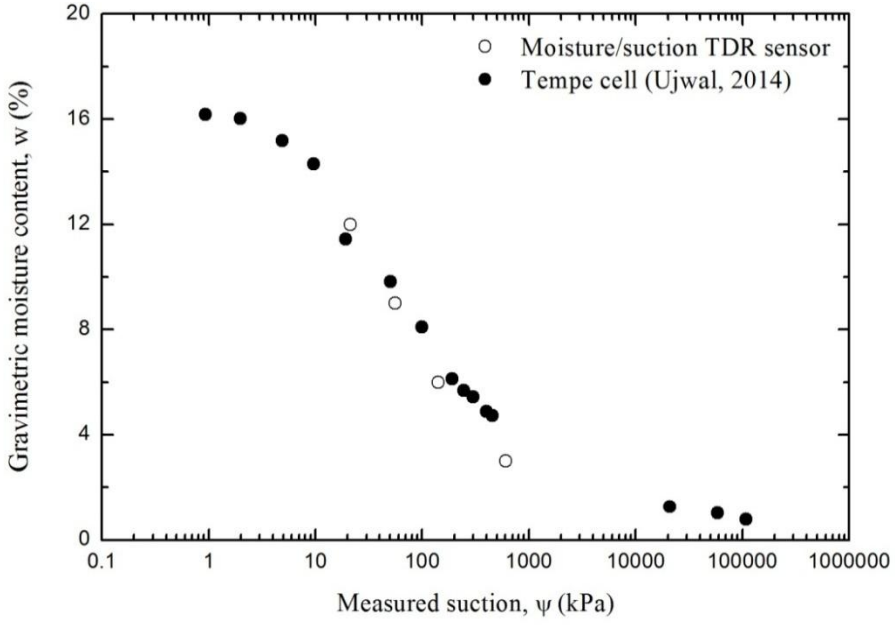

Figure 6-29 Comparison of the suction measurement between Tempe cell test (Patil, 2014) and the moisture/suction TDR probe

The comparison of measured suction by the moisture/suction probe with those obtained by the Tempe cell test in Patil's (2014) study is shown in Figure 6-29. It is obvious that the suction measurement from the two different methods agreed with each other very well in moisture content range 3% < w < 12.2%. However, the performance of the new probe in moisture content range, i.e., w > 12.2% or w < 3%, was not examined in the staged-drying test.

It is noted that the new probe may not be very sensitive in suction measurement, particularly when the soils are at high moisture contents, i.e., low suction levels. As shown in Figure 6-14, the K_a of the gypsum block was almost kept constant when $\psi < 50$ kPa. It also means the probe probably cannot provide accurate measurement within the above suction range. Another limitation of the probe is that the TDR-measured K_a at high suction levels was not included in the calibration equation (shown in Figure 6-14). Thus, the probe is not suitable for application to soils of low moisture contents or high suction levels. It is also observed that the measured suction by the new probe started to deviate from those of the Tempe cell test at 3%, as shown in Figure 6-29.

6.4.2.2 Absorption Test

Figure 6-30 shows the reflected TDR waveforms in the absorption test. It was found that the variation of the signal primarily occurred within the first hour after pouring the water into the mold. Because the silty sand has a relatively high hydraulic conductivity and it was a small sample size, the water penetrated the specimen rapidly in the beginning of the absorption test. The variation of K_a with time is shown in Figure 6-31. Similarly, the K_a of both gypsum and soils suddenly increased in the first hour, and then it varied slightly from 1 hour to 90 hours. It can also be inferred that the moisture was distributed uniformly in the specimen after 1 hour.

The measured suction with time obtained from the K_a of gypsum block was not plotted since the TDR-measured K_a exceeded K_{as} (i.e., 23.022) somewhat in the experiment; whereas the suction of specimen was supposed to be around 20 kPa at this moisture content (i.e. w=12.2%), as shown in Figure 6-17. It also demonstrated the insensitivity of the new probe in a low-suction measuring range. In addition, the average K_a of the sand specimen was 15.54 from 1 hour to 90 hours, and the predicted moisture content obtained from the calibration equation (shown in Figure 6-28) was 11.5%, which is very close to the actual value of 12.2%. Consequently, the high degree of measurement accuracy of moisture content by the new probe is corroborated.

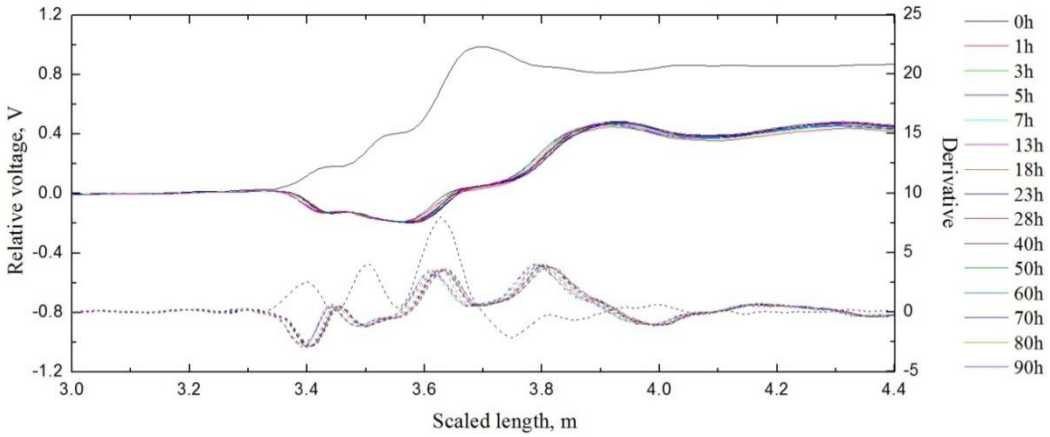

Figure 6-30 Reflected TDR waveforms in absorption test

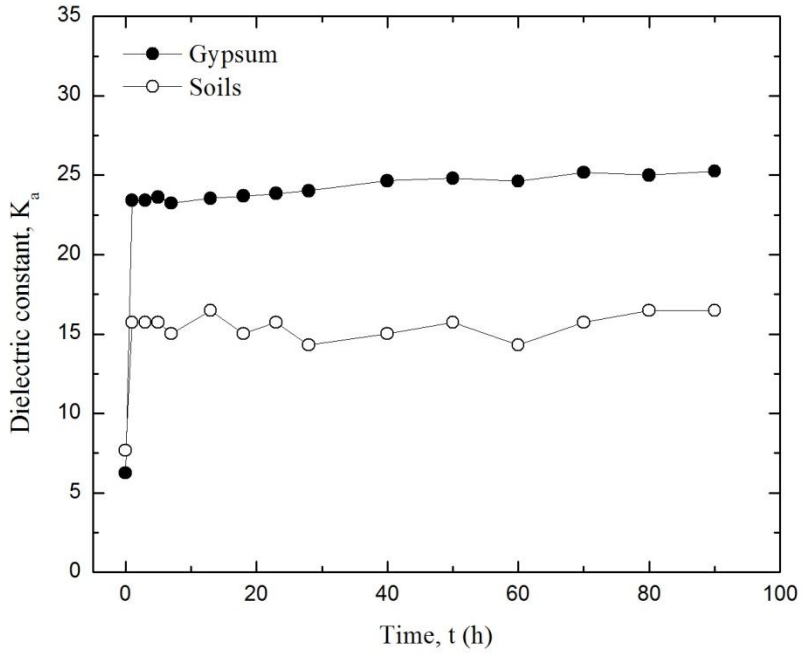

Figure 6-31 Variation of K_a with time in absorption test

6.4.2.3 Desorption Test

Figure 6-32 indicates the reflected TDR waveforms in the desorption test. It was found that the signal was shifting to the left with time continuously, which meant that the dielectric constants of both the gypsum block and soils were decreasing because of the moisture loss. The dielectric constants of gypsum (K_{a1}) and soil (K_{a2}) were calculated from TDR waveforms and are shown in Figure 6-33. It is illustrated that the K_{a1} was almost linearly decreased before 100 hours, and then did not change too much after that. But the K_{a2} dropped significantly in the first 24 hours, and then decreased slowly after that. This is because that the moisture in the top layer of the specimen was lost in the beginning, leading to the non-equilibrium in suction between the gypsum block and the surrounding soils. Then, the moisture in the gypsum block started moving into the specimen, resulting in a decrease in K_{a1}. Thus, the K_{a1} may decrease more slowly than the K_{a2} in the first 24 hours because of the hysteresis of the gypsum block.

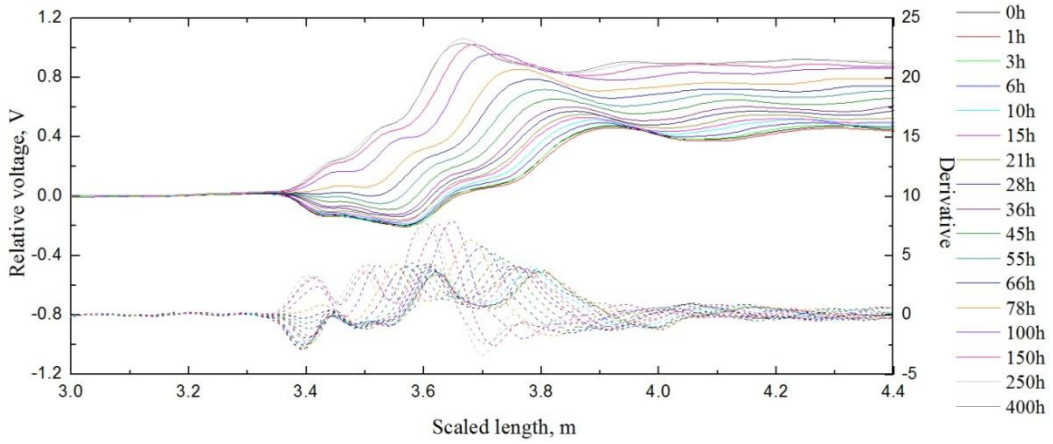

Figure 6-32 Reflected TDR waveforms in desorption test

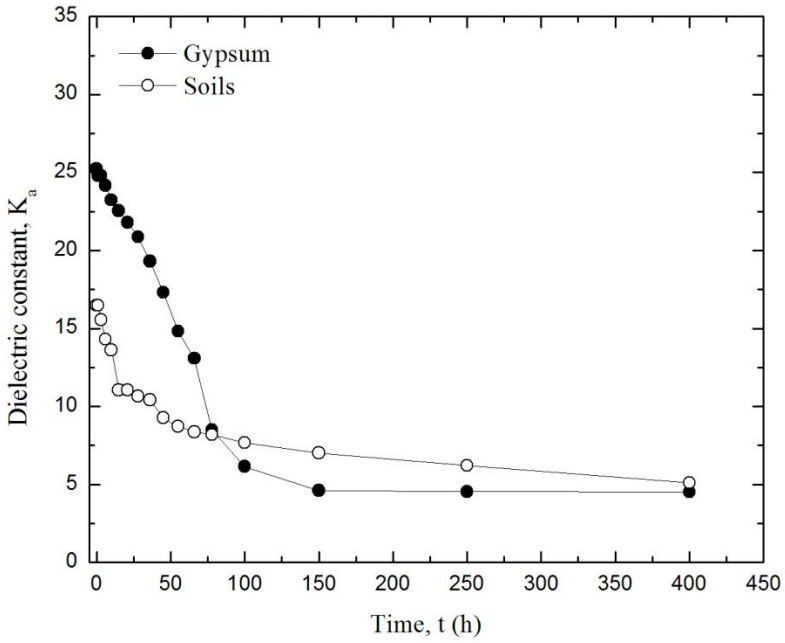

Figure 6-33 Variation of K_a with time in desorption test

According to the calibration equation shown in Figure 6-28, the moisture content of the specimen during the desorption process was predicted, based on the measured K_{a2}. Figure 6-34 shows the measured and predicted moisture content of the specimen with time. A slight difference was observed at low moisture content range, but it was also

found that the predicted values agreed with the measured results over a wide range of moisture contents.

Soil matric suction was also calculated from desorption test and shown in Figure 6-35. Compared with the results from the Tempe cell experiments in Patil's (2014) study, it was found that the measured suction by the probe was always lower than the Tempe cell experiments at suction levels below 300 kPa, and it reached the actual value after 10-25 hours. This is because the moisture flow driven by the matric suction from the gypsum block to the specimen takes time to get the suction equilibrium between them. However, a good agreement was observed at higher suction ranges, from 300 kPa to 2000 kPa. This is because the higher suction accelerated the speed of the moisture flow from the gypsum block to the specimen and reduced the time needed to attain the suction equilibrium. In addition, the measured suction at 250 hours was much lower than that obtained from the Tempe cell experiment since the calibration relationship for suction measurements was limited within a suction range between 10 and 750 kPa. Thus, the probe may not be applicable to soils at higher suction ranges.

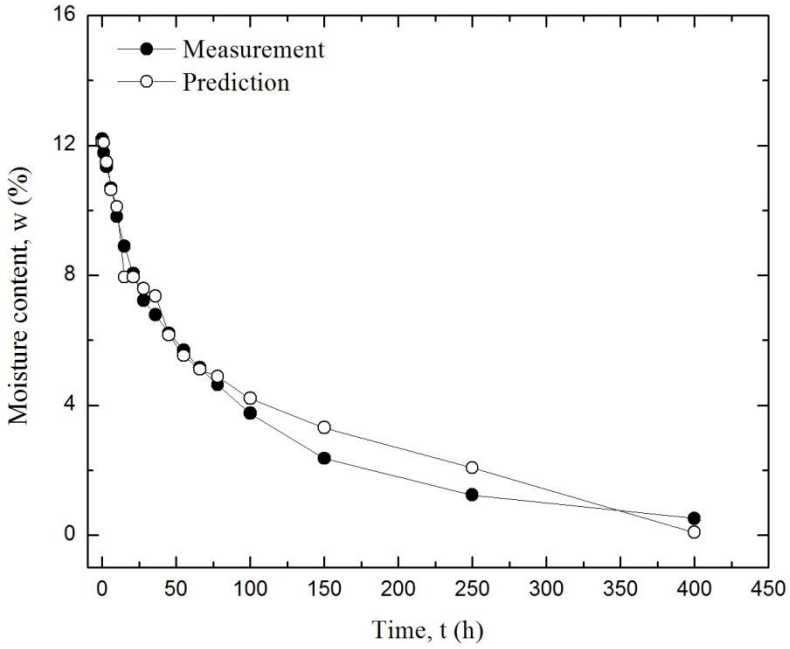

Figure 6-34 Measured and predicted moisture content in desorption test

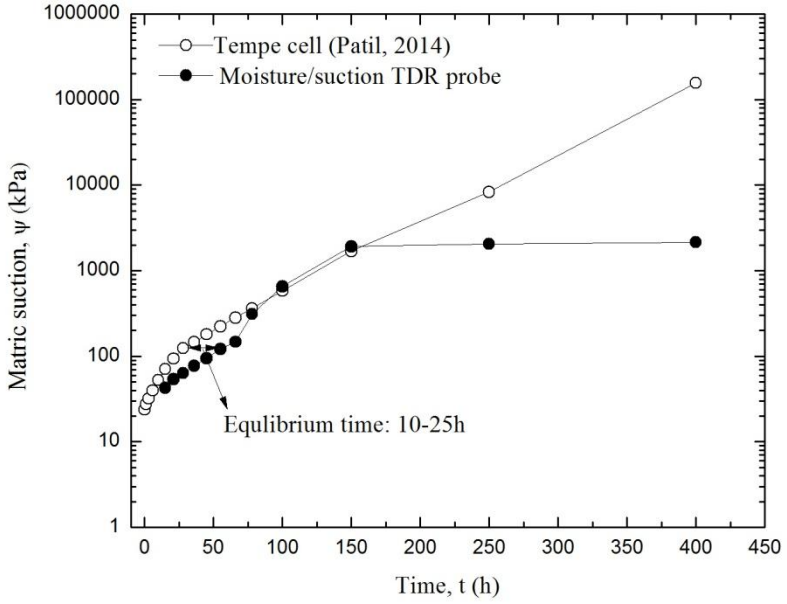

Figure 6-35 Measurement of matric suction with time: Tempe cell test (Patil, 2014) and the moisture/suction TDR probe

6.5 Summary

Based on the TDR technique, a new moisture/suction TDR probe was designed and fabricated to measure soil moisture content and matric suction simultaneously. The calibration equation for suction measurement was obtained by the pressure plate test, while the calibration relationship for soil moisture content measurement was established by the staged-drying test.

The evaluation of the probe was conducted through three tests on silty sand: staged-drying test, absorption test, and desorption test. The test results revealed that: (1) the moisture/suction probe can predict moisture content rapidly and accurately in wetting and drying processes; (2) the equilibrium time of the dry gypsum block in moist specimen with moisture content of 12.2% is around 48 hours; (3) the probe can measure the suction satisfactorily during the drying process at suction ranges between 300 kPa and 2000 kPa, whereas the equilibrium time of the gypsum block is around 10-25h at suction levels below 300 kPa; (4) the probe is only applicable in suction ranges from 10 to 2000 kPa, and it may underestimate soil suction at higher suction levels. The applicability of the probe in other soil types still needs to be studied in the future. In addition, the calibration curve for suction measurement can be extended by other methods (e.g., filter paper method) for soils at higher suction ranges.

Chapter 7

Summary, Conclusions and Recommendations

7.1 Introduction

This research mainly focuses on the development and validation of two different types of TDR-based sensors for thermal conductivity and soil suction measurements. The traditional measurement methods of soil thermal properties are time consuming and unreliable due to the moisture migration in the heating process. Moreover, simultaneous measurement of soil thermal property, moisture content, and dry density is a challenging issue, but very important to many geothermal-related applications in geotechnical engineering. Soil suction is also an important soil property in unsaturated soils, but it is not easily, rapidly, or accurately measured in the field.

In this research, a thermo-TDR probe was designed by integrating a dual heat probe with a TDR moisture sensor to measure soil thermal property, moisture content, and dry density simultaneously. The probe had one center probe and two outer probes with a diameter of 2 mm, length of 40.5 mm, and probe-to-probe spacing of 6 mm. The soils were heated in the experiments, and then the thermal properties were measured according to a line heat theory, in conjunction with the “peak value method” proposed by Bristow (1993). A KD2 standard probe was also used to compare the measured results. Based on the TDR technique, the prediction of moisture content and dry density of soils was accomplished by Topp’s et al. (1980) equation, the heat capacity method, and the one-step method, respectively. It was also validated against actual measurements by the oven-drying method.

Laboratory experiments, using the thermo-TDR probe, were performed on sand-sand and sand-clay mixtures under different moisture and dry density conditions after the evaluation of the probe was completed by testing three sands and one kaolin clay. The

effects of fines content, particle size, and clay content on thermal conductivity of mixtures were analyzed and discussed. A new continuum soil thermal conductivity model was also developed based on the test results of sand-clay mixtures and the normalized thermal conductivity concept proposed by Johansen (1975).

Another TDR-based sensor, the moisture/suction TDR probe, was designed and evaluated for simultaneous measurement of soil moisture and matric suction. The probe had two parts: a dual probe with a diameter of 2 mm and probe-to-probe spacing of 25 mm to measure soil moisture content, and the same dual probe with a smaller spacing of 5 mm and encapsulated in a gypsum block to measure soil matric suction. The calibration equation for suction measurement was obtained by employing the pressure plate test under different suction levels, i.e., 7.5, 4.0, 2.0, 1.0, 0.8, 0.5, 0.3, 0.1 bars. The probe evaluation was conducted by three different tests on a silty sand: staged-drying test, absorption test, and desorption test. In the meantime, the calibration equation of moisture content measurement was also obtained from the first test. Moreover, the equilibrium time and the response time of the new probe in the measurements of soil moisture and matric suction were also analyzed and discussed based on the test results.

7.2 Summary and Conclusions

The two types of TDR--based sensors designed in this research are promising tools which can measure soil thermal properties, moisture content, dry density, and matric suction rapidly and accurately, both in the laboratory and in the field. The major summaries and conclusions of this research are listed below:

Compared with previously designed TDR probes, the design of this probe was further optimized in this research. The probe-to-probe spacing was reduced to avoid probe deflection, and the pointed tip was also adopted to minimize the soil disturbance as much as possible during the insertion process.

1) From the calibration of the thermo-TDR probe, the test results revealed that the thermo-TDR probe can measure both dielectric constant (K_a) and electrical conductivity (EC_b) accurately from reflected TDR waveforms by using the Baker and Allmaras (1990) method.
2) The thermos-TDR probe's performance in soil thermal properties measurement was evaluated against the standard KD2 (TR-1) single probe and (SH-1) dual probe. The relative deviation of measured thermal conductivity, thermal diffusivity, and volumetric heat capacity of three sands and one kaolin clay were within 10%, 20%, and 25%, respectively.
3) Based on the TDR technique, the moisture content and dry density of the above three sands and one kaolin clay were also predicted by the Topp et al. (1980) equation, the heat capacity method, and the one-step method. Two new relationships between the dielectric constant and the volumetric moisture content for sands and clay were proposed, which were different from the Topp et al. (1980) equation. In addition, the heat capacity method exhibited reasonably well-predicted results for soil dry density. The one-step method showed he highest degree of accuracy in the prediction of both soil moisture content and dry density, with deviations of 10% and 5%, respectively.
4) The application of the thermo-TDR probe in measuring thermal properties, moisture content, and dry density of sand-clay mixtures was also studied. The clay content in mixtures ranged from 0% , 5%, 10%, 20%, to 30% by dry weight. The differences between the thermo-TDR probe and KD2 (SH-1) dual probe in measured thermal conductivity, thermal diffusivity, and volumetric heat capacity were 10%, 15%, and 20%, respectively. The one-step method still exhibited the best performance in the prediction of moisture content and dry density, with at least 90% accuracyl.

5) From the laboratory experiments in which the thermo-TDR probe was used, it is concluded that the thermal conductivity of soil increases with moisture content because the water has a greater thermal conductivity value (i.e., 0.59 W $m^{-1}K^{-1}$) than air (i.e. 0.026 W $m^{-1}K^{-1}$). The elevated dry density also leads to an increase in soil thermal conductivity, which is attributed to the decrease in thermal resistance due to the increase in the number of physical contact points among soil particles. But the dry density effect was not considerable compared with that of the moisture content in this study. In addition, the quartz content had a big effect on soil thermal conductivity because of the higher thermal conductivity of quartz (i.e., 7.7-8.4 W $m^{-1}K^{-1}$) compared with other soil minerals.

6) From the study on sand-sand mixtures, it is concluded that fine sands have the lower thermal conductivity at dry condition but higher thermal conductivity at low moisture content conditions compared with coarse sands because of the particle size effect. The thermal conductivity of moist sands was much greater than that of dry sands. The thermal conductivity of coarse sands increased to peak value by increasing fine sand contents to critical fines content (F_{cr}). Moreover, F_{cr} increased with a decrease in d_f/d_c ratio in the experiments.

7) Due to the considerable effect of quartz content on soil thermal conductivity, the fine-graded sand with known quartz content was selected to perform the laboratory experiments on sand-clay mixtures; thereby, such effect can be studied quantitatively. The results revealed that the thermal conductivity of mixtures decreased bi-linearly as the clay content increased. The critical clay content (C_c) was found to be equal to 10% in the experiments. The decrease in thermal conductivity was much more pronounced at C_c <10% than that at C_c >10%.

8) In terms of thermal conductivity predictions, the improved model (Zhang et al., 2015a) can predict thermal conductivity of sands with high quartz content more precisely than the other five alternative thermal conductivity prediction models. The Modified Cote and Konrad (2005) model and the Lu et al. (2007) model, which account for a continuous change of model parameters κ and α with clay content, can predict thermal conductivity of sand-clay mixtures satisfactorily and guide the design of geothermal-related structures effectively for geothermal applications.
9) A new continuum soil thermal conductivity model was proposed based on a series of laboratory experiments on sand, kaolin clay, and sand-kaolin clay mixtures in different proportions, using the thermo-TDR probe. The model incorporated the degree of saturation, porosity, and quartz content as variables, and was capable of accounting for the quartz content effect and predicting soil thermal conductivity continuously. From the study of model validation, the predicted thermal conductivities were found to be in good agreement with the experimental data with at least 85% accuracy.
10) A new moisture/suction TDR probe was designed and fabricated for simultaneous measurement of soil moisture content and matric suction. The probe can measure the soil moisture content accurately and rapidly based on the TDR technique. It also measures the soil suction reasonably well at suction ranges between 10 kPa and 2000 kPa. The equilibrium time of suction measurement in the drying process is around 10-24 hours.

7.3 Novelty and Limitations of Studies

The novelty items of this research are listed below:

1) Although the thermo-TDR probe was designed and used to measure soil thermal properties, moisture content, and dry density, the performance of the probe still

needs to be improved due to some design flaws. A comprehensive evaluation of the probe was studied through the laboratory experiments on three sands, kaolin clay, and sand-clay mixtures for simultaneous measurement of the above mentioned soil properties.

2) The effects of fines content, particle size, and clay content on soil thermal conductivity was experimentally studied by using the thermo-TDR probe. The critical clay content (C_c) was found for the sand-clay mixtures. Then, the variation of thermal behavior of soils, ranging from sand to clay, was better understood.

3) The continuum soil thermal conductivity model proposed in this research surpasses the existing models because it can predict soil thermal conductivity continuously over the entire range of soil types and can account for the quartz content effects in some cases.

4) The moisture/suction TDR probe was first designed and used in geotechnical engineering for simultaneous measurement of soil moisture content and matric suction. The study of probe calibration and evaluation attests to the strong performance of the TRD probe, as well as its great potential for better achieving the previously cited goals in the future.

7.4 Recommendations for Future Study

The recommendations for future study are listed below:

1) The measured thermal diffusivity and heat capacity of the thermos-TDR probe deviated somewhat from those obtained by the KD2 probe, which is probably because of the effects of moisture migration on the experimental results. The improper assumption of line heat theory for the probe with certain diameters can also cause some measurement errors. Hence, the possible sources of measurement error

need to be further studied to improve the measurement accuracy for future applications.

2) For the moisture/suction TDR probe, the calibration curve for soil suction is limited to suction ranges of less than 750 kPa. It can be extended to higher suction levels by other methods, such as the filter paper method. The equilibrium and response time of the gypsum block under different environmental conditions still need to be further evaluated. Moreover, the material loss of the gypsum itself for long term operation in the field was not considered in this research. This effect on measured soil moisture content and matric suction needs to be studied in the future.

References

ASTM C177-13, Standard Test Method for Steady-State Heat Flux Measurements and Thermal Transmission Properties by Means of the Guarded-Hot-Plate Apparatus, ASTM International, West Conshohocken, PA, 2013.

ASTM C778-13, Standard Specification for Standard Sand, ASTM International, West Conshohocken, PA, 2013.

ASTM D2216-10, Standard Test Methods for Laboratory Determination of Water (Moisture) Content of Soil and Rock by Mass, ASTM International, West Conshohocken, PA, 2010.

ASTM D4643-08, Standard Test Method for Determination of Water (Moisture) Content of Soil by Microwave Oven Heating, ASTM International, West Conshohocken, PA, 2008.

ASTM D4959-07, Standard Test Method for Determination of Water (Moisture) Content of Soil By Direct Heating, ASTM International, West Conshohocken, PA, 2007.

ASTM D4944-11, Standard Test Method for Field Determination of Water (Moisture) Content of Soil by the Calcium Carbide Gas Pressure Tester, ASTM International, West Conshohocken, PA, 2011.

ASTM D3017-05, Standard Test Method for Water Content of Soil and Rock in Place by Nuclear Methods (Shallow Depth) (Withdrawn 2007), ASTM International, West Conshohocken, PA, 2005.

ASTM D5195-14, Standard Test Method for Density of Soil and Rock in Place at Depths Below Surface by Nuclear Methods, ASTM International, West Conshohocken, PA, 2014.

ASTM D4564-08e1, Standard Test Method for Density and Unit Weight of Soil in Place by the Sleeve Method (Withdrawn 2013), ASTM International, West Conshohocken, PA, 2008.

ASTM D2937-10, Standard Test Method for Density of Soil in Place by the Drive-Cylinder Method, ASTM International, West Conshohocken, PA, 2010.

ASTM D1556 / D1556M-15, Standard Test Method for Density and Unit Weight of Soil in Place by Sand-Cone Method, ASTM International, West Conshohocken, PA, 2015.

ASTM D2167-08, Standard Test Method for Density and Unit Weight of Soil in Place by the Rubber Balloon Method, ASTM International, West Conshohocken, PA, 2008.

ASTM D5298-10, Standard Test Method for Measurement of Soil Potential (Suction) Using Filter Paper, ASTM International, West Conshohocken, PA, 2010. .

ASTM D5334-08, Standard Test Method for Determination of Thermal Conductivity of Soil and Soft Rock by Thermal Needle Probe Procedure, ASTM International, West Conshohocken, PA, 2008.

ASTM D0698-12e1, Standard Test Methods for Laboratory Compaction Characteristics of Soil Using Standard Effort (12 400 ft-lbf/ft^3 (600 kN-m/m^3)), ASTM International, West Cons/hohocken, PA, 2012.

Abdulla, S. A.K. Mohammed, and H. Al-Rizzo (1988). "The complex dielectric constant of Iraqi soils as a function of water content and texture." *Geoscience and Remote Sensing, IEEE Transactions on*, 26(6), 882-885.

Abiodun, R. O., and O. Edwin "Modelling the mechanical, thermo-physical, and filtration properties of dried clay-sand mixtures for water storage vessel using regression method."

Abramowitz, M., and I. A.. Stegun, I. A. (1972). *Handbook of mathematical functions*, Dover New York.

Abu-Hamdeh, N. H. (2003). "Thermal properties of soils as affected by density and water content." *Biosystems Engineering*, 86(1), 97-102.

Abu-Hamdeh, N. H., and R. C. Reeder (2000). "Soil thermal conductivity effects of density, moisture, salt concentration, and organic matter." *Soil Science Society of America Journal*, 64(4), 1285-1290.

Åkesson, M., A. Ledesma, C. Gatabin, A. C. Jacinto, and M. Sanchez (2009). "Bentonite THM behaviour at high temperatures: experimental and numerical analysis." *Géotechnique*, 59(4), 307-318.

Akrouch, G. A., M. Sanchez, and J. L. Briaud (2015). "Effect of the Unsaturated Soil Condition on the Thermal Efficiency of Energy Piles." *IFCEE 2015*, 1618-1627.

Al-Khafaf, S., and R. Hanks (1974). "Evaluation of the filter paper method for estimating soil water potential." *Soil Science*, 117(4), 194-199.

Baker, J., and R. Allmaras (1990). "System for automating and multiplexing soil moisture measurement by time-domain reflectometry." *Soil Science Society of America Journal*, 54(1), 1-6.

Baker, J., and R. Lascano (1989). "The spatial sensitivity of time-domain reflectometry." *Soil Science*, 147(5), 378-384.

Balland, V., and P. A. Arp (2005). "Modeling soil thermal conductivities over a wide range of conditions." *Journal of Environmental Engineering and Science*, 4(6), 549-558.

Baumgartner, N., G. W. Parkin, and D. E. Elrick (1994). "Soil water content and potential measured by hollow time domain reflectometry probe." *Soil Science Society of America Journal*, 58(2), 315-318.

Bennett, D., and R. Gens (2008). "Overview of European concepts for high-level waste and spent fuel disposal with special reference waste container corrosion." *Journal of Nuclear Materials*, 379(1), 1-8.

Benson, C. H., and P. J. Bosscher (1999). "Time-domain reflectometry (TDR) in geotechnics: a review." *Nondestructive and Automated Testing for Soil and Rock Properties, ASTM STP*, 1350, 113-136.

Beziat, A., M. Dardaine, and E. Mouche (1992). "Measurements of the thermal conductivity of clay-sand and clay-graphite mixtures used as engineered barriers for high-level radioactive waste disposal." *Applied Clay Science*, 6(4), 245-263.

Bilskie, J., R. Horton, and K. Bristow (1998). "Test of a dual-probe heat-pulse method for determining tehrmal properties of porous materials." *Soil Science*, 163(5), 346-355.

Blackwell, J. (1956). "The axial-flow error in the thermal-conductivity probe." *Canadian Journal of Physics*, 34(4), 412-417.

Blumm, J., and J. Opfermann (2002). "Improvement of the mathematical modeling of flash measurements." *High Temperatures. High Pressures*, 34(5), 515-521.

Boutin, C., G. Kacprzak, and D. Thiep (2011). "Compressibility and permeability of sand-kaolin mixtures. Experiments versus non-linear homogenization schemes." *International Journal for Numerical and Analytical Methods in Geomechanics*, 35(1), 21-52.

Brandl, H. (2003). *Geothermal heating and cooling of buildings*, na.

Brandl, H. (2006). "Energy foundations and other thermo-active ground structures." *Géotechnique*, 56(2), 81-122.

Brigaud, F., D. S. Chapman, and S. Le Douaran (1990). "Estimating thermal conductivity in sedimentary basins using lithologic data and geophysical well logs (1)." *AAPG Bulletin*, 74(9), 1459-1477.

Bristow, K. L., J. R. Bilskie, G. J. Kluitenberg, and R. Horton (1995). "Comparison of techniques for extracting soil thermal properties from dual probe heat pulse data." *Soil Science*, 160(1), 1-7.

Bristow, K. L., G. S. Campbell, and K. Calissendorff (1993). "Test of a heat-pulse probe for measuring changes in soil water content." *Soil Science Society of America Journal*, 57(4), 930-934.

Bristow, K. L., G. J. Kluitenberg, and R. Horton (1994a). "Measurement of soil thermal properties with a dual-probe heat-pulse technique." *Soil Science Society of America Journal*, 58(5), 1288-1294.

Bristow, K. L., R. D. White, and G. J. Kluitenberg (1994b). "Comparison of single and dual probes for measuring soil thermal properties with transient heating." *Soil Research*, 32(3), 447-464.

Campbell, G., C. Calissendorff, and J. Williams (1991). "Probe for measuring soil specific heat using a heat-pulse method." *Soil Science Society of America Journal*, 55(1), 291-293.

Campbell, G. S., G. W. Gee, and A. Klute (1986). "Water potential: miscellaneous methods." *Methods of soil analysis. Part 1. Physical and mineralogical methods*, 619-633.

Carslaw, H. S., and J. C. Jaeger (1959). *Conduction of heat in solids*, Clarendon Press Oxford.

Cassel, D., and A. Klute (1986). "Water potential: tensiometry." *Methods of Soil Analysis: Part 1—Physical and Mineralogical Methods*(methodsofsoilan1), 563-596.

Chandler, R., M. Crilly, M. Smith, and M. Smith. "A low-cost method of assessing clay desiccation for low-rise buildings." *Proceedings of the ICE-Civil Engineering*, Thomas Telford, 82-89.

Chandler, R., and C. Gutierrez (1986). "The filter-paper method of suction measurement." *Géotechnique*, 36(2), 265-268.

Chen, S. X. (2008). "Thermal conductivity of sands." *Heat and Mass Transfer*, 44(10), 1241-1246.

Chen, Y. (2010). "An experimental investigation of the behavior of compacted clay/sand mixtures." University of Delaware.

Chiu, T.-F., and C. D. Shackelford (1998). "Unsaturated hydraulic conductivity of compacted sand-kaolin mixtures." *Journal of Geotechnical and Geoenvironmental Engineering*, 124(2), 160-170.

Chung, C. C., and C. P. Lin (2009). "Apparent dielectric constant and effective frequency of TDR measurements: Influencing factors and comparison." *Vadose Zone Journal*, 8(3), 548.

Cortes, D. D. (2015). "The physical nature of thermal conduction in dry granular media." *Géotechnique Letters*, 5(January – March), 1-5.

Côté, J., and J. M. Konrad (2005). "A generalized thermal conductivity model for soils and construction materials." *Canadian Geotechnical Journal*, 42(2), 443-458.

Côté, J., and J. M. Konrad (2005). "Thermal conductivity of base-course materials." *Canadian Geotechnical Journal*, 42(1), 61-78.

Cui, Y. J., N. Sultan, and P. Delage (2000). "A thermomechanical model for saturated clays." *Canadian Geotechnical Journal*, 37(3), 607-620.

Dalton, F., W. Herkelrath, D. Rawlins, and J. Rhoades (1984). "Time-domain reflectometry: Simultaneous measurement of soil water content and electrical conductivity with a single probe." *Science*, 224(4652), 989-990.

Dasberg, S., and J. Hopmans (1992). "Time domain reflectometry calibration for uniformly and nonuniformly wetted sandy and clayey loam soils." *Soil Science Society of America Journal*, 56(5), 1341-1345.

Davis, J. (1975). "Relative permittivity measurements of a sand and clay soil in situ." *Geological Survey Canada, Ottawa*, 75-71C.

De Vries, D. A. (1952). "A nonstationary for determining thermal conductivity of soil in situ." *Soil Science*, 73(2), 83-90.

De Vries, D. A. (1963). "Thermal properties of soils." *Physics of plant environment*.

Deka, R., M. Wairiu, P. Mtakwa, C. Mullins, E. Veenendaal, and J. Townend (1995). "Use and accuracy of the filter-paper technique for measurement of soil matric potential." *European Journal of Soil Science*, 46(2), 233-238.

Devices, D. (2011). "KD2 Pro thermal properties analyzer operator's manual version 4." *Decagon Devices, Pullman, WA. KD2 Pro thermal properties analyzer operator's manual version*, 4.

Dirksen, C., and S. Dasberg (1993). "Improved calibration of time domain reflectometry soil water content measurements." *Soil Science Society of America Journal*, 57(3), 660-667.

Dobson, M. C., F. T. Ulaby, M. T. Hallikainen, and M. A. El-Rayes (1985). "Microwave dielectric behavior of wet soil-Part II: Dielectric mixing models." *Geoscience and Remote Sensing, IEEE Transactions on*(1), 35-46.

Donazzi, F., E. Occhini, and A. Sepp (1979). "Soil thermal and hydrological characteristics in designing underground cables." *Electrical Engineers, Proceedings of the Institution of*, 126(6), 506-516.

Dong, Y., J. S. McCartney, and N. Lu (2015). "Critical review of thermal conductivity models for unsaturated soils." *Geotechnical and Geological Engineering*, 33(2), 207-221.

Drnevich, V., C. Lin, O. Yi, and J. Lovell (2001). "Real-time determination of soil type, water content, and density using electromagnetics." *Joint Transportation Research Program*, 177.

Drnevich, V. P., X. Yu, and J. E. Lovell (2003). "Beta testing implementation of the Purdue Time Domain Reflectometry (TDR) method for soil water content and density measurement."

Farouki, O. T. (1981). "Thermal properties of soils." DTIC Document.

Fawcett, R., and N. Collis-George (1967). "A filter-paper method for determining the moisture characteristics of soil." *Animal Production Science*, 7(25), 162-167.

Flynn, D. R., and T. Watson (1969). "Measurements of the thermal conductivity of soils to high temperatures. Final Report." National Bureau of Standards, Washington, DC.

Forbes, J. D. (1846). *Account of Some Experiments on the Temperature of the Earth, at Different Depths and in Different Soils, Near Edinburgh: From the Transact. of the Roy. Soc. of Edinb. Vol. XVI*, Rob. Grant.

Fredlund, D., J. K. Gan, and P. Gallen (1995). "Suction measurements on compacted till specimens and indirect filter paper calibration technique." *Transportation research record*, 1481, 3-9.

Fredlund, D. G., and H. Rahardjo, H. (1993). *Soil mechanics for unsaturated soils*, John Wiley & Sons.

Furmanski, M. G. a. P. (2013). "Predicting the effective thermal conductivity of dry granular media using artificial neural networks." *Journal of Power Technologies*, 93(2), 59-66.

Gangadhara Rao, M., and D. N. Singh (1999). "A generalized relationship to estimate thermal resistivity of soils." *Canadian Geotechnical Journal*, 36(4), 767-773.

Gardner, R. (1937). "A method of measuring the capillary tension of soil moisture over a wide moisture range." *Soil Science*, 43(4), 277-284.

Gemant, A. (1950). "The thermal conductivity of soils." *Journal of Applied Physics*, 21(8), 750-752.

Giese, K., and R. Tiemann (1975). "Determination of the complex permittivity from thin-sample time domain reflectometry improved analysis of the step response waveform." *Advances in Molecular Relaxation Processes*, 7(1), 45-59.

Gori, F. "A theoretical model for predicting the effective thermal conductivity of unsaturated frozen soils." *Proc. Int. Conf. on Permafrost, 4th, Fairbanks, AL. Natl. Acad. Press, Washington, DC*, 363-368.

Gori, F., and S. corasaniti (2002). "Theoretical prediction of the soil thermal conductivity at moderately high temperatures." *Journal of Heat Transfer*, 124(6), 1001-1008.

Greacen, E., G. Walker, and P. Cook (1987). "Evaluation of the filter paper method for measuring soil water suction."

Griffiths, C., N. Brereton, R. Beausillon, and D. Castillo (1992). "Thermal conductivity prediction from petrophysical data: a case study." *Geological Society, London, Special Publications*, 65(1), 299-315.

Guymon, G. L., and J. N. Luthin (1974). "A coupled heat and moisture transport model for arctic soils." *Water Resources Research*, 10(5), 995-1001.

Gylys, J., T. Zdankus, and M. Gylys (2013). "Investigation of heat transfer from inclined flat surface to aqueous foam." *International Journal of Heat and Mass Transfer*, 59, 272-278.

Haigh, S. K. (2012). "Thermal conductivity of sands." *Géotechnique*, 62(7), 617-625.

Halliday, D., R. Resnick, and J. Walker (2010). *Fundamentals of physics extended*, John Wiley & Sons.

Ham, J., and E. Benson (2004). "On the construction and calibration of dual-probe heat capacity sensors." *Soil Science Society of America Journal*, 68(4), 1185-1190.

Hamblin, A. (1981). "Filter-paper method for routine measurement of field water potential." *Journal of Hydrology*, 53(3), 355-360.

Heimovaara, T. (1993). "Design of triple-wire time domain reflectometry probes in practice and theory." *Soil Science Society of America Journal*, 57(6), 1410-1417.

Heimovaara, T., .W. Bouten, and J. Verstraten (1995). "Assessing temporal variations in soil water composition with time domain reflectometry." *Soil Science Society of America Journal*, 59(3), 689-698.

Hoekstra, P., A. Delaney, and R. Atkins (1973). "Measuring the thermal properties of cylindrical specimens by the use of sinusoidal temperature waves." DTIC Document.

Horai, K. i. (1971). "Thermal conductivity of rock-forming minerals." *Journal of Geophysical Research*, 76(5), 1278-1308.

Houston, S., W. Houston, and A. M. Wagner (1994). "Laboratory filter paper suction measurements." *ASTM geotechnical testing journal*, 17(2), 185-194.

Hoyos, L. R. (1998). "Experimental and computational modeling of unsaturated soil behavior under true triaxial stress states." School of Civil and Environmental Engineering, Georgia Institute of Technology.

Huisman, J., C. Lin, L. Weihermüller, and H. Vereecken (2008). "Accuracy of bulk electrical conductivity measurements with time domain reflectometry." *Vadose Zone Journal*, 7(2), 426-433.

Hutcheon, N., and J. Paxton (1952). "Moisture migration in a closed guarded hot plate." *Transactions American Society Healing & Ventilating Engineers*, 58, 301-320.

Incropera, F. P. (2011). *Fundamentals of heat and mass transfer*, John Wiley & Sons.

Jackson, A., J. Adams, and R. Millar (1978). "Thermal conductivity measurements on high-temperature fibrous insulations by the hot-wire method." *Thermal Transmission Measurements of Insulations, ASTM STP*, 660, 154-171.

Jacobsen, O. H., and P. Schjønning (1993). "A laboratory calibration of time domain reflectometry for soil water measurement including effects of bulk density and texture." *Journal of Hydrology*, 151(2), 147-157.

Jaeger, J. C. (1965). "Application of the theory of heat conduction to geothermal measurements." *Terrestrial heat flow*, 7-23.

Jenny, H. (1941). *Factors of soil formation*, McGraw-Hill Book Company New York, NY.

Johansen, O. (1977). "Thermal conductivity of soils." DTIC Document.

Jones, F., and F. Pascal (1994). "Numerical model calculations of the effects of grain sizes and orientations on the thermal conductivities of composites." *Geothermics*, 23(4), 365-371.

Kaplar, C. W. (1971). "Evaluation of a 20-Inch Guarded Hot-Plate Thermal Conductivity Apparatus Range-50 Degrees F to+ 250 Degrees F." DTIC Document.

Kersten, M. S. (1949). "Laboratory research for the determination of the thermal properties of soils." DTIC Document.

Kluitenberg, G., B. Das, and K. Bristow (1995). "Error analysis of heat pulse method for measuring soil heat capacity, diffusivity, and conductivity." *Soil Science Society of America Journal*, 59(3), 719-726.

Kluitenberg, G., J. Ham, and K. L. Bristow (1993). "Error analysis of the heat pulse method for measuring soil volumetric heat capacity." *Soil Science Society of America Journal*, 57(6), 1444-1451.

Knight, J. (1992). "Sensitivity of time domain reflectometry measurements to lateral variations in soil water content." *Water Resources Research*, 28(9), 2345-2352.

Knoll, M. D., and R. Knight. "Relationships between dielectric and hydrogeologic properties of sand-clay mixtures." *Proc., Fifth International Conferention on Ground Penetrating Radar*.

Kraus, J. (1984). "Electromagnetics, McGrawHill." *Inc., USA*.

Larson, T. (1988). "Thermal measurement of soils using a multineedle probe with a pulsed-point source." *Geophysics*, 53(2), 266-270.

Lee, J., Y. S. Kim, H. S. Kim, J. M. Kang, and G. J. Bae (2012). "Assessment of Calculation Methods for Thermal Conductivity of Saturated Kaolinite." *International Journal of Offshore and Polar Engineering*, 22(2), 172-175.

Leong, E. C., L. He, and H. Rahardjo (2002). "Factors affecting the filter paper method for total and matric suction measurements." *ASTM Geotechnical Testing Journal*, 25(3), 322-333.

Lide, D., and W. Haynes (2009). *CRC handbook of chemistry and physics: a ready-reference book of chemical and physical data-/editor-in-chief, David R. Lide; ass. ed. WM" Mickey" Haunes*, Boca Raton, Fla: CRC.

Liu, X., T. Ren, and R. Horton (2008). "Determination of soil bulk density with thermo-time domain reflectometry sensors." *Soil Science Society of America Journal*, 72(4), 1000.

Lu, N., and Y. Dong (2015). "Closed-form equation for thermal conductivity of unsaturated soils at room temperature." *Journal of Geotechnical and Geoenvironmental Engineering*, 04015016.

Lu, N., and W. J. Likos (2004). *Unsaturated soil mechanics*, J. Wiley.

Lu, S., T. Ren, Y. Gong, and R. Horton (2007). "An improved model for predicting soil thermal conductivity from water content at room temperature." *Soil Science Society of America Journal*, 71(1), 8.

Lubimova, H., L. Lusova, F. Firsov, G. Starikova, and A. Shushpanov (1961). "Determination of surface heat flow in Mazesta (USSR)." *Annals of Geophysics*, 14(2), 157-167.

Malicki, M., R. Plagge, and C. Roth (1996). "Improving the calibration of dielectric TDR soil moisture determination taking into account the solid soil." *European Journal of Soil Science*, 47(3), 357-366.

Malicki, M. A., and W. M. Skierucha (1989). "A manually controlled TDR soil moisture meter operating with 300 ps rise-time needle pulse." *Irrigation Science*, 10(2), 153-163.

Marion, D., A. Nur, H. Yin, and D. H. Han (1992). "Compressional velocity and porosity in sand-clay mixtures." *Geophysics*, 57(4), 554-563.

McGaw, R. (1969). "Heat conduction in saturated granular materials." *Highway Research Board Special Report*(103).

McGeary, R. (1961). "Mechanical packing of spherical particles." *Journal of the American ceramic Society*, 44(10), 513-522.

McKenna, T. E., J. M. Sharp Jr, and F. L. Lynch (1996). "Thermal conductivity of Wilcox and Frio sandstones in south Texas (Gulf of Mexico Basin)." *AAPG Bulletin*, 80(8), 1203-1215.

Midttømme, K., and E. Roaldset (1998). "The effect of grain size on thermal conductivity of quartz sands and silts." *Petroleum Geoscience*, 4(2), 165-172.

Mochlinski, K. (1964). "Some industrial. measurements of thermal properties of soils'." *International study group on soils. Cambridge, England, July*, 12-26.

Monzo, P. M., J. Acuña, and B. Palm (2011). "Comparison of different line source model approaches for analysis of thermal response test in a u-pipe borehole heat exchanger." *Stockholm, Sweden*.

Mortensen, A. P., J. W. Hopmans, Y. Mori, and J. Šimůnek (2006). "Multi-functional heat pulse probe measurements of coupled vadose zone flow and transport." *Advances in Water Resources*, 29(2), 250-267.

Nakano, Y., and J. Brown (1971). "Effect of a freezing zone of finite width on the thermal regime of soils." *Water Resources Research*, 7(5), 1226-1233.

Noborio, K. (2001). "Measurement of soil water content and electrical conductivity by time domain reflectometry: a review." *Computers and electronics in agriculture*, 31(3), 213-237.

Noborio, K., R. Horton, and C. Tan (1999). "Time domain reflectometry probe for simultaneous measurement of soil matric potential and water content." *Soil Science Society of America Journal*, 63(6), 1500-1505.

Noborio, K., K. McInnes, and J. Heilman (1996). "Measurement of soil water content, heat capacity and thermal conductivity with a single TDR probe." *Soil Science*, 161(1), 22-28.

O'Connor, K. M., and C. H. Dowding (1999). *Geomeasurements by pulsing TDR cables and probes*, CRC Press.

Ohga, H., and K. Mikoda. "Energy performance of borehole thermal energy storage systems." *Proc., Seventh International IBPSA Conference, Brazil*, 1009-1016.

Pan, H., Y. Qing, and L. Pei-yong (2010). "Direct and indirect measurement of soil suction in the laboratory." *Electronic Journal of Geotechnical Engineering*, 15(3), 1.

Parker, W., R. Jenkins, C. Butler, and G. Abbott (1961). "Flash method of determining thermal diffusivity, heat capacity, and thermal conductivity." *Journal of Applied Physics*, 32(9), 1679-1684.

Patil, U. D. (2014). *Response of unsaturated silty sand over a wider range of suction states using a novel double-walled triaxial testing system*, THE UNIVERSITY OF TEXAS AT ARLINGTON.

Perera, J. P., Y, Y., Houston, W., and Fredlund, D. "A new soil-water characteristic curve device." *Proc., Advanced Experimental Unsaturated Soil Mechanics: Proceedings of the International Symposium on Advanced Experimental Unsaturated Soil Mechanics, Trento, Italy, 27-29 June 2005*, CRC Press, 15.

Perry, R. H., D. W. Green, J. O. Maloney, M. M. Abbott, C. M. Ambler, and R. C. Amero (1997). *Perry's chemical engineers' handbook*, McGraw-hill New York.

Petersen, L. W., A. Thomsen, P. Moldrup, O. H. Jacobsen, and D. Rolston (1995). "HIGH-RESOLUTION TIME DOMAIN REFLECTOMETRY: SENSITIVITY DEPENDENCY ON PROBE-DESIGN." *Soil Science*, 159(3), 149&hyhen.

Pigford, T. (1982). "Geological disposal of radioactive waste." *Chem. Eng. Prog.;(United States)*, 78(3).

Polvani, C. (1977). "Objectives, concepts and strategies for the management of radioactive waste arising from nuclear power programmes." *Report by a Group of Experts of the OECD Nuclear Energy Agency, OECD/NEA, Paris*, 153.

Ponizovsky, A., S/ Chudinova, and Y. A. Pachepsky (1999). "Performance of TDR calibration models as affected by soil texture." *Journal of Hydrology*, 218(1), 35-43.

Qian-lin, Z., and L. Xiao-chun. "Migration of moisture under temperature gradient in unsaturated soil." *Proc., Electric Technology and Civil Engineering (ICETCE), 2011 International Conference on*, IEEE, 4213-4216.

Rawlins, S. L., and G. S. Campbell (1986). "Water potential: Thermocouple psychrometry." *Methods of Soil Analysis: Part 1—Physical and Mineralogical Methods*(methodsofsoilan1), 597-618.

Reece, C. (1998). "Simple method for determining cable length resistance in time domain reflectometry systems." *Soil Science Society of America Journal*, 62(2), 314-317.

Ren, T., K. Noborio, and R. Horton (1999). "Measuring soil water content, electrical conductivity, and thermal properties with a thermo-time domain reflectometry probe." *Soil Science Society of America Journal*, 63(3), 450-457.

Ren, T., T. E. Ochsner, and R. Horton (2003). "Development of thermo-time domain reflectometry for vadose zone measurements." *Vadose Zone Journal*, 2(4), 544-551.

Revil, A., and N. Lu (2013). "Unified water isotherms for clayey porous materials." *Water Resources Research*, 49(9), 5685-5699.

Ridley, A., S. Houston, W. Houston, and A. M. Wagner (1995). "Discussion on Laboratory filter paper suction measurements. Closure." *ASTM geotechnical testing journal*, 18(3), 391-396.

Ridley, A., and W. Wray. "Suction measurement: a review of current theory and practices." *Proc., Proceedings of the first international conference on unsaturated soils/sat95/Paris/France/6-8 September 1995. Volume 3*.

Sass, J., A. H. Lachenbruch, and R. J. Munroe (1971). "Thermal conductivity of rocks from measurements on fragments and its application to heat-flow determinations." *Journal of Geophysical Research*, 76(14), 3391-3401.

Schwerdtfeger, P. (1970). "The measurement of heat flow in the ground and the theory of heat flux meters." DTIC Document.

Scott, R. F. (1964). *Heat exchange at the ground surface*, US Army Materiel Command Cold Regions Research and Engineering Laboratory.

Shannon, W., and W. Wells. "Tests for thermal diffusivity of granular materials." *Proc., Proceedings-American Society for Testing and Materials*, Amer Soc Testing Materials 100 Barr Harbor Dr, W Conshohochen, PA 19428-2959, 1044-1055.

Siddiqui, S., and V. Drnevich (1995). *A new method of measuring density and moisture content of soil using the technique of time domain reflectometry*, Joint Highway Research Project, Purdue University.

Siddiqui, S., V. Drnevich, and R. Deschamps (2000). "Time domain reflectometry development for use in geotechnical engineering." *Geotechnical Testing Journal*, 23(1).

Sihvola, A. H. (1999). *Electromagnetic mixing formulas and applications*, Iet.

Smith, W., and H. Byers (1939). "The thermal conductivity of dry soils of certain of the great soil groups." *Soil Science Society of America Journal*, 3(C), 13-19.

Smith, W. O. (1942). "The thermal conductivity of dry soil." *Soil Science*, 53(6), 435-460.

Spaans, E. J., and J. M. Baker (1993). "Simple baluns in parallel probes for time domain reflectometry." *Soil Science Society of America Journal*, 57(3), 668-673.

Stalhane, B., and S. Pyk (1931). "New method for determining the coefficients of thermal conductivity." *Tek. Tidskr*, 61(28), 389-393.

Stephan, K., and A. Laesecke (1985). "The thermal conductivity of fluid air." *Journal of Physical and Chemical Reference Data*, 14(1), 227-234.

Tarnawski, V. R., W. H. Leong, and T. Momose (2009). "Assessing the impact of quartz content on the prediction of soil thermal conductivity." *Géotechnique*, 59(4), 331-338.

Thermitus, M. "New beam size correction for thermal diffusivity measurement with the flash method." *Proc., Gaal, Daniela D.; Gaal, peter S.(eds) Thermal Conductivity Conference/18th International Thermal Expansion Synposion. Lancaster PA: Destech Publications*, 217.

Timlin, D., and Y. A. Pachepsky (1996). "Comparison of three methods to obtain the apparent dielectric constant from time domain reflectometry wave traces." *Soil Science Society of America Journal*, 60(4), 970-977.

Tong, F., L. Jing, and R. W. Zimmerman (2009). "An effective thermal conductivity model of geological porous media for coupled thermo-hydro-mechanical systems with multiphase flow." *International Journal of Rock Mechanics and Mining Sciences*, 46(8), 1358-1369.

Tong, F., L. Jing, and R. W. Zimmerman (2010). "A fully coupled thermo-hydro-mechanical model for simulating multiphase flow, deformation and heat transfer in buffer material and rock masses." *International Journal of Rock Mechanics and Mining Sciences*, 47(2), 205-217.

Topp, G., J. Davis, and A. Annan (1982). "Electromagnetic determination of soil water content using TDR: II. Evaluation of installation and configuration of parallel transmission lines." *Soil Science Society of America Journal*, 46(4), 678-684.

Topp, G., J. Davis, and A. P.Annan (1980). "Electromagnetic determination of soil water content: Measurements in coaxial transmission lines." *Water Resources Research*, 16(3), 574-582.

Topp, G., M. Yanuka, W. Zebchuk, and S. Zegelin (1988). "Determination of electrical conductivity using time domain reflectometry: Soil and water experiments in coaxial lines." *Water Resources Research*, 24(7), 945-952.

Van Genuchten, M. T. (1980). "A closed-form equation for predicting the hydraulic conductivity of unsaturated soils." *Soil Science Society of America Journal*, 44(5), 892-898.

Van Wijk, W., and P. Bruijn, P. (1964). "Determination of thermal conductivity and volumetric heat capacity of soils near the surface." *Soil Science Society of America Journal*, 28(4), 461-464.

Vanpelt, D. (1976). "Thermal conductivity measurements of crushed stone and gravel aggregate." *CRREL Technical Note*, 6, 25-28.

Venkanna, B. (2010). *Fundamentals of heat and mass transfer*, PHI Learning Pvt. Ltd.

Welch, S., G. Kluitenberg, and K. L. Bristow (1996). "Rapid numerical estimation of soil thermal properties for a broad class of heat-pulse emitter geometries." *Measurement Science and Technology*, 7(6), 932.

Whalley, W., P. Leeds-Harrison, P. Joy, and P. Hoefsloot (1994). "Time domain reflectometry and tensiometry combined in an integrated soil water monitoring system." *Journal of Agricultural Engineering Research*, 59(2), 141-144.

White, N. K. (2004). "Accuracy and bias of TDR measurements in compacted sands."

Wiener, O. (1912). "Abhandl. Math-Phys." *Kl. Sachs. Akad. Wiss*, 32, 509.

Winterkorn, H. F. (1960). "Water and Its Conduction in Soils." *Soil Science*, 89(2), 113.

Wolfe, L. H., and J. O. Thieme (1964). "Physical and thermal properties of frozen soil and ice." *Society of Petroleum Engineers Journal*, 4(01), 67-72.

Woodside, W., and J. B. Cliffe (1959). "Heat and moisture transfer in closed systems of two granular materials." *Soil Science*, 87(2), 75-82.

Wu, R. (2013). "Coupled heat and moisture transfer in unsaturated soil for the modeling of shallow horizontal ground loops." University of Wisconsin-Madison

Yanuka, M., G. Topp, S. Zegelin, and W. Zebchuk (1988). "Multiple reflection and attenuation of time domain reflectometry pulses: Theoretical considerations for applications to soil and water." *Water Resources Research*, 24(7), 939-944.

Yu, X., P. Asheesh, N. Zhang, B. Thapa, and S. Tjuatja. "Thermo-TDR Probe for Measurement of Soil Moisture, Density, and Thermal Properties." *Proc., Geo-Congress 2014 Technical Papers@ sGeo-characterization and Modeling for Sustainability*, ASCE, 2804-2813.

Yu, X., and V. P. Drnevich (2004). "Soil water content and dry density by time domain reflectometry." *Journal of Geotechnical and Geoenvironmental Engineering*, 130(9), 922-934.

Yu, X., N. Zhang, and P. Asheesh. "Development and Evaluation of a Thermo-TDR Probe." *Proc., Soil Behavior and Geomechanics*, ASCE, 434-444.

Zegelin, S., I. White, and D. Jenkins (1989). "Improved field probes for soil water content and electrical conductivity measurement using time domain reflectometry." *Water Resources Research*, 25(11), 2367-2376.

Zhang, N., X. Yu, A. Pradhan, and A. J. Puppala (2015a). "Thermal conductivity of quartz sands by thermo-time domain reflectometry probe and model prediction." *Journal of Materials in Civil Engineering*, 04015059.

Zhang, N., X. Yu, A. Pradhan, and A. J. Puppala. "Effects of Particle Size and Fine Content on Thermal Conductivity of Quartz Sands." *Proc., Transportation Research Board 94th Annual Meeting*.

Biographical Information

Nan Zhang was born on 17th November in 1986 in China. He graduated from Hohai University in China and obtained a Bachelor's Degree in Civil Engineering in 2005. After that, he was admitted to the Geotechnical Research Institute in Hohai University for study for a master's degree.. He mainly worked on "Sedimentation and Consolidation of Soil Particles in Dredged Slurry" and other related fields, such as solidification/consolidation of dredged materials with Prof. Wei Zhu. He graduated in 2012 with a Master's Degree in Geotechnical Engineering.

In 2012, he came to the U.S. and entered the doctoral program in the Department of Civil Engineering at the University of Texas at Arlington (UTA), majoring in Geotechnical Engineering with advisor, Dr. Xinbao Yu and co-advisor, Dr. Anand J. Puppala. His doctoral research topic is "Development and Validation of TDR-Based Sensors for Thermal Conductivity and Soil Suction Measurements." He mainly worked on the design and evaluation of a thermo-TDR sensor and a moisture/suction TDR sensor for geothermal applications, and the development of soil thermal conductivity prediction models. He successfully completed all the course work and research for the Degree of Doctor of Philosophy in Civil Engineering in August, 2015.